Numerical Analysis of Radial Basis Function Based Implicit-Explicit Finite Difference Methods for Option Pricing Problems

Thesis submitted in partial fulfilment
for the Award of Degree

Doctor of Philosophy

by

RAJESH YADAV

RAJIV GANDHI INSTITUTE OF PETROLEUM TECHNOLOGY
JAIS - 229304

21MA0002

2026

CERTIFICATE

It is certified that the work contained in the thesis titled ***"Numerical Analysis of Radial Basis Function Based Implicit-Explicit Finite Difference Methods for Option Pricing Problems"*** by ***"Rajesh Yadav"*** has been carried out under our supervision and that this work has not been submitted elsewhere for a degree.

It is further certified that the student has fulfilled all the requirements of Comprehensive, Candidacy and SOTA.

(Dr. Gobinda Rakshit)
Supervisor

(Dr. Alpesh Kumar)
Co-Supervisor

DECLARATION BY THE CANDIDATE

I, ***"Rajesh Yadav"***, certify that the work embodied in this thesis is my own bona fide work and carried out by me under the supervision of ***"Dr. Gobinda Rakshit"*** and ***"Dr. Alpesh Kumar"*** from ***"August 2021"*** to ***"January 2026"*** at Rajiv Gandhi Institute of Petroleum Technology, Jais (India). The matter embodied in this thesis has not been submitted for the award of any other degree. I declare that I have faithfully acknowledged and given credits to the research workers wherever their works have been cited in my work in this thesis. I further declare that I have not wilfully copied any other's work, paragraphs, text, data, results, etc., reported in journals, books, magazines, reports, dissertations, thesis, etc., or available at websites and have not included them in this thesis and have not cited as my own work.

Date:

Place:

(RAJESH YADAV)

Roll No: 21MA0002

CERTIFICATE BY THE SUPERVISOR

It is certified that the above statement made by the student is correct to the best of our knowledge.

(Dr. Gobinda Rakshit)
Supervisor

(Dr. Alpesh Kumar)
Co-Supervisor

(Head of Department)
Mathematical Sciences

CERTIFICATE

CERTIFIED that the work contained in the thesis titled **"Numerical Analysis of Radial Basis Function Based Implicit-Explicit Finite Difference Methods for Option Pricing Problems"** by **Mr. Rajesh Yadav** has been carried out under my supervision. It is also certified that he fulfilled the mandatory requirement of two quality publications arose out of his thesis work.

It is further certified that the two publications (copies enclosed) of the aforesaid **Mr. Rajesh Yadav** have been published in the Journals indexed by –

(a) SCI

(b) SCI Extended

(c) SCOPUS

(Dr. Gobinda Rakshit)	(Dr. Alpesh Kumar)	(Dr. Sudeep Kundu)
Supervisor	**Co-Supervisor**	**Convener, DPGC**

COPYRIGHT TRANSFER CERTIFICATE

Title of the Thesis : Numerical Analysis of Radial Basis Function Based Implicit-Explicit Finite Difference Methods for Option Pricing Problems

Name of the Student : Rajesh Yadav

Copyright Transfer

The undersigned hereby assigns to the Rajiv Gandhi Institute of Petroleum Technology, Jais all rights under copyright that may exist in and for the above thesis submitted for the award of the "*DOCTOR OF PHILOSOPHY*".

Date:

Place:

RAJESH YADAV

Roll No: 21MA0002

Dedicated

To

*My Sweet **Grandparents***

Lt. Sanjya Devi & Shri Bhagirath Mal Yadav

*My Beloved **Parents***

Smt. Santosh Devi & Shri Bhoop Singh Yadav

*My Supportive **Supervisors***

Dr. Alpesh Kumar & Dr. Gobinda Rakshit

&

*My Wonderful **Siblings***

Deepak, Nikhil, Vishal, Piyush.

ACKNOWLEDGEMENTS

This Ph.D. journey has been much more than an academic pursuit for me; it has been a deeply personal experience. It has carried moments of uncertainty and confusion, years filled with unanswered questions, slow learning, silent struggles, and countless long nights spent reading, writing, rewriting, and quietly doubting myself. What sustained me through all of this was a small but unwavering hope that my work would one day find its place. I had often heard that research is not a straight path, but living through it taught me its true meaning. This journey tested my patience, confidence, and belief, and shaped me to face rejection with resilience and to move forward even when appreciation was scarce.

This journey was never meant to be walked alone. Behind every step forward was the support, encouragement, and understanding of people who believed in me, even when I struggled to believe in myself. Acknowledging them is not merely a tradition, but a sincere expression of gratitude and responsibility. The order in which they are mentioned here does not imply any hierarchy; each one has contributed in their own way, and I simply had to begin somewhere.

First and foremost, I offer my deepest gratitude to *Hanumanji* for His constant guidance, strength, and grace. In moments of doubt, exhaustion, and uncertainty, His presence gave me courage, faith, and the strength to continue through every phase of my Ph.D. journey.

I am deeply grateful to my supervisors, *Dr. Alpesh Kumar* and *Dr. Gobinda Rakshit*, whose invaluable guidance, calm support, trust, and constant encouragement shaped this journey. Their patience, insights and belief in my abilities played a crucial role in my academic and personal growth throughout the course of my research.

I sincerely thank the RPEC members, *Dr. Dhrubasish Bhattacharya* and *Dr. Rohit Bansal*, for their constructive feedback and critical comments, which significantly improved the quality of the research work on which this thesis is based. I am extremely grateful to *Dr. Alpesh Kumar*, *Dr. Gobinda Rakshit*, *Dr. Soniya Dhama*, *Dr. Sudeep Kundu*, and *Prof. Chanchal Kundu* for their guidance and teaching during my Ph.D. course, which provided a strong foundation for my research. I also thank *Dr. Manoj K. Rajpoot*, and *Dr. Pradeep Das* for their assistance and support with administrative and official procedures throughout my Ph.D. tenure. I am deeply thankful to *Soniya Ma'am*, who has been a motherly figure to me throughout this journey. Her calm voice, kindness, and constant encouragement provided comfort and strength during difficult moments and helped me move forward with confidence.

At this point, I cannot forget my family, whose love and sacrifices form the foundation of everything I have achieved. I express my deepest gratitude to *Mummy* (my mother), whose unconditional love has been a constant source of strength, and to *Papa* (my father), my hero, whose values, guidance, and unwavering belief in me shaped who I am today. I owe a special debt of gratitude to my brother, *Deepak Bhai Sahab*, who inspired the beginning of my Ph.D. journey and stood by me unwaveringly until its completion. He is also co-author of the research articles related to this thesis, and his academic contributions, guidance, and constant encouragement have been invaluable. It is only because of his constant support that I am now very close to completing my Ph.D. and receiving the title of *Dr.*

I lovingly remember *Maa* (my late grandmother); though she is no longer with us, I know that her blessings continue to guide and protect me, and she would have been immensely proud of this achievement. I am also grateful to *Baba* (my grandfather), *Chacha*, *Chachi*, and my siblings, *Nikhil*, *Piyush*, *Vishal* and *Sachin*, for their love, encouragement, and faith in me. Whatever I am today and what I may become in the future is deeply rooted in their support.

I would like to thank my seniors, *Dr. Akanksha Bhardwaj*, *Dr. Deepak K. Yadav*, and *Dr. Jyoti*, for their unconditional support and encouragement. I feel blessed to have such wonderful batchmates, *Poulami* and *Shashank*, as well as semi-batchmates, *Puja*, *Shishupal*, and *Vidit*. I am equally grateful to my supportive junior, *Heeraballabh*, *Aman*, and *Mritunjay* for making the lab environment positive and encouraging.

Without friends, any journey can become stressful and boring. I am deeply thankful to *Puja* for always being by my side in every situations. I sincerely thank *Krishna* for taking the time to talk to me and making me feel special and supported. I will always cherish *Puja*, *Poulami*, and *Shishupal* for being my friends when I first arrived at the institute, far away from home. I also acknowledge my weekend-cricket and badminton friends, whose company and time in the field provided much-needed therapy and balance during this journey.

At this phase, I cannot forget my long-time friends, *Vijay*, *Braj Gopal*, *Ishwar*, *Jatin*, and *Chetna*. Although they were not physically present with me during this journey, they remained in constant touch and offered support and encouragement. I am also thankful to *Deepak*, *Simran*, *Antima*, *Hari Om*, and *Kanav*, whom I met only for a few days during workshops, yet whose warmth and connection made it feel otherwise.

I sincerely acknowledge CSIR, India, for providing me with financial support, without which I would not have imagined pursuing a Ph.D. I am also grateful to *Rajiv Gandhi Institute of Petroleum Technology, Jais*, for offering me admission to its Ph.D. program and for providing excellent research facilities and accommodation, which made my long stay here productive and comfortable.

I am particularly grateful to the non-teaching staff of RGIPT, especially *Joshi Sir*, *Shashi Ma'am*, and *Pachouri Sir*, for their kind administrative support. Last but not least, I extend my gratitude to *Shalini Ma'am*, *Anuj* and *Mohsin Bhaiya*, the non-teaching staff of the department, for their invaluable assistance with documents and related formalities.

During this long period of four and a half years I met many people, all of whom helped me in some way or another to complete this thesis. It is not possible to mention all of them. I thank you all and want forgiveness if I forget someone unintentionally.

RGIPT, Jais **Rajesh Yadav**

January, 2026

Contents

List of Figures

List of Tables

Notations and Abbreviations

$\mathbb{R}$	Set of Real Numbers
Ω	Domain
Ω_i	Sub-domain corresponding to pont x_i
S	Stock Price
K	Strike Price
Φ	Payoff
$\mathbb{E}$	Expectation
T	Maturity
λ	Jump intensity
σ	Volatility
μ_J	Mean
σ_J	Variance
r	Risk free interest rate
φ	Multivariate radial function
ϕ	Univariate function corresponds to φ
k	Temporal mesh length
$\mathscr{L}$	Any linear differential operator
W	Wiener process
κ	Expected relative jump size
η	Impulse function
$\mathbb{P}$	Probability
$\mathcal{F}$	Filtration
$\mathcal{A}$	Generator of the Markov chain
$\mathcal{X}_\tau$	Markov chain
$\mathcal{M}_\tau$	Martingale
M	Spatial points
N	Temporal points

BS	Black Scholes
PDE	Partial Differential Equation
SDE	Stochastics Differential Equation
JD	Jump-Diffusion
RSJD	Regime-Switching Jump-Diffusion
PIDE	Partial Integro-Differential Equation
LCP	Linear Complementarity Problem
ODE	Ordinary Differential Equation
RBF	Radial Basis Function
TPS	Thin Plate Spline
FD	Finite Difference
IMEX	Implicit-Explicit
CNLF	Crank–Nikolson Leap-Frog
CNAB	Crank-Nikolson Adam-Bashforth
BDF2	Backward Difference Formula of Second Order
BDF1	Backward Difference Formula of First Order
OS	Operator Splitting
OTC	Over The Counter

Abstract

Radial basis functions (RBFs) are highly effective for approximating multivariable functions through linear combinations of univariate radial functions that depend only on the distance from a center. Their mesh-free nature makes them naturally suitable for solving problems. They are particularly useful when the dataset is known only at a finite set of discrete points, providing a smooth approximation that can be evaluated quickly and repeatedly. Beyond their role in function approximations, RBFs have also emerged as a robust tool for advancing higher-order numerical methods for solving complex partial differential equations (PDEs), partial integro-differential equations (PIDEs), and linear complementarity problems (LCPs) particularly in computational finance. Their global support and inherent smoothness make RBFs an appropriate choice for achieving higher-order accuracy. By selecting suitable RBFs from the various types available in literature and by optimizing the shape parameters, these methods can attain high convergence rates while significantly reducing numerical errors.

In this thesis, we developed a radial basis function based finite difference (RBF-FD) scheme for solving various types of option pricing problems. Spatial discretization using RBF-FD method is combined with implicit-explicit (IMEX) temporal schemes to provide a reliable and efficient framework for computational finance problems with improved accuracy. Stability analyses for the proposed time semi-discretization methods are also presented. In addition, numerical experiments are performed to demonstrate the order of convergence, accuracy, and efficiency of the proposed numerical schemes. These RBF-FD–IMEX methods are efficiently applied to several stochastic models arising in option pricing. Specifically, we consider cases where the underlying asset follows a jump-diffusion process with local volatility, European and American options in an extended Markovian regime-switching jump-diffusion (RSJD) framework, Asian options governed by moving-boundary partial integro-differential equations with regime-switching jump-diffusion, and European and American options under liquidity shocks modeled through PDE system and semi-linear complementarity problems. These contributions establish high order, computationally efficient RBF-FD methods, capable of handling jumps, regime switching, path dependence, and liquidity effects, with direct application in option pricing.

In Chapter 1, a brief overview of financial markets and derivative securities is provided, with a particular focus on options and their fundamental concepts. The chapter also includes a literature review of recent numerical methods for option pricing and an introduction to the basic principles of radial basis function approximation. It presents the motivation of the study and outlines the problems addressed, together with the preliminaries that will be used extensively in the subsequent chapters.

Chapter 2 presents efficient and accurate RBF-FD–IMEX methods for pricing options when the underlying asset follows a jump-diffusion process with local volatility. For time semi-discretization, we introduce three numerical techniques: Crank–Nicolson Leap-Frog (CNLF), Crank-Nicolson Adam-Bashforth (CNAB), and the second order Backward difference formula (BDF2), all incorporated with the RBF-FD method. The stability of the time semi-discretized schemes is also analyzed. The computational methods developed for European options are extended to American options. In particular, the RBF-FD IMEX methods are integrated with an operator splitting (OS) technique to solve the linear complementarity problem with variable parameters, which determines the price of an American option. To validate the effectiveness and accuracy of the proposed techniques, numerical results for European and American put options under the Merton and Kou models are presented. Part of the work in this chapter has been published in *Engineering Analysis with Boundary Elements*.

Chapter 3 introduces three RBF-FD IMEX methods for pricing European and American options in an extended Markovian regime-switching jump-diffusion economy. A PIDE is used to compute European option values, while a linear complementarity problem determines American option prices. To solve the LCP, the proposed scheme is combined with operator splitting methods, eliminating the need for fixed-point iterations at each economic stage and time step. The stability of the proposed time discretization methods is analyzed, and numerical experiments are used to validate the second-order convergence and computational efficiency of the three IMEX methods (BDF2, CNAB, CNLF) under the extended RSJD model. Part of the work in this chapter has been published in *Numerical Algorithms*.

Chapter 4 investigates the construction of a RBF-FD IMEX method for solving moving-boundary PIDE systems governing regime-switching jump-diffusion for Asian option pricing. The RBF-FD scheme is employed for spatial discretization and paired with the IMEX schemes for temporal discretization. The stability of the time semi-discretization method is also established theoretically. Numerical examples are presented to demonstrate the efficacy of the proposed scheme in terms of convergence and accuracy. Part of the work in this chapter has been published in *Engineering Analysis with Boundary Elements*.

Chapter 5 introduces two accurate and efficient finite difference RBF-FD methods for pricing European and American options under liquidity shocks. The problems are formulated as semi-linear complementarity and PDE systems for American and European options, respectively. For temporal semi-discretization, two backward difference formulas of order one and two (BDF1 & BDF2) are employed. The stability and convergence analysis of the proposed methods are provided. For American options, the semi-linear system of complementarity problems is solved by combining the RBF-FD approach with an operator splitting method. Numerical examples are provided for both European and American call options, and the superiority of results are validated against existing literature. Additionally, Greeks (Delta and Gamma) plots are presented for the American options to illustrate the sensitivity of option prices. Part of the work in this chapter has been published in *International Journal of Computer Mathematics*.

Chapter 6 is the concluding chapter, in which the contributions of the thesis are summarized and directions for future research are outlined.

The references cited in this thesis are listed in the *Bibliography*, followed by a list of published/communicated articles based on this work.

CHAPTER 1

Introduction and mathematical preliminaries

During the last few decades, derivatives have expanded rapidly and have emerged as one of the most significant developments in modern finance. Financial derivatives are financial contracts whose value is derived from the value of underlying assets such as, stocks, bonds, currencies, commodities, or market indices. They are used primarily for risk management, hedging, speculation, and arbitrage. Common types of financial derivatives include options, futures, forwards, and swaps [63]. These contracts can be standardized and traded on exchanges or customized and traded over the counter (OTC). The valuation of derivative contracts plays a central role in modern financial theory and practice. Since options are the primary focus of this study, we provide a detailed discussion of their structure, properties, classifications, pricing models and associated simulation techniques.

1.1 Options

Options are among the most actively traded derivatives in the financial world. An option is a financial contract that gives the holder the right, but not the obligation, to buy or sell an underlying asset S at a specific price (the strike price K) before or at expiration (maturity date T). There are two main types of options: a call option, which gives the right to buy the underlying asset, and a put option, which gives the right to sell it. Among the various option styles, the most common are the European, American and Asian options, which differ in the time restrictions placed on exercising the option and the average price of the underlying asset.

1.1.1 European Options

A European option is a financial derivative that can be exercised only at maturity. It gives the holder the right, but not the obligation, to exercise underlying asset at a predetermined strike price exclusively on the expiration date. European options are of two types: European call option, which gives the right to buy the underlying asset at maturity, and European put option, which gives the right to sell the underlying asset at maturity. The payoff function, which determines the final cash flow, for European call and put options are respectively given as follows:

$$\Phi(S,T) = \max(S-K,0), \quad \text{and} \quad \Phi(S,T) = \max(0,K-S).$$

For a European call option, if the asset price at maturity exceeds the strike price, the holder makes a profit, otherwise, payoff is zero. Conversely, for a European put option, if the asset price at maturity is below the strike price, the holder gains, otherwise, payoff is zero.

European options exist for a wide range of assets, including stocks, stock indices, commodities, currencies, bonds, and even cryptocurrencies. The buyer pays an upfront premium to the seller, which represents the maximum possible loss if the option expires worthless. Due to their fixed-expiry exercise feature, the seller cannot be forced to fulfill the contract before the maturity date. Their standardized terms and simpler settlement procedures, make European options widely traded on major stock indices, particularly in European markets. The most common mathematical model for valuing European options is the Black-Scholes model.

1.1.2 American Options

American options are financial derivatives that give the holder the right, but not the obligation, to exercise the option at any time up to its expiration date. Unlike European options, American options allow for early exercise, providing flexibility to take advantage of favorable price movements, maximize profits, or limit losses during the life of the option. Similar to European options, there are two main types of American options: call option, which gives the holder the right to buy the underlying asset at a fixed strike price and put option, which gives the holder the right to sell the underlying asset at the strike price. The payoff function of American call and put options are, repectively, as follows:

$$\Phi(S,t) = \max(S-K,0), \quad \text{and} \quad \Phi(S,t) = \max(0,K-S), \quad 0 \leq t \leq T.$$

The early exercise feature generally increases the premium of American options compared to European options. They are widely used in U.S. markets, particularly for stocks, commodities, where traders often exploit short-term market shifts. American options are frequently chosen for underlying assets that pay dividends, as early exercise allows investors to capture dividend payouts.

1.1.3 Asian Options

Asian options are path-dependent financial derivatives whose payoff depends on the average value of the underlying asset over a certain time period, rather than its price at maturity. The payoff function of Asian call and put options are, respectively, as follows:

$$\Phi(S) = \max(S_{avg} - K, 0) \quad \text{and} \quad \Phi(S) = \max(0, K - S_{avg}).$$

where K is the strike price and S_{avg} is the average price of the underlying asset over the specified period. Asian options reduce sensitivity to short-term market fluctuations and price manipulation, making them generally less volatile and cheaper than European options. They can be structured as either European-style or American-style options, and both types are path-dependent.

- The European-style Asian options can only be exercised at Maturity, and their payoff depends on the average price of the underlying asset over a specified period.
- The American-style Asian options can be exercised at any time up to and including maturity. Their payoff also depends on the average price of the underlying asset, but the holder can choose the optimal exercise time before expiration.

1.2 Option Pricing models

Option pricing is a fundamental problem in financial mathematics, concerned with determining the value of derivative securities whose payoff depends on the price of underlying asset. Pricing derivatives enables investors to hedge risk and minimize losses arising from fluctuations in asset prices. Underlying assets are financial objects whose current values are known but may change in the future.

In 1973, Black and Scholes [14] and Merton [97] introduced a pioneering framework for option pricing, showing that option values can be formulated using deterministic partial differential equations. This Black-Scholes model soon became a cornerstone of quantitative finance, especially for European options, due to its simplicity and practical relevance. However, the standard Black-Scholes models [14] assumes constant volatility and log-normal stock price dynamics, which do not fully align with real market behavior. In practice, option prices exhibit volatility smiles or skews, where different strikes and maturity imply different volatilities.

To overcome these limitations, several extensions of the Black-Scholes model have been proposed. One approach is the local volatility model, where volatility is treated as deterministic function of underlying asset price and time. Another important development is the stochastic volatility model [57], [61], where volatility follows a mean-reverting diffusion process, often correlated with the asset price. A third widely used approach is the jump-diffusion model [96], which incorporates sudden jumps in asset prices to better captures volatility skews. Further extensions include Kou's log-double-exponential jump model [79] and a variety of Lévy process-based models (see, [8], [21], [30], [94]), allowing for richer jump dynamics. Although hybrid models combining both stochastic volatility and jumps have also been developed, they are often computationally expensive and difficult to implement. As a result, researchers frequently rely on jump-diffusion models with time- and price-dependent volatility as a more balanced and effective alternative.

American options give rise to additional challenges because they can be exercised at any time before expiration. This early-exercise feature transforms the pricing problem into a free boundary problem [95, 124]. An alternative formulation using variational inequalities was developed in [49] and [13]. Numerical methods based on these variational inequality techniques are now widely used for approximating American option prices.

While numerous extensions and alternative financial models have been developed in the existing literature, this thesis focuses specifically on the following financial model problems:

1.2.1 The Black–Scholes Model

The Black–Scholes model is fundamental to modern derivative pricing, financial risk management, and market efficiency. It provides a mathematical framework for valuing options and serves as the foundation for many advanced pricing models used today. The model describes the evolution of an option price through a PDE derived using stochastic calculus, Itô's lemma, and no arbitrage principle. The European option price satisfies the following degenerate and backward-in-time parabolic partial differential equation,

$$\frac{\partial U}{\partial \tau} + \frac{1}{2}\sigma^2 S^2 \frac{\partial^2 U}{\partial S^2} + (r-d)\, S\frac{\partial U}{\partial S} - rU = 0. \tag{1.2.1}$$

By using the transformations $\tau = T - t$, $S = Ke^x$ and $u(x,t) = U(Ke^x, T-t)$, the partial differential equation (1.2.1) is transformed into a non-degenerate and forward in time, as

$$\frac{\partial u}{\partial t} = \mathcal{L}u(x,t), \tag{1.2.2}$$

where the spatial operator $\mathcal{L}$ is defined as

$$\mathcal{L}u(x,t) = \frac{1}{2}\sigma^2\frac{\partial^2 u}{\partial x^2} + \left(r - d - \frac{1}{2}\sigma^2\right)\frac{\partial u}{\partial x} - ru. \tag{1.2.3}$$

Where, $x = \ln\left(\frac{S}{K}\right)$ represents the logarithmic transformation of asset price with respect to the strike price K, T is the maturity, and the parameter r is the risk-free interest rate, d is the dividend, σ is the volatility corresponding to asset price.

American Option Formulation

In contrast, an American option can be exercised at any time before or on the expiration date. This early-exercise feature leads to a Linear Complementarity Problem formulation based on the same underlying stochastic differential equation:

$$\begin{cases} \dfrac{\partial u}{\partial t} - \mathcal{L}u & \leq & 0, \quad (x,t) \in \mathbb{R} \times J, \\ u(x,t) - \Phi(Ke^x) & \geq & 0, \quad (x,t) \in \mathbb{R} \times J, \\ \left(\dfrac{\partial u}{\partial t} - \mathcal{L}u\right)\big(u(x,t) - \Phi(Ke^x)\big) & = & 0, \quad (x,t) \in \mathbb{R} \times J, \\ u(x,0) & = & \Phi(Ke^x), \quad x \in \mathbb{R}. \end{cases} \tag{1.2.4}$$

where $J = (0,T]$.

1.2.2 Black-Scholes Jump-diffusion model

The Black-Scholes Jump Diffusion Model mathematically extends the classical Black-Scholes model by incorporating a jump into the standard diffusion process to capture sudden and discontinuous movements in asset price. This leads to a Partial Integro-Differential Equation, since the diffusion terms of the Black–Scholes PDE are supplemented by an integral term representing jumps. The value of an option can be obtained by solving the following PIDE

$$\frac{\partial u}{\partial t} = \mathcal{L}u(x,t) = \mathcal{D}u(x,t) + \mathcal{I}u(x,t), \tag{1.2.5}$$

where,

$$\mathcal{D}u(x,t) = \frac{1}{2}\sigma^2(x,t)\frac{\partial^2 u}{\partial x^2} + \delta(x,t)\frac{\partial u}{\partial x} + \beta(x,t)u, \tag{1.2.6}$$

$$\mathcal{I}u(x,t) = \lambda \int_{-\infty}^{\infty} u(y,t) f(y-x)dy. \tag{1.2.7}$$

Where the maturity is given by T, $x = \ln(\frac{S}{K})$ represents the logarithmic asset price relative to the strike price K, λ denotes the jumps intensity, and $f(x)$ is the density function of jump sizes of the log-return x. The coefficients are given by

$$\delta(x,t) = r - \frac{\sigma^2(x,t)}{2} - \lambda\kappa \quad \text{and} \quad \beta(x,t) = -(r+\lambda).$$

We consider the density function $f(y)$ as

$$f(y) = \begin{cases} \frac{1}{\sqrt{2\pi}\sigma_J}\exp(-\frac{(y-\mu_J)^2}{2\sigma_J^2}) & \text{Merton's model,} \\ p\eta_1 e^{-\eta_1 y}\mathcal{H}(y) + q\eta_2 e^{-\eta_2 y}\mathcal{H}(-y) & \text{Kou's model,} \end{cases}$$

and $u(x,t)$ satisfies the following localised PIDE:

$$\frac{\partial u}{\partial t} = \frac{1}{2}\sigma^2(x,t)\frac{\partial^2 u}{\partial x^2} + \delta(x,t)\frac{\partial u}{\partial x} + \beta(x,t)u + \lambda \int_{-\infty}^{\infty} u(y,t) f(y-x)dy.$$

with the initial and boundary conditions for European put option as follows

$$u(x,0) = \max(K - Ke^x, 0),$$

$$u(x,t) = \begin{cases} Ke^{-rt} - Ke^{x} & : \quad x \to -\infty, \\ 0 & : \quad x \to +\infty. \end{cases}$$

Since the American option can be exercised at any time prior to maturity, its valuation problem can be formulated as a linear complementarity problem derived from the underlying stochastic differential equation, as follows:

$$\begin{cases} \frac{\partial u}{\partial t} - \mathcal{L}u & \leq & 0 \quad (x,t) \in \mathbb{R} \times J, \\ u(x,t) - \Phi(Ke^{x}) & \geq & 0 \quad (x,t) \in \mathbb{R} \times J, \\ (\frac{\partial u}{\partial t} - \mathcal{L}u)\,(u(x,t) - \Phi(Ke^{x})) & = & 0 \quad (x,t) \in \mathbb{R} \times J, \\ u(x,0) & = & \Phi(Ke^{t}) \qquad x \in \mathbb{R}, \end{cases} \tag{1.2.8}$$

where $J = (0,T]$ and the spatial operator can be defined as described above and the boundary condition for American option is

$$u(x,t) = \begin{cases} K - Ke^{x} & : \quad x \to -\infty, \\ 0 & : \quad x \to +\infty. \end{cases}$$

1.2.3 Regime-switching Jump-diffusion model

The RSJD model is a sophisticated financial framework that extends classical jump-diffusion processes by allowing the drift, volatility, jump intensity, and jump size to switch among a finite set of regimes. These regime changes are governed by an underlying Markov or semi-Markov process evolving at random times.

Under the risk-neutral measure, the price of the European option at the jth regime, $u(x,t,\mathfrak{e}_j)$, in the RSJD model satisfies the following PIDE:

$$\frac{\partial u}{\partial t}(x,t,\mathfrak{e}_j) - \mathcal{L}u(x,t,\mathfrak{e}_j) = 0, \quad (x,t,\mathfrak{e}_j) \in \mathbb{R} \times J \times \mathcal{H}, \tag{1.2.9}$$

where $J = (0,T]$ and the spatial differential operator can be defined as

$$\begin{aligned} \mathcal{L}u(x,t,\mathfrak{e}_j) \quad = \quad & \frac{1}{2}(\sigma_j(x,t))^2 \frac{\partial^2 u}{\partial x^2}(x,t,\mathfrak{e}_j) + \left(r_j - d_j - \frac{(\sigma_j(x,t))^2}{2} - \lambda_j \kappa_j \right) \frac{\partial u}{\partial x}(x,t,\mathfrak{e}_j) - (r_j + \lambda_j) u(x,t,\mathfrak{e}_j) \\ & + \lambda_j \int_{-\infty}^{\infty} u(y,t,\mathfrak{e}_j) f(y-x,\mathfrak{e}_j)\, dy + \langle \mathbf{u_n} \,,\, \mathcal{A}\mathfrak{e}_j \rangle. \end{aligned} \tag{1.2.10}$$

The option value $u(x,t,\mathfrak{e}_j)$ at the time of maturity T is termed as the payoff function. For the European put option, the payoff function is given by:

$$u_0^j(x) = \max(K - Ke^{x}, 0) \tag{1.2.11}$$

with a strike price of K. Here $x = \ln(\frac{S}{K})$ is the log asset price with respect to a strike price K and $\mathcal{L} = \mathcal{D} + \mathcal{I} + \mathcal{E}$, such that

$$\mathcal{D}u(x,t,\mathfrak{e}_j) = \frac{1}{2}(\sigma_j(x,t))^2 \frac{\partial^2 u}{\partial x^2}(x,t,\mathfrak{e}_j) + \left(r_j - d_j - \frac{(\sigma_j(x,t))^2}{2} - \lambda_j \kappa_j \right) \frac{\partial u}{\partial x}(x,t,\mathfrak{e}_j) - (r_j + \lambda_j) u(x,t,\mathfrak{e}_j), \tag{1.2.12}$$

$$\mathcal{I}u(x,t,\mathfrak{e}_j) = \lambda_j \int_{-\infty}^{\infty} u(x,t,\mathfrak{e}_j) f(y-x,\mathfrak{e}_j)dy, \tag{1.2.13}$$

$$\text{and} \;\; \mathcal{E}u(x,t,\mathfrak{e}_j) = \langle \mathbf{u_n} \; , \; \mathcal{A}\mathfrak{e}_j \rangle, \tag{1.2.14}$$

where $\langle \mathbf{u_n} \; , \; \mathcal{A}\mathfrak{e}_j \rangle = \sum_{i=1}^{Q} u_n^i q_{i,j}$, $\mathbf{u_n}$ is a Q dimensional vector $\mathbf{u_n} = (u_n^1, u_n^2, u_n^3, \cdots, u_n^Q)^T$ with $u^j(x,t) = u(x,t,\mathfrak{e}_j)$, $1 \le j \le Q$ and the function $f(y,\mathfrak{e}_j)$ can be written as:

$$f(y,\mathfrak{e}_j) = \begin{cases} \frac{1}{\sqrt{2\pi}\sigma_J^j} \exp -\frac{(y-\mu_J^j)^2}{2(\sigma_J^j)^2} & \text{Merton model,} \\ p_j \eta_1^j e^{-\eta_1^j y}\mathcal{H}(y) + q_j \eta_2^j e^{-\eta_2^j y}\mathcal{H}(-y) & \text{Kou model.} \end{cases}$$

The valuation of an American option $u(x,t,\mathfrak{e}_j)$ under RSJD model address the following linear complementarity problem:

$$\begin{cases} \frac{\partial u}{\partial t}(x,t,\mathfrak{e}_j) - \mathcal{L}u(x,t,\mathfrak{e}_j) & \ge & 0, & (x,t,\mathfrak{e}_j) \in \mathbb{R} \times J \times \mathcal{H}, \\ u(x,t,\mathfrak{e}_j) - \Phi^j(Ke^x) & \ge & 0, & (x,t,\mathfrak{e}_j) \in \mathbb{R} \times J \times \mathcal{H}, \\ \left(\frac{\partial u}{\partial t}(x,t,\mathfrak{e}_j) - \mathcal{L}u(x,t,\mathfrak{e}_j)\right)\left(u(x,t,\mathfrak{e}_j) - \Phi^j(Ke^x)\right) & = & 0, & (x,t,\mathfrak{e}_j) \in \mathbb{R} \times J \times \mathcal{H}, \\ u_0^j(x) & = & \Phi^j(Ke^x), & x \in \mathbb{R}. \end{cases} \tag{1.2.15}$$

For the American put option, the payoff function is given by:

$$u_0^j(x) = \max(K - Ke^x, 0) \tag{1.2.16}$$

with a strike price of K.

RSJD model for European-style Asian options

Since Asian options depend on the average of the underlying asset price, the state space must be extended to include both the asset price and its running average. Accordingly, under regime j, the regime switching model with a change of variables for the pricing of a European-style Asian option satisfies the following PIDE [81]:

$$\frac{\partial u}{\partial t}(x,t;\mathfrak{e}_j) \;\; = \;\; \mathcal{D}u(x,t;\mathfrak{e}_j) + \mathcal{I}u(x,t;\mathfrak{e}_j) + \mathcal{E}u(x,t;\mathfrak{e}_j), \;\; x \in (-\infty, 0], \;\; t \in (0,T], \tag{1.2.17}$$

where,

$$\begin{aligned} \mathcal{D}u(x,t;\mathfrak{e}_j) \;\; = \;\; & \frac{\sigma_j^2}{2}\frac{\partial^2 u}{\partial x^2}(x,t;\mathfrak{e}_j) + \left(\frac{e^x-1}{Te^x}\frac{1}{Z-\frac{T-t}{T}} - r_j - \frac{\sigma_j^2}{2} + d_j + \lambda_j\alpha_j\right)\frac{\partial u}{\partial x}(x,t;\mathfrak{e}_j) \\ & -(\lambda_j + d_j + \lambda_j\alpha_j - a_{jj})u(x,t;\mathfrak{e}_j), \end{aligned} \tag{1.2.18}$$

$$\mathcal{I}u(x,t;\mathfrak{e}_j) = \lambda_j \int_{-\infty}^{\infty} e^y u(x-y,t;\mathfrak{e}_j) f(y;\mathfrak{e}_j)dy, \tag{1.2.19}$$

$$\mathcal{E}u(x,t;\mathfrak{e}_j) = \sum_{l=1, l\ne j}^{d} a_{jl}u(x,t;l), \tag{1.2.20}$$

subject to the following initial condition:

$$u(x,0;\mathfrak{e}_j)=0,\quad x\in(-\infty,0], \tag{1.2.21}$$

and the boundary conditions:

$$u(-\infty,t;\mathfrak{e}_j)=\frac{1}{(d_j-r_j)T}(e^{-r_jt}-e^{-d_jt}),\quad t\in(0,T], \tag{1.2.22}$$

$$u(0,t;\mathfrak{e}_j)=0,\quad t\in(0,T]. \tag{1.2.23}$$

1.2.4 Liquidity-switching model

Liquidity shock models in finance examine the impact of sudden changes in market liquidity, that is, the ease with which assets can be traded without significantly affecting prices, on asset dynamics and option valuation. These models capture the risk of abrupt market liquidity, which can significantly alter price evaluation and trading strategies. By explicitly considering liquidity as a stochastic, and in some cases regime-switching factor, liquidity shock models extend traditional option pricing frameworks to account for sudden market frictions and price impacts. As a result, these models provide more realistic valuations and offer improved guidance for hedging strategies, particularly under stressed market conditions.

The resulting pricing equations are typically coupled through switching terms, which are commonly governed by a continuous-time Markov chain or a related regime-switching process describing transitions between liquid and illiquid market states. The indifference prices $p=R^0+\frac{\ln F_0(\tau)}{\gamma}$, $q=R^1+\frac{\ln F_1(\tau)}{\gamma}$, will satisfy the parabolic-ordinary system

$$\begin{cases} p_\tau+\frac{1}{2}\sigma^2S^2p_{SS}-\frac{\nu_{01}}{\gamma}e^{-\gamma(q-p)}+\frac{(d_0+\nu_{01})}{\gamma}-\frac{1}{\gamma}\frac{F_0^{'}}{F_0}=0,\\ q_\tau-\frac{\nu_{10}}{\gamma}e^{-\gamma(p-q)}+\frac{\nu_{10}}{\gamma}-\frac{1}{\gamma}\frac{F_1^{'}}{F_1}=0. \end{cases} \tag{1.2.24}$$

with the terminal conditions $p(S,T)=q(S,T)=\Phi(S)$. Although the problem is degenerate and backward in time, we can transform it into a non-degenerate and forward in-time problem by using the transformations $t=T-\tau$, $u=\gamma R^0$ and $v=\gamma R^1$, i.e.

$$u_t=\frac{1}{2}\sigma^2S^2u_{SS}-ae^{-(v-u)}+b,\qquad v_t=c-ce^{-(u-v)}, \tag{1.2.25}$$

where $a=\nu_{01}$, $b=d_0+\nu_{01}$, $c=\nu_{10}$, $\gamma=1$, and the initial conditions are $u(S,0)=v(S,0)=\gamma\Phi(S)$. Consider the solutions $u(S,t)$ and $v(S,t)$ of the following localised system of PDE:

$$\frac{\partial u}{\partial t}=\mathcal{L}u(S,t)\ \text{ and }\ \frac{\partial v}{\partial t}=\mathcal{L}^*v(S,t) \tag{1.2.26}$$

in the spatial domain $\Omega=(S_L,S_R)$. Here, $\mathcal{L}u(S,t)=\frac{1}{2}\sigma^2S^2u_{SS}-ae^{-(v-u)}+b$, $\mathcal{L}^*v(S,t)=c-ce^{-(u-v)}$ and the initial condition is given as $u(S,0)=v(S,0)=\max(S-K,0)$. The boundary condition for a call option can be defined as

$$u(S_L,t)=v(S_L,t)=0,\ u(S_R,t)=v(S_R,t)=S_R-K. \tag{1.2.27}$$

The possibility of early exercise for the American option leads to the solution of the following non-linear complementarity problem:

$$\begin{cases} \frac{\partial u}{\partial t} - \mathcal{L}u(S,t) \geq 0,\ \frac{\partial v}{\partial t} - \mathcal{L}^* v(S,t) \geq 0, \\ u(S,t) - \Phi(S) \geq 0,\ \left(\frac{\partial u}{\partial t} - \mathcal{L}u(S,t)\right)(u(S,t) - \Phi(S)) = 0, \\ v(S,t) - \Phi(S) \geq 0,\ \left(\frac{\partial v}{\partial t} - \mathcal{L}^* v(S,t)\right)(v(S,t) - \Phi(S)) = 0, \\ u(S,0) = \Phi(S),\ v(S,0) = \Phi(S),\ (S,t) \in \Omega \times J, \end{cases} \tag{1.2.28}$$

where $J = (0, T]$ and the boundary conditions are defined in (1.2.27).

1.3 Radial basis function based numerical methods

Accurate and efficient numerical schemes are essential for solving the partial differential equations and partial integro-differential equations associated with complex option pricing models, particularly those incorporating features such as jumps, stochastic volatility, and regime-switching dynamics. In this thesis, we focus exclusively on RBF based finite difference schemes, and therefore provide only a brief discussion of these methods.

1.3.1 Radial basis function

Radial basis function is a real valued function which depends only on the distance between the input vector and a center point. Radial basis functions are well known for approximating multivariate function, which are known only at a finite number of points. A function $\varphi : \mathbb{R}^d \to \mathbb{R}$ is called radial basis function provided there exists a univariate function $\phi : [0, \infty) \to \mathbb{R}$ such that $\varphi(\mathbf{x}) = \phi(\tilde{r})$, where $\tilde{r} = \|\mathbf{x}\|$ and $\|\cdot\|$ is some norm on $\mathbb{R}^d$. These functions can be broadly classified into two classes, infinitely smooth and piecewise

Table 1.1: Radial basis functions and their order

RBF	$\phi(\tilde{r}), \tilde{r} > 0$	Order
Multiquadric (MQ)	$(1 + (\epsilon\tilde{r})^2)^{\upsilon}, \upsilon > 0, \upsilon \notin \mathbb{N}$	$s = \lceil \upsilon \rceil$
Inverse multiquadric (IMQ)	$(1 + (\epsilon\tilde{r})^2)^{\upsilon}, \upsilon < 0, \upsilon \notin \mathbb{N}$	s=0
Gaussian (GA)	$e^{-(\epsilon\tilde{r})^2}$	s=0
Polyharmonic spline	$\begin{cases} \tilde{r}^{\upsilon},\ \upsilon > 0 \text{ if } \upsilon \in 2\mathbb{N}-1 \\ \tilde{r}^{\upsilon}\log(\tilde{r}),\ \text{if } \upsilon \in 2\mathbb{N} \end{cases}$	$s = \begin{cases} \lceil \frac{\upsilon}{2} \rceil \\ \frac{\upsilon}{2} + 1 \end{cases}$

smooth radial basis functions. Classical choices of RBF are given in Table 1.1 with their order, where for any $\mathbf{x} \in \mathbb{R}$, the symbol $\lceil \mathbf{x} \rceil$ denotes as usual the smallest integer greater than or equal to $\mathbf{x}$.

1.3.2 Radial basis function approximation

RBF approximation approximates a function as the linear combination of radial basis functions $\phi(\|\mathbf{x}-\mathbf{x}_j\|)$, which is radially symmetric about its center. RBF approximation for a given set of distinct nodes $\Omega := \{x_i \in R^d; i = 1, 2, ..., n\}$ and corresponding function values $f(\mathbf{x}_i), i = 1, 2, ..., n$, is of the following form:

$$f(\mathbf{x}_i) = \sum_{j=1}^{n} \ell_j \phi(\|\mathbf{x}_i - \mathbf{x}_j\|). \tag{1.3.1}$$

Imposing the interpolation conditions to (1.3.1) yields a symmetric linear system, given as

$$f = \hat{\phi}\ell, \tag{1.3.2}$$

where $f = [f_1, f_2, \dots, f_n]^T$, $\hat{\phi} = (\|\phi(\mathbf{x}_i - \mathbf{x}_j)\|_{1\le i,j\le n})$ and $\ell = [\ell_1, \ell_2, \dots, \ell_n]^T$.
Let $\Omega_{\mathfrak{M}} := \{\mathbf{x}_1, \mathbf{x}_2, \dots, \mathbf{x}_{\mathfrak{M}}\}$ be a set of arbitrary discrete points in the domain Ω. Using local RBF based finite difference method, any linear differential operator $\mathscr{L}$ at any arbitary node $\mathbf{x}_i \in \Omega_{\mathfrak{M}}$ can be approximated locally as follows:

$$\mathscr{L}v(\mathbf{x}_i) = \sum_{j=1}^{m_i} \omega_j v(\mathbf{x}_j), \tag{1.3.3}$$

where ω_j are the unknown differential weights, and $m_i (<< \mathfrak{M})$ is the stencil size in the sub-domain $\Omega_i \subset \Omega$ containing the approximation point $\mathbf{x}_i$. Note that, the set Ω_i precisely contain closest m_i nodes of $\Omega_{\mathfrak{M}}$ in the neighbourhood of $\mathbf{x}_i$. One of the main components in the approximation of $\mathscr{L}v(\mathbf{x}_i)$ using expression (1.3.3) is the computation of the weights ω_j, which depend on the approximation point $\mathbf{x}_i$.

In the traditional finite difference method, generally, the discretization points are equally spaced and the weights ω_j are calculated efficiently by the use of conventional polynomial interpolation. However, unlike the classical finite difference scheme, in the radial basis function method, the underline interpolation strategy does not constraint by the uniform distribution of discretization points and can be incorporated seamlessly even for the randomly distributed nodes. For the radial basis functions interpolation with polynomial precision, Let $\hat{v}(\mathbf{x})$ stand for the RBF interpolant, which takes the input function $v(\mathbf{x})$ and interpolates it at the points $\{\mathbf{x}_i\}_{i=1}^{m_i}$ in the sub-domain Ω_i. Then, we can express $\hat{v}(\mathbf{x})$ as

$$\hat{v}(\mathbf{x}) = \sum_{j=1}^{m_i} \ell_j \phi(\|\mathbf{x} - \mathbf{x}_j\|) + \sum_{j=1}^{l} \gamma_j p_j(\mathbf{x}),$$

where $\|\cdot\|$ represents the Euclidean norm and $\{p_j(x)\}_{j=1}^{l}$ denote basis of $\prod_{s-1}^{d}$, which is space of d-variate polynomials of total degree $\le s-1$, where s is the order of radial basis function ϕ.

1.3.3 Radial basis function based methods

RBF approximation based methods provide a flexible, meshfree framework for the numerical solution of differential equations. Over the past years, RBF approximation techniques have been applied to a wide range of numerical methods to solve various classes of problems. In particular, RBF approximations have been integrated into Runge-Kutta (RK) methods to improve accuracy and convergence order of classical RK schemes for solving initial value problems [137]. They have also been combined with weighted essentially non-oscillatory (WENO) schemes to enhance the accuracy and to better capture oscillations when solving hyperbolic partial differential equations. In addition, RBF-based techniques have been successfully applied to the numerical solution of integral equations.

RBF methods have been widely employed in scientific and engineering applications due to their flexibility in handling irregular node distributions, ability to achieve high-order accuracy, and effectiveness in treating complex geometries and multidimensional problems. Because of their inherent suitability for scattered data approximation, RBFs can be used to construct both global and localized discretizations for PDEs.

Over the time, RBF methods have evolved from global interpolation techniques to computationally efficient local formulations, such as RBF-based finite difference methods and RBF-based partition of unity methods. In particular, RBF based finite difference method replaces classical finite-difference schemes by constructing local meshfree stencils based on RBFs. The RBF-FD method combines the meshfree flexibility of RBF approximation with the computational efficiency of local finite difference discretizations. Its main idea is to approximate spatial derivatives at given node by constructing a local RBF interpolant over a set of neighboring points, followed differentiation of the interpolant to obtain sparse diffferentiation weigths. This localization naturally leads to sparse system matrices, similar to those arising in classical finite difference methods, while preserving the high accuracy and geometric flexibility inherent to RBF approximation. As a result, RBF-FD methods have emerged as a powerful and versatile tool for solving PDEs on irregular domains, scattered data sets, and in higher dimensional settings.

An important aspect affecting the performance of RBF-FD methods is the interplay between the conditioning of the local interpolation matrices and the selection of the shape parameter. For infinitely smooth radial basis functions, such as Gaussian and multiquadric kernels, the shape parameter governs the flatness of the basis functions and consequently influences both approximation accuracy and numerical stability. In general, smaller shape parameter values yield flatter basis functions and often improve approximation accuracy; however, they simultaneously increase the condition number of the interpolation matrix, leading to ill-conditioning and a greater sensitivity to round-off errors. Conversely, larger shape parameter values improve matrix conditioning but may reduce the accuracy of the resulting approximation. This trade-off, commonly referred to as the accuracy-conditioning dilemma, represents a fundamental challenge in RBF-based numerical methods. The use of local RBF-FD stencils significantly alleviates the severe conditioning difficulties typically encountered in global RBF collocation methods, since only small local systems are solved when constructing differentiation weights. However, this thesis primarily employs thin plate spline

(TPS) radial basis functions, which do not require a shape parameter and therefore avoid the complexities associated with shape parameter selection.

1.4 Literature review on numerical methods for option pricing

We now briefly review the literature on numerical solution approaches for financial problems formulated as differential equations. Although analytical solutions are available for some classical models, many practically relevent financial models do not admit closed-form solutions. For example, when the volatility is not constant, analytical solutions of the Black-Scholes model generally do not exist, even for European-style options. This limitation has motivated extensive research into the development of efficient and accurate numerical methods for option pricing and related financial problems.

The development of numerical methods for option pricing within the Black-Scholes framework began with lattice-based techniques [33, 62]. From a numerical perspective, these lattice methods can be interpreted as explicit time-stepping schemes. A clear and comprehensive presentation of their formulation and implementation is provided in [58]. Alongside lattice approaches, classical finite difference methods have played a central role in solving option pricing problems numerically. The first finite-difference method for option pricing was proposed by Brennan and Schwartz [18]. When the coefficients of Black-Scholes equation are constant or spatially independent, the equation can be transformed into a standard diffusion equation. This transformation significantly simplifies the numerical treatment and has led to the development of a wide range of effective finite difference schemes. However, when the coefficients vary in space, such a transformation is no longer applicable, and the resulting PDEs must be solved directly, presenting additional numerical challenges. Finite difference methods designed for Black-Scholes-type equations with spatially varying coefficients have therefore been investigated in several studies, including [118] and [146].

Beyond the classical Black-Scholes models, a wide variety of financial models have been proposed in the literature, including jump-diffusion model [79, 96], the regime-switching based models [102], Lévy-process based models [30], the local volatility model [40, 44], and the stochastic volatility framework [57]. Andersen and Andreasen [7] introduced a straightforward numerical approach for pricing options under a jump-diffusion process with deterministic volatility depending on both the asset price and time. Regime-switching models have emerged as one of the rapidly growing areas of interest in computational option pricing, as they enable the modeling of changing market conditions. In particular, the regime-switching techniques introduced by Yang *et al.*[138] provide an effective mechanism to capture stochastic volatility and fat tailed return distribution, thereby overcoming the limitation of the constant volatility assumption inherent in lognormal models. In addition to classical finite difference approaches, several meshfree and advanced numerical techniques have been proposed for option pricing under jump-diffusion and related models. Mollapourasl *et al.*[100] presented radial basis function partition of unity (RBF-PU) method for the numerical solution of the PIDE arising in European option pricing under jump-diffusion models with variable coefficients.

For American options, the pricing problem is commonly formulated as a linear complementarity problem. A free-boundary problem for the price function and the optimal exercise boundary for American option was first derived by McKean [95], expressing the option price in terms of this boundary. This formulation was later extended by van Moerbeke [124], who analyzed key properties of the optimal exercise boundary. Building on these analytical studies, Courtadon [32] and Schwartz [113] developed numerical methods to approximate the resulting free-boundary problem. In the context of jump-diffusion models, several numerical approaches have been developed to solve the LCP and estimate American option prices [24, 28, 59, 82, 111, 112]. Shirzadi *et al.*[114, 115] proposed a mesh-free moving least-squares approximation and derived the optimal uniform error bounds under the jump-diffusion models for the pricing option. Kwon and Lee [83] introduced a three-time level implicit numerical method combined with operator splitting, while using a penalty approach, Huang et al. [59] developed a finite difference scheme on a piecewise uniform grid to approximate American put option prices under jump-diffusion dynamics. In addition, several finite element methods have been proposed for related option pricing models [68, 71].

Markovian regime-switching models extends the classical Geometric Brownian Motion (GBM) model by incorporating a finite-state Markov chain [55]. These models include additional flexibility and unpredictability into the Black-scholes framework, allowing better capture of changes in macro-market conditions while maintaining a manageable level of model complexity. This is achieved by permitting model parameters, including volatility, rate of return, interest rate, and dividend rate, to vary across distinct regimes. Within this framework, the Regime-switching jump-diffusion model leads to a PIDE for European options and a LCP for American options, both of which require numerical solution techniques. Costabile *et al.*[31] proposed a multinomial technique for pricing the European and American options under the RSJD model, achieving first-order accuracy in time. Huang *et al.*[60] investigated several techniques using a penalty approach for American options under a regime switching stochastic processes. Salmi and Toivanen [111] developed an iterative method and a family of implicit-explicit time discretization techniques for option pricing problems. Kadalbajoo *et al.*[67, 70, 69] examined the effectiveness of mesh-free methods using local RBFs for option pricing. More recently, Haghi *et al.*[52] applied an RBF-FD method for pricing American options under the jump-diffusion models, and Li *et al.*[87] extended this approach to solve systems of PDEs arising under regime-switching models.

The pricing and hedging problems associated with European options in markets vulnerable to liquidity shocks are studied in [92]. The authors introduce a distinct Markovian liquidity component to construct a regime-switching description of market liquidity and develop the utility-indifference approach for derivative valuation. A key contribution of this work is the formulation and analysis of a semi-linear coupled Hamilton-Jacobi-Bellman equation satisfied by the indifference price, representing the option value that keeps an investor's optimal utility unchanged regardless of whether the option is held. The concept of indifference pricing, which is closely related to utility-based pricing [20], is particularly relevant in incomplete markets. In this framework, European options under liquidity shocks are modeled by a coupled system of PDEs, where one equation is a degenerate parabolic and the other lacks a diffusion term. Koleva *et al.*[77] presented a fourth-order compact scheme to solve this parabolic-ordinary system for European options pricing.

Other studies relevant to option pricing theory are reviewed in later chapters, where these studies are incorporated as needed to support the proposed methodologies.

1.5 Motivation and Objectives of the work

Despite the extensive literature on numerical methods for option pricing, many existing approaches encounter significant challenges when applied to modern and realistic financial models. Classical grid-based techniques, such as finite difference and finite element methods, rely on structured meshes and often become inefficient or unstable in the presence of jump integrals, strong regime coupling, semi-linear PDE-ODE systems, or moving boundaries, as encountered, for example, in Asian options. Monte Carlo methods [17, 88], while flexible, typically suffer from slow convergence and are poorly suited for handling early-exercise features of American options for accurately computing PDE-based sensitivities (Greeks). Global RBF collocation methods [69, 107, 131] offer high accuracy, but their reliance on dense and often ill-conditioned system matrices makes them computationally expensive for higher-dimensional problems or for models involving multiple regimes and jump components. In contrast, the local mesh-free RBF techniques provide an attractive alternative by significantly reducing matrix ill-conditioning through localized supports, while retaining an implementation simplicity similar to classical finite difference methods. Their flexibility in stencil construction, controllable accuracy via the shape parameter, and natural scalability to higher dimensions make it particularly attractive for complex option pricing models.

Motivated by the need to incorporate key market features, such as local volatility, jump diffusion, regime switching, path dependence and liquidity shocks, within a unified and computationally robust framework, this thesis focuses on the development of numerical methods for the PIDE systems arising in European option pricing, the LCP formulations for American-style options, and path-dependent options such as Asian contracts. These formulations characterize the indifference prices for both the option writer and the buyer in incomplete market environments. To overcome the shortcomings of existing approaches, this study proposes a unified numerical framework that combines RBF-FD spatial discretization with the IMEX time-stepping and operator splitting techniques. The RBF-FD approach construct sparse and well-conditioned system matrices, enabling efficient computation on irregular and moving domains. The IMEX schemes allow stiff diffusion terms to be treated implicitly, while jump integrals, regime-switching interactions, and nonlinear liquidity components are handled explicitly, ensuring both stability and computational efficiency. Operator splitting further simplifies the treatment of early-exercise constraints by avoiding expensive nonlinear LCP solvers associated with American option pricing.

Overall, the main objective of the proposed framework is to provide a general, stable, and computationally efficient numerical methodology for solving complex PIDE systems arising in modern option pricing models, thereby addressing important gaps in the existing literature. The main objectives of this thesis are summarized as follows:

- To develop and analyze RBF-FD based IMEX numerical schemes for pricing options under jump-diffusion, regime-switching, stochastic volatility, and liquidity shock models.
- To establish theoretical stability and convergence results for the proposed time semi-discretization schemes.
- To conduct comprehensive numerical experiments assessing accuracy, convergence, stability, and computational efficiency, including comparisons across different option types and model settings.

1.6 Organization of the thesis

This thesis is organized into six chapters. **Chapter 1** introduces the research context, reviews the relevant literature, and outlines the motivation and objectives of the present work.

Chapter 2 focuses on the development of RBF-FD–based IMEX schemes for option pricing under a jump-diffusion model with local volatility. Three time semi-discretization approaches, namely, Crank-Nikolson Leap-Frog, Crank-Nikolson Adam-Bashforth, and second-order Backward difference formula, combined with RBF-FD spatial discretization are proposed, and their stability properties are analyzed. The proposed framework is further extended to American options through an operator splitting approach for handling early-exercise constraints. Numerical experiments under standard jump-diffusion models (Merton and Kou) are presented to validate the proposed methods. Part of the work presented in this chapter has been published in *Engineering Analysis with Boundary Elements*.

Chapter 3 extends the developed numerical framework to Markovian regime-switching jump-diffusion models, addressing both European and American options. Efficient solution strategies are developed for the corresponding PIDE and LCP formulations, and their stability and convergence properties are investigated through numerical studies. Part of the work presented in this chapter has been published in *Numerical Algorithms*.

Chapter 4 addresses the pricing of Asian options governed by moving-boundary PIDE systems under regime-switching jump-diffusion dynamics. A suitable RBF-FD–IMEX scheme is developed, and its stability, accuracy, and effectiveness are validated through theoretical analysis and numerical experiments. Part of the work presented in this chapter has been published in *Engineering Analysis with Boundary Elements*.

Chapter 5 investigates option pricing models under liquidity shocks, formulating the problem as coupled PDE and linear complementarity systems. Stable and efficient RBF-FD–based schemes are developed and validated through numerical experiments, including the computation of option sensitivities (Greeks). Part of the work presented in this chapter has been published in *International journal of computer mathematics*.

Finally, **Chapter 6** summarizes the main contributions of the thesis and provides directions for future research.

Along with the bibliography, a list of papers published or communicated arising from this thesis, as well as other work completed during the PhD programme, is provided at the end. To maintain the self-contained nature of each chapter, certain definitions and results are repeated where appropriate.

CHAPTER 2

RBF based some Implicit-Explicit finite difference schemes for pricing option under extended jump-diffusion model [1]

This chapter aims to develop and analyze radial basis function-based finite difference implicit-explicit temporal semi-discretization for pricing the options under Merton and Kou jump-diffusion process with local volatility.

2.1 Introduction

One of the most extensively used models in option pricing is the Black-Scholes (BS). The volatility in the typical BS partial differential equation is constant. The constant volatility BS model is generally acknowledged to be practically inadequate since real financial market data exhibit non-constant volatility behavior. The constant volatility does not represent volatility skew or smile. The volatility smile phenomena are best explained by extended BS models, which characterize volatilities as a time- and price-dependent function. The deterministic local volatility function has significant limitations. For beginners, several empirical investigations have demonstrated that the local volatility function works poorly for hedging in [4, 43]. As a second point, local volatility models are inadequate for capturing market fluctuations. Much recent research [10, 42, 66, 89] have proven the presence of jumps and their market influence. The local volatility function may be calibrated to produce consistent option pricing. Such models have also been considered

[1]The results discussed in this chapter have been published in *Engineering Analysis with Boundary Elements*, 156, 392-406 (2023), https://doi.org/10.1016/j.enganabound.2023.08.021.

in [7, 44, 75, 84, 100].

In this chapter, we consider a local volatility jump-diffusion model for pricing the value of European and American options. In order to price the value of options numerically, Andersen and Andreasen [7] suggested a straightforward alternative in which stock dynamics are defined by a jump-diffusion process, and the diffusion volatility serves as the deterministic volatility function of time and stock price. Recently, Mollapourasl et al. [100] present an RBF-PU approach to solving the partial integro-differential equation with variable coefficients in the jump-diffusion model. Meshfree techniques based on radial basis functions are commonly utilized for solving PDEs because they may give spectral convergence for smooth solutions in complicated geometries. In recent works, Kadalbajoo *et al.*[67, 69, 70] examined the efficiency of meshfree method to deal with option pricing problems based on the local radial basis function for numerically solving the multi-dimensional option pricing problem and solved the PIDE that occurs when the underlying asset act in accordance with the jump-diffusion process using an RBF-based approach. Other mesh-free work can be found in [38, 52, 99, 108, 120] and references therein.

The solution of a linear complementarity problem with a nonlocal integral element is required to estimate the price of an American option under the jump-diffusion local volatility process. To handle the discretized linear complementarity problem that arises in American option pricing, numerous solutions have been offered in the literature [24, 28, 59, 82, 105, 111, 112, 132].

Throughout this chapter, we primarily concentrate on numerical pricing of options using an RBD-FD based IMEX-BDF2, IMEX-CNLF, and IMEX-CNAB methods with careful investigation of the related numerical techniques for both the Merton [96] and Kou [79] local volatility jump-diffusion models. We discuss the class of methods for solving the LCP for the American option, considered to be of paramount importance, viz., the method of operator splitting introduced in [64]. The method of operator splitting is discovered to be an effective strategy for overcoming the problem of linear complementarity for determining the price of American-style options. Aside from effectively applying to a variety of Black-Scholes models. It is also extremely simple to implement, because both the differential and complementarity requirements can be readily separated and are known to be rather straightforward to solve. The splitting associated with the slack function and its complementarity criteria represents the major problem. Many authors [15, 22, 65] have successfully applied the operator splitting technique to solve the LCPs. Lee et al. [83] suggested a three-time level implicit numerical method combined with an operator splitting technique to approximate the value of American options when the underlying asset behaves according to a jump-diffusion model for these kinds of issues.

In this work, we proposed radial basis function finite difference-based implicit-explicit techniques for pricing option in local volatility jump-diffusion models that leads to tridiagonal coefficient matrices. Although there are a variety of approaches for solving LCPs, we employ the operator splitting method [64] to deal with the inequality restrictions. To avoid iterative procedures, we paired the Backward difference methods with the operator splitting method to evaluate the value of the American option.

The rest of the chapter is structured in the following manner. In Sect. 2.2, we start with defining the notations and preliminaries for the local volatility jump-diffusion model, describing the basic notations, symbols, and presumptions used throughout this chapter and the construction of the PIDE and its associated characteristics. In Sect. 2.3, we propose three discretization schemes. In Sect. 2.4 we present the IMEX-OS discretization for the American option. In Sect. 2.5, we provide some numerical experiments in support of our results and associated discussions.

2.2 Jump Diffusion Model with Local Volatility

In this section, we'll go over the mathematical concepts behind the "jump-diffusion process" described in options. Consider the asset's equity price to be $S(\tau)$. We assume that the time-series analysis of this variable is described by a jump diffusion process of the form,

$$\frac{dS(\tau)}{S(\tau_-)} = (r-\kappa\lambda)d\tau + \sigma(S(\tau_-),\tau)dW(\tau) + (\eta-1)dq(\tau), \tag{2.2.1}$$

where $\{\eta(\tau)\}_{\tau\geq 0}$ is a sequence of positive, independent random variables with a maximum density function of $\mathscr{G}(\cdot;\tau)$, that varies with time and follow the given properties: $\mathscr{G}(\eta)\geq 0$, $\forall\ \eta$ and $\int\limits_0^\infty \mathscr{G}(\eta)d\eta = 1$. $\sigma(S,\tau)$ is a bounded time and space dependent local volatility function, τ is the time to maturity, dW is an enhancement of standard Gauss-Wiener process, r is the risk-free interest rate. Here λ is taken as the intensity of the independent Poisson process dq

$$dq = \begin{cases} 0 & \text{if probability is } 1-\lambda d\tau, \\ 1 & \text{if probability is } \lambda d\tau. \end{cases}$$

Here κ is expected relative jump size that is $\kappa = \mathbb{E}(\eta-1)$, $\mathbb{E}[\cdot]$ represent the expectation operator and $\eta - 1$ is a impulse function producing jump from S to S_η.

Under the aforementioned assumptions, the value of a European-style contingent claim $U(S,\tau)$ satisfies the following backward partial integro-differential equation depending on the underlying stock price S and time τ (see [50, 103]).

$$\begin{aligned} \frac{\partial U}{\partial \tau} &= \frac{1}{2}\sigma^2(S,\tau)S^2\frac{\partial^2 U}{\partial s^2} + (r-\kappa\lambda)S\frac{\partial U}{\partial S} - rU \\ &+ \lambda\left\{\int\limits_0^\infty U(Sz,\tau)\mathscr{G}(z;\tau)dz - U(S,\tau)\right\}, \quad (S,\tau)\in(0,\infty)\times[0,T). \end{aligned} \tag{2.2.2}$$

The option value $U(S,T)$ at the time of maturity T is termed as pay-off function. For put option the pay-off function is given by:

$$\Phi(S) = \max(K-S,0) \tag{2.2.3}$$

with strike price K. The notation $\mathscr{G}(\eta)$ stands for the log-normal density in Merton's jump-diffusion model

$$\mathscr{G}(\eta) := \frac{1}{\sqrt{2\pi}\sigma_J \eta} \exp - \frac{(\ln \eta - \mu_J)^2}{2\sigma_J^2},$$

where $\kappa := \mathbb{E}(\eta - 1) = \exp\left(\mu_J + \frac{\sigma_J^2}{2}\right) - 1$, μ_J and σ_J^2 are the mean and the variance of jump in return. According to the Kou's model, the log-double-exponential density is represented by $\mathscr{G}(\eta)$,

$$\mathscr{G}(\eta) := \frac{1}{\eta}\left(p\eta_1 e^{-\eta_1 \ln(\eta)}\mathcal{H}(\ln(\eta)) + q\eta_2 e^{-\eta_2 \ln(\eta)}\mathcal{H}(-\ln(\eta))\right),$$

where $\mathcal{H}(\cdot)$ represents a Heaviside function with $p > 0$, $q = 1 - p$, $\eta_1 > 1$, $\eta_2 > 0$ and κ is given by $\kappa := \frac{p\eta_1}{\eta_1 - 1} + \frac{q\eta_2}{\eta_1 + 1} - 1$.

After implementing the variable swap $t = T - \tau$ and $x = \ln(\frac{S}{K})$ in (2.2.2), we have

$$\frac{\partial u}{\partial t} = \mathcal{L}u(x,t) := \mathcal{D}u(x,t) + \mathcal{I}u(x,t), \tag{2.2.4}$$

$$\mathcal{D}u(x,t) = \frac{1}{2}\sigma^2(x,t)\frac{\partial^2 u}{\partial x^2} + \delta(x,t)\frac{\partial u}{\partial x} + \beta(x,t)u, \tag{2.2.5}$$

$$\mathcal{I}u(x,t) = \lambda \int_{-\infty}^{\infty} u(y,t) f(y-x)dy. \tag{2.2.6}$$

The time left before maturity T, denoted by $t = (T - \tau)$, $x = \ln(\frac{S}{K})$ is the asset's logarithmic price at a specified strike price K, $u(x,t) = U(Ke^x, T-\tau)$, λ is taken as the jumps intensity and $f(x)$ is the density function of jump sizes of the log return x. Where $\delta(x,t) = r - \frac{\sigma^2(x,t)}{2} - \lambda\kappa$ and $\beta(x,t) = -(r+\lambda)$.

After applying the given transformation, we can write the function $f(y)$ as:

$$f(y) := \begin{cases} \frac{1}{\sqrt{2\pi}\sigma_J}\exp(-\frac{(y-\mu_J)^2}{2\sigma_J^2}) & \text{Merton's model,} \\ p\eta_1 e^{-\eta_1 y}\mathcal{H}(y) + q\eta_2 e^{-\eta_2 y}\mathcal{H}(-y) & \text{Kou's model.} \end{cases}$$

Consider the solution of the following localised PIDE, $u(x,t)$

$$\frac{\partial u}{\partial t} = \frac{1}{2}\sigma^2(x,t)\frac{\partial^2 u}{\partial x^2} + \delta(x,t)\frac{\partial u}{\partial x} + \beta(x,t)u + \lambda\int_{-\infty}^{\infty} u(y,t)f(y-x)dy.$$

$$u(x,0) = \max(K - Ke^x, 0),$$

$$u(x,t) = \begin{cases} Ke^{-rt} - Ke^x & : \quad x \to -\infty, \\ 0 & : \quad x \to +\infty \end{cases}$$

As we can exercise the American option at any time up to the life of the option and we can formulate it as the linear complementarity problem based on the SDE (2.2.1),

$$\begin{cases} \frac{\partial u}{\partial t} - \mathcal{L}u & \geq & 0 \quad (x,t) \in \mathbb{R}\times J, \\ u(x,t) - \Phi(Ke^x) & \geq & 0 \quad (x,t) \in \mathbb{R}\times J, \\ (\frac{\partial u}{\partial t} - \mathcal{L}u)\,(u(x,t) - \Phi(Ke^x)) & = & 0 \quad (x,t) \in \mathbb{R}\times J, \\ u(x,0) & = & \Phi(Ke^x) \quad x \in \mathbb{R}, \end{cases} \tag{2.2.7}$$

where $J = (0, T]$ and the spatial operator can be defined as described above and the boundary condition for American option is

$$u(x,t) = \begin{cases} K - Ke^x & : \quad x \to -\infty, \\ 0 & : \quad x \to +\infty \end{cases}$$

2.3 Discretization

In this part, we will discuss the Crank-Nicolson Leap-Frog, Crank-Nicolson Adam Bashforth, and BDF2, implicit-explicit temporal discretization techniques for the subsequent PIDE (2.3.1) on the reduced domain Ω.

$$\frac{\partial u}{\partial t} = \mathcal{D}u(x,t) + \mathcal{I}u(x,t), \tag{2.3.1}$$

For numerical approximation of the integral operator $\mathcal{I}u(x,t)$, firstly we separate the integral into two different parts on $\Omega := (x_L, x_R)$ and on $\Omega^c := R \setminus \Omega$ and split the integral operator as

$$\mathcal{I}u(x,t) = \lambda \int_{\Omega} u(y,t) f(y-x) dy + R(x,t). \tag{2.3.2}$$

Because of the asymptotic behaviour of the option over the domain $R \setminus \Omega$, the integral is defined as

$$R(x,t) := \lambda \int_{\Omega^c} (Ke^{-rt} - Ke^y) f(y-x) dy. \tag{2.3.3}$$

In case of the European put option, $R(x,t)$ is defined as:

$$R(x,t) := \begin{cases} Ke^{-rt}\mathcal{N}\left(\frac{x_L - x - \mu_j}{\sigma_j}\right) - Ke^{x+\mu_j+\frac{\sigma_j^2}{2}}\mathcal{N}\left(\frac{x_L - x - \mu_j - \sigma_j^2}{\sigma_j}\right) & \text{Merton's model,} \\ K(1-p)e^{-rt+\eta_2(x_L - x)} - K(1-p)\frac{\eta_2}{\eta_2+1}e^{-\eta_2 x + (\eta_2+1)x_L} & \text{Kou's model.} \end{cases}$$

We can reformulate the above expression for American put option as:

$$R(x,t) := \begin{cases} K\mathcal{N}\left(\frac{x_L - x - \mu_j}{\sigma_j}\right) - Ke^{x+\mu_j+\frac{\sigma_j^2}{2}}\mathcal{N}\left(\frac{x_L - x - \mu_j - \sigma_j^2}{\sigma_j}\right) & \text{Merton's model,} \\ K(1-p)e^{\eta_2(x_L - x)} - K(1-p)\frac{\eta_2}{\eta_2+1}e^{-\eta_2 x + (\eta_2+1)x_L} & \text{Kou's model,} \end{cases}$$

where $\mathcal{N}(\cdot)$ represents the cumulative normal distribution. To approximate the integral term on truncated domain Ω, we used the composite trapezoidal rule.

2.3.1 Time Discretization

Let the system (2.3.1), be initially discretized in time with uniform grid $t_n = nk$, $n = 0, 1, 2, \ldots, N$ with uniform temporal mesh length k, with $u(x, t_n)$ abbreviated as u_n.

Now, we have a brief discussion about three IMEX methods for the temporal discretization of PIDE (2.3.1).

IMEX-BDF2 method

$$\frac{3u_{n+1} - 4u_n + u_{n-1}}{2k} = \mathcal{D}u_{n+1} + \lambda\mathcal{I}(\mathcal{E}_1 u_n) \quad n \geq 1, \tag{2.3.4}$$

$$u_{n+1}(x_L) = Ke^{-rt_{n+1}} - Ke^{x_L}, \qquad u_{n+1}(x_R) = 0, \tag{2.3.5}$$

where, $\mathcal{E}_1 u_n = 2u_n - u_{n-1}$.

IMEX-CNAB method

$$\frac{u_{n+1} - u_n}{k} = \mathcal{D}(\frac{u_{n+1} + u_n}{2}) + \lambda\mathcal{I}(\mathcal{E}_2 u_n) \quad n \geq 1, \tag{2.3.6}$$

$$u_{n+1}(x_L) = Ke^{-rt_{n+1}} - Ke^{x_L}, \qquad u_{n+1}(x_R) = 0, \tag{2.3.7}$$

where, $\mathcal{E}_2 u_n = \frac{3u_n - u_{n-1}}{2}$.

IMEX-CNLF method

$$\frac{u_{n+1} - u_{n-1}}{2k} = \mathcal{D}(\frac{u_{n+1} + u_{n-1}}{2}) + \lambda\mathcal{I}(u_n) \quad n \geq 1, \tag{2.3.8}$$

$$u_{n+1}(x_L) = Ke^{-rt_{n+1}} - Ke^{x_L}, \qquad u_{n+1}(x_R) = 0. \tag{2.3.9}$$

IMEX-BDF2, IMEX-CNAB and IMEX-CNLF techniques require two starting numbers on the zeroth and first time levels, where initial condition gives the value u_0 at the zeroth time level, and the value u_1 can be evaluated by using the implicit-explicit backward difference technique of order one. Now we prove the stability of all the above discussed time discretization schemes. The PIDE (2.3.1) variable coefficients are subject to various assumptions (A1, A2) for the stability investigation, as detailed in [2].

(A1) Theoretical Analysis of the suggested techniques requires that all variable coefficients, σ, δ, and β, be continuous and adequately regular.

(A2) Let there exists $\underline{\sigma} > 0$ and $\bar{\sigma} > 0$ such that for all $(x,t) \in \bar{\Omega} \times (0,T]$, $0 < \underline{\sigma} < \sigma(x,t) < \bar{\sigma}$.

We will frequently use the following result through out our analysis:

$$\begin{aligned}
(\mathcal{D}U, U) &= \frac{1}{2}(\bar{\sigma})^2(U_{xx}, U) + (r - \frac{1}{2}(\bar{\sigma})^2 - \lambda\kappa)(U_x, U) - (r+\lambda)(U,U) \\
&= -\frac{(\bar{\sigma})^2}{2}\left(\|U_x - \frac{(r - \frac{(\bar{\sigma})^2}{2} - \lambda\kappa)}{(\bar{\sigma})^2}U\|^2\right) + \frac{(r - \frac{(\bar{\sigma})^2}{2} - \lambda\kappa)^2 - 2(r+\lambda)(\bar{\sigma})^2}{2(\bar{\sigma})^2}\|U\|^2 \\
&\leq \frac{\left(r - \frac{(\bar{\sigma})^2}{2} - \lambda\kappa\right)^2 - \left(2(r+\lambda)(\bar{\sigma})^2\right)}{2(\bar{\sigma})^2}\|U\|^2 \\
&\leq \alpha\|U\|^2,
\end{aligned} \tag{2.3.10}$$

where $\alpha = |\frac{(r - \frac{(\bar{\sigma})^2}{2} - \lambda\kappa)^2 - \left(2(r+\lambda)(\bar{\sigma})^2\right)}{2(\bar{\sigma})^2}|$.

We will frequently use the Young's inequality for all $a, b \in \mathbb{R}$ with ϵ^* (valid for every $\epsilon^* > 0$), i.e,

$$(a,b) \leq \epsilon^* a^2 + \frac{1}{4\epsilon^*}b^2. \tag{2.3.11}$$

We shall use the following result in analysis, for all $u(\cdot,t) \in L^2(\Omega)$, $t \in (0,T)$ such that

$$\overline{u}(x,t) = u(x,t) : (x,t) \in \Omega \times [0,T], \qquad \text{and} \qquad \overline{u}(x,t) = 0 : (x,t) \in \Omega^c \times [0,T].$$

Mathematical requirement that the integral operator $\mathcal{I}u$ is given as

$$\|\mathcal{I}\overline{u}(\cdot,t)\| \leq \mathcal{C}_I \|u(\cdot,t)\|,$$

where $\mathcal{C}_I$ is a constant that is independent of t and $\|u\| := \left(\int_\Omega |u(x)|^2 dx\right)^{\frac{1}{2}}$.
Consider the solutions u_n and $\tilde{u}_n$ to the equations (2.3.4) and the perturbed equation (2.3.12), respectively.

$$\frac{3\tilde{u}_{n+1} - 4\tilde{u}_n + \tilde{u}_{n-1}}{2k} = \mathcal{D}\tilde{u}_{n+1} + \lambda\mathcal{I}(\mathcal{E}_1\tilde{u}_n) + \mathcal{T}_{n+1} \quad n \geq 1 \tag{2.3.12}$$

combined with the conditions at the boundaries

$$\tilde{u}_{n+1}(x_L) = Ke^{-rt_{n+1}} - Ke^{x_L}, \qquad \tilde{u}_{n+1}(x_R) = 0 \tag{2.3.13}$$

As we go forward in time, we will analyse the impact of the $\mathcal{T}_n$ perturbation on the data at each successive time level t_n. To prove stability in time discretization, we will demonstrate that the error at each time level is limited by the error at the starting time level (t_0 & t_1; for all mentioned approaches) and is a bounded multiple of the discussed perturbations.

Now we can provide an accurate description of the error representation $\epsilon_n := \tilde{u}_n - u_n$. Since we are addressing the same boundary conditions, in both the referenced (2.3.4 − 2.3.5) and perturbed equations (2.3.12−2.3.13). Therefore, ϵ_n will be zero-valued at the boundaries. Similarly we can get the perturbation equation for other schemes.

Theorem 2.3.1 (BDF2)**.** *Under the assumption $k < \frac{1}{2(2\alpha+1+\lambda\mathcal{C}_I)}$ the scheme is stable in the following sense:*

$$\|\epsilon_m\|^2 \leq C[\|\epsilon_0\|^2 + \|\epsilon_1\|^2 + \max_{2\leq n\leq m} \sum_{n=2}^{m} \|\mathcal{T}_n\|^2],$$

where C is a constant that depends on the parameters C_I, r, σ, λ and T.

Proof. Consider the equations (2.3.4) and (2.3.12), we get,

$$\frac{3\epsilon_{n+1} - 4\epsilon_n + \epsilon_{n-1}}{2k} = \mathcal{D}\epsilon_{n+1} + \lambda\mathcal{I}(\mathcal{E}_1\epsilon_n) + \mathcal{T}_{n+1} \tag{2.3.14}$$

$$\epsilon_{n+1}(x_L) = 0, \qquad \epsilon_{n+1}(x_R) = 0 \tag{2.3.15}$$

Taking the inner product of both sides of the equation (2.3.14) with $4k\epsilon_{n+1}$

$$\left(\frac{3\epsilon_{n+1} - 4\epsilon_n + \epsilon_{n-1}}{2k}, 4k\epsilon_{n+1}\right) = (\mathcal{D}\epsilon_{n+1}, 4k\epsilon_{n+1}) + (\lambda\mathcal{I}(\mathcal{E}_1\epsilon_n), 4k\epsilon_{n+1}) + (\mathcal{T}_{n+1}, 4k\epsilon_{n+1}) \tag{2.3.16}$$

Now, we will use the identity $2\,(3a-4b+c,a) = a^2+(2a-b)^2-b^2-(2b-c)^2+(a-2b+c)^2$ in LHS of (2.3.16), we get

$$\begin{aligned}\|\epsilon_{n+1}\|^2-\|\epsilon_n\|^2+\|2\epsilon_{n+1}-\epsilon_n\|^2-\|2\epsilon_n-\epsilon_{n-1}\|^2 \;&\le\; 4k(\mathcal{D}\epsilon_{n+1},\epsilon_{n+1})+4k\lambda(\mathcal{I}(\mathcal{E}_1\epsilon_n),\epsilon_{n+1})\\ &\quad +4k(\mathcal{T}_{n+1},\epsilon_{n+1}). \end{aligned} \tag{2.3.17}$$

Now the relation (2.3.10) implies,

$$\begin{aligned}\|\epsilon_{n+1}\|^2-\|\epsilon_n\|^2+\|2\epsilon_{n+1}-\epsilon_n\|^2-\|2\epsilon_n-\epsilon_{n-1}\|^2 \;&\le\; 4k\alpha\|\epsilon_{n+1}\|^2+4k\lambda(\mathcal{I}(\mathcal{E}_1\epsilon_n),\epsilon_{n+1})\\ &\quad +4k(\mathcal{T}_{n+1},\epsilon_{n+1}). \end{aligned} \tag{2.3.18}$$

$$\begin{aligned}\|\epsilon_{n+1}\|^2-\|\epsilon_n\|^2+\|2\epsilon_{n+1}-\epsilon_n\|^2-\|2\epsilon_n-\epsilon_{n-1}\|^2 \;&\le\; k\left(4\alpha+2+2\lambda\mathcal{C}_I\right)\|\epsilon_{n+1}\|^2+16k\lambda\mathcal{C}_I\|\epsilon_n\|^2\\ &\quad +4k\lambda\mathcal{C}_I\|\epsilon_{n-1}\|^2+2k\|\mathcal{T}_{n+1}\|^2. \end{aligned} \tag{2.3.19}$$

Summing up the above inequality for $n=1$ to $n=m-1$, we get

$$\begin{aligned}&\|\epsilon_m\|^2-\|\epsilon_1\|^2-\|2\epsilon_1-\epsilon_0\|^2\\ &\le k[4\lambda\mathcal{C}_I\|\epsilon_0\|^2+20\lambda\mathcal{C}_I\|\epsilon_1\|^2+(4\alpha+2+22\lambda\mathcal{C}_I)\sum_{n=2}^{m-1}\|\epsilon_n\|^2+2\sum_{n=2}^{m}\|\mathcal{T}_n\|^2+\left(4\alpha+2+2\lambda\mathcal{C}_I\right)\|\epsilon_m\|^2].\end{aligned}$$

Now imagine that the k is small enough such that $(1-k(4\alpha+2+2\lambda\mathcal{C}_I))>0$ or $k<\frac{1}{(4\alpha+2+2\lambda\mathcal{C}_I)}$, then above inequality implies,

$$\begin{aligned}\|\epsilon_m\|^2 &\le C[\|\epsilon_0\|^2+\|\epsilon_1\|^2+k\sum_{n=2}^{m-1}\|\epsilon_n\|^2+k\sum_{n=2}^{m}\|\mathcal{T}_n\|^2]\\ &\le C[\|\epsilon_0\|^2+\|\epsilon_1\|^2+k\sum_{n=2}^{m-1}\|\epsilon_n\|^2+mk\max_{2\le n\le m}\sum_{n=2}^{m}\|\mathcal{T}_n\|^2]. \end{aligned} \tag{2.3.20}$$

We know that $mk\le T$, then we have

$$\|\epsilon_m\|^2\le C[\|\epsilon_0\|^2+\|\epsilon_1\|^2+k\sum_{n=2}^{m-1}\|\epsilon_n\|^2+\max_{2\le n\le m}\sum_{n=2}^{m}\|\mathcal{T}_n\|^2], \tag{2.3.21}$$

where C is a generic constant that is unaffected by the extent of the grid. The discrete Gronwall's inequality (for more information, see Lemma 3.1 in [70]) is now applied, and the outcome is obtained. □

Theorem 2.3.2 (IMEX-CNLF). *Under the assumption $k<\frac{1}{\beta}$ the scheme is stable in the following sense:*

$$\|\epsilon_m\|^2\le C[\|\epsilon_0\|^2+\|\epsilon_1\|^2+\max_{2\le n\le m}\sum_{n=2}^{m}\|\mathcal{T}_n\|^2],$$

where C is a constant that depends on the parameters C_I, r, σ, λ and T.

Proof. Consider the equations (2.3.8) and (2.3.12), we get,

$$\frac{\epsilon_{n+1}-\epsilon_{n-1}}{2k} = \mathcal{D}\left(\frac{\epsilon_{n+1}+\epsilon_{n-1}}{2}\right) + \lambda\mathcal{I}(\epsilon_n) + \mathcal{T}_{n+1}, \tag{2.3.22}$$

$$\epsilon_{n+1}(x_L) = 0, \qquad \epsilon_{n+1}(x_R) = 0. \tag{2.3.23}$$

Taking the inner product of both sides of the equation (2.3.14) with $2k\epsilon_{n+1}$

$$\begin{aligned}\left(\frac{\epsilon_{n+1}-\epsilon_{n-1}}{2k}, 2k(\epsilon_{n+1}+\epsilon_{n-1})\right) &= \left(\mathcal{D}\left(\frac{\epsilon_{n+1}+\epsilon_{n-1}}{2}\right), 2k(\epsilon_{n+1}+\epsilon_{n-1})\right) \\ &+ \left(\lambda\mathcal{I}(\epsilon_n), 2k(\epsilon_{n+1}+\epsilon_{n-1})\right) + \left(\mathcal{T}_{n+1}, 2k(\epsilon_{n+1}+\epsilon_{n-1})\right).\end{aligned} \tag{2.3.24}$$

Simplifying the left hand side of (2.3.24), we get

$$\begin{aligned}\|\epsilon_{n+1}\|^2 - \|\epsilon_{n-1}\|^2 &= \left(\mathcal{D}\left(\frac{\epsilon_{n+1}+\epsilon_{n-1}}{2}\right), 2k(\epsilon_{n+1}+\epsilon_{n-1})\right) + \left(\lambda\mathcal{I}(\epsilon_n), 2k(\epsilon_{n+1}+\epsilon_{n-1})\right) \\ &+ \left(\mathcal{T}_{n+1}, 2k(\epsilon_{n+1}+\epsilon_{n-1})\right).\end{aligned} \tag{2.3.25}$$

Now the relation (2.3.10) implies,

$$\begin{aligned}\|\epsilon_{n+1}\|^2 - \|\epsilon_{n-1}\|^2 &\leq k\alpha\|\epsilon_{n+1}+\epsilon_{n-1}\|^2 + \left(\lambda\mathcal{I}(\epsilon_n), 2k(\epsilon_{n+1}+\epsilon_{n-1})\right) \\ &+ \left(\mathcal{T}_{n+1}, 2k(\epsilon_{n+1}+\epsilon_{n-1})\right),\end{aligned} \tag{2.3.26}$$

$$\begin{aligned}\|\epsilon_{n+1}\|^2 - \|\epsilon_{n-1}\|^2 &\leq 2k(\alpha+\lambda\mathcal{C}_I+1)(\|\epsilon_{n+1}\|^2 + \|\epsilon_{n-1}\|^2) \\ &+ k\lambda\mathcal{C}_I\|\epsilon_n\|^2 + k\|\mathcal{T}_{n+1}\|^2.\end{aligned} \tag{2.3.27}$$

Let $\beta_1 = 2(\alpha+\lambda\mathcal{C}_I+1)$, $\beta_2 = \lambda\mathcal{C}_I$ and we have choose a parameter β such that

$$\beta = \max\{\beta_1, \beta_2\}.$$

We have,

$$\|\epsilon_{n+1}\|^2 - \|\epsilon_{n-1}\|^2 \leq k\beta(\|\epsilon_{n+1}\|^2 + \|\epsilon_{n-1}\|^2 + \|\epsilon_n\|^2) + k\|\mathcal{T}_{n+1}\|^2. \tag{2.3.28}$$

In order to maintain the generality, let's suppose that m is an integer. Then, after summing up the inequality (2.3.28), for $n=1$ to $n=m-1$

$$\begin{aligned}&\|\epsilon_m\|^2 + \|\epsilon_{m-1}\|^2 - \|\epsilon_0\|^2 - \|\epsilon_1\|^2 \\ &\leq k\beta[\|\epsilon_0\|^2 + 2\|\epsilon_1\|^2 + 3\sum_{n=2}^{m-1}(\|\epsilon_n\|^2) + (\|\epsilon_m\|^2 - \|\epsilon_{m-1}\|^2)] + k\sum_{n=1}^{m-1}\|\mathcal{T}_{n+1}\|^2.\end{aligned}$$

Now imagine that the k is tiny enough such that $(1-k\beta) > 0$ or $k < \frac{1}{\beta}$, then above inequality implies,

$$\|\epsilon_m\|^2 + \|\epsilon_{m-1}\|^2 \leq C[\|\epsilon_0\|^2 + \|\epsilon_1\|^2 + k\sum_{n=2}^{m-1}\|\epsilon_n\|^2 + k\sum_{n=2}^{m}\|\mathcal{T}_n\|^2]$$

$$\leq \quad C[\|\epsilon_0\|^2 + \|\epsilon_1\|^2 + k\sum_{n=2}^{m-1}\|\epsilon_n\|^2 + mk\max_{2\leq n\leq m}\sum_{n=2}^{m}\|\mathcal{T}_n\|^2]. \tag{2.3.29}$$

We know that $mk \leq T$, then we have

$$\|\epsilon_m\|^2 \leq C[\|\epsilon_0\|^2 + \|\epsilon_1\|^2 + k\sum_{n=2}^{m-1}\|\epsilon_n\|^2 + \max_{2\leq n\leq m}\sum_{n=2}^{m}\|\mathcal{T}_n\|^2], \tag{2.3.30}$$

where C is a generic constant that is unaffected by the extent of the grid. The discrete Gronwall's inequality (more details see, Lemma 3.1 in [70]) is now applied, and the outcome is obtained. □

Theorem 2.3.3 (IMEX-CNAB)**.** *Under the assumption $k < \frac{1}{\gamma}$ the scheme is stable in the following sense:*

$$\|\epsilon_m\|^2 \leq C[\|\epsilon_0\|^2 + \|\epsilon_1\|^2 + \max_{2\leq n\leq m}\sum_{n=2}^{m}\|\mathcal{T}_n\|^2].$$

Where $\gamma_1 = \alpha + \lambda\mathcal{C}_I + 1$, $\gamma_2 = \alpha + \frac{13}{4}\lambda\mathcal{C}_I + 1$, $\gamma_3 = \frac{\lambda\mathcal{C}_I}{4}$. $\gamma = \max\{\gamma_1, \gamma_2, \gamma_3\}$ and C is a constant that depends on the parameters C_I, r, σ, λ,T.

Proof. The proof is similar to that of Theorem 2.3.2. □

In the following subsection, we describe the radial basis function based finite difference technique that we use to solve the resulting temporal semi discretize algorithm.

2.3.2 Spatial Discretization

A function $\varphi : \mathbb{R}^d \to \mathbb{R}$ is called radial provided there exists a univariate function $\phi : [0, \infty) \to \mathbb{R}$ such that $\varphi(\mathbf{x}) = \phi(\tilde{r})$, where $\tilde{r} = \|\mathbf{x}\|$ and $\|\cdot\|$ is Euclidean norm on $\mathbb{R}^d$. These functions can be broadly classified into two classes, infinitely smooth and piecewise smooth radial basis functions. Classical choices of RBF are given in Table 1.1 with their order, where for any $\mathbf{x} \in \mathbb{R}$, the symbol $\lceil \mathbf{x} \rceil$ denotes as usual the smallest integer greater than or equal to $\mathbf{x}$. The Gaussian and inverse Multiquadric are positive definite functions where as thin plate spline and multiquadric are conditionally positive definite functions of order $s > 0$. In this section, we briefly discuss the implementation of the local radial basis function-based finite difference scheme because, as we pointed out in the introduction, the proposed numerical scheme uses the radial basis function meshless method for spatial discretization.

Let $\Omega_{\mathfrak{M}} := \{\mathbf{x}_1, \mathbf{x}_2, \ldots, \mathbf{x}_{\mathfrak{M}}\}$ be a set of arbitray discrete points in the domain Ω then using local RBF-FD based method, any linear differential operator $\mathscr{L}$ at any arbitrary node $\mathbf{x}_i \in \Omega_{\mathfrak{M}}$ can be approximated locally as follows:

$$\mathscr{L}v(\mathbf{x}_i) = \sum_{j=1}^{m_i}\omega_j v(\mathbf{x}_j), \tag{2.3.31}$$

where ω_j are the unknown differential weights, and $m_i (<< \mathfrak{M})$ is the stencil size in the sub-domain $\Omega_i \subset \Omega$ containing the approximation point $\mathbf{x}_i$. Note that, the set Ω_i precisely contain closest m_i nodes of $\Omega_{\mathfrak{M}}$ in the neighbourhood of $\mathbf{x}_i$. One of the main component in the approximation of $\mathscr{L}v(\mathbf{x}_i)$ by means of expression (2.3.31) is the computation of weights ω_j as it depend on the approximation point $\mathbf{x}_i$. In the traditional finite difference method, generally, the discretization points are equally spaced, and the weights ω_j are calculated efficiently by the use of conventional polynomial interpolation. However, unlike the classical finite difference scheme, in the radial basis function method, the underline interpolation strategy does not constraint by the uniform distribution of discretization points and can be incorporated seamlessly even for the randomly distributed nodes. The RBF interpolation strategy that we have used for approximation of weights ω_j describes in what follows.

Let $\hat{v}(\mathbf{x})$ stand for the RBF interpolant, which takes the input function $v(\mathbf{x})$ and interpolates it at the points $\{\mathbf{x}_i\}_{i=1}^{m_i}$ in the sub-domain Ω_i. Then, we can express $\hat{v}(\mathbf{x})$ as

$$\hat{v}(\mathbf{x}) = \sum_{j=1}^{m_i} \ell_j \phi(\|\mathbf{x}-\mathbf{x}_j\|) + \sum_{j=1}^{l} \gamma_j p_j(\mathbf{x}), \tag{2.3.32}$$

where $\|\cdot\|$ represents the Euclidean norm and $\{p_j(x)\}_{j=1}^{l}$ denote basis of $\prod_{s-1}^{d}$, which is space of d-variate polynomials of total degree $\leq s-1$, where s is the order of radial basis function ϕ.

By enforcing the following interpolation and orthogonality constraints, the coefficients ℓ_j and γ_j utilised in equation (2.3.32) can be obtained;

$$\begin{aligned} \hat{v}(\mathbf{x}_i) &= v(\mathbf{x}_i),\ 1 \leq i \leq m_i, & (2.3.33)\\ \sum_{j=1}^{m_i} \ell_j p_k(\mathbf{x}_j) &= 0, \qquad 1 \leq k \leq l. & (2.3.34) \end{aligned}$$

Now all the unknowns in the (2.3.32) can be obtained by solving the following linear system

$$\begin{bmatrix} \Psi & \mathscr{P} \\ \mathscr{P}^\intercal & O \end{bmatrix} \begin{bmatrix} \ell \\ \gamma \end{bmatrix} = \begin{bmatrix} v\,|_{\Omega_i} \\ O \end{bmatrix}, \tag{2.3.35}$$

where $\Psi := (\phi_{ij})_{1\leq i,j\leq m_i} := (\phi\|\mathbf{x}_i-\mathbf{x}_j\|)_{1\leq i,j\leq m_i} \in \mathbb{R}^{m_i\times m_i}$, $\mathscr{P} := (p_j(\mathbf{x}_i))_{1\leq i\leq m_i, 1\leq j\leq l} \in \mathbb{R}^{m_i\times l}$.

We can compute the differential weights w_j used in the equation by forcing the linear combination (2.3.31) to be accurate for RBFs $\{\phi(\|\mathbf{x}-\mathbf{x}_i\|)\}_{i=1}^{m_i}$, centred at each of the grid assessment points in sub-domain Ω_i. Therefore, the weights are derived by solving the following linear system using RBFs and polynomials up to degree l.

$$\begin{bmatrix} \Psi & \mathscr{P} \\ \mathscr{P}^\intercal & O \end{bmatrix} \begin{bmatrix} \omega \\ u \end{bmatrix} = \begin{bmatrix} [\mathscr{L}\phi(\|\mathbf{y}_i-\mathbf{y}_j\|)_{j=1}^{m_i}]^\intercal \\ [\mathscr{L}p_j(\mathbf{y}_i)_{j=1}^{l}]^\intercal \end{bmatrix} \tag{2.3.36}$$

it is crucial to know that the equation on the right (2.3.36) is simply

$$[\mathscr{L}\phi(\|\mathbf{x}_i-\mathbf{x}_1\|)\ \mathscr{L}\phi(\|\mathbf{x}_i-\mathbf{x}_2\|)\ldots\mathscr{L}\phi(\|\mathbf{x}_i-\mathbf{x}_{m_i}\|)\mid \mathscr{L}p_1(\mathbf{x}_i)\ \mathscr{L}p_2(\mathbf{x}_i)\ldots\mathscr{L}p_l(\mathbf{x}_i)]^\intercal.$$

It is easy to see that the linear system (2.3.36) is significantly smaller than the global RBF collocation system (size $\mathfrak{M}+l$) since its size is just m_i+l. Therefore, it offers an equation system that is more reliable and productive.

2.4 American Option

The RBF-based IMEX technique described in the preceding part can be adapted to solve LCP (2.2.7) for American option problems using the operator splitting method introduced by the Ikonen and Toivanen [64] for determining the American put option. The primary idea behind introduction of the operator splitting method is to derive an expression with the help of an additional variable ψ such that $\psi = u_t - \mathcal{D}u$. We can reformulate LCP (2.2.7) as:

$$\begin{cases} \frac{\partial u}{\partial t} - \mathcal{D}u - \lambda\mathcal{I}(u_n) &= \psi, \\ (u(x,t) - \Phi(Ke^x))\cdot\psi &= 0, \\ u(x,t) - \Phi(Ke^x) &\geq 0, \\ \psi &\geq 0, \end{cases} \tag{2.4.1}$$

in the region $\Omega \times J$.

2.4.0.1 IMEX-BDF2-OS method

Let us assume that the values $\{u_n, \psi_n\}$ and $\{u_{n-1}, \psi_{n-1}\}$ are a priori known at the points t_n and t_{n-1}. Now, we perform two sub-step at discrete point t_{n+1}; in first step, we compute an intermediate value $\tilde{u}_{n+1}$ using the following BVP

$$\begin{cases} \frac{1}{k}\left(\frac{3}{2}\tilde{u}_{n+1} - 2u_n + \frac{1}{2}u_{n-1}\right) &= \mathcal{D}\tilde{u}_{n+1} + \lambda\mathcal{I}(\mathcal{E}_1 u_n) + \psi_n, \\ \tilde{u}_{n+1}(x_L) = K, & \tilde{u}_{n+1}(x_R) = 0. \end{cases} \tag{2.4.2}$$

Here, the second step of the operator splitting method proceeds with projecting the $\tilde{u}_{n+1}$ on constraint space to obtain u_{n+1} with following correction terms

$$\begin{cases} \frac{3}{2}\frac{u_{n+1} - \tilde{u}_{n+1}}{k} &= \psi_{n+1} - \psi_n, \\ u_{n+1} &\geq \Phi, \\ \psi_{n+1} &\geq 0, \\ \psi_{n+1}(u_{n+1} - \Phi) &= 0. \end{cases} \tag{2.4.3}$$

By solving the problems (2.4.3), in (u_{n+1}, ψ_{n+1}) plane, we get

$$(u_{n+1}, \psi_{n+1}) = \begin{cases} (\Phi, \psi_n + \frac{3}{2}\frac{\Phi - \tilde{u}_{n+1}}{k}) & \text{if } \tilde{u}_{n+1} - \frac{2k}{3}\psi_n \leq \Phi, \\ (\tilde{u}_{n+1} - \frac{2k}{3}\psi_n, 0) & \text{otherwise.} \end{cases} \tag{2.4.4}$$

Hence, one can perform the first step by solving discrete equation (2.4.2) and the second step with the help of the revised formula (2.4.4). The aforementioned implicit method with three levels of time needs the values obtained from the earlier two time levels. The pair (u_0, ψ_0) at zeroth time level can be acquired by making use of the initial condition and assigning the value given by $\psi_0 = 0$. To get the pair (u_1, ψ_1) at the next level succeeding the zeroth time level, we can use BDF1-OS method.

2.4.0.2 IMEX-CNLF-OS method

Following the previous procedure, for this case in the first step, we compute the intermediate value $\tilde{u}_{n+1}$ from the equations

$$\left(\frac{\tilde{u}_{n+1} - u_{n-1}}{2k}\right) = \mathcal{D}\left(\frac{\tilde{u}_{n+1} + u_{n-1}}{2}\right) + \lambda\mathcal{I}u_n + \psi_n. \tag{2.4.5}$$

Similarly, from previous steps, we use this intermediate solution in the second step to obtain u_{n+1} with following correction:

$$\begin{cases} \frac{u_{n+1}-\tilde{u}_{n+1}}{2k} &= \psi_{n+1} - \psi_n, \\ \psi_{n+1}(u_{n+1} - \Phi) &= 0, \\ u_{n+1} &\geq \Phi, \\ \psi_{n+1} &\geq 0. \end{cases} \tag{2.4.6}$$

Now we will update (u_{n+1}, ψ_{n+1}), with

$$(u_{n+1}, \psi_{n+1}) = \begin{cases} (\Phi, \psi_n + \frac{\Phi - \tilde{u}_{n+1}}{2k}) & \text{if } \tilde{u}_{n+1} - 2k\psi_n \leq \Phi, \\ (\tilde{u}_{n+1} - 2k\psi_n, 0) & \text{otherwise.} \end{cases} \tag{2.4.7}$$

Since, the above operator splitting scheme is three step scheme, for computing first step (u_1, ψ_1) we can use BDF1-OS method.

2.4.0.3 IMEX-CNAB-OS method

Now, we find an expression for the CNAB discretization. Following the previous procedure, the two sub-step performed at t_{n+1}. In the first step, we compute the intermediate value $\tilde{u}_{n+1}$ from the equations

$$\left(\frac{\tilde{u}_{n+1} - u_n}{k}\right) = \mathcal{D}\left(\frac{\tilde{u}_{n+1} + u_n}{2}\right) + \lambda\mathcal{I}(\mathcal{E}_2 u_n) + \psi_n. \tag{2.4.8}$$

Similarly, from previous steps, we use this intermediate solution in the second step to obtain u_{n+1} with following correction:

$$\begin{cases} \frac{u_{n+1}-\tilde{u}_{n+1}}{k} &= \psi_{n+1} - \psi_n, \\ \psi_{n+1}(u_{n+1} - \Phi) &= 0, \\ u_{n+1} &\geq \Phi, \\ \psi_{n+1} &\geq 0. \end{cases} \tag{2.4.9}$$

Finally, in second step, we can be solve in (u_{n+1}, ψ_{n+1}) plane, with adaptation of

$$(u_{n+1}, \psi_{n+1}) = \begin{cases} (\Phi, \psi_n + \frac{\Phi - \tilde{u}_{n+1}}{k}) & \text{if } \tilde{u}_{n+1} - k\psi_n \leq \Phi, \\ (\tilde{u}_{n+1} - k\psi_n, 0) & \text{otherwise.} \end{cases} \tag{2.4.10}$$

Since, the IMEX-CNAB operator splitting scheme is three step scheme, for computing first step (u_1, ψ_1) we can use BDF1-OS method.

2.5 Computational Results

In this section, we discuss a number of computational experiments to demonstrate the effectiveness and precision of the proposed numerical methods in order to determine the value of European and American put options using local volatility models with jumps. To compute the differential operator, we use the thin plate spline ($\tilde{r}^4 \ln \tilde{r}$) radial basis functions. To discretize the integral term (2.3.2) on truncated domain Ω, we used the composite trapezoidal rule. We applied the Fast Fourier Transformation (FFT) algorithm [5, 83] to compute the product of a dense matrix and a column vector in the discrete integral operator. The computational error generated by the numerical methods was calculated by the double mesh principle at different asset prices by maintaining the shape parameter constant. In all computational examples, equal distance grid with $m_i = 3$ is used. In all the computational investigations first step is calculated by IMEX-BDF1 method. We used MATLAB R2022b on a PC with Processor Intel(R) Core(TM) i5-10500 CPU @ 3.10GHz, 3096 Mhz, 6 Core(s), 12 Logical Processor(s) and 16.00GB RAM.

We have shown the option value and the computational errors for all the three cases when the option holder is in the money, at the money or out the money $S = 90,\ 100,\ 110$. To compute the errors we used the difference between successive numerical solutions as the following formula,

$$\text{Error} = \left| U(k,h) - U(\frac{k}{2}, \frac{h}{2}) \right|,$$

where $U(k,h)$ is the computed price of option with temporal mesh length k and spatial mesh length h. We showed the option value and some greeks value of option for the local volatility $\sigma_1(x,t)$.

The operator splitting approach was used to handle the inequality restrictions in the LCP for American option pricing. We applied the IMEX-BDF2, IMEX-CNLF and IMEX-CNAB techniques joined with the operator splitting method, it produced a linear system at each time step that can be easily solved by LU decomposition without the use of fixed point iteration.

To estimate the price of option at non-grid points of stock price, we applied the piecewise cubic Hermite interpolation. In connection to the spatial variable, the cubic spline was applied to ensure accuracy of given methods. Throughout all of the tests, we have calculated the error at different stock price $S = 90,\ 100,\ 110$ with M spatial discretization points in the spatial computational domain $\Omega := [-1.5, 1.5]$ and N is denoting to the temporal discretization points.

Since volatility is an important factor in investing decisions, modeling and forecasting volatility are of paramount importance for market practitioners. In order to price derivative securities, financial institutions need to forecast stock price volatility. The volatility smile phenomena is best explained by local volatility

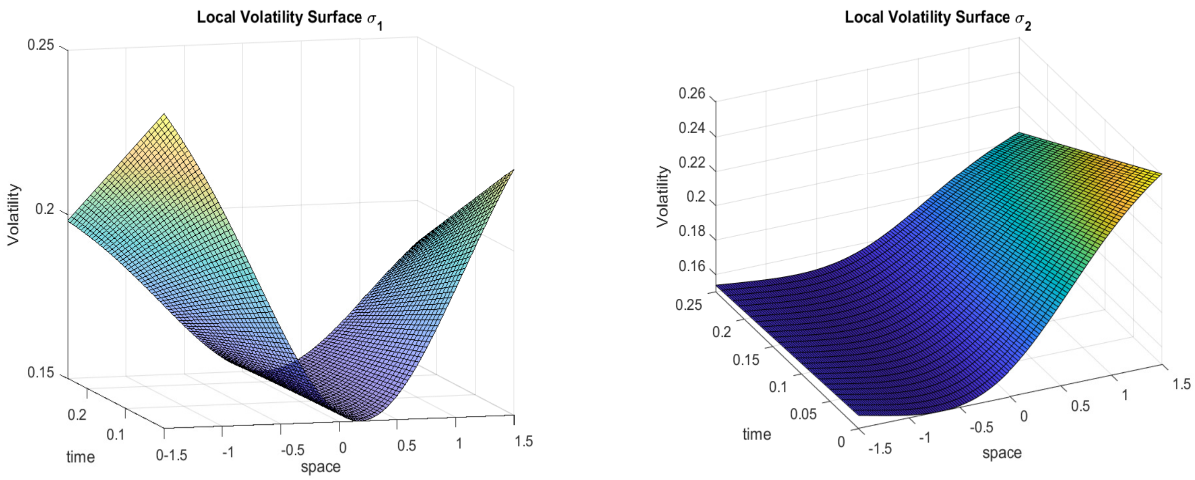

Figure 2.1: Local volatility surfaces for both the functions.

models, which define volatilities as a deterministic function of current stock prices and time. In [75] Kim and Lee explained the challenges of constant and Local volatility and then address the numerical and theoretical treatments for these challenges. For the generalised Black-Scholes equation, Kim [76] provide a mathematical approach for the reliable and precise construction of a local volatility surface. To perform numerical simulation, we have taken two local volatility functions to decribe the effects of local volatility surface in option pricing:

$$\sigma_1(x,t) = 0.15 + 0.15(0.5 + 2(T-t))\frac{(\frac{Ke^x}{100} - 1.2)^2}{((\frac{Ke^x}{100})^2 + 1.44)}, \tag{2.5.1}$$

which was also used in [121], and

$$\sigma_2(x,t) = 0.15 + 0.15(0.5 + 2(T-t))\frac{(\frac{Ke^x}{100} - 0.5)^2}{((\frac{Ke^x}{100})^2 + 1.44)}, \tag{2.5.2}$$

which was also employed in [70]. Both the volatility surfaces are shown in Figure (2.1) with respect to time and asset price, where asset price is denoted by space. The Kou model in [79] and Merton model in [96] are the two jump-diffusion models that are most prominently adopted for pricing option value. We begin by taking into account the Merton model, where suitable parameters are given by:

$$\sigma = \sigma_1 \ \text{ and } \ \sigma_2,\ r = 0.05,\ T = 0.25,\ K = 100,\ \sigma_J = 0.45,\ \mu_J = -0.90,\ \lambda = 0.10, \tag{2.5.3}$$

and for Kou model we have taken the parameters as:

$$\sigma = \sigma_1 \text{ and } \sigma_2,\ r = 0.05,\ T = 0.25,\ K = 100,\ \eta_1 = 3.0465,\ \eta_2 = 3.0775,\ p = 0.3445,\ \lambda = 0.10. \tag{2.5.4}$$

In order to price the European and American put options with a reduced domain of $x_L = -1.5$ and $x_R = 1.5$, [69, 70, 121] also use these parameters.

2.5.1 European Option

Example 2.5.1. *First, we consider the Merton's jump diffusion model to price the European put option, where* $\sigma(x,t) = \sigma_1(x,t)$.

We have computed the error and option value at different asset prices for IMEX-BDF2, IMEX-CNLF and IMEX-CNAB methods under Merton's model for pricing European put options and data are given in Table 2.1. We can observe that the convergence rate attains its asymptotic order when the temporal mesh is sufficiently small. We saw that, all the proposed methods are nearly second order accurate in time. We have shown the option values and some greeks for IMEX-BDF2, IMEX-CNLF and IMEX-CNAB methods in Fig. 2.2. The graphs show that there is little to no erratic movement in option values close to the strike price.

Table 2.1: Numerical results for European put options under the Merton's jump-diffusion model with local volatility $\sigma_1(x,t)$ using the specified parameters at various stock prices as given in (2.5.3).

			$S = 90$		$S = 100$		$S = 110$	
Method	M	N	Value	Error	Value	Error	Value	Error
BDF2	129	25	9.336388	-	3.182687	-	1.410097	-
	257	50	9.323776	1.2612e-02	3.184479	1.7919e-03	1.409032	1.0643e-03
	513	100	9.320533	3.2426e-03	3.184987	5.0817e-04	1.408816	2.1582e-04
	1025	200	9.319720	8.1358e-04	3.185118	1.3099e-04	1.408765	5.1671e-05
CNLF	129	25	9.334524	-	3.181724	-	1.409849	-
	257	50	9.321732	1.2792e-02	3.183375	1.6506e-03	1.408444	1.4046e-03
	513	100	9.318526	3.2067e-03	3.183671	2.9625e-04	1.408027	4.1664e-04
	1025	200	9.317674	8.5195e-04	3.183726	5.5213e-05	1.407875	1.5261e-04
CNAB	129	25	9.335030	-	3.181437	-	1.409787	-
	257	50	9.322055	1.2975e-02	3.183207	1.7694e-03	1.408374	1.4130e-03
	513	100	9.318614	3.4408e-03	3.183648	4.4092e-04	1.407990	3.8416e-04
	1025	200	9.317700	9.1473e-04	3.183730	8.2257e-05	1.407856	1.3457e-04

Example 2.5.2. *Next, we consider the Kou's jump diffusion model to price the European put option, where* $\sigma(x,t) = \sigma_1(x,t)$.

In example 2.5.2 , we execute the same simulation for IMEX-BDF2, IMEX-CNLF and IMEX-CNAB methods for Kou's model, and numerical results are provided in Table 2.2. We observe that for all the proposed methods the errors were reducing with ratio nearly four, thus the discretization schemes are approximatly second order convergent in time, as given in the Table 2.2. We have plotted the option

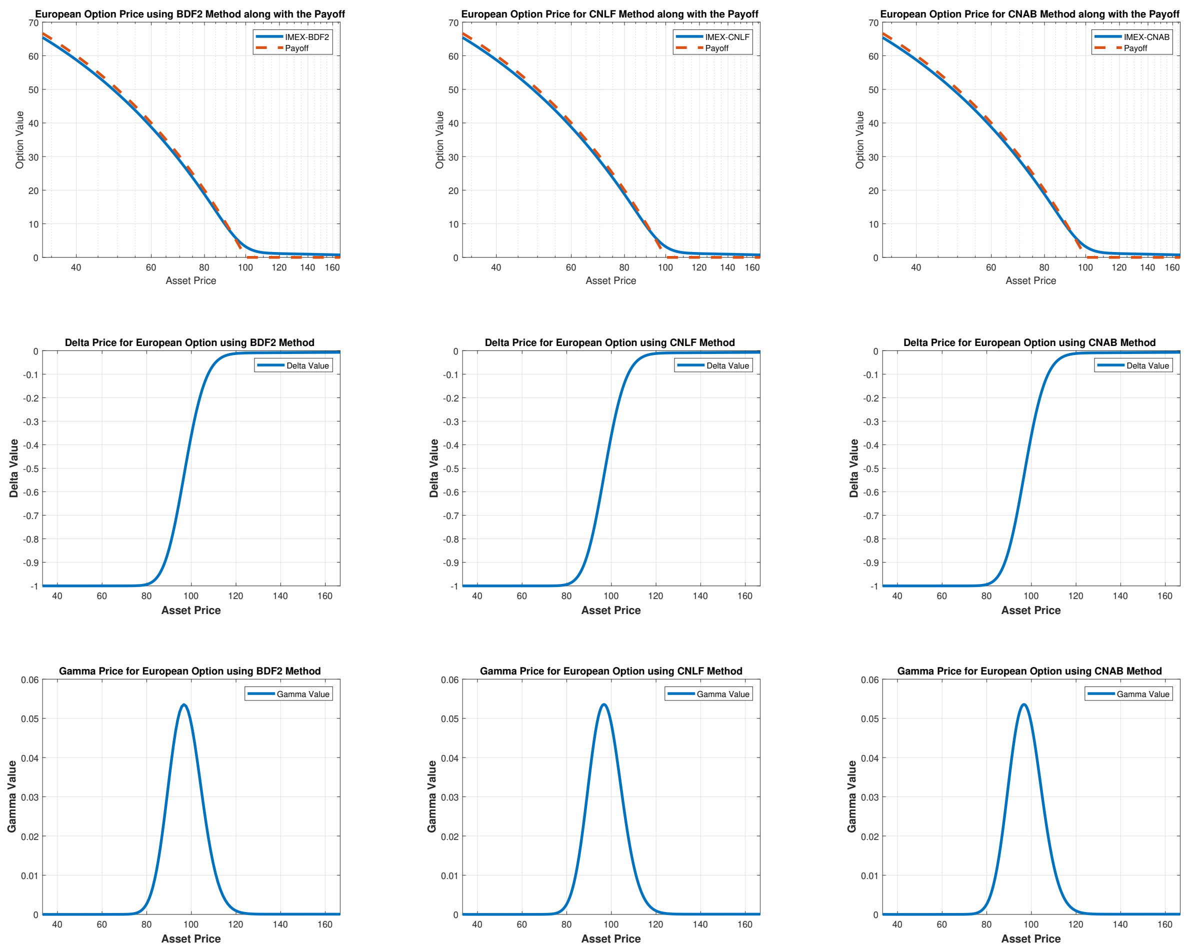

Figure 2.2: European option value and some greeks, under the Merton's jump-diffusion model with parameters as provided in the example 2.5.1.

values and some greeks in Fig. 2.3.

In Table 2.3, we present the temporal convergence order of the IMEX-BDF2 method for both the Merton and Kou jump diffusaion model. We have fixed the spatial points $M = 10^3 + 1$, in the spatial domain $\Omega = [-5, 5]$ and shown the results for different temporal points. From Table 2.3, we can observe that the error is reducing by the factor of approximate four at different values of N, this shows that our method has approximate second order convergence rate in time for both the Merton and Kou models.

Example 2.5.3. *We consider the Merton's jump diffusion model to price the European put option, where* $\sigma(x,t) = \sigma_2(x,t)$.

In Example 2.5.3, we perform the simulation for IMEX-BDF2, IMEX-CNLF and IMEX-CNAB methods for Merton's and Kou's model with variable coefficients $\sigma_2(x,t)$. The numerical results are reported

Table 2.2: Numerical results for European put options under the Kou's jump-diffusion model with local volatility $\sigma_1(x,t)$ using the specified parameters at various stock prices as given in (2.5.4).

			$S = 90$		$S = 100$		$S = 110$	
Method	M	N	Value	Error	Value	Error	Value	Error
BDF2	129	25	9.468647	-	2.767410	-	0.566071	-
	257	50	9.459640	9.0065e-03	2.767574	1.6370e-04	0.562383	3.6882e-03
	513	100	9.457313	2.3273e-03	2.767658	8.3770e-05	0.561513	8.7058e-04
	1025	200	9.456728	5.8508e-04	2.767681	2.3509e-05	0.561296	2.1622e-04
CNLF	129	25	9.467679	-	2.766714	-	0.565822	-
	257	50	9.459025	8.6537e-03	2.767245	5.3147e-04	0.562210	3.6117e-03
	513	100	9.456969	2.0561e-03	2.767383	1.3850e-04	0.561389	8.2158e-04
	1025	200	9.456494	4.7510e-04	2.767478	9.4799e-05	0.561197	1.9222e-04
CNAB	129	25	9.468350	-	2.766719	-	0.566094	-
	257	50	9.459382	8.9676e-03	2.767208	4.8898e-04	0.562310	3.7842e-03
	513	100	9.457102	2.2807e-03	2.767432	2.2394e-04	0.561426	8.8425e-04
	1025	200	9.456549	5.5304e-04	2.767520	8.7318e-05	0.561212	2.1398e-04

Table 2.3: Numerical results for European put options under the Merton's and Kou's jump-diffusion models with local volatility $\sigma_1(x,t)$ using the specified parameters at various stock prices as given in (2.5.3)-(2.5.4).

		$S = 90$		$S = 100$		$S = 110$	
Model	N	Value	Error	Value	Error	Value	Error
Merton	50	9.417792	-	3.578447	-	1.969447	-
	100	9.417715	7.7353e-05	3.578493	4.5228e-05	1.969506	5.9541e-05
	200	9.417696	1.9284e-05	3.578504	1.1444e-05	1.969521	1.4749e-05
	400	9.417691	4.8167e-06	3.578507	2.8786e-06	1.969525	3.6707e-06
	800	9.417690	1.2037e-06	3.578508	7.2189e-07	1.969526	9.1564e-07
	1600	9.417689	3.0090e-07	3.578508	1.8075e-07	1.969526	2.2865e-07
Kou	50	9.607426	-	2.928799	-	0.703181	-
	100	9.607418	7.7338e-06	2.928866	6.6915e-05	0.703233	5.2466e-05
	200	9.607416	1.9701e-06	2.928882	1.6848e-05	0.703246	1.2974e-05
	400	9.607416	4.9829e-07	2.928887	4.2276e-06	0.703249	3.2257e-06
	800	9.607416	1.2536e-07	2.928888	1.0588e-06	0.703250	8.0422e-07
	1600	9.607416	3.1446e-08	2.928888	2.6497e-07	0.703250	2.0077e-07

in Table 2.4 and Table 2.5 for Merton and Kou models respectively. We can see from the Table 2.4 and Table 2.5, that all the proposed methods have approximate second order convergence rate in time.

Example 2.5.4. *We consider the Kou's jump diffusion model to price the European put option, where*

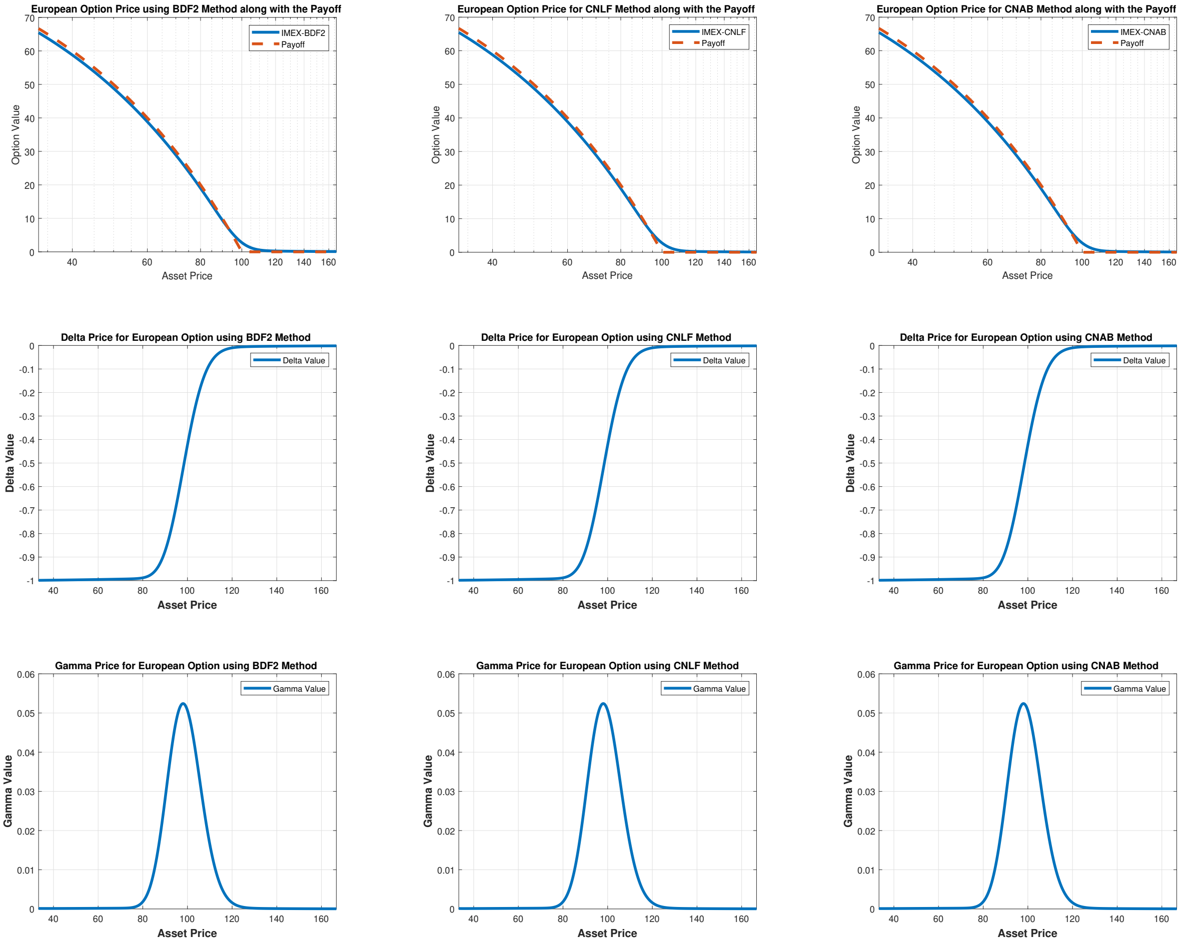

Figure 2.3: European option value and some greeks, under the Kou's jump-diffusion model with parameters as provided in the example 2.5.2.

$\sigma(x,t) = \sigma_2(x,t)$.

All the considered examples show that the proposed methods have approximate second order convergence rate in time, although the order of convergence at the early exercise boundary is less precise for both Merton's and Kou's models.

Although the concept of smoothing the payoff has been addressed in prior finance literature, we considered the European put option pricing under Merton's jump diffusion model with local volatility $\sigma_1(x,t)$ with parameters provided in (2.5.3). We studied the situations where the payoffs were discontinuous, and we employed the IMEX-CNLF time stepping technique combined with the Tavella, D. and C. Randall's mesh shifting technique as suggested in [106]. We obtained slightly better results with the improved accuracy of the proposed method. We demonstrated the numerical results in Table 2.6 and compared it

Table 2.4: Numerical results for European put options under the Merton's jump-diffusion model with local volatility $\sigma_2(x,t)$ using the specified parameters at various stock prices as given in (2.5.3).

			$S = 90$		$S = 100$		$S = 110$	
Method	M	N	Value	Error	Value	Error	Value	Error
BDF2	129	25	9.411279	-	3.361633	-	1.484906	-
	257	50	9.400236	1.1043e-02	3.362923	1.2897e-03	1.483607	1.2993e-03
	513	100	9.397391	2.8448e-03	3.363297	3.7444e-04	1.483323	2.8393e-04
	1025	200	9.396678	7.12961e-04	3.363394	9.7022e-05	1.483254	6.9481e-05
CNLF	129	25	9.407028	-	3.355629	-	1.482211	-
	257	50	9.397255	9.7730e-03	3.358962	3.3332e-03	1.481707	5.0419e-04
	513	100	9.394810	2.4456e-03	3.360604	1.6419e-03	1.481873	1.6585e-04
	1025	200	9.394318	4.9128e-04	3.361325	7.2154e-04	1.482031	1.5765e-04
CNAB	129	25	9.408822	-	3.357860	-	1.483420	-
	257	50	9.397924	1.0898e-02	3.360377	2.5169e-03	1.482336	1.0845e-03
	513	100	9.395167	2.7564e-03	3.361317	9.3990e-04	1.482183	1.5248e-04
	1025	200	9.394503	6.6449e-04	3.361683	3.6661e-04	1.482185	1.5175e-06

Table 2.5: Numerical results for European put options under the Kou's jump-diffusion model with local volatility $\sigma_1(x,t)$ using the specified parameters at various stock prices as given in (2.5.4).

			$S = 90$		$S = 100$		$S = 110$	
Method	M	N	Value	Error	Value	Error	Value	Error
BDF2	129	25	9.530477	-	2.953432	-	0.663080	-
	257	50	9.522590	7.8871e-03	2.953536	1.0389e-04	0.659413	3.6672e-03
	513	100	9.520546	2.0444e-03	2.953601	6.5076e-05	0.658537	8.7620e-04
	1025	200	9.520032	5.1325e-04	2.953619	1.8659e-05	0.658319	2.1838e-04
CNLF	129	25	9.527920	-	2.947926	-	0.660121	-
	257	50	9.521127	6.7924e-03	2.950755	2.8294e-03	0.657833	2.2876e-03
	513	100	9.519769	1.3578e-03	2.952089	1.3335e-03	0.657700	1.3398e-04
	1025	200	9.519580	1.8907e-04	2.952794	7.0571e-04	0.657859	1.5985e-04
CNAB	129	25	9.529427	-	2.950305	-	0.661782	-
	257	50	9.521921	7.5067e-03	2.951936	1.6307e-03	0.658646	3.1359e-03
	513	100	9.520121	1.7996e-03	2.952754	8.1805e-04	0.658096	5.5078e-04
	1025	200	9.519745	3.7641e-04	2.953146	3.9190e-04	0.658055	4.0838e-05

with the corresponding results in Table 1 of Lee [84], where authors have provided results for pricing the European and American option under local volatility model with jumps. From the Table 2.6, we can observe that although both methods achieve approximately second order rate in financial domain but the proposed method provides better result than Lee [84]. We have also shown the results for American option in Table 2.8 and compared with the Table 3 of Lee [84].

Table 2.6: Comparison of numerical results of IMEX-CNLF method for pricing European option with Table 1 of Lee [84].

		$S = 90$		$S = 100$		$S = 110$	
M	N	Lee [84]	Present Method	Lee [84]	Present Method	Lee [84]	Present Method
256	50	0.001251	0.001411	0.027544	0.027431	0.006320	0.005825
512	100	0.000567	0.000428	0.006597	0.006558	0.001604	0.001398
1024	200	0.000147	0.000065	0.001642	0.001609	0.000404	0.000305
2048	400	0.000037	0.000007	0.000410	0.000390	0.000101	0.000052

2.5.2 American Option

For pricing American options, authors [45] suggested an implicit discretization accompanied by a penalty approach, and authors [83] provided the three time level IMEX approach combined with OS technique. We used the operator splitting technique to handle the inequality constraints for pricing the American put option under the jump diffusion model with local volatility $\sigma_1(x, t)$ and $\sigma_2(x, t)$.

Example 2.5.5. *First, we consider the Merton's jump diffusion model to price the American put option, where* $\sigma(x, t) = \sigma_1(x, t)$.

In Example 2.5.5, we execute the simulation for IMEX-BDF2-OS, IMEX-CNLF-OS and IMEX-CNAB-OS methods for pricing American option under Merton's model with parameters in (2.5.3). The numerical results are reported in Table 2.7 for Merton's model. We observe that, all the proposed methods are convergent with approximate second order in time. We have plotted the option values and Greeks for Merton model in Figure 2.4.

Example 2.5.6. *We consider the Kou's jump diffusion model to price the American put option, where* $\sigma(x, t) = \sigma_1(x, t)$.

In Example 2.5.6, we perform the simulation for IMEX-BDF2-OS, IMEX-CNLF-OS and IMEX-CNAB-OS methods for pricing American option under Kou's model with parameters in (2.5.4). The numerical results are reported in Table 2.9 for Kou's model. We observe that, all the proposed methods are convergent with approximate second order in time. We have plotted the option values, Delta and Gamma values for Kou model in Figure 2.5.

In Table 2.8, we have shown the results for American put option using the mesh shifting technique and results are compared it with Table 3 of Lee [84]. From the table we can observe that although both methods achieved second order convergence rate in time but the proposed method provides better accuracy than Lee [84].

Table 2.7: Numerical results for American put options under the Merton's jump-diffusion model with local volatility $\sigma_1(x,t)$ using the specified parameters at various stock prices as given in (2.5.3).

			$S=90$		$S=100$		$S=110$	
Method	M	N	Value	Error	Value	Error	Value	Error
BDF2	129	25	9.996996	-	3.261637	-	1.426582	-
	257	50	10.010091	1.3095e-02	3.270957	9.3207e-03	1.426207	3.7494e-04
	513	100	10.007914	2.1764e-03	3.273861	2.9034e-03	1.426302	9.4784e-05
	1025	200	10.008732	8.1757e-04	3.274674	8.1343e-04	1.426366	6.4481e-05
CNLF	129	25	9.996992	-	3.261568	-	1.426978	-
	257	50	10.010339	1.3348e-02	3.271568	9.9994e-03	1.426476	5.0149e-04
	513	100	10.007791	2.5478e-03	3.274065	2.4971e-03	1.426404	7.2394e-05
	1025	200	10.008760	9.6803e-04	3.274720	6.5532e-04	1.426400	3.3514e-06
CNAB	129	25	9.997013	-	3.260062	-	1.426800	-
	257	50	10.009905	1.2892e-02	3.270245	1.0182e-02	1.426246	5.5340e-04
	513	100	10.007824	2.0813e-03	3.273557	3.3120e-03	1.426302	5.5167e-05
	1025	200	10.008684	8.5988e-04	3.274541	9.8456e-04	1.426359	5.7592e-05

Table 2.8: Comparison of numerical results of IMEX-CNLF-OS method for pricing American option with Table 3 of Lee [84].

		$S=90$		$S=100$		$S=110$	
M	N	Lee [84]	Present Method	Lee [84]	Present Method	Lee [84]	Present Method
256	50	0.003397	0.002762	0.032421	0.032459	0.006771	0.006432
512	100	0.007377	0.007417	0.007556	0.007658	0.001749	0.001639
1024	200	0.000132	0.000127	0.001944	0.002001	0.000473	0.000439
2048	400	0.000153	0.000143	0.000453	0.000489	0.000120	0.000112

Example 2.5.7. *Next, we consider the Merton's jump diffusion model to price the American put option, where* $\sigma(x,t) = \sigma_2(x,t)$.

In Example 2.5.7, we demonstrate the numerical experiments for American put option under Merton model with the local volatility function $\sigma_2(x,t)$. To handle the inequality conditions in the LCP, the operator splitting method is used. The implicit methods with three time levels combined with the operator splitting method results in a linear system at each time step that can be easily solved using LU decomposition without fixed point iteration. Table 2.10 shows that the pointwise errors for the American put option are decreasing with the approximate second order in time, despite the fact that the option values at $S=90$ are volatile due to the early exercise boundaries.

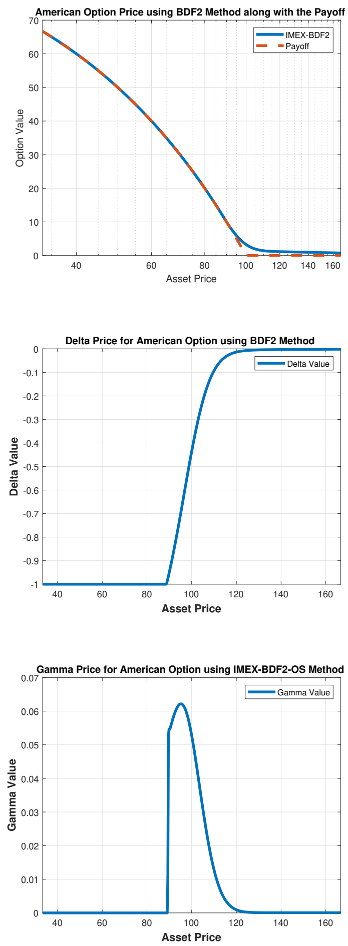

Figure 2.4: Option values and Greeks for American option under the Merton's jump-diffusion model with parameters as provided in the example 2.5.5.

Example 2.5.8. *We consider the Kou's jump diffusion model to price the American put option, where* $\sigma(x,t) = \sigma_2(x,t)$.

In Example 2.5.8, we perform the numerical experiment for American put option under Kou model with the local volatility function $\sigma_2(x,t)$. To handle the inequality conditions in the LCP, the operator splitting technique is used. The implicit methods with three time levels joined by the operator splitting method results in a linear system at each time step that can be easily solved using LU decomposition without fixed point iteration. Table 2.11 shows that the pointwise errors for the American put option are decreasing with the approximate second order in time, despite the fact that the option values at $S = 90$ are volatile due to the early exercise boundaries.

Choosing the basis functions is a necessary step in the implementation of radial basis function (RBF) approaches, and radial basis functions are specified by a shape parameter that must also be chosen. The

Table 2.9: Numerical results for American put options under the Kou's jump-diffusion model with local volatility $\sigma_1(x,t)$ using the specified parameters at various stock prices as given in (2.5.4).

			$S=90$		$S=100$		$S=110$	
Method	M	N	Value	Error	Value	Error	Value	Error
BDF2	129	25	9.997825	-	2.833644	-	0.574283	-
	257	50	10.010444	1.2619e-02	2.840246	6.6023e-03	0.571325	2.9576e-03
	513	100	10.010050	3.9385e-04	2.842316	2.0698e-03	0.570762	5.6322e-04
	1025	200	10.010298	2.4725e-04	2.842938	6.2131e-04	0.570671	9.0797e-05
CNLF	129	25	9.997427	-	2.833522	-	0.574185	-
	257	50	10.010606	1.3179e-02	2.840575	7.0536e-03	0.571334	2.8508e-03
	513	100	10.010158	4.4788e-04	2.842290	1.7152e-03	0.570737	5.9733e-04
	1025	200	10.010364	2.0544e-04	2.842925	6.3457e-04	0.570666	7.1173e-05
CNAB	129	25	9.997447	-	2.832021	-	0.574370	-
	257	50	10.010284	1.2837e-02	2.839458	7.4365e-03	0.571271	3.0988e-03
	513	100	10.009927	3.5624e-04	2.841973	2.5158e-03	0.570713	5.5808e-04
	1025	200	10.010237	3.0977e-04	2.842786	8.1296e-04	0.570642	7.1068e-05

Table 2.10: Numerical results for American put options under the Merton's jump-diffusion model with local volatility $\sigma_2(x,t)$ using the specified parameters at various stock prices as given in (2.5.3).

			$S=90$		$S=100$		$S=110$	
Method	M	N	Value	Error	Value	Error	Value	Error
BDF2	129	25	10.012810	-	3.441046	-	1.502343	-
	257	50	10.026396	1.3586e-02	3.449681	8.6352e-03	1.502001	3.4196e-04
	513	100	10.029761	3.3648e-03	3.452295	2.6141e-03	1.502095	9.4039e-05
	1025	200	10.030300	5.3932e-04	3.453055	7.5988e-04	1.502173	7.8502e-05
CNLF	129	25	10.010923	-	3.436614	-	1.500452	-
	257	50	10.025792	1.4869e-02	3.447940	1.1326e-02	1.501111	6.5879e-04
	513	100	10.029895	4.1030e-03	3.451184	3.2441e-03	1.501589	4.7776e-04
	1025	200	10.030314	4.1910e-04	3.452488	1.3038e-03	1.501916	3.2720e-04
CNAB	129	25	10.011758	-	3.438303	-	1.501638	-
	257	50	10.025902	1.4144e-02	3.448221	9.9175e-03	1.501551	8.7151e-05
	513	100	10.029439	3.5363e-03	3.451570	3.3491e-03	1.501845	2.9426e-04
	1025	200	10.030177	7.3792e-04	3.452693	1.1234e-03	1.502040	1.9458e-04

choices of shape parameter have a tremendous impact on the accuracy of the results and the numerical stability of the method used. Finding the optimal shape parameter is a challenging task and an ongoing research area [48, 101]. Figure 2.6 demonstrate the effects of the shape parameters with the error (successive difference of computed solutions) for Gaussian radial basis function for pricing European and American option under local volatility jump-diffusion model.

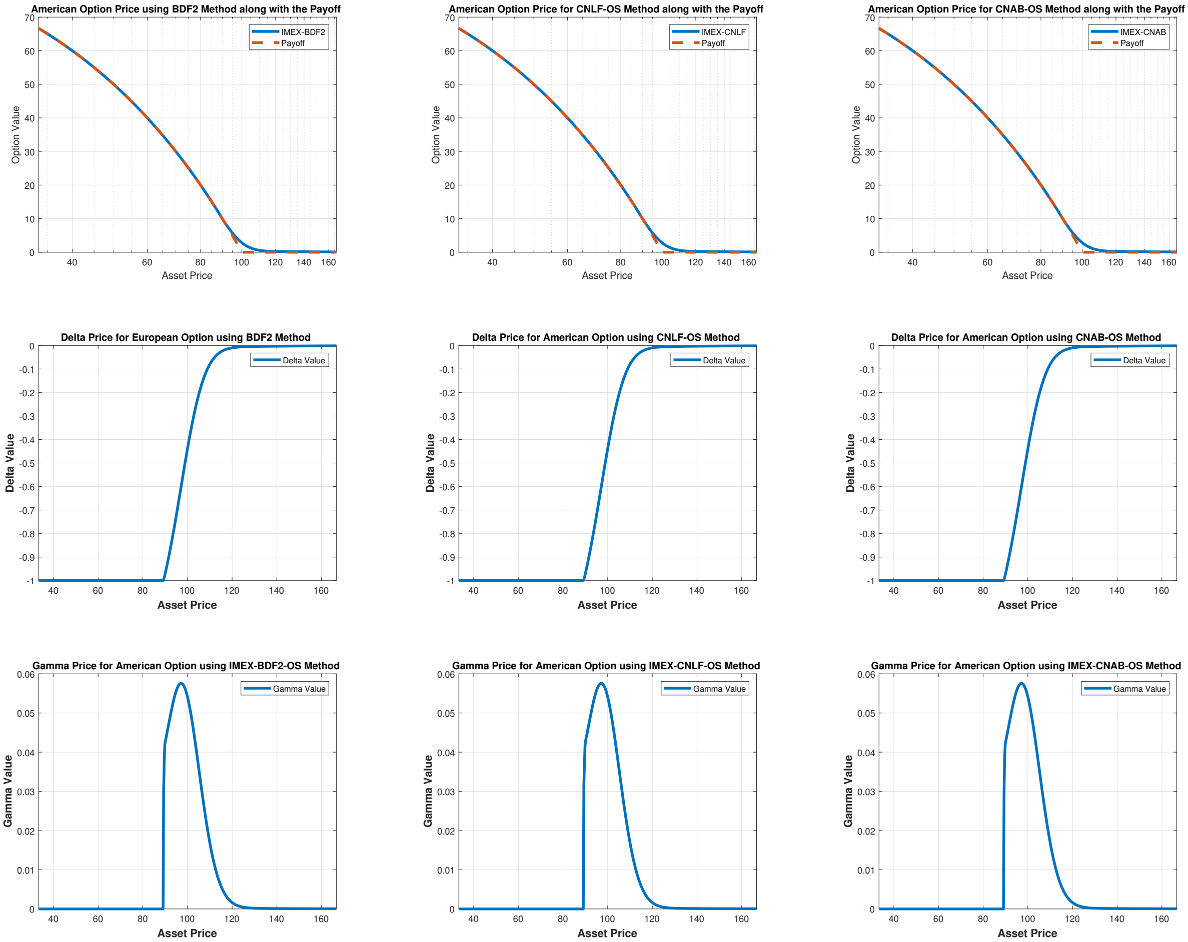

Figure 2.5: Option values and Greeks for American option under the Kou's jump-diffusion model with parameters as provided in the example 2.5.6.

2.6 Conclusion

We have presented RBF based three IMEX finite difference techniques namely; BDF2, CNLF and CNAB, for solving the PIDEs that arises when an underlying asset exhibits behaviour consistent with the extended jump diffusion method. An RBF-based finite difference method is used to solve the linear differential equations that come from temporal semi-discretization of the governing equation, and a composite trapezoidal method is used to calculate the integral term involved in PIDE. We applied the IMEX-BDF2, IMEX-CNLF and IMEX-CNAB techniques joined with the operator splitting method to handle the inequality restrictions in the LCP for pricing American option pricing, it produces a linear system at each time step that can be easily solved by LU decomposition without the use of fixed point iteration. The numerical experiments with European put and American put options are performed using the Merton and Kou model with local volatility. The numerical results demonstrate that the proposed methods are precise and effective. The

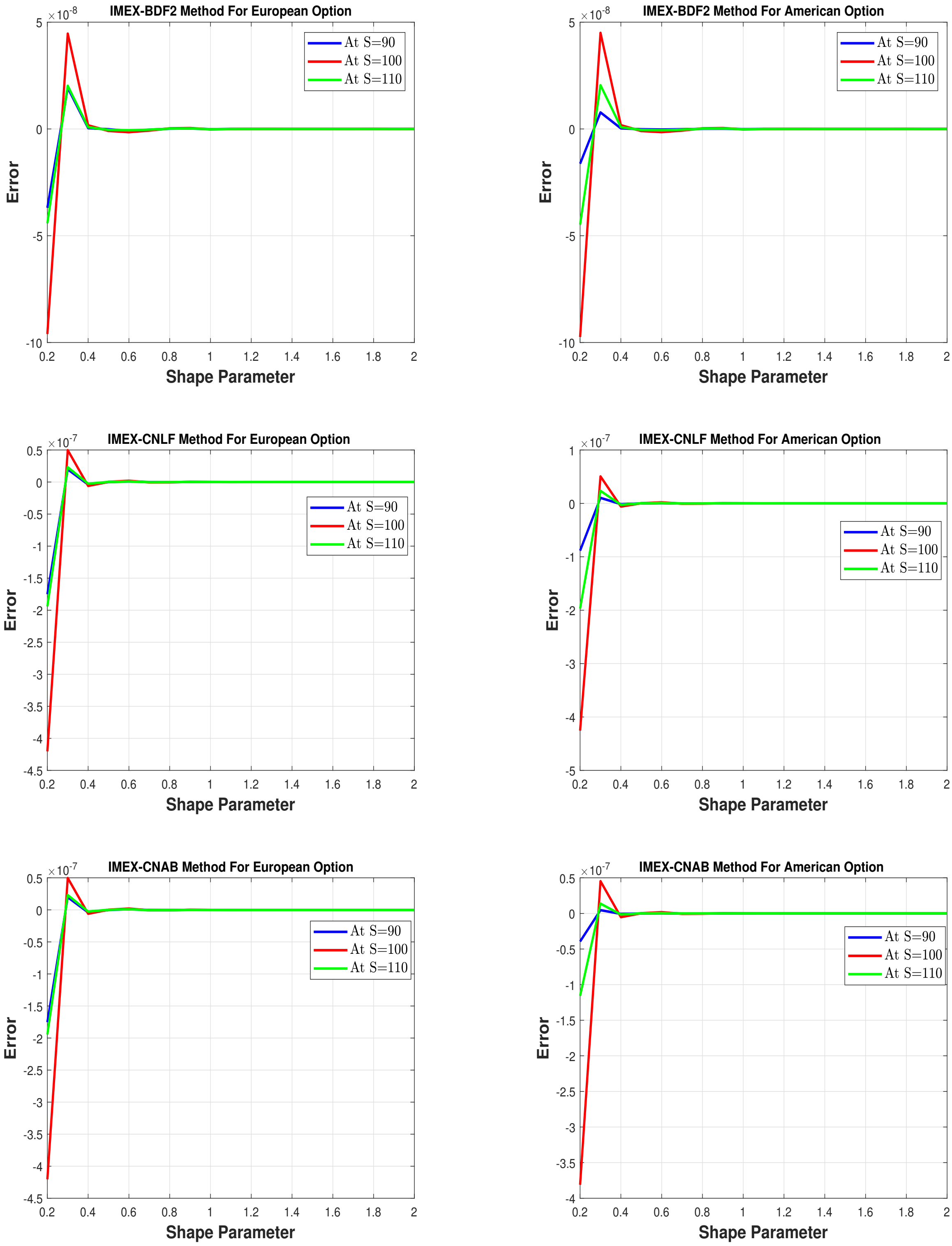

Figure 2.6: Effects of the shape parameters on error for pricing European and American option under the Kou's jump-diffusion model with local volatility $\sigma_1(x,t)$ at N=50 and M=256, rest of the parameters are given as in (2.5.4).

Table 2.11: Numerical results for American put options under the Kou's jump-diffusion model with local volatility $\sigma_2(x,t)$ using the specified parameters at various stock prices as given in (2.5.4).

			$S=90$		$S=100$		$S=110$	
Method	M	N	Value	Error	Value	Error	Value	Error
BDF2	129	25	10.018328	-	3.019847	-	0.672227	-
	257	50	10.028372	1.0044e-02	3.025721	5.8742e-03	0.669384	2.84356e-03
	513	100	10.030544	2.1714e-03	3.027722	2.0008e-03	0.668897	4.8704e-04
	1025	200	10.030888	3.4384e-04	3.028316	5.9372e-04	0.668831	6.6035e-05
CNLF	129	25	10.017045	-	3.014446	-	0.669374	-
	257	50	10.028143	1.1098e-02	3.023542	9.0962e-03	0.667983	1.3909e-03
	513	100	10.030462	2.3198e-03	3.026582	3.0399e-03	0.668204	2.2115e-04
	1025	200	10.030839	3.7659e-04	3.027690	1.1075e-03	0.668472	2.6772e-04
CNAB	129	25	10.017698	-	3.016892	-	0.671041	-
	257	50	10.027965	1.0268e-02	3.024191	7.2992e-03	0.668702	2.3392e-03
	513	100	10.030345	2.3797e-03	3.026946	2.7549e-03	0.668531	1.7106e-04
	1025	200	10.030787	4.4225e-04	3.027932	9.8663e-04	0.668643	1.1220e-04

option value and some "Greeks" can be precisely estimated using the proposed numerical methods.

Chapter 3

RBF-FD based Implicit-Explicit methods for pricing option under regime-switching jump-diffusion model with variable coefficients [1]

This chapter aims to develop and analyze radial basis function-based finite difference implicit-explicit temporal semi-discretizations techniques for pricing options under an extended Markovian regime-switching jump-diffusion economy.

3.1 Introduction

One of the most extensively used models in option pricing is the Black-Scholes. The volatility in the classical BS partial differential equation is constant. The constant volatility BS model is generally acknowledged to be practically inadequate since real financial market data exhibit non-constant volatility behavior. The constant volatility does not represent volatility skew or smile. Numerous stochastic models, including the local volatility model [40, 44], the regime-switching approach [102], the jump-diffusion framework [79, 96], and the stochastic volatility framework [57], have been proposed to address these limitations.

The volatility smile phenomena are best explained by extended BS models, which characterize volatilities as a time- and price-dependent function. The deterministic local volatility function, on the other hand, has significant limitations. For beginners, several empirical investigations have demonstrated that

[1] The results discussed in this chapter have been published in *Numerical Algorithms*, 97, 645-685 (2024). https://doi.org/10.1007/s11075-023-01719-2.

the local volatility function works poorly for hedging in [4, 43]. However, local volatility models are inadequate for capturing market fluctuations. Much recent research [10, 42, 66, 89] has proven the presence of jumps and their market influence. Dehghan *et al.*[37] explained the asymptotic expansion of the solutions of Black–Scholes equation near the maturity for pricing the American option.

In this study, we focus on the regime-switching jump-diffusion model, which combines the regime-switching and jump-diffusion models. The parameters in the RSJD model are viewed as variable coefficients in the temporal and spatial directions, specifically including the volatility smile, the time inhomogeneity, the sudden regime shift, and the deterministic volatility function, as demonstrated in the financial market. Under the RSJD model, the partial integrodifferential equation for a European option and the linear complementarity problem for an American option could potentially be solved numerically using several different techniques. Costabile *et al.*'s [31] recommendation for pricing the European and American options under the RSJD model included an explicit formula and a multinomial technique. The multinomial technique provides first-order precision in the time variable with constant coefficients. Haghi *et al.*[52] introduced a new combination of an RBF-FD method for pricing American options if the underlying asset acts in accordance with the jump-diffusion models. Dehghan *et al.*[38] presented a new class of radial basis function and explored its efficiency in option pricing problems. Rad *et al.*[109] presented radial basis point interpolation for pricing European and American options. For the numerical simulation of the prostate tumor growth model, Mohammadi *et al.*[98] presented the RBF-FD method. Shirzadi *et al.*[114, 115] introduced the mesh-free moving least-squares approximation and derived the optimal uniform error bounds for the pricing option under jump-diffusion models. The authors of [39] applied the homotopy perturbation method (HPM) and variational iteration method (VIM) for pricing the barrier option under the BS model. In [36], the time-splitting techniques for the solution of the two-dimensional transport equation are presented. In order to investigate the time-dependent incompressible Navier-Stokes equation with varying density, authors of [1] developed an impressively quick RBF-FD based numerical method. Some other applications of the mesh-free method for option pricing problems can be found in Kadalbajoo *et al.*[67, 68, 69] and references therein.

This chapter's goal is to provide numerical techniques for evaluating European and American pricing using the RSJD model with variable coefficients. Even if there are many research articles on pricing financial derivatives, the constant parameters under the RSJD model have already been taken into account. Thus, it is important to concentrate on the variable coefficients that allow us to accurately replicate financial market data. To solve the PIDE for the European option, we provide three implicit-explicit numerical methods: Crank-Nicolson Adam Bashfourth, Crank-Nicolson Leap-Frog, and a two-step backward differentiation formula. When the jump intensity is high enough, it is noted in [112] that the three implicit approaches in which the zeroth derivative term is implicitly discretized provide more stable results than the explicit treatment of the zeroth derivative term. The three numerical techniques we provide for the RSJD model with variable coefficients are intended for the linear system associated with the inverse of a tridiagonal matrix at each stage of the economy and time step. As a result, it can be effectively solved using a LU decomposition. The regime-switching framework also ranks among the most rapid advancements that are gaining a substantial amount of attention for computing the price of an option.

Regime-switching approaches provide a straightforward technique to record stochastic volatility and as a result, fat tails, avoiding the shortcoming of the standard lognormality assumption of constant volatility. The addition of a jump component to the regime-switching context helps to explain some of the empirical biases observed by the classical lognormal model more precisely. The finite state Markov chain of the regime-switching model generates switches of the drift and volatility parameters that efficiently account for the impact of major financial forces on asset price dynamics. Some handful examples of regime switching implementations are, insurance [56], power markets [53, 128], natural gas [6, 26], optimum forestry management [24], trading methods [34], valuation of stock loans [144], convertible bond pricing [29], and interest rate dynamics [72]. In contrary to a stochastic volatility jump-diffusion model, regime switching models are intuitively enticing and computationally inexpensive. In our recent work [135], we have presented the RBF-FD based IMEX methods for pricing European and American option under local volatility jump-diffusion model.

A plethora of strategies have been put together for addressing the American options in regime-switching frameworks (see, for example, [27, 60, 86, 134, 140, 143]). When the underlying asset is subjected to a regime-switching jump-diffusion model for pricing the American option, Bastani *et al.*[9] presented an RBF-based collocation method, Tour *et al.*[122] introduced a spectral element method. Kumar *et al.*[82], Mollapourasl *et al.*[100], Rad and Parand [108], Tour *et al.*[123] proposed radial basis function approach, Chen *et al.*[22], Patel *et al.*[104] used the compact finite difference approaches. Egorova *et al.*[46] suggested a novel, more efficient numerical method for solving the American option in the regime-switching framework.

In this work, we proposed some radial basis function finite difference based implicit-explicit methods for pricing European and American options in a regime-switching jump-diffusion model with local volatility that leads to tridiagonal coefficient matrices. Although there are a variety of approaches for solving LCPs, we employ the operator splitting method [64] to deal with the inequality restrictions. To avoid iterative procedures, we paired the proposed methods with the operator splitting method to evaluate the value of the American option. Operator splitting technique has been used proficiently in several Black-Scholes models [23, 65, 73, 87, 133], and it is robust and efficient to apply since the differential equation and complementarity conditions are disentangled and rapidly solved on their own.

The rest of the chapter is structured in the following manner. We start with defining the notations and preliminaries for the regime-switching jump-diffusion model with local volatility, describing the basic notations, symbols, and presumptions used throughout this chapter and the construction of the PIDE and its associated characteristics. In Sect. 3.3, we provide the discretization, and we demonstrate the stability of the proposed approaches with the second-order convergence rate. After that, we present the IMEX-OS discretization for the American option. In Sect. 3.4, we provide numerical experiments to validate accuracy, order of convergence for the proposed methods.

3.2 Regime-Switching Jump-Diffusion Models

In this section, we consider a regime-switching jump-diffusion model with varying coefficients to integrate the various regimes and the behavior of volatility smiles. These models explain the various phases of an economy as well as the effects of jumps in the underlying asset. We briefly present an RSJD model for an underlying asset S_τ on a filtered probability space $(\Omega,\ \mathcal{F},\ \{\mathcal{F}\}_{\tau\geq 0},\ \mathbf{P})$, in which the financial market allows us to have no arbitrage opportunities. A continuous Markov chain process $(\mathcal{X}_\tau)_{\tau\geq 0}$, is defined on a probability space $(\Omega,\ \mathcal{F},\ \mathbf{P})$, so as to take a value in a finite state space $\mathcal{H} = \{\mathfrak{e}_1, \mathfrak{e}_2, \cdots, \mathfrak{e}_Q\}$ with the following property.

$$\mathbf{P}(\mathcal{X}_{\tau+\delta\tau} = \mathfrak{e}_i | \mathcal{X}_\tau = \mathfrak{e}_j) = \begin{cases} q_{ij}\delta\tau + O(\delta\tau) & \text{for} \quad i \neq j, \\ 1 + q_{ij}\delta\tau + O(\delta\tau) & \text{for} \quad i = j, \end{cases} \tag{3.2.1}$$

for a Q-dimensional vector $\mathfrak{e}_j := \mathfrak{e}_j^i$ such that

$$\mathfrak{e}_j^i = \begin{cases} 0 \quad for \quad i \neq j, \\ 1 \quad for \quad i = j. \end{cases} \tag{3.2.2}$$

We postulate that the economy switches from one state to another state regulated by the finite state continuous time Markov chain $\mathcal{X}_\tau$ with the state space $\{1, \cdots, Q\}$.

A Markov chain process can be written as

$$d\mathcal{X}_\tau = d\mathcal{M}_\tau + \mathcal{A}\mathcal{X}_{\tau-}d\tau,$$

where $\mathcal{A} = [q_{ij}]_{Q\times Q}$ is the generator of the Markov chain $\mathcal{X}_\tau$, and $\mathcal{M}_\tau$ is a martingale.
The entry element q_{ij} satisfies the condition: If $i \neq j$, $q_{ij} \geq 0$ and $q_{jj} = -\sum_{i\neq j} q_{ij}$ for $i = 1, 2, \cdots, Q$.

The local volatility σ_τ is the function of time and space variables, and risk-free interest rate r_τ is given as $\sigma_\tau = \langle \sigma, \mathcal{X}_\tau \rangle$ and $r_\tau = \langle r, \mathcal{X}_\tau \rangle$ respectively, where $\sigma := (\sigma_1, \sigma_2, \cdots, \sigma_Q)^T$ and $r := (r_1, r_2, \cdots, r_Q)^T$ are Q dimensional vectors with $\sigma_j \geq 0$ and $r_j \geq 0$ for all $1 \leq j \leq Q$. Here, $(\cdots)^T$ reflects the matrix's transposition, and $\langle \cdot, \cdot \rangle$ specifies the dot product in $\mathbb{R}^Q$.

Suppose the underlying asset S_τ behaves according to RSJD then,

$$\frac{dS_\tau}{S_{\tau-}} = \quad (r_\tau - d_\tau - \lambda_\tau\kappa_\tau)d\tau + \eta_\tau dN_\tau + \sigma_\tau dW_\tau, \tag{3.2.3}$$

where $N_\tau := \langle \mathcal{N}_\tau \ , \ \mathcal{X}_\tau \rangle$ is a Poisson process with $\mathcal{N}_\tau := (N_\tau^1, N_\tau^2, N_\tau^3, \cdots, N_\tau^Q)^T$ and the intensity λ_τ of the Poisson process is defined as $\lambda_\tau := \langle \lambda \ , \ \mathcal{X}_\tau \rangle$ with $\lambda := (\lambda_1, \lambda_2, \lambda_3, \cdots, \lambda_Q)^T$, $d_\tau := \langle \lceil_\tau \ , \ \mathcal{X}_\tau \rangle$ is a continuous dividend with $\lceil_\tau := (d_\tau^1, d_\tau^2, d_\tau^3, \cdots, d_\tau^Q)^T$, W_τ is a Wiener process, $\eta_\tau := \langle \eta \ , \ \mathcal{X}_\tau \rangle$ with $\eta := (\eta_1, \eta_2, \eta_3, \cdots, \eta_Q)^T$ is a random variable to generate jump size from $S_{\tau -}$ to S_τ and $\kappa_\tau := \langle \kappa \ , \ \mathcal{X}_\tau \rangle$ with $\kappa := (\kappa_1, \kappa_2, \kappa_3, \cdots, \kappa_Q)^T$ with $\kappa_j = \mathbb{E}[\eta_j]$ for $1 \le j \le Q$.

In the risk-neutral RSJD model (3.2.3), the price of the European option $u(x, t, \mathfrak{e}_j)$ can be calculated by solving the following partial integro-differential equation:

$$\frac{\partial u}{\partial t}(x, t, \mathfrak{e}_j) - \mathcal{L}u(x, t, \mathfrak{e}_j) = 0, \quad (x, t, \mathfrak{e}_j) \in \mathbb{R} \times J \times \mathcal{H}, \tag{3.2.4}$$

where $J = (0, T]$ and the spatial differential operator can be defined as

$$\begin{aligned} \mathcal{L}u(x, t, \mathfrak{e}_j) \quad &= \quad \frac{1}{2}(\sigma_j(x,t))^2 \frac{\partial^2 u}{\partial x^2}(x, t, \mathfrak{e}_j) + \left(r_j - d_j - \frac{(\sigma_j(x,t))^2}{2} - \lambda_j \kappa_j \right) \frac{\partial u}{\partial x}(x, t, \mathfrak{e}_j) - (r_j + \lambda_j) u(x, t, \mathfrak{e}_j) \\ &\quad + \lambda_j \int_{-\infty}^{\infty} u(y, t, \mathfrak{e}_j) f(y - x, \mathfrak{e}_j) dy + \langle \mathbf{u_n} \ , \ \mathcal{A}\mathfrak{e}_j \rangle. \end{aligned} \tag{3.2.5}$$

The option value $u(x, t, \mathfrak{e}_j)$ at the time of maturity T is termed as the payoff function. For the European put option, the payoff function is given by:

$$v_0^j(z) = \max(K - Ke^x, 0) \tag{3.2.6}$$

with a strike price of K.

Where $x = \ln(\frac{S}{K})$ is the log asset price with respect to a strike price K and $\mathcal{L} = \mathcal{D} + \mathcal{I} + \mathcal{E}$, such that

$$\mathcal{D}u(x, t, \mathfrak{e}_j) = \frac{1}{2}(\sigma_j(x,t))^2 \frac{\partial^2 u}{\partial x^2}(x, t, \mathfrak{e}_j) + \left(r_j - d_j - \frac{(\sigma_j(x,t))^2}{2} - \lambda_j \kappa_j \right) \frac{\partial u}{\partial x}(x, t, \mathfrak{e}_j) - (r_j + \lambda_j) u(x, t, \mathfrak{e}_j), \tag{3.2.7}$$

$$\mathcal{I}u(x, t, \mathfrak{e}_j) = \lambda_j \int_{-\infty}^{\infty} u(x, t, \mathfrak{e}_j) f(y - z, \mathfrak{e}_j) dy, \tag{3.2.8}$$

$$\mathcal{E}u(x, t, \mathfrak{e}_j) = \langle \mathbf{u_n} \ , \ \mathcal{A}\mathfrak{e}_j \rangle, \tag{3.2.9}$$

where $\langle \mathbf{u_n} \ , \ \mathcal{A}\mathfrak{e}_j \rangle = \sum_{i=1}^{Q} v_n^i q_{i,j}$, $\mathbf{u_n}$ is a Q dimensional vector $\mathbf{u_n} = (u_n^1, u_n^2, u_n^3, \cdots, u_n^Q)^T$ with $u^j(x,t) = u(x, t, \mathfrak{e}_j)$, $1 \le j \le Q$ and the function $f(y, \mathfrak{e}_j)$ can be written as:

$$f(y, \mathfrak{e}_j) = \begin{cases} \frac{1}{\sqrt{2\pi}\sigma_J^j} \exp - \frac{(y - \mu_J^j)^2}{2(\sigma_J^j)^2} & \text{Merton model,} \\ p_j \eta_1^j e^{-\eta_1^j y} \mathcal{H}(y) + q_j \eta_2^j e^{-\eta_2^j y} \mathcal{H}(-y) & \text{Kou model.} \end{cases}$$

To numerically approximate the integral operator $\mathcal{I}u(x, t, \mathfrak{e}_j)$, we first split the integral into two portions on Ω and Ω^c.

The integral operator may now be divided into two parts:

$$\mathcal{I}u(x, t, \mathfrak{e}_j) = \lambda_j \int_{\Omega} u(y, t, \mathfrak{e}_j) f(y - z, \mathfrak{e}_j) dy + \mathcal{R}(x, t, \mathfrak{e}_j). \tag{3.2.10}$$

By using the asymptotic behavior of the option, the integral over Ω^c is given by

$$\mathcal{R}(x,t,\mathfrak{e}_j) := \lambda_j \int_{\Omega^c} (Ke^{-r_j t} - Ke^{y}) f(y-z,\mathfrak{e}_j) dy. \tag{3.2.11}$$

For the European put option, the $\mathcal{R}(x,t,\mathfrak{e}_j)$ is given as

$$\mathcal{R}(x,t,\mathfrak{e}_j) := \begin{cases} Ke^{-r_j t}\mathcal{N}(\frac{x_{min}-x-\mu_J^j}{\sigma_J^j}) - Ke^{x+\mu_J^j+\frac{(\sigma_J^j)^2}{2}}\mathcal{N}(\frac{x_{min}-x-\mu_J^j-(\sigma_J^j)^2}{\sigma_J^j}) & \text{Merton's model,} \\ Ke^{-r_j t}(1-p_j)e^{\eta_2^j(x_{min}-x)} - K(1-p_j)\frac{\eta_2^j}{\eta_2^j+1}e^{-\eta_2^j x+(\eta_2^j+1)x_{min}} & \text{Kou's model.} \end{cases}$$

The above expression may be rewritten as follows in the case of the American put option:

$$\mathcal{R}(x,t,\mathfrak{e}_j) := \begin{cases} K\mathcal{N}(\frac{x_{min}-x-\mu_J^j}{\sigma_J^j}) - Ke^{x+\mu_J^j+\frac{(\sigma_J^j)^2}{2}}\mathcal{N}(\frac{x_{min}-x-\mu_J^j-(\sigma_J^j)^2}{\sigma_J^j}) & \text{Merton's model,} \\ K(1-p_j)e^{\eta_2^j(x_{min}-x)} - K(1-p_j)\frac{\eta_2^j}{\eta_2^j+1}e^{-\eta_2^j x+(\eta_2^j+1)x_{min}} & \text{Kou's model,} \end{cases}$$

where $\mathcal{N}(\cdot)$ is the cumulative normal distribution.

On the other hand, the value of American option $u(x,t,\mathfrak{e}_j)$ under RSJD model address the following linear complementarity problem:

$$\begin{cases} \frac{\partial u}{\partial t}(x,t,\mathfrak{e}_j) - \mathcal{L}u(x,t,\mathfrak{e}_j) \geq 0, & (x,t,\mathfrak{e}_j) \in \mathbb{R}\times J\times\mathcal{H}, \\ u(x,t,\mathfrak{e}_j) - \Phi^j(Ke^x) \geq 0, & (x,t,\mathfrak{e}_j) \in \mathbb{R}\times J\times\mathcal{H}, \\ \left(\frac{\partial u}{\partial t}(x,t,\mathfrak{e}_j) - \mathcal{L}u(x,t,\mathfrak{e}_j)\right)\left(u(x,t,\mathfrak{e}_j) - \Phi^j(Ke^x)\right) = 0, & (x,t,\mathfrak{e}_j) \in \mathbb{R}\times J\times\mathcal{H}, \\ u_0^j(x) = \Phi^j(Ke^x), & x\in\mathbb{R}. \end{cases} \tag{3.2.12}$$

For the American put option, the payoff function is given by:

$$u_0^j(x) = \max(K - Ke^x, 0) \tag{3.2.13}$$

with a strike price of K.

For the computational purposes, the problem (3.2.4) and (3.2.12) needs to be localized on a bounded domain $\Omega := (x_L, x_R)$, with $x_L \in \mathbb{R}$ and $x_R \in \mathbb{R}$ and consider $u(x,t,\mathfrak{e}_j)$ as a solution of the localized problem (3.2.14).

$$\begin{cases} \frac{\partial u^j}{\partial t} - \mathcal{L}u^j \geq 0 & (x,t,\mathfrak{e}_j) \in \Omega\times J\times\mathcal{H}, \\ u(x,t,\mathfrak{e}_j) - \Phi^j(Ke^x) \geq 0 & (x,t,\mathfrak{e}_j) \in \Omega\times J\times\mathcal{H}, \\ (\frac{\partial u^j}{\partial t} - \mathcal{L}u^j)\left(u(x,t,\mathfrak{e}_j) - \Phi^j(Ke^x)\right) = 0 & (x,t,\mathfrak{e}_j) \in \Omega\times J\times\mathcal{H}, \\ u_0^j(x) = \Phi^j(Ke^x) & x\in\Omega, \end{cases} \tag{3.2.14}$$

We use the asymptotic behavior of the European put option to establish a boundary condition for the log price outside the domain.

$$u^j(x,t) = \begin{cases} Ke^{-r_j t} - Ke^x & : \quad x\to-\infty, \\ 0 & : \quad x\to+\infty \end{cases}$$

On the other hand, asymptotic behaviors of the American put options are

$$u^j(x,t) = \begin{cases} K - Ke^x & : \quad x \to -\infty, \\ 0 & : \quad x \to +\infty \end{cases}$$

3.3 Discretization

This section describes how to build an implicit explicit time semi-discretization known as the Crank-Nicolson Leap-Frog, Crank-Nicolson Adam-Bashforth, BDF2 methods for the following coupled PIDE on the reduced domain Ω.

$$\frac{\partial u}{\partial t}(x,t,\mathfrak{e}_j) - \mathcal{L}u(x,t,\mathfrak{e}_j) = 0, \quad (x,t,\mathfrak{e}_j) \in \mathbb{R} \times J \times \mathcal{H}, \tag{3.3.1}$$

$$u_0^j(x) = \max(K - Ke^x, 0), \tag{3.3.2}$$

$$u^j(x,t) = \begin{cases} Ke^{-r_j t} - Ke^x & : \quad x \to -\infty, \\ 0 & : \quad x \to +\infty, \end{cases} \tag{3.3.3}$$

where $\mathcal{L}$ is the integro-differential operator in (3.2.5).

3.3.1 Time Discretization

Let the system (3.3.1), be initially discretized in time with uniform grid $t_n = nk$, $n = 0, 1, 2, \ldots, N$ with uniform temporal mesh length k, with $u(x, t_n, \mathfrak{e}_j)$ abbreviated as u_n^j.

Now, we have a brief discussion about three IMEX methods for the temporal discretization of PIDE (3.3.1).

3.3.1.1 IMEX-BDF2 method

$$\frac{3u_{n+1}^j - 4u_n^j + u_{n-1}^j}{2k} = \mathcal{D}{u^j}_{n+1} + \lambda_j \mathcal{I}(\mathcal{E}_1 {u^j}_n) + \mathcal{E}(\mathcal{E}_1 u_n^j), \quad n \geq 1, \tag{3.3.4}$$

$$u_{n+1}^j(x_L) = Ke^{-r_j \tau_{n+1}} - Ke^{x_L}, \qquad u_{n+1}^j(x_R) = 0, \tag{3.3.5}$$

where, $\mathcal{E}_1 u_n^j = 2u_n^j - u_{n-1}^j$.

The suggested technique requires two starting values on the zeroth and first time levels. The model problem's starting condition gives the value u_0^j at the zeroth time level, and the value u_1^j can be evaluated by using the implicit-explicit backward difference technique of order one.

3.3.1.2 IMEX-CNAB method

$$\frac{u_{n+1}^j - u_n^j}{k} = \mathcal{D}\left(\frac{u_{n+1}^j + u_n^j}{2}\right) + \lambda_j \mathcal{I}(\mathcal{E}_2 u_n^j) + \mathcal{E}(\mathcal{E}_2 u_n^j), \quad n \geq 1, \tag{3.3.6}$$

$$u_{n+1}^j(x_L) = Ke^{-r_j t_{n+1}} - Ke^{x_L}, \qquad u_{n+1}^j(x_R) = 0, \tag{3.3.7}$$

where, $\mathcal{E}_2 u_n^j = \frac{3u_n^j - u_{n-1}^j}{2}$.

3.3.1.3 IMEX-CNLF method

$$\frac{u_{n+1}^j - u_{n-1}^j}{2k} = \mathcal{D}\left(\frac{u_{n+1}^j + u_{n-1}^j}{2}\right) + \lambda_j \mathcal{I}(u_n^j) + \mathcal{E}(u_n^j), \quad n \geq 1, \tag{3.3.8}$$

$$u_{n+1}^j(x_L) = Ke^{-r_j t_{n+1}} - Ke^{x_L}, \qquad u_{n+1}^j(x_R) = 0. \tag{3.3.9}$$

The suggested technique requires two starting values on the zeroth and first time levels. The model problem's starting condition gives the value u_0^j at the zeroth time level, and the value u_1^j can be evaluated by using the implicit-explicit backward difference technique of order one. Now, we prove the stability of all the above discussed time discretization schemes. For the stability analysis, we impose some assumptions, which are described in [2], on the variable coefficients in the PIDE (3.3.1).

(A1) Variable coefficient $\sigma_j(x,t)$ is continuous and sufficiently smooth for the analysis of the proposed methods.

(A2) There are $\underline{\sigma}_j > 0$ and $\bar{\sigma}_j > 0$ such that for all $(x, t, \mathfrak{e}_j) \in \mathbb{R} \times J \times \mathcal{H}$, $0 < \underline{\sigma}_j < \sigma_j(x,t) < \bar{\sigma}_j$.

We will frequently use the following results throughout our analysis:

$$\begin{aligned}
(\mathcal{D}U^j, U^j) &= \frac{1}{2}(\bar{\sigma}_j)^2(U_{xx}^j, U^j) + (r_j - \frac{1}{2}(\bar{\sigma}_j)^2 - \lambda_j\kappa_j)(U_x^j, U^j) - (r_j + \lambda_j)(U^j, U^j)\\
&= -\frac{(\bar{\sigma}_j)^2}{2}\left(\|U_x^j - \frac{(r_j - \frac{(\bar{\sigma}_j)^2}{2} - \lambda_j\kappa_j)}{(\bar{\sigma}_j)^2}U^j\|^2\right) + \frac{(r_j - \frac{(\bar{\sigma}_j)^2}{2} - \lambda_j\kappa_j)^2 - 2(r^j + \lambda_j)(\bar{\sigma}_j)^2}{2(\bar{\sigma}_j)^2}\|U^j\|^2\\
&\leq \frac{\left(r_j - \frac{(\bar{\sigma}_j)^2}{2} - \lambda_j\kappa_j\right)^2 - \left(2(r_j + \lambda_j)(\bar{\sigma}_j)^2\right)}{2(\bar{\sigma}_j)^2}\|U^j\|^2\\
&\leq \alpha^j\|U^j\|^2,
\end{aligned} \tag{3.3.10}$$

where $\alpha^j = |\frac{(r_j - \frac{(\bar{\sigma}_j)^2}{2} - \lambda_j\kappa_j)^2 - \left(2(r_j+\lambda_j)(\bar{\sigma}_j)^2\right)}{2(\bar{\sigma}_j)^2}|$.

We will frequently use the Young's inequality for all $a, b \in \mathbb{R}$ with ϵ^* (valid for every $\epsilon > 0$), i.e,

$$(a,b) \leq \epsilon^* a^2 + \frac{1}{4\epsilon^*}b^2, \tag{3.3.11}$$

and an identity

$$2\,(3a - 4b + c, a) = a^2 + (2a-b)^2 - b^2 - (2b-c)^2 + (a - 2b + c)^2. \tag{3.3.12}$$

We shall use the following result in analysis for all $u^j(\cdot,t) \in L^2(\Omega)$, $t \in (0,T)$ such that

$$\overline{u}^j(x,t) = \begin{cases} u^j(x,t) & : \quad (x,t) \in \Omega \times [0,T], \\ 0 & : \quad (x,t) \in \Omega^c \times [0,T]. \end{cases}$$

The integral operator $\mathcal{I}u^j$ follow the condition $\|\mathcal{I}\overline{u}^j(\cdot,t)\| \leq \mathcal{C}_I\|u^j(\cdot,t)\|$, where $\mathcal{C}_I$ is a constant that is independent of t and $\|u^j\| := \left(\int_\Omega |u^j(x)|^2 dx\right)^{\frac{1}{2}}$.

We can bound the regime-switching term $\langle \mathbf{u_n}\ ,\ \mathcal{A}\mathfrak{e}_j\rangle$ by the inequality

$$|\langle \mathbf{u_n}\ ,\ \mathcal{A}\mathfrak{e}_j\rangle| = \left|\sum_{i=1}^{Q} u_n^i q_{i,j}\right| \leq \sum_{i=1}^{Q} \max_{i=1,2,\ldots,Q} |u_n^i||q_{i,j}|.$$

Let $u_n^{i_n} := \max_{i=1,2,\ldots,Q} |u_n^i|$. Then

$$|\langle \mathbf{u_n}\ ,\ \mathcal{A}\mathfrak{e}_j\rangle| \leq \left|u_n^{i_n}\sum_{i=1}^{Q}|q_{i,j}|\right| = 2|q_{j,j}||u_n^{i_n}|.$$

Let us suppose that u_n^j be the solution of the equation (3.3.4) and $\tilde{u}_n^j$ be the solution of perturbed equation (3.3.13)

$$\frac{3\tilde{u}_{n+1}^j - 4\tilde{u}_n^j + \tilde{u}_{n-1}^j}{2k} = \mathcal{D}\tilde{u}_{n+1}^j + \lambda_j\mathcal{I}(\mathcal{E}_1\tilde{u}_n^j) + \mathcal{E}(\mathcal{E}_1\tilde{u}_n^j) + \mathcal{T}_{n+1}^j \quad n \geq 1 \tag{3.3.13}$$

together with boundary condition

$$\tilde{u}_{n+1}^j(x_L) = Ke^{-r_j t_{n+1}} - Ke^{x_L}, \qquad \tilde{u}_{n+1}^j(x_R) = 0 \tag{3.3.14}$$

The $\mathcal{T}_n^j$ is the perturbation in the data at any time level t_n in the j^{th} state of the economy and what we will examine the effect of these perturbations on the error as we proceed in time. We will show that the error at any time level is bounded by the initial errors at initial time levels (t_0 & t_1; for all discussed techniques) and is a bounded multiple of the introduced perturbations; which establishes stability in time discretization.

Now define the error term $\epsilon_n^j := \tilde{u}_n^j - u_n^j$. Since we are treating boundary conditions exactly in the equations ($3.3.4 - 3.3.5$) and perturbed equations ($3.3.13 - 3.3.14$). Hence, the error term ϵ_n^j will be zero at the boundary points. Similarly, we can get the perturbation equation for other schemes.

Theorem 3.3.1 (IMEX-BDF2)**.** *Under the assumption $k < \frac{1}{2(2\alpha^j+1+2|q_{j,j}|+\lambda_j\mathcal{C}_I)}$ the scheme is stable in the following sense:*

$$\|\epsilon_m^j\|^2 \leq C\left(\max_{i=1,2,\cdots,Q}\|\epsilon_0^i\|^2 + \max_{i=1,2,\cdots,Q}\|\epsilon_1^i\|^2 + \max_{2\leq n\leq m}\|\mathcal{T}_n^j\|^2\right), \quad \forall\ 2 \leq m \leq \frac{T}{N}, \tag{3.3.15}$$

where C is a constant that depends on the parameters C_I, r_j, σ_j, λ_j and T.

Proof. Consider the equations (3.3.4) and (3.3.13), we get,

$$\frac{3\epsilon_{n+1}^j - 4\epsilon_n^j + \epsilon_{n-1}^j}{2k} = \mathcal{D}\epsilon_{n+1}^j + \lambda_j\mathcal{I}(\mathcal{E}_1\epsilon_n^j) + \mathcal{E}(\mathcal{E}_1\epsilon_n^j) + \mathcal{T}_{n+1}^j \tag{3.3.16}$$

$$\epsilon_{n+1}^j(x_L) = 0, \qquad \epsilon_{n+1}^j(x_R) = 0 \tag{3.3.17}$$

Taking the inner product of both sides of the equation (3.3.16) with $4k\epsilon^j_{n+1}$

$$\begin{aligned}\left(\frac{3\epsilon^j_{n+1}-4\epsilon^j_n+\epsilon^j_{n-1}}{2k},4k\epsilon^j_{n+1}\right) &= \left(\mathcal{D}\epsilon^j_{n+1},4k\epsilon^j_{n+1}\right)+\left(\lambda_j\mathcal{I}(\mathcal{E}_1\epsilon^j_n),4k\epsilon^j_{n+1}\right)\\ &+\left(\mathcal{E}(\mathcal{E}_1\epsilon^j_n),4k\epsilon^j_{n+1}\right)+\left(\mathcal{T}^j_{n+1},4k\epsilon^j_{n+1}\right) \qquad (3.3.18)\end{aligned}$$

Using the identity (3.3.12) in LHS, we get

$$\begin{aligned}\|\epsilon^j_{n+1}\|^2-\|\epsilon^j_n\|^2 &+ \|2\epsilon^j_{n+1}-\epsilon^j_n\|^2-\|2\epsilon^j_n-\epsilon^j_{n-1}\|^2\\ &\le 4k(\mathcal{D}\epsilon^j_{n+1},\epsilon^j_{n+1})+4k\lambda_j(\mathcal{I}(\mathcal{E}_1\epsilon^j_n),\epsilon^j_{n+1})+\left(\mathcal{E}(\mathcal{E}_1\epsilon^j_n),4k\epsilon^j_{n+1}\right)+4k(\mathcal{T}^j_{n+1},\epsilon^j_{n+1}).\end{aligned}$$

Now the relation (3.3.10) implies,

$$\begin{aligned}\|\epsilon^j_{n+1}\|^2-\|\epsilon^j_n\|^2 &+ \|2\epsilon^j_{n+1}-\epsilon^j_n\|^2-\|2\epsilon^j_n-\epsilon^j_{n-1}\|^2\\ &\le 4k\alpha^j\|\epsilon^j_{n+1}\|^2+4k\lambda_j(\mathcal{I}(\mathcal{E}_1\epsilon^j_n),\epsilon^j_{n+1})+4k\left(\sum_{i=1}^{Q}(\mathcal{E}_1\epsilon^i_n)q_{i,j},\epsilon^j_{n+1}\right)+4k(\mathcal{T}^j_{n+1},\epsilon^j_{n+1}).\end{aligned}$$

$$\begin{aligned}\|\epsilon^j_{n+1}\|^2-\|\epsilon^j_n\|^2 &+ \|2\epsilon^j_{n+1}-\epsilon^j_n\|^2-\|2\epsilon^j_n-\epsilon^j_{n-1}\|^2\\ &\le k\left(4\alpha^j+2+4|q_{j,j}|+2\lambda_j\mathcal{C}_I\right)\|\epsilon^j_{n+1}\|^2+16k\lambda_j\mathcal{C}_I\|\epsilon^j_n\|^2+32k|q_{j,j}|\|\epsilon^{i_n}_n\|^2\\ &+8k|q_{j,j}|\|\epsilon^{i_{n-1}}_{n-1}\|^2+4k\lambda_j\mathcal{C}_I\|\epsilon^j_{n-1}\|^2+2k\|\mathcal{T}^j_{n+1}\|^2.\end{aligned}$$

Summing up the above inequality between $n=1$ to $n=m-1$, for $1\le m\le N$, we get

$$\begin{aligned}\|\epsilon^j_m\|^2-\|\epsilon^j_1\|^2 &- \|2\epsilon^j_1-\epsilon^j_0\|^2\\ &\le k(4\lambda_j\mathcal{C}_I\|\epsilon^j_0\|^2+20\lambda_j\mathcal{C}_I\|\epsilon^j_1\|^2+\left(4\alpha^j+2+4|q_{j,j}|+22\lambda_j\mathcal{C}_I\right)\sum_{n=2}^{m-1}\|\epsilon^j_n\|^2\\ &+\sum_{n=1}^{m-1}32k|q_{j,j}|\|\epsilon^{i_n}_n\|^2+\sum_{n=1}^{m-1}8k|q_{j,j}|\|\epsilon^{i_{n-1}}_{n-1}\|^2+2\sum_{n=2}^{m}\|\mathcal{T}^j_n\|^2+(4\alpha+2+2\lambda_j\mathcal{C}_I)\|\epsilon^j_m\|^2).\end{aligned}$$

Case 1. If $\epsilon^{i_n}_n:=\max_{i=1,2,\cdots,Q}|\epsilon^i_n|=\epsilon^j_n$, for $1\le n\le m$, then

$$\begin{aligned}&\|\epsilon^j_m\|^2-\|\epsilon^j_1\|^2-\|2\epsilon^j_1-\epsilon^j_0\|^2\\ &\le k(4\lambda_j\mathcal{C}_I\|\epsilon^j_0\|^2+20\lambda_j\mathcal{C}_I\|\epsilon^j_1\|^2+\left(4\alpha^j+2+44|q_{j,j}|+22\lambda_j\mathcal{C}_I\right)\sum_{n=2}^{m-1}\|\epsilon^j_n\|^2\\ &+2\sum_{n=2}^{m}\|\mathcal{T}^j_n\|^2+\left(4\alpha^j+2+4|q_{j,j}|+2\lambda_j\mathcal{C}_I\right)\|\epsilon^j_m\|^2).\end{aligned}$$

Assume that k is sufficiently small such that $\left(1-k(4\alpha^j+2+4|q_{j,j}|+2\lambda_j\mathcal{C}_I)\right)>0$ or $k<\frac{1}{(4\alpha^j+2+4|q_{j,j}|+2\lambda_j\mathcal{C}_I)}$, then above inequality implies,

$$\|\epsilon^j_m\|^2 \quad\le\quad C(\|\epsilon^j_0\|^2+\|\epsilon^j_1\|^2+k\sum_{n=2}^{m-1}\|\epsilon^j_n\|^2+k\sum_{n=2}^{m}\|\mathcal{T}^j_n\|^2)$$

$$\leq \quad C(\|\epsilon_0^j\|^2 + \|\epsilon_1^j\|^2 + k\sum_{n=2}^{m-1}\|\epsilon_n^j\|^2 + mk\max_{2\leq n\leq m}\|\mathcal{T}_n^j\|^2). \tag{3.3.19}$$

We know that $mk \leq T$, then we have

$$\|\epsilon_m^j\|^2 \leq C(\|\epsilon_0^j\|^2 + \|\epsilon_1^j\|^2 + k\sum_{n=2}^{m-1}\|\epsilon_n^j\|^2 + \max_{2\leq n\leq m}\|\mathcal{T}_n^j\|^2). \tag{3.3.20}$$

where C is a generic constant that is unaffected by the extent of the grid. The application of the discrete Gronwall's inequality is leads to the result,

$$\|\epsilon_m^j\|^2 \leq C(\|\epsilon_0^j\|^2 + \|\epsilon_1^j\|^2 + \max_{2\leq n\leq m}\|\mathcal{T}_n^j\|^2). \tag{3.3.21}$$

Case 2. If $\epsilon_n^{i_n} := \max_{i=1,2,\cdots,Q}|\epsilon_n^i| \neq \epsilon_n^j$ then $|\epsilon_0^j| < |\epsilon_0^i|, |\epsilon_1^j| < |\epsilon_1^i|$ and let us consider $\epsilon_n^i = \max\{\epsilon_1^{i_1}, \epsilon_2^{i_2}, \epsilon_3^{i_3}, \ldots, \epsilon_n^{i_n}\}$. Then we obtain

$$\begin{aligned}
&\|\epsilon_m^j\|^2 - \|\epsilon_1^j\|^2 - \|2\epsilon_1^j - \epsilon_0^j\|^2 \\
&\leq k(4\lambda^j\mathcal{C}_I\|\epsilon_0^j\|^2 + 20\lambda_j\mathcal{C}_I\|\epsilon_1^j\|^2 + \left(4\alpha^j + 2 + 4|q_{j,j}| + 22\lambda_j\mathcal{C}_I\right)\sum_{n=2}^{m-1}\|\epsilon_n^j\|^2 \\
&+ \sum_{n=1}^{m-1}32k|q_{j,j}|\|\epsilon_n^i\|^2 + \sum_{n=1}^{m-1}8k|q_{j,j}|\|\epsilon_{n-1}^i\|^2 + 2\sum_{n=2}^{m}\|\mathcal{T}_n^j\|^2 + \left(4\alpha^j + 2 + 4|q_{j,j}| + 2\lambda_j\mathcal{C}_I\right)\|\epsilon_m^j\|^2).
\end{aligned}$$

Now imagine that the k is tiny enough such that $\left(1 - k(4\alpha^j + 2 + 4|q_{j,j}| + 2\lambda_j\mathcal{C}_I)\right) > 0$ or $k < \frac{1}{(4\alpha^j+2+4|q_{j,j}|+2\lambda_j\mathcal{C}_I)}$, then above inequality implies,

$$\begin{aligned}
\|\epsilon_m^j\|^2 \quad &\leq \quad C(\|\epsilon_0^j\|^2 + \|\epsilon_1^j\|^2 + \|\epsilon_0^i\|^2 + \|\epsilon_1^i\|^2 + k\sum_{n=2}^{m-1}\|\epsilon_n^i\|^2 + 2\sum_{n=2}^{m}\|\mathcal{T}_n^j\|^2). \\
&\leq C(\|\epsilon_0^i\|^2 + \|\epsilon_1^i\|^2 + k\sum_{n=2}^{m-1}\|\epsilon_n^i\|^2 + mk\max_{2\leq n\leq m}\|\mathcal{T}_n^j\|^2).
\end{aligned} \tag{3.3.22}$$

Now, we know that the left hand side of the inequality is satisfied for all the $1 \leq j \leq Q$, since $\mathfrak{e}_j \in \mathcal{H}$, then we can write as:

$$\|\epsilon_m^i\|^2 \leq C(\|\epsilon_0^i\|^2 + \|\epsilon_1^i\|^2 + k\sum_{n=2}^{m-1}\|\epsilon_n^i\|^2 + \max_{2\leq n\leq m}\|\mathcal{T}_n^j\|^2). \tag{3.3.23}$$

The application of the discrete Gronwall's inequality (for more information, see Lemma 3.1 in [70]) is now applied, and we get,

$$\|\epsilon_m^i\|^2 \leq C(\|\epsilon_0^i\|^2 + \|\epsilon_1^i\|^2 + \max_{2\leq n\leq m}\|\mathcal{T}_n^j\|^2). \tag{3.3.24}$$

Now, from (3.3.21) and (3.3.24), we obtained the outcome (3.3.15), and this completes the proof of Theorem 3.3.1. □

Theorem 3.3.2 (IMEX-CNLF). *Under the assumption $k < \frac{1}{\beta^j}$ the scheme is stable in the following sense:*

$$\|\epsilon_m^j\|^2 \leq C\left(\max_{i=1,2,\cdots,Q}\|\epsilon_0^i\|^2 + \max_{i=1,2,\cdots,Q}\|\epsilon_1^i\|^2 + \max_{2\leq n\leq m}\|\mathcal{T}_n^j\|^2\right), \quad \forall\ 2 \leq m \leq \frac{T}{N}, \tag{3.3.25}$$

where C is a constant that depends on the parameters C_I, r_j, σ_j, λ_j and T, and $\beta_1^j = 2(\alpha^j + \lambda_j\mathcal{C}_I + 1)$, $\beta_2^j = \lambda_j\mathcal{C}_I$, $\beta_3^j = 2|q_{j,j}|$, $\beta^j = \max\{\beta_1^j, \beta_2^j, \beta_3^j\}$.

Proof. Consider the equations (3.3.5) and (3.3.9), we get,

$$\frac{\epsilon_{n+1}^j - \epsilon_{n-1}^j}{2k} = \mathcal{D}\left(\frac{\epsilon_{n+1}^j + \epsilon_{n-1}^j}{2}\right) + \lambda_j\mathcal{I}(\epsilon_n^j) + \mathcal{E}(\epsilon_n^j) + \mathcal{T}_{n+1}^j \tag{3.3.26}$$

$$\epsilon_{n+1}^j(x_L) = 0, \qquad \epsilon_{n+1}^j(x_R) = 0 \tag{3.3.27}$$

Taking the inner product of both sides of the equation (3.3.11) with $2k(\epsilon_{n+1}^j + \epsilon_{n-1}^j)$

$$\begin{aligned}\left(\frac{\epsilon_{n+1}^j - \epsilon_{n-1}^j}{2k}, 2k(\epsilon_{n+1}^j + \epsilon_{n-1}^j)\right) &= \left(\mathcal{D}\left(\frac{\epsilon_{n+1}^j + \epsilon_{n-1}^j}{2}\right), 2k(\epsilon_{n+1}^j + \epsilon_{n-1}^j)\right) \\ &+ \left(\lambda_j\mathcal{I}(\epsilon_n^j), 2k(\epsilon_{n+1}^j + \epsilon_{n-1}^j)\right) + \left(\mathcal{E}(\epsilon_n^j), 2k(\epsilon_{n+1}^j + \epsilon_{n-1}^j\right) \\ &+ \left(\mathcal{T}_{n+1}^j, 2k(\epsilon_{n+1}^j + \epsilon_{n-1}^j)\right)\end{aligned} \tag{3.3.28}$$

Simplifying the left hand side of (3.3.28), we get

$$\begin{aligned}\|\epsilon_{n+1}^j\|^2 - \|\epsilon_{n-1}^j\|^2 &= \left(\mathcal{D}\left(\frac{\epsilon_{n+1}^j + \epsilon_{n-1}^j}{2}\right), 2k(\epsilon_{n+1}^j + \epsilon_{n-1}^j)\right) + \left(\lambda_j\mathcal{I}(\epsilon_n), 2k(\epsilon_{n+1}^j + \epsilon_{n-1}^j)\right) \\ &+ \left(\mathcal{E}(\epsilon_n^j), 2k(\epsilon_{n+1}^j + \epsilon_{n-1}^j\right) + \left(\mathcal{T}_{n+1}^j, 2k(\epsilon_{n+1}^j + \epsilon_{n-1}^j)\right)\end{aligned} \tag{3.3.29}$$

Now the relation (3.3.7) implies,

$$\begin{aligned}\|\epsilon_{n+1}^j\|^2 - \|\epsilon_{n-1}^j\|^2 &\leq k\alpha^j\|\epsilon_{n+1}^j + \epsilon_{n-1}^j\|^2 + \left(\lambda_j\mathcal{I}(\epsilon_n^j), 2k(\epsilon_{n+1}^j + \epsilon_{n-1}^j)\right) \\ &+ \left(\sum_{i=1}^{Q}(\epsilon_n^i)q_{k,j}, 2k(\epsilon_{n+1}^j + \epsilon_{n-1}^j)\right) + \left(\mathcal{T}_{n+1}^j, 2k(\epsilon_{n+1}^j + \epsilon_{n-1}^j)\right)\end{aligned}$$

$$\begin{aligned}\|\epsilon_{n+1}^j\|^2 - \|\epsilon_{n-1}^j\|^2 &\leq 2k(\alpha^j + |q_{j,j}| + \lambda_j\mathcal{C}_I + 1)(\|\epsilon_{n+1}^j\|^2 + \|\epsilon_{n-1}^j\|^2) + 2k|q_{j,j}|\|\epsilon_n^{i_n}\|^2 \\ &+ k\lambda_j\mathcal{C}_I\|\epsilon_n^j\|^2 + k\|\mathcal{T}_{n+1}^j\|^2\end{aligned} \tag{3.3.30}$$

Let $\beta_1^j = 2(\alpha^j + \lambda_j\mathcal{C}_I + 1)$, $\beta_2^j = \lambda_j\mathcal{C}_I$, $\beta_3^j = 2|q_{j,j}|$ and we have choose a parameter β such that

$$\beta^j = \max\{\beta_1^j, \beta_2^j, \beta_3^j\}.$$

We have,

$$\|\epsilon_{n+1}^j\|^2 - \|\epsilon_{n-1}^j\|^2 \leq k\beta^j(\|\epsilon_{n+1}^j\|^2 + \|\epsilon_{n-1}^j\|^2 + \|\epsilon_n^j\|^2 + \|\epsilon_n^{i_n}\|^2) + k\|\mathcal{T}_{n+1}^j\|^2 \tag{3.3.31}$$

In order to maintain the generality, let's suppose that $1 \leq m \leq N$ is an integer. Then summing up the above inequality between $n = 1$ to $n = m-1$, we get

$$\begin{aligned}
&\|\epsilon_m^j\|^2 + \|\epsilon_{m-1}^j\|^2 - \|\epsilon_0^j\|^2 - \|\epsilon_1^j\|^2 \\
&\leq k\beta^j(\|\epsilon_0^j\|^2 + 2\|\epsilon_1^j\|^2 + 3\sum_{n=2}^{m-1}(\|\epsilon_n^j\|^2) + (\|\epsilon_m^j\|^2 - \|\epsilon_{m-1}^j\|^2) + \sum_{n=1}^{m-1}\|\epsilon_n^{i_n}\|^2) + k\sum_{n=1}^{m-1}\|\mathcal{T}_{n+1}^j\|^2.
\end{aligned}$$

Case 1. If $\epsilon_n^{i_n} = \max_{i=1,2,\cdots,Q}|\epsilon_n^i| = \epsilon_n^j$, for $1 \leq n \leq m$, then

$$\begin{aligned}
&\|\epsilon_m^j\|^2 + \|\epsilon_{m-1}^j\|^2 - \|\epsilon_0^j\|^2 - \|\epsilon_1^j\|^2 \\
&\leq k\beta^j(\|\epsilon_0^j\|^2 + 3\|\epsilon_1^j\|^2 + 4\sum_{n=2}^{m-1}(\|\epsilon_n^j\|^2) + (\|\epsilon_m^j\|^2 - \|\epsilon_{m-1}^j\|^2)) + k\sum_{n=1}^{m-1}\|\mathcal{T}_{n+1}^j\|^2.
\end{aligned}$$

Now imagine that the k is tiny enough such that $\left(1 - k\beta^j\right) > 0$ or $k < \frac{1}{\beta^j}$, then above inequality implies,

$$\begin{aligned}
\|\epsilon_m^j\|^2 + \|\epsilon_{m-1}^j\|^2 &\leq C(\|\epsilon_0^j\|^2 + \|\epsilon_1^j\|^2 + k\sum_{n=2}^{m-1}\|\epsilon_n^j\|^2 + k\sum_{n=2}^{m}\|\mathcal{T}_n^j\|^2) \\
&\leq C(\|\epsilon_0^j\|^2 + \|\epsilon_1^j\|^2 + k\sum_{n=2}^{m-1}\|\epsilon_n^j\|^2 + mk\max_{2\leq n\leq m}\|\mathcal{T}_n^j\|^2). \qquad (3.3.32)
\end{aligned}$$

We know that $mk \leq T$, then we have

$$\|\epsilon_m^j\|^2 \leq C(\|\epsilon_0^j\|^2 + \|\epsilon_1^j\|^2 + k\sum_{n=2}^{m-1}\|\epsilon_n^j\|^2 + \max_{2\leq n\leq m}\|\mathcal{T}_n^j\|^2), \qquad (3.3.33)$$

where C is a generic constant that is unaffected by the extent of the grid. The application of the discrete Gronwall's inequality leads to the result,

$$\|\epsilon_m^j\|^2 \leq C(\|\epsilon_0^j\|^2 + \|\epsilon_1^j\|^2 + \max_{2\leq n\leq m}\|\mathcal{T}_n^j\|^2). \qquad (3.3.34)$$

Case 2. If $\epsilon_n^{i_n} = \max_{i=1,2,\cdots,Q}|\epsilon_n^i| \neq \epsilon_n^j$, then $|\epsilon_0^j| < |\epsilon_0^i|$, $|\epsilon_1^j| < |\epsilon_1^i|$ and let us consider $\epsilon_n^i = \max\{\epsilon_1^{i_1}, \epsilon_2^{i_2}, \epsilon_3^{i_3}, ..., \epsilon_n^{i_n}\}$. Then we obtain

$$\begin{aligned}
&\|\epsilon_m^j\|^2 + \|\epsilon_{m-1}^j\|^2 - \|\epsilon_0^j\|^2 - \|\epsilon_1^j\|^2 \\
&\leq k\beta^j(\|\epsilon_0^j\|^2 + 2\|\epsilon_1^j\|^2 + 3\sum_{n=2}^{m-1}(\|\epsilon_n^j\|^2) + (\|\epsilon_m^j\|^2 - \|\epsilon_{m-1}^j\|^2) + \|\epsilon_1^i\|^2 + \sum_{n=2}^{m-1}\|\epsilon_n^i\|^2) + k\sum_{n=1}^{m-1}\|\mathcal{T}_{n+1}^j\|^2.
\end{aligned}$$

Now imagine that the k is tiny enough such that $\left(1 - k\beta^j\right) > 0$ or $k < \frac{1}{\beta^j}$, then above inequality implies,

$$\begin{aligned}
\|\epsilon_m^j\|^2 + \|\epsilon_{m-1}^j\|^2 &\leq C(\|\epsilon_0^j\|^2 + \|\epsilon_1^i\|^2 + k\sum_{n=2}^{m-1}\|\epsilon_n^i\|^2 + k\sum_{n=2}^{m}\|\mathcal{T}_n^j\|^2). \\
&\leq C(\|\epsilon_0^j\|^2 + \|\epsilon_1^i\|^2 + k\sum_{n=2}^{m-1}\|\epsilon_n^i\|^2 + mk\max_{2\leq n\leq m}\|\mathcal{T}_n^j\|^2). \qquad (3.3.35)
\end{aligned}$$

We know that $mk \leq T$, then we have,

$$\|\epsilon_m^j\|^2 \leq C(\|\epsilon_0^j\|^2 + \|\epsilon_1^i\|^2 + k\sum_{n=2}^{m-1}\|\epsilon_n^i\|^2 + \max_{2\leq n\leq m}\|\mathcal{T}_n^j\|^2), \tag{3.3.36}$$

Now, we know that the left hand side of the inequality is satisfied for all the $1 \leq j \leq Q$, since $\mathfrak{e}_j \in \mathcal{H}$, then we can right as:

$$\|\epsilon_m^i\|^2 \leq C(\|\epsilon_0^i\|^2 + \|\epsilon_1^i\|^2 + k\sum_{n=2}^{m-1}\|\epsilon_n^i\|^2 + \max_{2\leq n\leq m}\|\mathcal{T}_n^j\|^2). \tag{3.3.37}$$

The application of the discrete Gronwall's inequality is now applied, and we get,

$$\|\epsilon_m^i\|^2 \leq C(\|\epsilon_0^i\|^2 + \|\epsilon_1^i\|^2 + \max_{2\leq n\leq m}\|\mathcal{T}_n^j\|^2). \tag{3.3.38}$$

Now, from (3.3.34) and (3.3.38), we obtained the outcome (3.3.25), and this completes the proof of Theorem 3.3.2. □

Theorem 3.3.3 (IMEX-CNAB)**.** *Under the assumption $k < \frac{1}{\gamma^j}$ the scheme is stable in the following sense:*

$$\|\epsilon_m^j\|^2 \leq C\left(\max_{i=1,2,\cdots,Q}\|\epsilon_0^i\|^2 + \max_{i=1,2,\cdots,Q}\|\epsilon_1^i\|^2 + \max_{2\leq n\leq m}\|\mathcal{T}_n^j\|^2\right), \quad \forall\ 2 \leq m \leq \frac{T}{N},$$

where C is a constant that depends on the parameters C_I, r_j, σ_j, λ_j and T, and $\gamma_1^j = (2\alpha^j + 41|q_{j,j}| + 2\lambda_j\mathcal{C}_I + 2)$, $\gamma_2^j = 2(\alpha^j + k|q_{j,j}| + \frac{13}{4}\lambda_j\mathcal{C}_I + 1)$, $\gamma_3^j = \frac{\lambda_j\mathcal{C}_I}{2}$ and we have choose a parameter γ^j such that

$$\gamma^j = \max\{\gamma_1^j, \gamma_2^j, \gamma_3^j\}.$$

Proof. The proof follows the same structure as the proof of Theorem 3.3.2. □

In the following subsection, we describe the radial basis function-based finite difference technique that we use to solve the resulting temporal semi-discretized algorithm.

3.3.2 Spatial Discretization

A function $\varphi : \mathbb{R}^d \to \mathbb{R}$ is called radial provided there exists a univariate function $\phi : [0,\infty) \to \mathbb{R}$ such that $\varphi(\mathbf{x}) = \phi(\tilde{r})$, where $\tilde{r} = \|\mathbf{x}\|$ and $\|\cdot\|$ is some norm on $\mathbb{R}^d$.

These functions can be broadly classified into two classes: infinitely smooth and piecewise smooth radial basis functions. Classical choices of RBF are given in Table 1.1 with their order, where for any $\mathbf{x} \in \mathbb{R}$, the symbol $\lceil\mathbf{x}\rceil$ denotes as usual the smallest integer greater than or equal to $\mathbf{x}$.

The Gaussian and inverse multiquadric are positive definite functions, whereas thin plate spline and multiquadric are conditionally positive definite functions of order $s > 0$. In this section, we briefly discuss the implementation of the local radial basis function based finite difference scheme because, as we pointed out in the introduction, the proposed numerical scheme uses the radial basis function meshless method for spatial discretization.

Let $\Omega_{\mathfrak{M}} := \{\mathbf{x}_1, \mathbf{x}_2, \ldots, \mathbf{x}_{\mathfrak{M}}\}$ be a set of arbitrary discrete points in the domain Ω then using local RBF-FD based method, any linear differential operator $\mathscr{L}$ at any arbitrary node $\mathbf{x}_i \in \Omega_{\mathfrak{M}}$ can be approximated locally as follows:

$$\mathscr{L}v(\mathbf{x}_i) = \sum_{j=1}^{m_i} \omega_j v(\mathbf{x}_j), \tag{3.3.39}$$

where ω_j are the unknown differential weights, and $m_i(<< \mathfrak{M})$ is the stencil size in the sub-domain $\Omega_i \subset \Omega$ containing the approximation point $\mathbf{x}_i$. Note that, the set Ω_i precisely contain closest m_i nodes of $\Omega_{\mathfrak{M}}$ in the neighbourhood of $\mathbf{x}_i$. One of the main components in the approximation of $\mathscr{L}v(\mathbf{x}_i)$ by means of expression (3.3.39) is the computation of integral weight ω_j as it depends on the approximation point $\mathbf{x}_i$. In the traditional finite difference method, generally, the discretization points are equally spaced, and the weights ω_j are calculated efficiently by the use of conventional polynomial interpolation. However, unlike the classical finite difference scheme, in the radial basis function method, the underline interpolation strategy is not constrained by the uniform distribution of discretization points and can be incorporated seamlessly even for the randomly distributed nodes. The RBF interpolation strategy that we have used for the approximation of integral weight ω_j is described in what follows.

Let $\hat{v}(\mathbf{x})$ stand for the RBF interpolant, which takes the input function $v(\mathbf{x})$ and interpolates it at the points $\{\mathbf{x}_i\}_{i=1}^{m_i}$ in the sub-domain Ω_i. Then, we can express $\hat{v}(\mathbf{x})$ as

$$\hat{v}(\mathbf{x}) = \sum_{j=1}^{m_i} \ell_j \phi(\|\mathbf{x} - \mathbf{x}_j\|) + \sum_{j=1}^{l} \gamma_j p_j(\mathbf{x}), \tag{3.3.40}$$

where $\|\cdot\|$ represents the Euclidian norm and $\{p_j(x)\}_{j=1}^{l}$ denote basis of $\prod_{s-1}^{d}$, which is space of d-variate polynomials of total degree $\leq s-1$, where s is the order of radial basis function ϕ.
By enforcing the following interpolation and orthogonality constraints, the coefficients ℓ_j and γ_j utilized in equation (3.3.40) can be obtained;

$$\hat{v}(\mathbf{x}_i) = v(\mathbf{x}_i),\ 1 \leq i \leq m_i, \tag{3.3.41}$$

$$\sum_{j=1}^{m_i} \ell_j p_k(\mathbf{x}_j) = 0, \qquad 1 \leq k \leq l. \tag{3.3.42}$$

Now, all the unknowns in the (3.3.40) can be obtained by solving the following linear system,

$$\begin{bmatrix} \Psi & \mathscr{P} \\ \mathscr{P}^{\mathsf{T}} & O \end{bmatrix} \begin{bmatrix} \ell \\ \gamma \end{bmatrix} = \begin{bmatrix} v\,|_{\Omega_i} \\ O \end{bmatrix}, \tag{3.3.43}$$

where $\Psi := (\phi_{ij})_{1\leq i,j\leq m_i} := (\phi\|\mathbf{x}_i - \mathbf{x}_j\|)_{1\leq i,j\leq m_i} \in \mathbb{R}^{m_i\times m_i}$, $\mathscr{P} := (p_j(\mathbf{x}_i))_{1\leq i\leq m_i, 1\leq j\leq l} \in \mathbb{R}^{m_i\times l}$.

We can compute the differential weights w_j used in the equation by forcing the linear combination (3.3.39) to be accurate for RBFs $\{\phi(\|\mathbf{x}-\mathbf{x}_i\|)\}_{i=1}^{m_i}$, centred at each of the grid assessment points in sub-domain Ω_i. Therefore, the weights are derived by solving the following linear system using RBFs and polynomials up to degree l.

$$\begin{bmatrix} \Psi & \mathscr{P} \\ \mathscr{P}^{\intercal} & O \end{bmatrix} \begin{bmatrix} \omega \\ u \end{bmatrix} = \begin{bmatrix} [\mathscr{L}\phi(\|\mathbf{x}_i-\mathbf{x}_j\|)_{j=1}^{m_i}]^{\intercal} \\ [\mathscr{L}p_j(\mathbf{x}_i)_{j=1}^{l}]^{\intercal} \end{bmatrix} \tag{3.3.44}$$

it is crucial to know that the equation on the right (3.3.44) is simply,

$$[\mathscr{L}\phi(\|\mathbf{x}_i-\mathbf{x}_1\|)\ \mathscr{L}\phi(\|\mathbf{x}_i-\mathbf{x}_2\|)\ldots\mathscr{L}\phi(\|\mathbf{x}_i-\mathbf{x}_{m_i}\|)\mid \mathscr{L}p_1(\mathbf{x}_i)\ \mathscr{L}p_2(\mathbf{x}_i)\ldots\mathscr{L}p_l(\mathbf{x}_i)]^{\intercal}.$$

It is easy to see that the linear system (3.3.44) is significantly smaller than the global RBF collocation system (size $\mathfrak{M}+l$) since its size is just m_i+l. Therefore, it offers an equation system that is more reliable and productive.

3.3.3 Operator Splitting Methods for American Option

The RBF based IMEX technique described in the preceding part can be adapted to solve LCP (3.2.8) for American option problems using the operator splitting method introduced by the Ikonen and Toivanen [64] for determining the American put option. The primary idea behind the introduction of the operator splitting method is to derive an expression with the help of an additional variable ψ^j such that $\psi^j = u_t^j - \mathcal{L}u^j$. We can reformulate LCP (3.2.14) as:

$$\begin{cases} \frac{\partial u^j}{\partial t} - \mathcal{L}u^j &= \psi^j, \\ (u(x,t,\mathfrak{e}_j) - \Phi^j(Ke^x))\cdot\psi^j &= 0, \\ u(x,t,\mathfrak{e}_j) - \Phi^j(Ke^x) &\geq 0, \\ \psi^j &\geq 0, \end{cases} \tag{3.3.45}$$

in the region $\Omega \times J \times \mathcal{H}$.

3.3.3.1 IMEX-BDF2-OS Method

Let us assume that the values $\{u_n^j, \psi_n^j\}$ and $\{u_{n-1}^j, \psi_{n-1}^j\}$ are a priory known at the points t_n and t_{n-1}. Now, we perform the two sub-steps at discrete point t_{n+1}, in first step, we compute an intermediate value $\tilde{u}_{n+1}^j$ using the following BVP

$$\begin{cases} \frac{1}{k}\left(\frac{3}{2}\tilde{u}_{n+1}^j - 2u_n^j + \frac{1}{2}u_{n-1}^j\right) - \mathcal{D}\tilde{u}_{n+1}^j - \lambda_j\mathcal{I}(\mathcal{E}_1u_n^j) - \mathcal{E}(\mathcal{E}_1u_n^j) = \psi_n^j, \\ \tilde{u}_{n+1}^j(x_L) = K, \qquad \tilde{u}_{n+1}^j(x_R) = 0, \end{cases} \tag{3.3.46}$$

where $\mathcal{E}_1u_n^j = 2u_n^j - u_{n-1}^j$.

Now, the operator splitting method's second step is to project the $\tilde{u}^j_{n+1}$ on constraint space to obtain u^j_{n+1} with the following correction terms

$$\begin{cases} \frac{3}{2}\frac{u^j_{n+1}-\tilde{u}^j_{n+1}}{k} &= \psi^j_{n+1} - \psi^j_n, \\ u^j_{n+1} &\geq \Phi^j, \\ \psi^j_{n+1} &\geq 0, \\ \psi^j_{n+1}(u^j_{n+1} - \Phi^j) &= 0. \end{cases} \tag{3.3.47}$$

Now by solving the problems (3.3.47), in $(u^j_{n+1}, \psi^j_{n+1})$ plane, we get

$$(u^j_{n+1}, \psi^j_{n+1}) = \begin{cases} (\Phi^j, \psi^j_n + \frac{3}{2}\frac{\Phi^j - \tilde{u}^j_{n+1}}{k}) & \text{if} \quad \tilde{u}^j_{n+1} - \frac{2k}{3}\psi^j_n \leq \Phi^j, \\ (\tilde{u}^j_{n+1} - \frac{2k}{3}\psi^j_n, 0) & \text{otherwise.} \end{cases} \tag{3.3.48}$$

Thus, the first step may be completed by solving a discrete equation (3.3.46), and the second step can be performed by using the updating formula (3.3.48). The value on the previous two-time levels is required by the implicit approach with three-time levels described above. Using initial condition and assigning value $\psi^j_0 = 0$, the pair (u^j_0, ψ^j_0) on the zeroth time level may be obtained. Alternatively, the algorithm described in [83] can be used. We may utilize the IMEX-BDF1-OS approach to determine the pair (u^j_1, ψ^j_1) at the first level.

3.3.3.2 IMEX-CNLF-OS method

Following the previous procedure, for this case in the first step, we compute the intermediate value $\tilde{u}_{n+1}$ from the equations

$$\left(\frac{\tilde{u}^j_{n+1} - u^j_{n-1}}{2k}\right) = \mathcal{D}\left(\frac{\tilde{u}^j_{n+1} + u^j_{n-1}}{2}\right) + \lambda_j \mathcal{I} u^j_n + \mathcal{E}(u^j_n) + \psi^j_n. \tag{3.3.49}$$

Similarly, from previous steps, we use this intermediate solution in the second step to obtain u^j_{n+1} with the following correction:

$$\begin{cases} \frac{u^j_{n+1}-\tilde{u}^j_{n+1}}{2k} &= \psi^j_{n+1} - \psi^j_n, \\ \psi^j_{n+1}(u^j_{n+1} - \Phi^j) &= 0, \\ u^j_{n+1} &\geq \Phi^j, \\ \psi^j_{n+1} &\geq 0. \end{cases} \tag{3.3.50}$$

Now we will update $(u^j_{n+1}, \psi^j_{n+1})$, with

$$(u^j_{n+1}, \psi^j_{n+1}) = \begin{cases} (\Phi^j, \psi^j_n + \frac{\Phi^j - \tilde{u}^j_{n+1}}{2k}) & \text{if}\, \tilde{u}^j_{n+1} - 2k\psi^j_n \leq \Phi^j, \\ (\tilde{u}^j_{n+1} - 2k\psi^j_n, 0) & \text{otherwise.} \end{cases} \tag{3.3.51}$$

Since the above operator splitting scheme is a three steps scheme, for computing the first step (u^j_1, ψ^j_1), we can use BDF1-OS method.

3.3.3.3 IMEX-CNAB-OS method

Now, we find an expression for the CNAB discretization. Following the previous procedure, the two sub-steps are performed at t_{n+1}. In the first step, we compute the intermediate value $\tilde{u}_{n+1}$ from the equations

$$\left(\frac{\tilde{u}^j_{n+1} - u^j_n}{k}\right) = \mathcal{D}\left(\frac{\tilde{u}^j_{n+1} + u^j_n}{2}\right) + \lambda_j \mathcal{I}(\mathcal{E}_2 u^j_n) + \mathcal{E}(\mathcal{E}_2 u^j_n) + \psi^j_n. \tag{3.3.52}$$

Similarly, from previous steps, we use this intermediate solution in the second step to obtain u^j_{n+1} with the following correction:

$$\begin{cases} \frac{u^j_{n+1} - \tilde{u}^j_{n+1}}{k} &= \psi^j_{n+1} - \psi^j_n, \\ \psi^j_{n+1}(u^j_{n+1} - \Phi^j) &= 0, \\ u^j_{n+1} &\geq \Phi^j, \\ \psi^j_{n+1} &\geq 0. \end{cases} \tag{3.3.53}$$

Finally, in the second step, we can solve in $(u^j_{n+1}, \psi^j_{n+1})$ plane, with the adaptation of

$$(u^j_{n+1}, \psi^j_{n+1}) = \begin{cases} (\Phi^j, \psi^j_n + \frac{\Phi^j - \tilde{u}^j_{n+1}}{k}) & \text{if } \tilde{u}^j_{n+1} - k\psi^j_n \leq \Phi^j, \\ (\tilde{u}^j_{n+1} - k\psi^j_n, 0) & \text{otherwise.} \end{cases} \tag{3.3.54}$$

Since the IMEX-CNAB operator splitting scheme is a three steps scheme, for computing the first step (u^j_1, ψ^j_1) we can use BDF1-OS method.

3.4 Numerical Discussion

In the present section, we provide ample numerical examples and scrutinize the convergence behavior of the discussed methods (BDF2, CNLF, CNAB) for pricing European and American put options under Kou and Merton regime-switching jump-diffusion models with variable coefficients. To compute the differential operator, we use the thin plate spline ($\tilde{r}^4 \ln \tilde{r}$) radial basis functions with the second-degree space augmented polynomial ($\prod_2 := \{1, x, x^2\}$). To discretize the integral term (3.3.2) on truncated domain Ω, we used the composite trapezoidal rule. We applied the Fast Fourier Transformation algorithm [5, 83] to compute the product of a dense matrix and a column vector in the discrete integral operator. To confront the inequality constraints in the LCP, we applied the three IMEX approaches in collaboration with the operator splitting method. Each of the three computational strategies is intended to prevent the use of fixed point iteration techniques for each economic condition and time step. The first two stages of all numerical experiments are computed using the IMEX-BDF1 technique, and an equispaced grid with $m_i = 3$ is employed. We used MATLAB R2022b on a PC with Processor Intel(R) Core(TM) i5-10500 CPU @ 3.10GHz, 3096 Mhz, 6 Core(s), 12 Logical Processor(s) and 16.00GB RAM.

In our numerical simulation, three economic states are used to examine the pricing of the European and American put options under the regime-switching Merton and Kou model with variable coefficients. We exhibit the option value and pointwise errors at various asset prices $S = 90, 100, 110$ of the corresponding numerical technique with M spatial discretization points and N temporal discretization points, and all the results are shown in the second state of the economy of the three states extended RSJD model. Using the double mesh methodology, we approximate the pointwise errors, and we used the piecewise cubic Hermite interpolation to analyze the price of the European and American put option at non-mesh points in the computational domain $\Omega := [-2, 2]$.

First, we perform the numerical experiments for IMEX-BDF2, IMEX-CNLF, and IMEX-CNAB schemes under the three states regime-switching jump-diffusion model, and the parameter values for the three states RSJD model used in the simulations are,

$$r = \begin{bmatrix} 0.05 \\ 0.05 \\ 0.05 \end{bmatrix}, \quad d = \begin{bmatrix} 0.00 \\ 0.00 \\ 0.00 \end{bmatrix}, \quad \sigma = \begin{bmatrix} \sigma_1 \\ \sigma_2 \\ \sigma_3 \end{bmatrix}, \quad \mathcal{A} = \begin{bmatrix} -0.8 & 0.6 & 0.2 \\ 0.2 & -1.0 & 0.8 \\ 0.1 & 0.3 & -0.4 \end{bmatrix}, \quad \lambda = \begin{bmatrix} 0.3 \\ 0.5 \\ 0.7 \end{bmatrix}. \tag{3.4.1}$$

Since volatility is an important factor in investing decisions, modeling and forecasting volatility are of paramount importance for market practitioners. In order to price derivative securities, financial institutions need to forecast stock price volatility. The volatility smile phenomenon is best explained by local volatility models, which define volatilities as a deterministic function of current stock prices and time. In [75], Kim and Lee explained the challenges of constant and Local volatility and then addressed the numerical and theoretical treatments for these challenges. For the generalized Black-Scholes equation, Kim [76] provides a mathematical approach for the reliable and precise construction of a local volatility surface. To perform numerical simulation, we have taken three local volatility functions for all three states of the RSJD model to describe the effects of local volatility surfaces in option pricing,

$$\sigma_1(x,t) = 0.25 + 0.35(0.5 + 3(T-t))\frac{(\frac{Ke^x}{100} - 1.5)^2}{((\frac{Ke^x}{100})^2 + 1.7)}, \tag{3.4.2}$$

$$\sigma_2(x,t) = 0.15 + 0.15(0.5 + 2(T-t))\frac{(\frac{Ke^x}{100} - 0.5)^2}{((\frac{Ke^x}{100})^2 + 1.44)}, \tag{3.4.3}$$

$$\sigma_3(x,t) = 1.9x^2 - 0.5x + (0.7x - 0.2)(T-t) + 0.35, \tag{3.4.4}$$

these local volatility surfaces also used in [85], and all three volatility surfaces are shown in Figure 3.1. The Kou [79] and Merton model [96] are the two jump-diffusion models most prominently adopted for pricing option value. We begin by taking into account the Merton model, where suitable parameters are given by:

$$\sigma_J = \begin{bmatrix} 0.35 \\ 0.45 \\ 0.55 \end{bmatrix}, \quad \mu_J = \begin{bmatrix} -0.95 \\ -0.90 \\ -0.85 \end{bmatrix}, \quad T = 0.25, \quad K = 100. \tag{3.4.5}$$

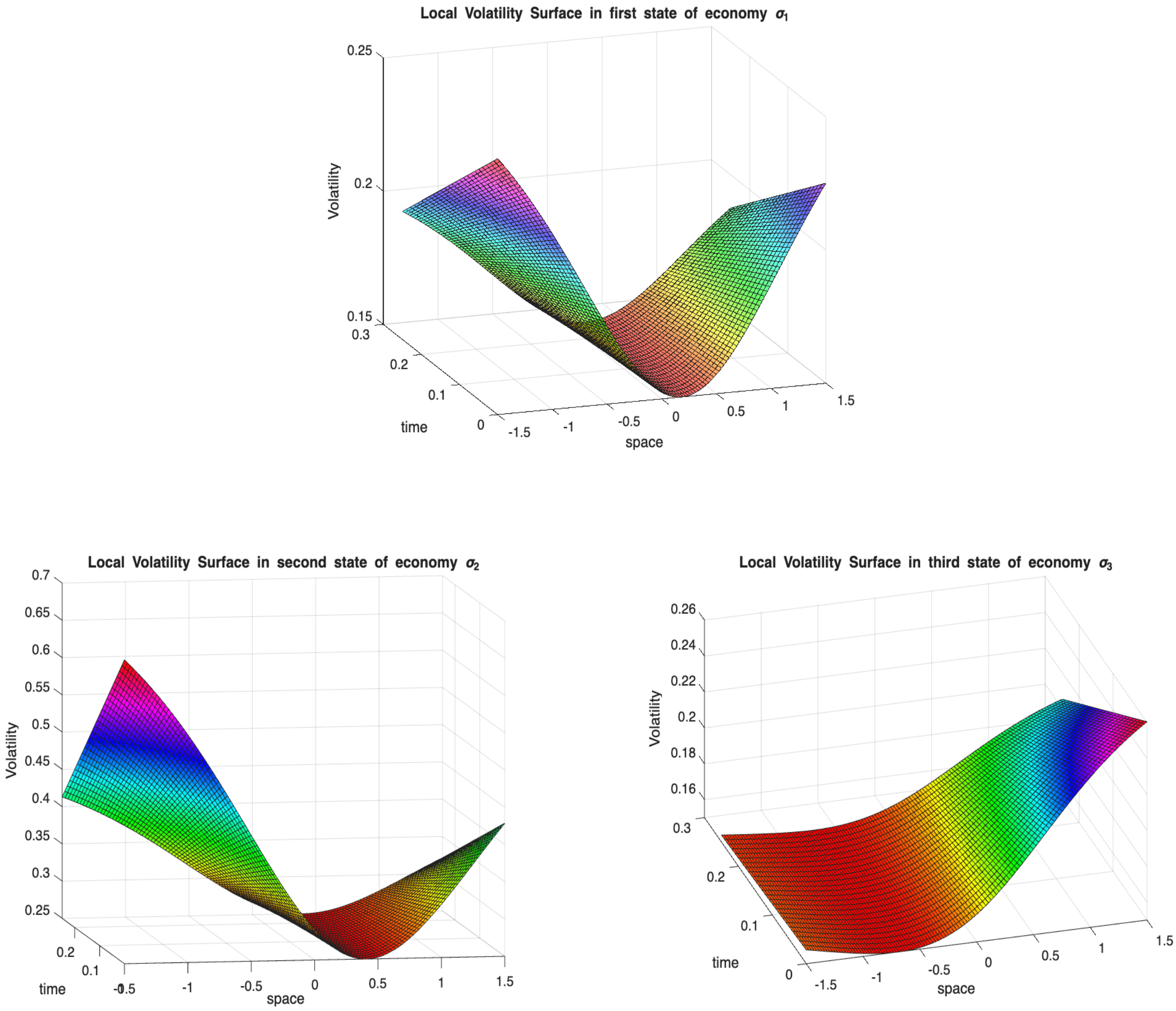

Figure 3.1: Local volatility surfaces for all three regimes.

and for the Kou model, we have taken the parameters:

$$\eta_1 = \begin{bmatrix} 3 \\ 3 \\ 3 \end{bmatrix}, \quad \eta_2 = \begin{bmatrix} 2 \\ 2 \\ 2 \end{bmatrix}, \quad T = 0.25, \quad K = 100, \quad p = \begin{bmatrix} 0.5 \\ 0.5 \\ 0.5 \end{bmatrix}. \tag{3.4.6}$$

3.4.1 European Option

In the first numerical simulation, we presented the results for pricing the European put option under Merton's jump-diffusion model. We showed the option value and error at different asset prices for IMEX-BDF2, IMEX-CNLF, and IMEX-CNAB methods under Merton's model and data are reported in Table 3.1. We can observe that the convergence rate reached its asymptotic order when the temporal mesh length is sufficiently small. We have shown that all the proposed methods have approximate second order accuracy with different values of M and N. We have also shown the European put option value for IMEX-BDF2, IMEX-CNLF, and IMEX-CNAB methods in Figure 3.2 (left) for Merton model, and the graphs show that there is little to no erratic movement in option values close to the strike price.

We performed the same simulation for Kou's model using the IMEX-BDF2, IMEX-CNLF, and IMEX-

Table 3.1: Numerical results for European put option under Merton's three state regime-switching jump-diffusion model with variable coeficients.

			$S = 90$		$S = 100$		$S = 110$	
Method	M	N	Value	Error	Value	Error	Value	Error
BDF2	50	25	11.245178	-	6.933952	-	5.877318	-
	100	50	11.008158	2.3702e-01	7.020822	8.6870e-02	5.924514	4.7197e-02
	200	100	10.970135	3.8022e-02	7.057014	3.6192e-02	5.931524	7.0101e-03
	400	200	10.960003	1.0132e-02	7.066011	8.9974e-03	5.933501	1.9765e-03
	800	400	10.957772	2.2312e-03	7.068246	2.2344e-03	5.933970	4.6940e-04
CNLF	50	25	11.244921	-	6.934132	-	5.877298	-
	100	50	11.008804	2.3612e-01	7.020976	8.6844e-02	5.924257	4.6959e-02
	200	100	10.970437	3.8366e-02	7.057152	3.6176e-02	5.931431	7.1742e-03
	400	200	10.960151	1.0287e-02	7.066096	8.9441e-03	5.933464	2.0324e-03
	800	400	10.957845	2.3056e-03	7.068292	2.1961e-03	5.933954	4.9042e-04
CNAB	50	25	11.243306	-	6.930666	-	5.874136	-
	100	50	11.005483	2.3782e-01	7.017840	8.7174e-02	5.921904	4.7768e-02
	200	100	10.967008	3.8475e-02	7.054201	3.6360e-02	5.929076	7.1716e-03
	400	200	10.956717	1.0291e-02	7.063219	9.0186e-03	5.931101	2.0254e-03
	800	400	10.954428	2.2893e-03	7.065446	2.2273e-03	5.931586	4.8523e-04

CNAB methods in the same lineup. The numerical results are shown in Table 3.2, and we can observe that the errors are decreasing with a ratio of about four for all of the suggested approaches. As seen in Table 3.2, the discretization methods converge with approximately second-order precision in time. In Figure 3.2 (right), we illustrated the values of the European put options for Kou model.

Next, we use the above defined parameters of Kou's model for the IMEX-BDF2 technique to select a fine enough spatial mesh length, $h = 1/2^{10}$, such that time discretization dominates the errors. In the second stage of the economy of three states RSJD model, we demonstrated the temporal convergence order of the RBF based IMEX-BDF2 strategy for various values of N. The data are presented in Table 3.3. From Table 3.3, we can observe that the convergence rate of the proposed method reached its asymptotic order when the temporal mesh length sufficiently small (viz. $k = \frac{1}{2^7}$).

We have also exhibited the option value, error, and spatial convergence order of all proposed methods with the CPU time (in seconds) at various asset prices in the second stage of the economy in Table 3.4

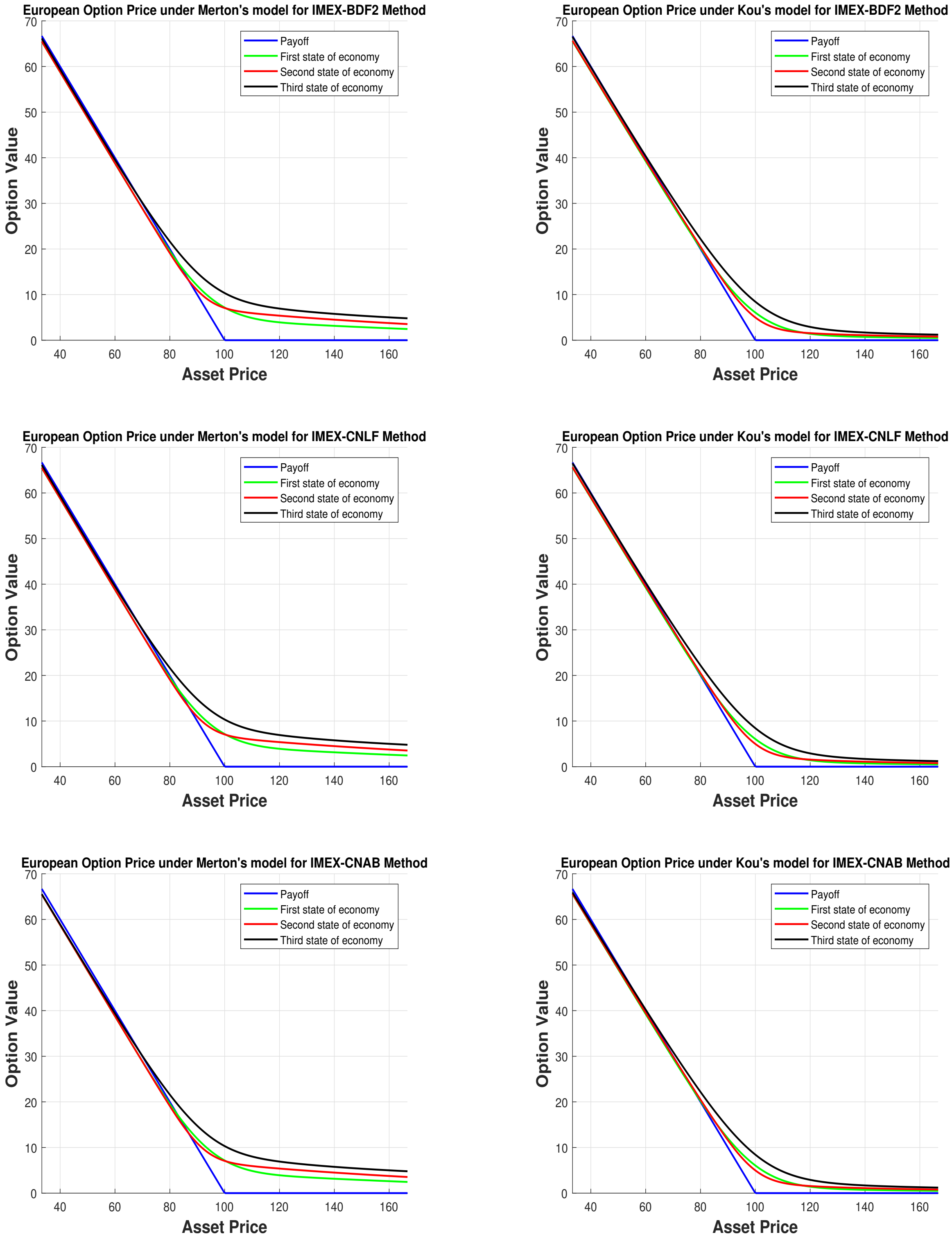

Figure 3.2: European put option value under three-state regime-switching jump-diffusion model with variable coefficients.

Table 3.2: Numerical results for European put option under Kou's three state regime-switching jump-diffusion model with variable coefficients.

			$S = 90$		$S = 100$		$S = 110$	
Method	M	N	Value	Error	Value	Error	Value	Error
BDF2	50	25	11.689794	-	5.051800	-	2.354535	-
	100	50	11.607938	8.1856e-02	4.987953	6.3846e-02	2.284626	6.9909e-02
	200	100	11.592725	1.5213e-02	4.984897	3.0560e-03	2.271090	1.3535e-02
	400	200	11.587811	4.9142e-03	4.984540	3.5737e-04	2.267141	3.9489e-03
	800	400	11.586681	1.1298e-03	4.984469	7.0640e-05	2.266242	8.9926e-04
CNLF	50	25	11.691574	-	5.053947	-	2.356302	-
	100	50	11.608842	8.2732e-02	4.988829	6.5119e-02	2.285473	7.0829e-02
	200	100	11.593212	1.5630e-02	4.985423	3.4069e-03	2.271552	1.3920e-02
	400	200	11.588063	5.1493e-03	4.984825	5.9724e-04	2.267382	4.1696e-03
	800	400	11.586809	1.2538e-03	4.984618	2.0757e-04	2.266365	1.0172e-03
CNAB	50	25	11.689570	-	5.050809	-	2.354549	-
	100	50	11.607579	8.1991e-02	4.987409	6.3400e-02	2.284543	7.0006e-02
	200	100	11.592145	1.5434e-02	4.984450	2.9596e-03	2.270819	1.3725e-02
	400	200	11.587108	5.0371e-03	4.984044	4.0550e-04	2.266760	4.0590e-03
	800	400	11.585915	1.1932e-03	4.983923	1.2089e-04	2.265801	9.5823e-04

Table 3.3: Numerical results for the temporal convergence order of RBF-BDF2 for pricing European option under kou's RSJD model with a fixed $M = 1024$.

		$S = 90$			$S = 100$			$S = 110$		
$k=\frac{1}{2^l}$	Value	Error	order	Value	Error	order	Value	Error	order	CPU Time
l=1	12.314884	-	-	5.846382	-	-	3.364397	-	-	0.163169
l=2	11.225824	1.089059e+00	-	3.982386	1.863995e+00	-	1.850260	1.514137e+00	-	0.166911
l=3	11.462359	2.365353e-01	2.2029	4.699346	7.169596e-01	1.3784	2.116495	2.662354e-01	2.5077	0.406020
l=4	11.546211	8.385175e-02	1.4961	4.923372	2.240264e-01	1.6782	2.217345	1.008493e-01	1.4005	0.818643
l=5	11.575821	2.960961e-02	1.5017	4.970056	4.668350e-02	2.2626	2.253394	3.604994e-02	1.4841	1.488376
l=6	11.583974	8.153356e-03	1.8605	4.980816	1.075962e-02	2.1172	2.263086	9.691343e-03	1.8952	2.925509
l=7	11.585915	1.940341e-03	2.0710	4.983541	2.725175e-03	1.9812	2.265386	2.300204e-03	2.0749	5.715759
l=8	11.586382	4.674953e-04	2.0532	4.984232	6.908606e-04	1.9798	2.265945	5.585278e-04	2.0420	11.364792
l=9	11.586496	1.144254e-04	2.0305	4.984406	1.743147e-04	1.9867	2.266082	1.375358e-04	2.0218	22.796509
l=10	11.586525	2.827664e-05	2.0167	4.984450	4.380926e-05	1.9923	2.266116	3.411314e-05	2.0114	45.944449
l=11	11.586532	7.026064e-06	2.0088	4.984461	1.098319e-05	1.9959	2.266125	8.493536e-06	2.0058	93.989520

using the above defined parameters of Merton's model with a fixed $N = 512$. It's demonstrated that all proposed methods are second-order convergent in spatial dimension.

From a computational perspective, the efficiency of the proposed IMEX schemes is primarily governed by the solution of the sparse linear systems arising from the RBF–FD spatial discretization at each time level. Since all schemes employ the same spatial discretization, the observed differences in CPU time are mainly attributable to the temporal integration strategy. The numerical results presented in Table 3.4 show that the IMEX-BDF2 scheme consistently requires less CPU time than the IMEX-CNLF and

Table 3.4: Numerical results for the spatial convergence order of all the proposed methods for pricing European option under Merton model with a fixed $N = 512$.

		$S=90$			$S=100$			$S=110$			
	M	Value	Error	order	Value	Error	order	Value	Error	order	CPU Time
BDF2	32	23.559360	-	-	20.662187	-	-	18.546241	-	-	0.128288
	64	23.612237	7.2473e-02	-	20.723654	5.1786e-02	-	18.594220	3.0677e-02	-	0.275653
	128	23.624984	1.5890e-02	2.1892	20.737036	1.1231e-02	2.2050	18.603088	3.4876e-03	3.1368	1.185904
	256	23.627679	3.0493e-03	2.3816	20.740241	2.7288e-03	2.0411	18.605151	7.6914e-04	2.1809	4.253184
	512	23.628387	8.3198e-04	1.8738	20.741031	6.7538e-04	2.0145	18.605657	1.8472e-04	2.0578	21.784663
	1024	23.628558	1.9848e-04	2.0675	20.741227	1.6805e-04	2.0067	18.605783	4.5617e-05	2.0177	91.669085
CNLF	32	21.597424	-	-	19.450693	-	-	17.909388	-	-	0.152058
	64	21.816733	2.1930e-01	-	19.625694	1.7500e-01	-	17.954515	4.5127e-02	-	0.265641
	128	21.866324	4.9590e-02	2.1448	19.649530	2.3836e-02	2.8761	17.958302	3.7872e-03	3.5747	1.297801
	256	21.877473	1.1149e-02	2.1531	19.654903	5.3731e-03	2.1493	17.959392	1.0903e-03	1.7963	4.739584
	512	21.880189	2.7159e-03	2.0373	19.656226	1.3224e-03	2.0225	17.959675	2.8315e-04	1.9451	24.190640
	1024	21.880870	6.8088e-04	1.9959	19.656561	3.3502e-04	1.9808	17.959752	7.7035e-05	1.8779	100.709713
CNAB	32	17.159722	-	-	12.331639	-	-	9.124172	-	-	0.167202
	64	17.056482	1.0323e-01	-	12.229500	1.0213e-01	-	9.008812	1.1535e-01	-	0.327920
	128	17.030091	2.6391e-02	1.9678	12.210377	1.9122e-02	2.4171	8.989653	1.9159e-02	2.5900	1.594833
	256	17.022327	7.7634e-03	1.7653	12.205892	4.4851e-03	2.0920	8.984925	4.7276e-03	2.0188	5.585655
	512	17.020580	1.7477e-03	2.1511	12.204796	1.0964e-03	2.0323	8.983783	1.1420e-03	2.0494	28.440750
	1024	17.020131	4.4855e-04	1.9621	12.20452	2.7036e-04	2.0197	8.983502	2.8077e-04	2.0241	116.358402

IMEX-CNAB schemes while maintaining comparable or superior accuracy. This improved efficiency can be attributed to the favorable stability properties of the BDF2 formulation, which allow accurate solutions to be obtained with reduced computational effort. Although IMEX-CNLF and IMEX-CNAB are straightforward to implement, their overall execution times are slightly higher for the problems considered. However, the lower CPU time of IMEX-BDF2, combined with its second-order temporal accuracy and robust performance, makes it particularly attractive for option pricing applications involving stiff PDEs and PIDEs.

We have also plotted the Gamma & Delta for European option, in Figure 3.3. For the Delta & Gamma, we used the above defined parameters for Kou's model at $N = 512$ and $M = 1024$ and plotted the curves at all economic stages under the three-states RSJD model with variable coefficients.

In Table 3.5, we showed the Errors at different values of M and N using the parameters of [85] and compared our computational results with Table 1 of [85]. From Table 3.5, we can observe our proposed method is giving better results than Lee [85].

Further, we took the large values for the intensity of the Poisson process λ and showed the convergence order of the BDF2 method for Merton's jump-diffusion model using the parameters of [85]. We took $\lambda_j = 10$ and $\lambda_j = 25$ and showed that the method is second-order convergent in time even if we choose the larger value of λ. In Table 3.6, we showed the option value, error, and temporal convergence order of the IMEX-BDF2 method with the CPU time (in seconds) at different asset prices in the third stage of the economy.

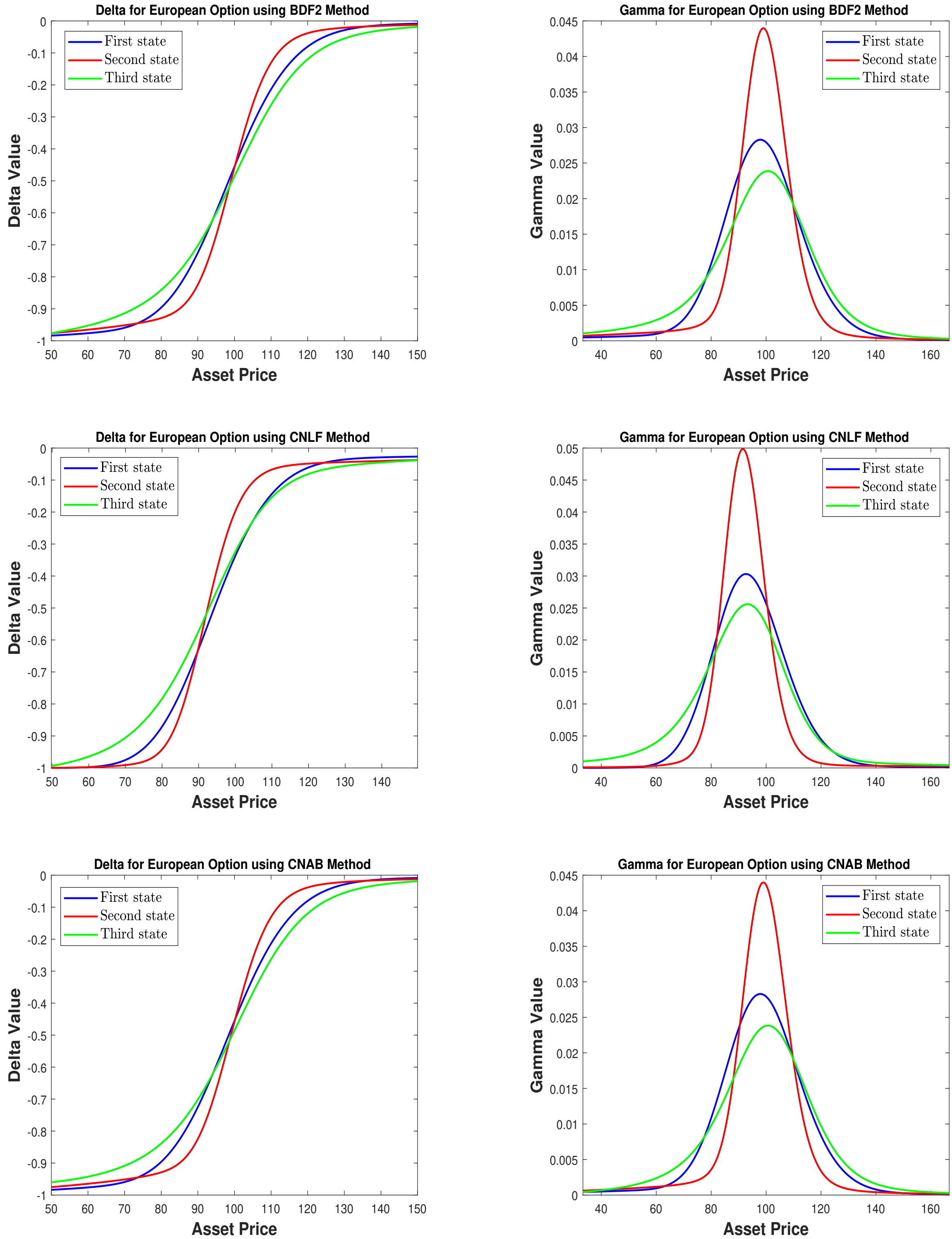

Figure 3.3: Under the three-states RSJD model with variable coefficients, European put option Delta (left) and Gamma (right) curves at all economic stages at $N = 512$ and $M = 1024$.

Table 3.5: Comparison of numerical errors for pricing European option with Table 1 of Lee [85].

		$S = 90$		$S = 100$		$S = 110$	
M	N	Lee [85]	Present Method	Lee [85]	Present Method	Lee [85]	Present Method
64	50	0.159998	0.063262	0.502315	0.056211	0.236599	0.045502
128	100	0.054960	0.016795	0.109948	0.002254	0.064131	0.002825
256	200	0.014193	0.005868	0.026055	0.001711	0.016214	0.000796
512	400	0.003569	0.000788	0.006443	0.000772	0.004063	0.000410
1024	800	0.000893	0.000070	0.001607	0.000354	0.001016	0.000183
2048	1600	0.000223	0.000070	0.000401	0.000168	0.000254	0.000084

Table 3.6: Numerical results for pricing European option using IMEX-BDF2 method for different values of λ with the parameters in [85].

			$S = 90$			$S = 100$			$S = 110$		
	N	Value	Error	order	Value	Error	order	Value	Error	order	CPU Time
	16	43.808411	-	-	41.122927	-	-	38.789901	-	-	2.834413
	32	43.948454	1.4004e-01	-	41.254108	1.3118e-01	-	38.915125	1.2522e-01	-	5.708413
$\lambda_j = 10$	64	43.979449	3.0994e-02	2.1757	41.283951	2.9842e-02	2.1361	38.944867	2.9741e-02	2.0739	11.647500
	128	43.986908	7.4594e-03	2.0548	41.291241	7.2900e-03	2.0333	38.952211	7.3437e-03	2.0179	22.591865
	256	43.988746	1.8372e-03	2.0215	41.293046	1.8051e-03	2.0138	38.954037	1.8255e-03	2.0081	45.695432
	16	61.544549	-	-	59.649727	-	-	57.913504	-	-	2.901904
	32	61.662526	1.1797e-01	-	59.763357	1.1363e-01	-	58.023232	1.0972e-01	-	5.493071
$\lambda_j = 25$	64	61.688508	2.5981e-02	2.1829	59.788241	2.4883e-02	2.1910	58.046774	2.3542e-02	2.2206	11.081254
	128	61.694636	6.1278e-03	2.0840	59.794123	5.8823e-03	2.0807	58.052382	5.6073e-03	2.0698	22.079019
	256	61.696143	1.5068e-03	2.0238	59.795574	1.4502e-03	2.0200	58.053767	1.3857e-03	2.0166	44.646502

3.4.2 American Option

For pricing such American options, authors in [116] combine an operator splitting approach with the dynamic least-squares approximation, and the author of [85] put forward the three-time level IMEX approach combined with the OS technique. We executed the same simulation for RBF-FD based IMEX-BDF2, IMEX-CNLF, and IMEX-CNAB methods combined with the operator splitting method for pricing the American option under Merton's and Kou's regime-switching jump-diffusion model with variable volatility. The proposed techniques with three-time levels joined by the operator splitting method result in a linear system at each time step that can be readily solved using LU decomposition without fixed point repetition. We presented the option value and error at different values of M and N for both the Merton and Kou models in Table 3.7 and Table 3.8 respectively.

From Table 3.7 and Table 3.8, we can observe that the pointwise errors for the American put option are decreasing with the ratio of approximately four. So, all the proposed methods are converging with approximate second order accuracy in time. We have shown the option values for the Merton and Kou models in Figure 3.4.

Table 3.7: Numerical results for American put option under Merton's three-state regime-switching jump-diffusion model with variable coefficients.

			$S = 90$		$S = 100$		$S = 110$	
Method	M	N	Value	Error	Value	Error	Value	Error
BDF2	50	25	11.354228	-	6.999497	-	5.942431	-
	100	50	11.188430	1.6579e-01	7.094424	9.4926e-02	5.990659	4.8229e-02
	200	100	11.183625	4.8052e-03	7.135321	4.0897e-02	5.998173	7.5141e-03
	400	200	11.184654	1.0290e-03	7.146444	1.1123e-02	6.000374	2.2003e-03
	800	400	11.185629	9.7480e-04	7.149409	2.9656e-03	6.000924	5.5038e-04
CNLF	50	25	11.354592	-	7.001242	-	5.943791	-
	100	50	11.188702	1.6589e-01	7.095136	9.3895e-02	5.991010	4.7219e-02
	200	100	11.183928	4.7745e-03	7.135723	4.0587e-02	5.998389	7.3794e-03
	400	200	11.184826	8.9819e-04	7.146653	1.0930e-02	6.000490	2.1013e-03
	800	400	11.185738	9.1173e-04	7.149522	2.8691e-03	6.000985	4.9464e-04
CNAB	50	25	11.354449	-	6.999679	-	5.942138	-
	100	50	11.188571	1.6588e-01	7.094453	9.4774e-02	5.990710	4.8572e-02
	200	100	11.183706	4.8655e-03	7.135391	4.0938e-02	5.998241	7.5317e-03
	400	200	11.184702	9.9600e-04	7.146510	1.1119e-02	6.000420	2.1784e-03
	800	400	11.185656	9.5376e-04	7.149450	2.9400e-03	6.000950	5.3042e-04

Determining the early exercise boundary is the most crucial aspect of the American put option, and Figure 3.5 shows these curves for all economic conditions. For the sensitivity analysis, we have taken above defined parameters for Merton model with $N = 256$ and $M = 400$ and different values of $\lambda_j = 0.1,\ 0.5,\ 1.0,\ 1.5,\ 2.0$, and showed the effects of the intensity of the Poisson process λ on the early exercise boundary for American put option in all three states of the economy of three states RSJD model with variable coefficients. In Table 3.9, we showed the errors at different asset prices using the parameters given in [85] for pricing the American put option, and results are compared with Table 3 of Lee [85]. From Table 3.9, we observed that although both methods achieved a second order convergence rate in time, but the proposed method provides a better result than Lee [85].

3.5 Conclusion

In this chapter, we presented the RBF based three IMEX finite difference methods, namely, BDF2, CNLF, and CNAB, for solving the PIDEs that come out when an underlying asset exhibits behavior consistent with the extended regime-switching jump diffusion method. An RBF based finite difference method is used to solve the linear differential equations that come from the temporal semi-discretization of the governing

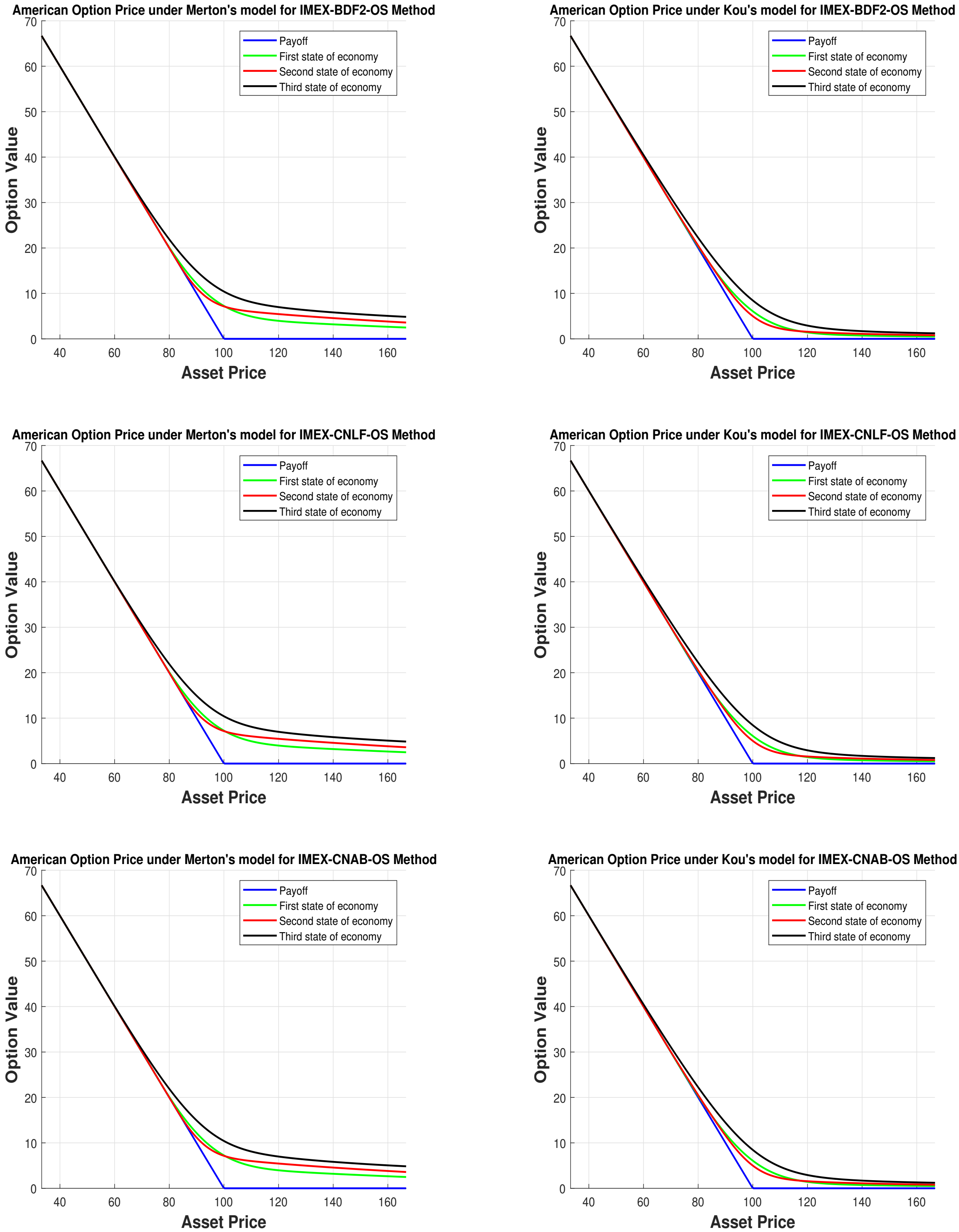

Figure 3.4: American put option value under three-state regime-switching jump-diffusion model with variable coefficients.

Table 3.8: Numerical results for American put option under Kou's three state regime-switching jump-diffusion model with variable coefficients.

			$S = 90$		$S = 100$		$S = 110$	
Method	M	N	Value	Error	Value	Error	Value	Error
BDF2	50	25	11.704588	-	5.063014	-	2.363686	-
	100	50	11.623311	8.1277e-02	4.999502	6.3511e-02	2.294042	6.9644e-02
	200	100	11.608237	1.5074e-02	4.996537	2.9655e-03	2.280573	1.3469e-02
	400	200	11.603358	4.8788e-03	4.996202	3.3478e-04	2.276641	3.9311e-03
	800	400	11.602236	1.1218e-03	4.996137	6.5202e-05	2.275746	8.9504e-04
CNLF	50	25	11.706839	-	5.065485	-	2.365711	-
	100	50	11.624426	8.2413e-02	5.000507	6.4978e-02	2.294989	7.0721e-02
	200	100	11.608826	1.5600e-02	4.997123	3.3837e-03	2.281082	1.3907e-02
	400	200	11.603659	5.1667e-03	4.996516	6.0710e-04	2.276905	4.1772e-03
	800	400	11.602388	1.2712e-03	4.996299	2.1738e-04	2.275880	1.0248e-03
CNAB	50	25	11.705389	-	5.062765	-	2.364301	-
	100	50	11.623883	8.1505e-02	4.999635	6.3130e-02	2.294510	6.9791e-02
	200	100	11.608535	1.5348e-02	4.996732	2.9032e-03	2.280825	1.3685e-02
	400	200	11.603509	5.0262e-03	4.996334	3.9804e-04	2.276772	4.0529e-03
	800	400	11.602312	1.1970e-03	4.996211	1.2248e-04	2.275813	9.5945e-04

Table 3.9: Comparison of numerical errors for pricing American option with Table 3 of Lee [85].

		$S = 90$		$S = 100$		$S = 110$	
M	N	Lee [85]	Present Method	Lee [85]	Present Method	Lee [85]	Present Method
64	50	0.180968	0.059502	0.468914	0.068911	0.223403	0.035978
128	100	0.049768	0.018486	0.100028	0.004249	0.058720	0.005140
256	200	0.012693	0.007057	0.023656	0.002164	0.014867	0.001053
512	400	0.003183	0.001223	0.005848	0.000677	0.003729	0.000429
1024	800	0.000796	0.000312	0.001458	0.000199	0.000933	0.000138
2048	1600	0.000199	0.000077	0.000364	0.000052	0.000233	0.000038

equation, and a composite trapezoidal method is used to calculate the integral term involved in PIDE. We applied the IMEX-BDF2, IMEX-CNLF, and IMEX-CNAB techniques joined with the operator splitting method to handle the inequality restrictions in the LCP for pricing American option; it produces a linear system at each time step that can be easily solved by LU decomposition without the use of fixed-point iteration. The numerical experiments with European and American put options are performed using the Merton and Kou model with local volatility. The numerical results demonstrate that the suggested techniques are precise and effective. The option value, error, and some Greeks (Delta & Gamma) can be precisely estimated using the suggested techniques.

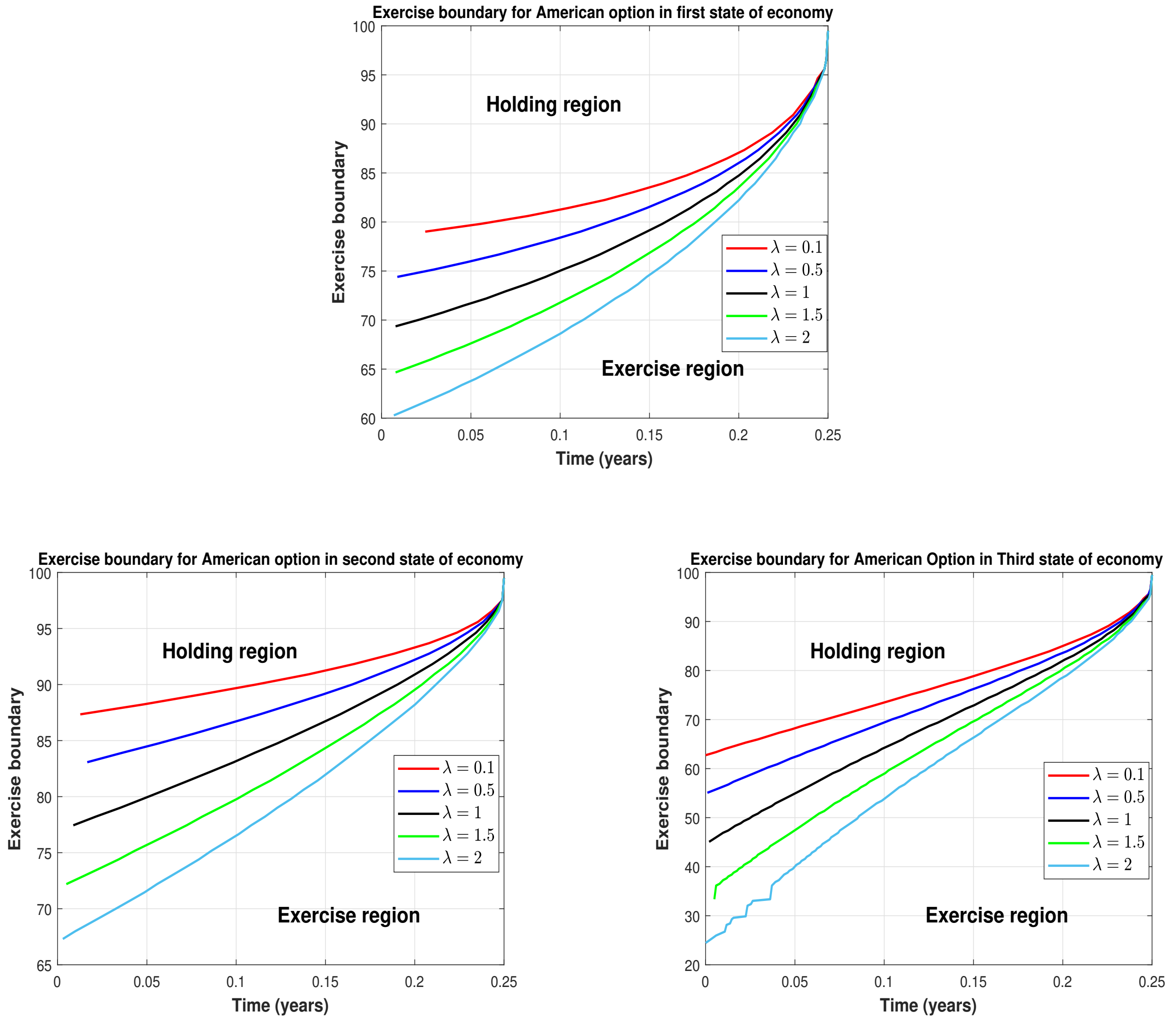

Figure 3.5: Using the operator splitting method in conjunction with the RBF-FD based IMEX-CNLF method, the early exercise boundary curves for the American put option were derived under the regime-switching Merton model with variable coefficients at $N = 256$ and $M = 400$.

CHAPTER 4

Radial basis function-based finite difference schemes for pricing Asian options under a regime-switching jump diffusion model [1]

This chapter delves into the construction of RBF-FD implicit-explicit difference temporal semi-discretization schemes for solving a moving boundary partial integro-differential equation system governing regime-switching jump-diffusion for Asian option pricing.

4.1 Introduction

Asian options are a kind of financial derivative whose payoff is dependent on the average price of the underlying asset over a given time period rather than only on the asset's price at maturity. Investors and traders prefer these options since they assist to minimize the impact of market manipulation on the underlying asset near expiration. Pricing Asian options, therefore, presents major difficulties as the distribution of the average asset price is usually not analytically tractable, especially under the typically assumed geometric Brownian motion model. Though difficult, Asian options are crucial tools in financial markets as they provide clear benefits for both speculative methods and risk management. Consequently, several computational techniques have been introduced to precisely price these derivatives such as Monte Carlo simulation techniques suggested by Broadie et al. [19] and Kemna and Vorst [74], dimension reduction methods presented by Vecer [125], and perturbation techniques developed by Zhang [142]. All of these

[1] The results discussed in this chapter have been published in *Engineering Analysis with Boundary Elements* , 97, 645-685 (2025). https://doi.org/10.1016/j.enganabound.2025.106400.

studies fall within the Black-Scholes paradigm. The BS model, while widely used, is recognised to have a number of flaws, including inconsistent implied volatility smiles (or skews) with market observations. The literature has proposed several BS model adaptations to provide more accurate representations of asset price movements. Specifically, the implied volatility grin (smirk) empirical behaviour has been taken into account by extending the BS model. The two most often used extensions are jump-diffusions and regime-switching models.

Adding a finite-state Markov chain to the GBM model is one method of adding more unpredictability to the BS model; these models are known as Markovian regime-switching models [55]. Regime-switching models are able to better capture changes in macro-market conditions while maintaining some degree of model simplicity. This is accomplished by permitting the model parameters, including volatility, rate of return, interest rate, and dividend rate, to assume varying values across distinct regimes. Furthermore, as shown by Yao et al. [139], regime-switching models may produce implied volatility smiles that are often seen in empirical research. A handful of studies, including Boyle and Draviam [16], Yuen and Yang [141] have addressed the valuation of Asian options within regime-switching frameworks, despite the extensive literature available on the pricing of European and American options under similar models.

Adding jumps to the GBM is a significant additional approach for BS model expansions, as shown in [96]. Compared to the standard BS model, there is comparatively less published research on pricing Asian options under a jump diffusion framework. The partial integro-differential equation may be directly solved using a semi-Lagrangian method as demonstrated in [41] and by Vecer and Xu [126], who provide a representation for Asian options inside semi-martingale frameworks through the analysis of the PIDE. The method suggested in [11] builds upon the work of Vecer and Xu [126] by creating a series of functions that converge uniformly to option price.

The pricing of Asian options using RSJD models that incorporate both regime-switching and jump-diffusions, is the primary emphasis of this work. We draw attention to the two pertinent gaps in the body of literature that served as the inspiration for this effort. First and foremost, the literature on pricing options under RSJD models is restricted to European and American options despite the fact that there has been a lot of interest in applying these models to a wide range of financial challenges. Examples include modeling electricity prices [130], short rates [117], portfolio selection [145], and option pricing [31, 110]. Second, it is unrealistic to assume that the Markov chain is independent of Brownian motion as is often done in the literature on Markovian RS models, particularly when it comes to options that are based on significant indexes like the S&P 500. To be more precise, this assumption means that although the asset price may be affected by the regime transition, the asset price itself has no bearing on how quickly or slowly the regime changes. This independence assumption is not feasible for options written on large indexes, even if it seems reasonable for options written on individual stocks because we may assume that the price movement of the specific stock has no effect on the market as a whole. This is due to the possibility that the index itself may serve as an indication of market conditions in this instance, necessitating consideration of the index's impact on the market as a whole. This is the reason why it is extremely desirable to loosen the independence assumption indicated above and allow the regime-switching to depend on the underlying asset process whenever pricing options written on key indexes under a regime-switching model. For a thorough examination of this novel and significant class of stochastic models, we direct the reader to the most current work by Yin and Zhu [90].

In this chapter, we provide two finite difference techniques based on RBF that preserve the positivity of the solution to the differential issue. We concentrate on the numerical solution of a moving boundary PIDE system governing RSJD model for pricing Asian option. Since radial basis function mesh-free methods provide spectral convergence for smooth solutions in complicated geometry, they are often used in the solution of partial differential equations. There is no spectrum convergence with RBF-FD. Nevertheless, spectral convergence can only be attained by RBF when applied throughout the whole domain, notwithstanding potential stability issues. In this regard, Li *et al.*[87] expanded the concept to solve the system of PDE emerging in options pricing under the RS model, and Haghi *et al.*[52] provided an RBF-FD approach for American options under the JD models. While Rad *et al.*[109] proposed an interpolation technique utilising radial basis functions to predict the price of options, Bastani *et al.*[9] developed a radial basis collocation method. Kadalbajoo *et al.*[67, 69, 70] investigated the effectiveness of the meshfree technique in solving one and high-dimensional option pricing issues using the local radial basis function. Shirzadi *et al.*[114, 115] proposed a mesh-free moving least-squares approach for jump-diffusion models, which resulted in an optimal uniform error estimates for pricing. Under the local volatility jump-diffusion framework, we have developed the RBF-FD based IMEX methods for pricing options [135]. A hybrid RBF-FD solution combining Gaussian and multiquadric functions has recently been provided by [3] to solve high-dimensional PDE for multi-asset options utilising parabolic time-dependent models. [38, 100, 116, 136] and references therein include further mesh-free work on option pricing. For more on the IMEX methods one can see [22, 70, 71, 73, 86, 112, 127, 129].

The purpose of this chapter is to provide stability estimates and the RBF-FD based BDF2 and CNLF temporal semi-discretization methods for pricing Asian options in a Markovian regime-switching jump-diffusion framework.

The rest of the chapter is structured as follows. First, we define the Markovian regime-switching jump-diffusion model and discuss the fundamental terms, symbols, and premises that will be utilised in this work. We also discuss how the moving-boundary PIDE is derived and its associated characteristics. We describe the RBF-FD based discretization methods and provide a stability analysis of the provided schemes in Section 4.3. The spatial discretization is shown in Section 4.4. To validate the theoretical results, numerical experiments for pricing Asian options are demonstrated in Section 4.5.

4.2 RSJD Model For Asian Option

In accordance with the regime-switching jump-diffusion model, this study focuses on the aforementioned subject matter. It is assumed, in accordance with risk-neutral measures, that the underlying asset S_τ adheres to the RSJD model:

$$\frac{dS_\tau}{S_\tau} = (r(\rho(\tau)) - d(\rho(\tau)) - \lambda(\rho(\tau))\kappa(\rho(\tau)))d\tau + \eta(\rho(\tau) - 1)dN_\tau + \sigma(\rho(\tau))dW_\tau, \tag{4.2.1}$$

Let (W_τ) indicate a standard Brownian motion, and let $(\rho(\tau))$ represent a continuous-time Markov chain with a finite state space $\{\mathfrak{e}_1, \mathfrak{e}_2, \ldots, \mathfrak{e}_q\}$. We suppose for any state $\rho(\tau) = \mathfrak{e}_j$, with $j \in Q = \{1, 2, \ldots, q\}$, that the interest rate $r(\mathfrak{e}_j) = r_j$, the dividend yield $d(\mathfrak{e}_j) = d_j$, and the volatility $\sigma(\mathfrak{e}_j) = \sigma_j$ are all non-negative constants. In addition, we consider a Poisson jump process N_τ characterized by the following parameters: the jump intensity is given by $\lambda(\mathfrak{e}_j) = \lambda_j > 0$, the jump amplitude is $\eta(\mathfrak{e}_j) - 1 = \eta_j - 1$, and the expected value of the jump size is $\kappa(\mathfrak{e}_j) = \kappa_j = \mathbb{E}[\eta_j - 1]$. The random variable η_j is defined here as $\eta_j = e^{Y(\mathfrak{e}_j)} = e^{Y_j}$, where Y_j is the logarithmic jump size. For each $j \in Q$, the random variables Y_j are considered to be independent and follow Gaussian distributions.

$$f(y; \mathfrak{e}_j) = \frac{1}{\sqrt{2\pi}\sigma_J^j} \exp\left(-\frac{(y - \mu_J^j)^2}{2(\sigma_J^j)^2}\right), \tag{4.2.2}$$

using the constants $j > 0$ and μ_j for $j \in Q$ as the variables. Utilize the notation $A = (a_{jl})_{j,l\in Q}$ to represent the generation matrix of the Markov chain mechanism. This matrix is characterised by constant entries that satisfy the condition $a_{jl} > 0$ for $j \neq l \in Q$ and $j, l \in Q$, and $\sum_{l=1}^{q} a_{jl} = 0$ for $j \in Q$. In conclusion, let us assert that the variables $\rho(\tau)$, W_τ, and N_τ are independent under certain conditions.

Provide

$$A_\tau = \int_0^\tau S_l dl \tag{4.2.3}$$

So, the Asian option's price that's based on the continuous arithmetical average is given by

$$U(S_\tau, A_\tau, \tau; \mathfrak{e}_j) = e^{-r_j(T-\tau)}\mathbb{E}_\tau[\max(A_T/T - K, 0)], \quad j \in Q, \tag{4.2.4}$$

In this context, $\mathbb{E}_\tau$ denotes the conditional expectation at present time τ, with T signifying the expiry date and K representing the strike price.

As per [35, 93], the value $U(S, A, \tau; \mathfrak{e}_j)$, including the dummy variables S and A, conforms to the subsequent PIDE setup,

$$\frac{\partial U}{\partial \tau}(S_\tau, A_\tau, \tau; \mathfrak{e}_j) + \mathcal{L}U(S_\tau, A_\tau, \tau; \mathfrak{e}_j) = 0, \quad j \in Q. \tag{4.2.5}$$

The spatial differential operator is defined as

$$\mathcal{L}U(S_\tau, A_\tau, \tau; \mathfrak{e}_j) = \frac{1}{2}\sigma_j^2 S^2 \frac{\partial^2 U}{\partial S^2}(S_\tau, A_\tau, \tau; \mathfrak{e}_j) + (r_j - d_j - \lambda_j\kappa_j)\frac{\partial U}{\partial S}(S_\tau, A_\tau, \tau; \mathfrak{e}_j)$$

$$
\begin{aligned}
&-(r_j+\lambda_j-a_{jj})U(S_\tau,A_\tau,\tau;\mathfrak{e}_j)+S\frac{\partial U}{\partial A}(S_\tau,A_\tau,\tau;\mathfrak{e}_j)\\
&+\lambda_j\int_{-\infty}^{\infty}U(e^yS_\tau,A_\tau,\tau;j)f(y;\mathfrak{e}_j)dy+\sum_{l=1}^{l=d}a_{jl}U(S_\tau,A_\tau,\tau;l),
\end{aligned}
\tag{4.2.6}
$$

where the boundary condition $U(S,-\infty,\tau;\mathfrak{e}_j)=0$ for $j\in Q$ and $U(S,A,T;\mathfrak{e}_j)=\max(A/T-K,0)$ is the terminal condition that determines the boundary of the set. In order to effectively address the issue, Ma and Wang [93] have identified an accurate solution for system (4.2.6) in the area where $A\geq KT$ for any $t\leq T$.

$$
U(S,A,\tau;\mathfrak{e}_j)=(\frac{A}{T}-K)e^{-r_j(T-\tau)}+\frac{S}{(d_j-r_j)T}(e^{-r_j(T-\tau)}-e^{-d_j(T-\tau)}),\quad j\in Q, \tag{4.2.7}
$$

afterwards, by performing the change of variables, for each $j\in Q$,

$$
z=\frac{T-t}{T}+\frac{K-A/T}{S},\quad V(z,t;\mathfrak{e}_j)=\frac{U(S,A,\tau;\mathfrak{e}_j)}{S},\tau=T-t,\quad j\in Q. \tag{4.2.8}
$$

Therefore, the solution (4.2.7) may be interpreted as

$$
V(z,t;\mathfrak{e}_j)=-(z-\frac{T-t}{T})e^{-r_jt}+\frac{1}{(d_j-r_j)T}(e^{-r_jt}-e^{-d_jt}),\quad z\in(-\infty,\frac{T-t}{T}], \tag{4.2.9}
$$

and for $j\in Q$, the PIDE system (4.2.6) has been transformed as a one-dimensional PIDE system's moving boundary problem, which describes the following:

$$
\begin{aligned}
\frac{\partial V}{\partial t}(z,t;\mathfrak{e}_j)\quad-\quad&\frac{1}{2}\sigma_j^2(z-\frac{T-t}{T})^2\frac{\partial^2 V}{\partial z^2}(z,t;\mathfrak{e}_j)+(r_j-d_j-\lambda_j\kappa_j)\,(z-\frac{T-t}{T})\frac{\partial V}{\partial z}(z,t;\mathfrak{e}_j)\\
&+(d_j+\lambda_j+\lambda_j\kappa_j-a_{jj})V(z,t;\mathfrak{e}_j)-\lambda_j\int_{-\infty}^{\infty}e^yV\left(\frac{(z-\frac{T-t}{T})}{e^y}+\frac{T-t}{T},t;\mathfrak{e}_j\right)f(y;\mathfrak{e}_j)dy\\
&-\sum_{l=1}^{l=d}a_{jl}V(z,t;l)=0,\quad z\in(\frac{T-t}{T},\infty),\quad t\in(0,T]
\end{aligned}
\tag{4.2.10}
$$

using the following starting and stopping conditions,

$$
V(z,0;\mathfrak{e}_j)=0,\quad z\in[1,\infty), \tag{4.2.11}
$$

$$
V(\frac{T-t}{T},t;\mathfrak{e}_j)=\frac{1}{(d_j-r_j)T}(e^{-r_jt}-e^{-d_jt}),\quad t\in(0,T], \tag{4.2.12}
$$

$$
V(+\infty,t;\mathfrak{e}_j)=0,\quad z\in[1,\infty). \tag{4.2.13}
$$

4.2.1 IMEX Methods

A finite interval $\Omega_T=\left[\frac{T-t}{T},Z\right]$ is created by truncating the semi-infinite domain $\left[\frac{T-t}{T},+\infty\right)$ for computational efficiency. Z is a well-determined cutoff such that the option value satisfies $V(Z,t;\mathfrak{e}_j)\approx 0$. This presumption guarantees that the numerical solution is minimally affected by the boundary at Z. Next, a change of variables is performed to make the analysis and calculation easier, as follows:

$$x = \ln\left(\frac{z - \frac{T-t}{T}}{Z - \frac{T-t}{T}}\right)$$

and denoting $u(x,t;\mathfrak{e}_j) = V(\frac{T-t}{T} + e^x(Z - \frac{T-t}{T}), t; \mathfrak{e}_j)$, we can transform the system (4.2.10) into

$$\frac{\partial u(x,t;\mathfrak{e}_j)}{\partial t} = \mathcal{D}u(x,t;\mathfrak{e}_j) + \mathcal{I}u(x,t;\mathfrak{e}_j) + \mathcal{E}u(x,t;\mathfrak{e}_j), \; x \in (-\infty, 0], \; t \in (0,T], \tag{4.2.14}$$

where,

$$\begin{aligned}\mathcal{D}u(x,t;\mathfrak{e}_j) &= \frac{\sigma_j^2}{2}\frac{\partial^2 u(x,t;\mathfrak{e}_j)}{\partial x^2} + \left(\frac{e^x - 1}{Te^x}\frac{1}{Z - \frac{T-t}{T}} - r_j - \frac{\sigma_j^2}{2} + d_j + \lambda_j\alpha_j\right)\frac{\partial u(x,t;\mathfrak{e}_j)}{\partial x} \\ &\quad -(\lambda_j + d_j + \lambda_j\alpha_j - a_{jj})u(x,t;\mathfrak{e}_j),\end{aligned} \tag{4.2.15}$$

$$\mathcal{I}u(x,t;\mathfrak{e}_j) = \lambda_j \int_{-\infty}^{\infty} e^y u(x-y,t;\mathfrak{e}_j) f(y;\mathfrak{e}_j)dy, \tag{4.2.16}$$

$$\mathcal{E}u(x,t;\mathfrak{e}_j) = \sum_{l=1, l\neq j}^{d} a_{jl}u(x,t;l), \tag{4.2.17}$$

subject to the following initial points

$$u(x,0;\mathfrak{e}_j) = 0, \quad x \in (-\infty, 0], \tag{4.2.18}$$

and the final points

$$u(-\infty,t;\mathfrak{e}_j) = \frac{1}{(d_j - r_j)T}(e^{-r_j t} - e^{-d_j t}), \quad t \in (0,T], \tag{4.2.19}$$

$$u(0,t;\mathfrak{e}_j) = 0, \quad t \in (0,T]. \tag{4.2.20}$$

The infinite domain $(-\infty, 0]$ for the variable x is trimmed to the finite interval $[-X, 0]$, where $X > 0$ is chosen so that $e^{-X} \approx 0$, hence minimizing the impact of the truncation on the solution. The system (4.2.14) represents a linear parabolic equation characterized by continuous coefficients and beginning conditions. Consequently, the solutions u exhibit high-order regularity, indicating they possess considerable smoothness. We will now examine the IMEX strategy to address the PIDE (4.2.14). We divide the uniform temporal and spatial meshes as outlined below:

$$t_n = nk, \quad n = 0,1,...,N, \qquad x_i = -X + i\Delta x, \quad i = 0,1,...,M.$$

Let M be a positive integer with $\Delta x = \frac{X}{M}$ and N is also a positive integer with $k = \frac{T}{N}$, where Δx and k represents step sizes in both spatial and temporal domain.

Assume $\zeta = x_i - y$, then in view of boundary condition (4.2.19), the integral part in (4.2.14) can be discretized at the mesh point $(x_i, t_n; \mathfrak{e}_j)$ as follows:

$$\begin{aligned}
\int_{-\infty}^{+\infty} e^{x_i-\zeta} u(x_i - y, t_n; \mathfrak{e}_j) f(y; \mathfrak{e}_j) dy &= \int_{-\infty}^{+\infty} e^{x_i-\zeta} u(\zeta, t_n; \mathfrak{e}_j) f(x_i - \zeta; \mathfrak{e}_j) d\zeta \\
&\approx \sum_{j=1}^{M} \int_{x_{j-1}}^{x_j} \left[e^{x_j - x_j} \frac{\zeta - x_i}{x_{j-1} - x_j} u(x_{j-1}, t_n; \mathfrak{e}_j) f(x_i - \zeta; \mathfrak{e}_j) \right. \\
&\quad \left. + e^{x_i-\zeta} \frac{\zeta - x_{j-1}}{x_j - x_{j-1}} u(x_j, t_n; \mathfrak{e}_j) f(x_i - \zeta; \mathfrak{e}_j) \right] d\zeta + \mathcal{R}(x_i, t_n; \mathfrak{e}_j) \\
&= \mathcal{I}(x_i, t_n; \mathfrak{e}_j) + \mathcal{R}(x_i, t_n; \mathfrak{e}_j), \quad j \in \mathbb{D} \qquad (4.2.21)
\end{aligned}$$

where the expression $\mathcal{R}(x_i, t_n; \mathfrak{e}_j)$ may be readily computed as follows

$$\mathcal{R}(x_i, t_n; \mathfrak{e}_j) = \frac{e^{-r_j t_n} - e^{-d_j t_n}}{(d_j - r_j)T} \left[1 - \phi \left(\frac{x_i + X - \mu_j - \varrho_j^2}{\varrho_j} \right) \right] e^{\mu_j + \frac{\varrho_j^2}{2}}, \qquad (4.2.22)$$

here $\phi(\cdot)$ represents the function of the standard normal distribution. We can directly calculate the term in (4.2.21) as follows:

$$\begin{aligned}
\int_{x_{j-1}}^{x_j} e^{x_i-\zeta} \frac{\zeta - x_j}{x_{j-1} - x_j} f(x_i - \zeta; \mathfrak{e}_j) d\zeta &= -\exp\left(\mu_j + \frac{\varrho_j^2}{2} \right) \int_{x_{j-1}}^{x_j} \frac{\zeta - x_j}{x_{j-1} - x_j} dF(x_i - \zeta; \mathfrak{e}_j) \\
&= \exp\left(\mu_j + \frac{\varrho_j^2}{2} \right) \left[F(x_i - x_{j-1}; \mathfrak{e}_j) - \frac{\int_{x_{j-1}}^{x_j} F(x_i - \zeta; \mathfrak{e}_j) d\zeta}{x_j - x_{j-1}} \right],
\end{aligned}$$

where $F(x; \mathfrak{e}_j) = \Phi\left(\frac{x - \mu_j - \varrho_j^2}{\varrho_j} \right)$. In the same way, for $j \in D$,

$$\begin{aligned}
\int_{x_{j-1}}^{x_j} e^{x_i-\zeta} \frac{\zeta - x_{j-1}}{x_j - x_j - 1} f(x_i - \zeta; \mathfrak{e}_j) d\zeta &= -\exp\left(\mu_j + \frac{\varrho_j^2}{2} \right) \int_{x_{j-1}}^{x_j} \frac{\zeta - x_{j-1}}{x_j - x_{j-1}} dF(x_i - \zeta; \mathfrak{e}_j) \\
&= -\exp\left(\mu_j + \frac{\varrho_j^2}{2} \right) \left[F(x_i - x_j; \mathfrak{e}_j) - \frac{\int_{x_{j-1}}^{x_j} F(x_i - \zeta; \mathfrak{e}_j) d\zeta}{x_j - x_{j-1}} \right],
\end{aligned}$$

4.3 Time Discretization

Take into account the system (4.2.14) that was first discretized in time using a uniform grid $t_n = nk$, $n = 0, 1, 2, \ldots, N$ with a uniform temporal mesh length k. $u(x, t_n, \mathfrak{e}_j)$ is abbreviated as u_n^j. In order to discretize PIDE across time, we will now quickly look at two different IMEX methods (4.2.14).

4.3.0.1 IMEX-BDF2 method

$$\frac{3u_{n+1}^j - 4u_n^j + u_{n-1}^j}{2k} = \mathcal{D}u_{n+1}^j + \lambda_j \mathcal{I}(2u_n^j - u_{n-1}^j) + \mathcal{E}(2u_n^j - u_{n-1}^j), \quad n \geq 1, \qquad (4.3.1)$$

$$u_{n+1}^j(x_L) = \frac{1}{(d_j - r_j)T}(e^{-r_j t} - e^{-d_j t}), \qquad u_{n+1}^j(x_R) = 0. \qquad (4.3.2)$$

4.3.0.2 IMEX-CNLF method

$$\frac{u^j_{n+1} - u^j_{n-1}}{2k} = \mathcal{D}(\frac{u^j_{n+1} + u^j_{n-1}}{2}) + \lambda_j \mathcal{I}(u^j_n) + \mathcal{E}(u^j_n), \quad n \geq 1, \tag{4.3.3}$$

$$u^j_{n+1}(x_L) = \frac{1}{(d_j - r_j)T}(e^{-r_j t} - e^{-d_j t}), \qquad u^j_{n+1}(x_R) = 0, \tag{4.3.4}$$

where,

$$\begin{aligned}\mathcal{I}(u^j_n) \quad &= \quad \exp\left(\mu_j + \frac{\varrho_j^2}{2}\right) \sum_{l=1}^{M} u^j_{l-1,n} \left[F(x_i - x_{l-1}; \mathfrak{e}_j) - \frac{\int_{x_{l-1}}^{x_l} F(x_i - \zeta; \mathfrak{e}_j) d\zeta}{x_l - x_{l-1}}\right] \\ &\quad - \exp\left(\mu_j + \frac{\varrho_j^2}{2}\right) \sum_{l=1}^{M} u^j_{l,n} \left[F(x_i - x_l; \mathfrak{e}_j) - \frac{\int_{x_{l-1}}^{x_l} F(x_i - \zeta; \mathfrak{e}_j) d\zeta}{x_l - x_{l-1}}\right] \end{aligned} \tag{4.3.5}$$

Two values, one for the zeroth time level and one for the first time level, are required by the suggested techniques. At the zeroth time level, the initial condition of the model problem gives the value u^j_0, and as per [80], the BDF1 may be used to calculate the value u^j_1. Assume that u^j_n is the solution to equation (4.3.1) and $\tilde{u}^j_n$ is the solution to the perturbed equation (4.3.6).

$$\frac{3\tilde{u}^j_{n+1} - 4\tilde{u}^j_n + \tilde{u}^j_{n-1}}{2k} = \mathcal{D}\tilde{u}^j_{n+1} + \lambda_j \mathcal{I}(2\tilde{u}^j_n - \tilde{u}^j_{n-1}) + \mathcal{E}(2\tilde{u}^j_n - \tilde{u}^j_{n-1}) + \mathcal{T}^j_{n+1}, \ n \geq 1 \tag{4.3.6}$$

along with boundary condition

$$\tilde{u}^j_{n+1}(x_L) = \frac{1}{(d_j - r_j)T}(e^{-r_j t} - e^{-d_j t}), \ \tilde{u}^j_{n+1}(x_R) = 0. \tag{4.3.7}$$

As time goes on, we will examine how these perturbations affect the inaccuracy; the $\mathcal{T}^j_n$ stands for the perturbation in the data at any temporal level t_n in the j^{th} economic state. We will show that the beginning errors at the beginning time levels (t_0 & t_1; for all methods discussed) limit the error at each time level and are a finite multiple of the perturbations that have been provided, thereby validating the stability of the discretization process across time.

Let $\epsilon^j_n := \tilde{u}^j_n - u^j_n$ be the definition of the error term. In the perturbed equations (4.3.6 – 4.3.7) and the equations (4.3.1 – 4.3.2), we are specifically dealing with boundary conditions. As a result, at the boundary locations, the error ϵ^j_n will be zero. For different methods, we may get the perturbation equation in a comparable way.

4.3.1 Stability Analysis

Theorem 4.3.1 (IMEX-BDF2). *Assuming that $k < \frac{1}{2(2\alpha^j + 1 + 2|q_{j,j}| + \lambda_j C_I)}$, the scheme exhibits stability in the following manner:*

$$\|\epsilon^j_m\|^2 \leq C\left(\max_{i=1,2,\cdots,Q} \|\epsilon^i_0\|^2 + \max_{i=1,2,\cdots,Q} \|\epsilon^i_1\|^2 + \max_{2\leq n\leq m} \|\mathcal{T}^j_n\|^2\right), \quad \forall\ 2 \leq m \leq \frac{T}{N}, \tag{4.3.8}$$

where C is a constant contingent upon parameters C_I, r_j, σ_j, λ_j, and T.

Proof. Upon examining equations (4.3.1) and (4.3.6), we obtain,

$$\frac{3\epsilon^j_{n+1} - 4\epsilon^j_n + \epsilon^j_{n-1}}{2k} = \mathcal{D}\epsilon^j_{n+1} + \lambda_j \mathcal{I}(2\epsilon^j_n - \epsilon^j_{n-1}) + \mathcal{E}(2\epsilon^j_n - \epsilon^j_{n-1}) + \mathcal{T}^j_{n+1} \tag{4.3.9}$$

$$\epsilon^j_{n+1}(x_L) = 0, \qquad \epsilon^j_{n+1}(x_R) = 0 \tag{4.3.10}$$

Obtaining the inner product of both sides of the equation (4.3.9) with $4\Delta t e^j_{n+1}$

$$\begin{aligned}\left(\frac{3\epsilon^j_{n+1} - 4\epsilon^j_n + \epsilon^j_{n-1}}{2k}, 4k\epsilon^j_{n+1}\right) &= \left(\mathcal{D}\epsilon^j_{n+1}, 4k\epsilon^j_{n+1}\right) + \left(\lambda_j \mathcal{I}(2\epsilon^j_n - \epsilon^j_{n-1}), 4k\epsilon^j_{n+1}\right) \\ &\quad + \left(\mathcal{E}(2\epsilon^j_n - \epsilon^j_{n-1}), 4k\epsilon^j_{n+1}\right) + \left(\mathcal{T}^j_{n+1}, 4k\epsilon^j_{n+1}\right) \end{aligned} \tag{4.3.11}$$

Using the identity $2\,(3a_1 - 4a_2 + a_3, a_1) = a_1^2 + (2a_1 - a_2)^2 - a_2^2 - (2a_2 - a_3)^2 + (a_1 - 2a_2 + a_3)^2$ in the left hand side, we get

$$\begin{aligned}\|\epsilon^j_{n+1}\|^2 - \|\epsilon^j_n\|^2 &+ \|2\epsilon^j_{n+1} - \epsilon^j_n\|^2 - \|2\epsilon^j_n - \epsilon^j_{n-1}\|^2 \\ &\le 4k(\mathcal{D}\epsilon^j_{n+1}, \epsilon^j_{n+1}) + 4k\lambda_j(\mathcal{I}(2\epsilon^j_n - \epsilon^j_{n-1}), \epsilon^j_{n+1}) \\ &\quad + \left(\mathcal{E}(2\epsilon^j_n - \epsilon^j_{n-1}), 4k\epsilon^j_{n+1}\right) + 4k(\mathcal{T}^j_{n+1}, \epsilon^j_{n+1}). \end{aligned} \tag{4.3.12}$$

First term in right hand side of (4.3.12) can be approximate as:

$$\begin{aligned}\left(\mathcal{D}\epsilon^j_{n+1}, \epsilon^j_{n+1}\right) &= \frac{1}{2}(\bar\sigma_j)^2((\epsilon^j_{xx})_{n+1}, \epsilon^j_{n+1}) + c^j_1((\epsilon^j_x)_{n+1}, \epsilon^j_{n+1}) - c^j_2(\epsilon^j_{n+1}, \epsilon^j_{n+1}) \\ &= -\frac{1}{2}(\bar\sigma_j)^2\|(\epsilon^j_{xx})_{n+1}\|^2 + c^j_1((\epsilon^j_x)_{n+1}, \epsilon^j_{n+1}) - c^j_2\|\epsilon^j_{n+1}\|^2 \\ &= -\frac{(\bar\sigma_j)^2}{2}\left(\|(\epsilon^j_x)_{n+1} - \frac{c^j_1}{(\bar\sigma_j)^2}\epsilon^j_{n+1}\|^2\right) + \frac{(c^j_1)^2 - 2(c^j_2)(\bar\sigma_j)^2}{2(\bar\sigma_j)^2}\|\epsilon^j_{n+1}\|^2 \\ &\le \frac{(c^j_1)^2 - (2c^j_2(\bar\sigma_j)^2)}{2(\bar\sigma_j)^2}\|\epsilon^j_{n+1}\|^2 \\ &\le \alpha^j\|\epsilon^j_{n+1}\|^2, \end{aligned} \tag{4.3.13}$$

where $\alpha^j = \frac{(c^j_1)^2 - (2c^j_2(\bar\sigma_j)^2)}{2(\bar\sigma_j)^2}$.

The integral operator $\mathcal{I}(u^j)$ defined in (4.2.21) is as follow:

$$\mathcal{I}(u^j) = \int_{-X}^{0} e^{x-\zeta} u(\zeta, t_n; \mathfrak{e}_j) f(x - \zeta; \mathfrak{e}_j) d\zeta, \;\; x \in [-X, 0]. \tag{4.3.14}$$

For the integral operator $u^j(\cdot, t) \in L^2([-X, 0])$, $t \in (0, T)$ such that

$$\overline{u}^j(x,t) = \begin{cases} u^j(x,t) & : \quad (x,t) \in [-X,0] \times [0,T], \\ 0 & : \quad (x,t) \in [-X,0]^c \times [0,T], \end{cases} \tag{4.3.15}$$

then it can be easily bounded as: $\|\mathcal{I}\overline{u}^j(\cdot,t)\| \le \mathbb{C}_{\text{Int}}\|u^j(\cdot,t)\|$, where $\mathbb{C}_{\text{Int}}$ is a constant that is independent of t and $\|u^j\| := \left(\int_{[-X,0]} |u^j(x)|^2 dx\right)^{\frac{1}{2}}$.

In the analysis, we will frequently employ Young's inequality for all $a, b \in \mathbb{R}$ with ϵ^* (true for every $\epsilon^* > 0$), that is,

$$(a, b) \leq \epsilon^* a^2 + \frac{1}{4\epsilon^*} b^2. \tag{4.3.16}$$

Using the above results, we bound the integral term in right hand side of (4.3.12) as:

$$\begin{aligned}(\lambda_j \mathcal{I}(2\epsilon_n^j - \epsilon_{n-1}^j), 4k\epsilon_{n+1}^j) &= 8k\lambda_j(\mathcal{I}(\epsilon_n^j), \epsilon_{n+1}^j) - 4k\lambda_j(\mathcal{I}(\epsilon_{n-1}^j), \epsilon_{n+1}^j) \\ &\leq 4k\lambda_j \mathbb{C}_{\text{Int}}(\|\epsilon_n^j\|^2 + \|\epsilon_{n+1}^j\|^2) + 2k\lambda_j \mathbb{C}_{\text{Int}}(\|\epsilon_{n-1}^j\|^2 + \|\epsilon_{n+1}^j\|^2) \\ &\leq 6k\lambda_j \mathbb{C}_{\text{Int}}\|\epsilon_{n+1}^j\|^2 + 4k\lambda_j \mathbb{C}_{\text{Int}}\|\epsilon_n^j\|^2 \\ &\quad +2k\lambda_j \mathbb{C}_{\text{Int}}\|\epsilon_{n-1}^j\|^2 \end{aligned} \tag{4.3.17}$$

We can bound the RS term (4.2.17) by the inequality

$$\left| \sum_{i=1, i\neq j}^{Q} u_n^i q_{i,j} \right| \leq \sum_{i=1, i\neq j}^{Q} \max_{i=1,2,\ldots,Q} |u_n^i||q_{i,j}|. \tag{4.3.18}$$

Let $u_n^{i_n} := \max_{i=1,2,\ldots,Q} |u_n^i|$. Then

$$\left| u_n^{i_n} \sum_{i=1, i\neq j}^{Q} |q_{i,j}| \right| = |q_{j,j}||u_n^{i_n}|. \tag{4.3.19}$$

then we get the

$$\left(\mathcal{E}(2\epsilon_n^j - \epsilon_{n-1}^j), 4k\epsilon_{n+1}^j\right) \leq 6k|q_{j,j}|\|\epsilon_{n+1}^j\|^2 + 4k|q_{j,j}|\|\epsilon_n^{i_n}\|^2 + 2k|q_{j,j}|\|\epsilon_{n-1}^{i_{n-1}}\|^2 \tag{4.3.20}$$

Combining the inequalities (4.3.12), (4.3.13), (4.3.17), (4.3.20), we have

$$\begin{aligned}\|\epsilon_{n+1}^j\|^2 - \|\epsilon_n^j\|^2 &+ \|2\epsilon_{n+1}^j - \epsilon_n^j\|^2 - \|2\epsilon_n^j - \epsilon_{n-1}^j\|^2 \\ &\leq 4k\alpha^j\|\epsilon_{n+1}^j\|^2 + 6k\lambda_j\mathbb{C}_{\text{Int}}\|\epsilon_{n+1}^j\|^2 + 4k\lambda_j\mathbb{C}_{\text{Int}}\|\epsilon_n^j\|^2 \\ &\quad +2k\lambda_j\mathbb{C}_{\text{Int}}\|\epsilon_{n-1}^j\|^2 + 6k|q_{j,j}|\|\epsilon_{n+1}^j\|^2 + 4k|q_{j,j}|\|\epsilon_n^{i_n}\|^2 \\ &\quad +2k|q_{j,j}|\|\epsilon_{n-1}^{i_{n-1}}\|^2 + 2k\|\epsilon_{n+1}^j\|^2 + 2k\|\mathcal{T}_{n+1}^j\|^2. \end{aligned}$$

$$\begin{aligned}\|\epsilon_{n+1}^j\|^2 - \|\epsilon_n^j\|^2 &+ \|2\epsilon_{n+1}^j - \epsilon_n^j\|^2 - \|2\epsilon_n^j - \epsilon_{n-1}^j\|^2 \\ &\leq 2k\left(2\alpha^j + 3|q_{j,j}| + 3\lambda_j\mathbb{C}_{\text{Int}} + 1\right)\|\epsilon_{n+1}^k\|^2 + 4k\lambda_j\mathbb{C}_{\text{Int}}\|\epsilon_n^j\|^2 \\ &\quad +4k|q_{j,j}|\|\epsilon_n^{i_n}\|^2 + 2k|q_{j,j}|\|\epsilon_{n-1}^{i_{n-1}}\|^2 \\ &\quad +4k\lambda_j\mathbb{C}_{\text{Int}}\|\epsilon_{n-1}^j\|^2 + 2k\|\mathcal{T}_{n+1}^j\|^2. \end{aligned} \tag{4.3.21}$$

By aggregating the aforementioned inequality (4.3.21) from $n = 1$ to $n = m - 1$ for $1 \leq m \leq N$, we obtain the following:

$$\|\epsilon_m^j\|^2 - \|\epsilon_1^j\|^2 - \|2\epsilon_1^j - \epsilon_0^j\|^2$$

$$\leq 4k\lambda_j\mathbb{C}_{\text{Int}}\|\epsilon_0^j\|^2 + 4k\lambda_j\mathbb{C}_{\text{Int}}\|\epsilon_1^j\|^2 + 2k\left(2\alpha^j + 3|q_{j,j}| + 5\lambda_j\mathbb{C}_{\text{Int}} + 1\right)\sum_{n=2}^{m-1}\|\epsilon_n^j\|^2$$
$$+\sum_{n=1}^{m-1}4k|q_{j,j}|\|\epsilon_n^{i_n}\|^2 + \sum_{n=1}^{m-1}2k|q_{j,j}|\|\epsilon_{n-1}^{i_{n-1}}\|^2 + 2k\sum_{n=2}^{m}\|\mathcal{T}_n^j\|^2$$
$$+2k\left(2\alpha^j + 3|q_{j,j}| + 3\lambda_j\mathbb{C}_{\text{Int}} + 1\right)\|\epsilon_m^j\|^2. \tag{4.3.22}$$

Case 1. If $\epsilon_n^{i_n} := \max\limits_{i=1,2,\cdots,Q}|\epsilon_n^i| = \epsilon_n^j$, for $1 \leq n \leq m$, then

$$\begin{aligned}
&\|\epsilon_m^j\|^2 - \|\epsilon_1^j\|^2 - \|2\epsilon_1^j - \epsilon_0^j\|^2\\
&\leq k(4\lambda^j\mathbb{C}_{\text{Int}} + 2|q_{j,j}|)\|\epsilon_0^j\|^2 + k(4\lambda^j\mathbb{C}_{\text{Int}} + 4|q_{j,j}|)\|\epsilon_1^j\|^2\\
&+2k\left(2\alpha^j + 6|q_{j,j}| + 5\lambda_j\mathbb{C}_{\text{Int}} + 1\right)\sum_{n=2}^{m-1}\|\epsilon_n^j\|^2\\
&+2k\sum_{n=2}^{m}\|\mathcal{T}_n^j\|^2 + 2k\left(2\alpha^j + 3|q_{j,j}| + 3\lambda_j\mathbb{C}_{\text{Int}} + 1\right)\|\epsilon_m^j\|^2.
\end{aligned} \tag{4.3.23}$$

Assume that k is sufficiently small such that $\left(1 - 2k\left(2\alpha^j + 3|q_{j,j}| + 3\lambda_j\mathbb{C}_{\text{Int}} + 1\right)\right) > 0$ or $k < \frac{1}{2(2\alpha^j + 3|q_{j,j}| + 3\lambda_j\mathbb{C}_{\text{Int}} + 1)}$, then above inequality implies,

$$\begin{aligned}
\|\epsilon_m^j\|^2 &\leq C(\|\epsilon_0^j\|^2 + \|\epsilon_1^j\|^2 + k\sum_{n=2}^{m-1}\|\epsilon_n^j\|^2 + k\sum_{n=2}^{m}\|\mathcal{T}_n^j\|^2)\\
&\leq C(\|\epsilon_0^j\|^2 + \|\epsilon_1^j\|^2 + k\sum_{n=2}^{m-1}\|\epsilon_n^j\|^2 + mk\max_{2\leq n\leq m}\|\mathcal{T}_n^j\|^2).
\end{aligned} \tag{4.3.24}$$

As we know $mk \leq T$, then we obtain

$$\|\epsilon_m^j\|^2 \leq C(\|\epsilon_0^j\|^2 + \|\epsilon_1^j\|^2 + k\sum_{n=2}^{m-1}\|\epsilon_n^j\|^2 + \max_{2\leq n\leq m}\|\mathcal{T}_n^j\|^2). \tag{4.3.25}$$

where C is a generic constant that is invariant regardless of the grid's extent. The implementation of the discrete Gronwall's inequality yields the conclusion,

$$\|\epsilon_m^j\|^2 \leq C(\|\epsilon_0^j\|^2 + \|\epsilon_1^j\|^2 + \max_{2\leq n\leq m}\|\mathcal{T}_n^j\|^2). \tag{4.3.26}$$

Case 2. If $\epsilon_n^{i_n} := \max\limits_{i=1,2,\cdots,Q}|\epsilon_n^i| \neq \epsilon_n^j$ then $|\epsilon_0^j| < |\epsilon_0^i|, |\epsilon_1^j| < |\epsilon_1^i|$ and let us consider $\epsilon_n^i = \max\{\epsilon_1^{i_1}, \epsilon_2^{i_2}, \epsilon_3^{i_3}, ..., \epsilon_n^{i_n}\}$. Then we obtain

$$\|\epsilon_m^j\|^2 - \|\epsilon_1^j\|^2 - \|2\epsilon_1^j - \epsilon_0^j\|^2$$
$$\leq 4k\lambda^j\mathbb{C}_{\text{Int}}\|\epsilon_0^j\|^2 + 4k\lambda_j\mathbb{C}_{\text{Int}}\|\epsilon_1^j\|^2 + 2k\left(2\alpha^j + 3|q_{j,j}| + 5\lambda_j\mathbb{C}_{\text{Int}} + 1\right)\sum_{n=2}^{m-1}\|\epsilon_n^j\|^2$$
$$+\sum_{n=1}^{m-1}4k|q_{j,j}|\|\epsilon_n^i\|^2 + \sum_{n=1}^{m-1}2k|q_{j,j}|\|\epsilon_{n-1}^i\|^2 + 2k\sum_{n=2}^{m}\|\mathcal{T}_n^j\|^2$$
$$+2k\left(2\alpha^j + 3|q_{j,j}| + 3\lambda_j\mathbb{C}_{\text{Int}} + 1\right)\|\epsilon_m^j\|^2. \tag{4.3.27}$$

Assume that the k is sufficiently small such that $\left(1-2k\left(2\alpha^j+3|q_{j,j}|+3\lambda_j\mathbb{C}_{\text{Int}}+1\right)\right)>0$ or $k<\frac{1}{2(2\alpha^j+3|q_{j,j}|+3\lambda_j\mathbb{C}_{\text{Int}}+1)}$, then above inequality implies,

$$\begin{aligned}\|\epsilon_m^j\|^2 &\le C(\|\epsilon_0^j\|^2+\|\epsilon_1^j\|^2+\|\epsilon_0^i\|^2+\|\epsilon_1^i\|^2+k\sum_{n=2}^{m-1}\|\epsilon_n^i\|^2+2\sum_{n=2}^{m}\|\mathcal{T}_n^j\|^2).\\ &\le C(\|\epsilon_0^i\|^2+\|\epsilon_1^i\|^2+k\sum_{n=2}^{m-1}\|\epsilon_n^i\|^2+mk\max_{2\le n\le m}\|\mathcal{T}_n^j\|^2).\end{aligned} \tag{4.3.28}$$

Since $e^j\in\mathcal{H}$, we may formulate the inequality as follows: for each $1\le j\le Q$, the left-hand component is satisfied,

$$\|\epsilon_m^i\|^2\le C(\|\epsilon_0^i\|^2+\|\epsilon_1^i\|^2+k\sum_{n=2}^{m-1}\|\epsilon_n^i\|^2+\max_{2\le n\le m}\|\mathcal{T}_n^j\|^2). \tag{4.3.29}$$

Now, the discrete Gronwall's inequality is employed, as detailed in Lemma 3.1 of [68], which yields the following result:

$$\|\epsilon_m^i\|^2\le C(\|\epsilon_0^i\|^2+\|\epsilon_1^i\|^2+\max_{2\le n\le m}\|\mathcal{T}_n^j\|^2). \tag{4.3.30}$$

From equations (4.3.26) and (4.3.30), we derived the result (4.3.8), which completes the proof of Theorem 4.3.1. □

Note: A similar strategy used to prove Theorem (4.3.1) can also be used to prove stability for the IMEX-CNLF scheme.

4.4 Spatial Discretization

Let $\mathbf{X}:=\{\mathbf{x}_1,\mathbf{x}_2,\ldots,\mathbf{x}_i,\ldots,\mathbf{x}_{\mathfrak{M}}\}$ denote a collection of arbitrary points inside the spatial domain $\Omega\subset\mathbb{R}^d$. Let the function $\phi:\Omega\times\Omega\to\mathbb{R}$ be a kernel defined by $\phi(\mathbf{x},\mathbf{y})=\phi(\|\mathbf{x}-\mathbf{y}\|)$ for $\mathbf{x},\mathbf{y}\in\Omega$ is called a radial basis functions. The RBF interpolation for a continuous function $u:\Omega\to\mathbb{R}$, defined at the points in $\mathbf{X}$, is expressed as

$$\mathfrak{I}_u(\mathbf{x})=\sum_{j=1}^{\mathfrak{M}}\ell_j\phi(\|\mathbf{x}-\mathbf{x}_j\|) \tag{4.4.1}$$

The interpolation coefficients $\{\ell_j\}_{j=1}^{\mathfrak{M}}$ are ascertained by positioning $\mathfrak{I}_u(\mathbf{x})$ to fulfill the condition $\mathfrak{I}_u(\mathbf{x}_i)=u(\mathbf{x}_i)$ for $i=1,2,\ldots,\mathfrak{M}$. The result is a set of linear equations that are symmetrical.

$$\underbrace{\begin{pmatrix}\phi(\|\mathbf{x}_1-\mathbf{x}_1\|) & \phi(\|\mathbf{x}_1-\mathbf{x}_2\|) & \cdots & \phi(\|\mathbf{x}_1-\mathbf{x}_{\mathfrak{M}}\|)\\ \phi(\|\mathbf{x}_2-\mathbf{x}_1\|) & \phi(\|\mathbf{x}_2-\mathbf{x}_2\|) & \cdots & \phi(\|\mathbf{x}_2-\mathbf{x}_{\mathfrak{M}}\|)\\ \vdots & \vdots & \ddots & \vdots\\ \phi(\|\mathbf{x}_{\mathfrak{M}}-\mathbf{x}_1\|) & \phi(\|\mathbf{x}_{\mathfrak{M}}-\mathbf{x}_2\|) & \cdots & \phi(\|\mathbf{x}_{\mathfrak{M}}-\mathbf{x}_{\mathfrak{M}}\|)\end{pmatrix}}_{\mathbf{A}}\underbrace{\begin{pmatrix}\ell_1\\ \ell_2\\ \vdots\\ \ell_{\mathfrak{M}}\end{pmatrix}}_{\ell}=\underbrace{\begin{pmatrix}u_1\\ u_2\\ \vdots\\ u_{\mathfrak{M}}\end{pmatrix}}_{\mathbf{u}} \tag{4.4.2}$$

The resultant coefficient matrix $\mathbf{A}$ is guaranteed to be invertible if the points in $\mathbf{X}$ are distinct and ϕ is a positive-definite radial kernel or a conditionally positive-definite kernel of order one on $\mathbb{R}^d$. Assume $\mathscr{L}$ be a linear differential operator and that $u : \Omega \to \mathbb{R}$ be a differentiable function. We want to estimate $\mathscr{L}u$ at scattered grids $\mathbf{X}$ utilizing local approximations based on finite-difference methodologies. Let $\Omega_{\mathfrak{M}}$ represent any subset of $\mathbf{X}$, defined as $\Omega_{\mathfrak{M}} := \{\mathbf{x}_1, \mathbf{x}_2, \ldots, \mathbf{x}_i, \ldots, \mathbf{x}_{m_i}\}$, containing $m_i << \mathfrak{M}$ nodes that are closest points to $\mathbf{x}_i$, as determined by Euclidean distance in $\mathbb{R}^d$. We denote $\Omega_{\mathfrak{M}}$ as the grid associated with $\mathbf{x}_i$. This is the way the values of u over the stencil $\Omega_{\mathfrak{M}}$ are linearly combined to approximate $\mathscr{L}u$ at $\mathbf{x}_i$:

$$\mathscr{L}(u(\mathbf{x}_i)) \approx \sum_{j=1}^{m_i} \omega_j u(\mathbf{x}_j) \tag{4.4.3}$$

where weights $\{\omega\}_{j=1}^{m_i}$ may be calculated using radial basis functions, a method referred to as RBF-FD. We may express (4.4.3) as $\mathscr{L}(u(\mathbf{x}_i)) \approx \mathrm{w}u_i$. Therefore, to compute RBF-FD weights, we first construct a local interpolant, resulting in

$$\mathfrak{I}_u(\mathbf{x}) = \sum_{j=1}^{m_i} \ell_j \phi(\|\mathbf{x} - \mathbf{x}_j\|). \tag{4.4.4}$$

The matrix-vector representation is given by $\mathbf{A}_i \ell = \mathbf{u}_i$, where $\mathbf{A}_i$ and $\mathbf{u}_i$ denote the local distance matrix and the known data associated with the stencil of $\mathbf{x}_i$, respectively. The unknown coefficients ℓ_j are ascertained via the equation $\ell = \mathbf{A}_i^{-1}\mathbf{u}_i$. Next, we take both sides of (4.4.4) and apply the differentiation operator $\mathscr{L}$ to them, resulting in

$$\mathscr{L}(\mathfrak{I}_u(\mathbf{x})) = \sum_{j=1}^{m_i} \ell_j \mathscr{L}(\phi(\|\mathbf{x} - \mathbf{x}_j\|)) \tag{4.4.5}$$

By collocating (4.4.5) at $\mathbf{x}_i$ and expressing it in matrix-vector form, we get

$$\mathscr{L}(u(\mathbf{x}_i)) = \mathscr{L}\hat{\phi}(\mathbf{x}_i)\ell = \mathscr{L}\hat{\phi}(\mathbf{x}_i)\mathbf{A}_i^{-1}\mathbf{u}_i \tag{4.4.6}$$

where $\mathscr{L}\hat{\phi}(\mathbf{x}_i) = [\mathscr{L}\phi(\|\mathbf{x}_i - \mathbf{x}_1\|), \mathscr{L}\phi(\|\mathbf{x}_i - \mathbf{x}_2\|), \ldots, \mathscr{L}\phi(\|\mathbf{x}_i - \mathbf{x}_{m_i}\|)]$. With the comparison of (4.4.3) and (4.4.6), we get $\mathrm{w} = \mathscr{L}\hat{\phi}(\mathbf{x}_i)\mathbf{A}_i^{-1}$.

The number of operations required to derive the differentiation matrix using the global RBF approach is $O(\mathfrak{M}^3)$, and the resulting matrix is dense. Conversely, the RBF-FD method necessitates $O(m_i^3)$ operations for each stencil, with $\mathfrak{M}$ stencils in total, leading to a cumulative computational cost of $O(m_i^3\mathfrak{M})$, excluding the expense of establishing the stencil grids. Given that $m_i << N$ and m_i remains constant as $\mathfrak{M}$ rises, the overall cost will be $O(\mathfrak{M})$.

Computing the interpolation weights calls for inverting each stencil's local distance matrix of size $m_i \times m_i$. The local distance matrix stays the same across all stencils as this matrix depends only on the pairwise distances between grid points and this work employs uniform grids. Hence its inverse has to be calculated just once, therefore greatly lowering the total processing expense. Because each stencil's differentiation matrix calculation is standalone, the RBF-FD methodology may be optimized for high-dimensional issues and adaptive algorithms using parallel approaches.

4.4.1 RBF-FD

For numerical analysis, a bounded domain is necessary; thus, we substitute the domain $\{(x,t) : x \in \mathbb{R}, t \in (0,T]\}$ with the domain $[x_L, x_R] \times (0,T]$, where the values x_L and x_R will be selected based on conventional financial reasoning, ensuring that the error resulting from reducing the solution domain is minimal. Now assume $\Omega := \{\mathbf{x}_1, \mathbf{x}_2, \ldots, \mathbf{x}_i, \ldots, \mathbf{x}_m\} \subset [x_L, x_R]$ such that $x_L = \mathbf{x}_1 < \mathbf{x}_2 < \cdots < \mathbf{x}_m = x_R$, and for each $\mathbf{x}_i$, we define the influence domain $\Omega_{m_i} := \{\mathbf{x}_1, \mathbf{x}_2, \ldots, \mathbf{x}_i, \ldots, \mathbf{x}_{m_i}\} \subset \Omega$, which represents a local area comprising the m_i closest interpolation points to the center node $\mathbf{x}_i$. The local radial basis function interpolant for every state is then constructed as follows:

$$u_k(x,t) \approx \hat{u}_k(\mathbf{x}) = \sum_{j=1}^{m_i} \ell_j \phi(\|\mathbf{x} - \mathbf{x}_j\|), \tag{4.4.7}$$

where $\{\ell_j\}_{j=1}^{m_i}$ are unknowns found by enforcing the interpolation requirements and resolving a system of linear equations. $\hat{\phi}^i \ell^i = \hat{u}_k^i$, where $\hat{\phi}^i = [\phi(\|\mathbf{x}_i - \mathbf{x}_j\|)], 1 \leq i,j \leq m_i$, $\ell^i = [\ell_1, \ell_2, \ldots \ell_N]$, $\hat{u}_k^i = [\hat{u}_k(x_1,t), \hat{u}_k(x_2,t), \ldots, \hat{u}_k(x_{m_i},t)]$, in light of the fact that $\hat{\phi}^i$ is invertible, therefore we've $\ell^i = (\hat{\phi}^i)^{-1}\hat{u}_k^i$. We apply the differential operator (4.2.15) to the local interpolant (4.4.7) for each point $\mathbf{x}_i \in \Omega_{m_i}$, thus we obtain

$$\mathcal{D}\hat{u}_k(x_i) = \sum_{j=1}^{m_i} \ell_j \mathcal{D}\phi(\|\mathbf{x}_i - \mathbf{x}_j\|) = \Psi_k^i \hat{u}_k^i \tag{4.4.8}$$

where

$$\Psi_k^i = [\mathcal{D}\phi(\|\mathbf{x}_i - \mathbf{x}_1\|), \mathcal{D}\phi(\|\mathbf{x}_i - \mathbf{x}_2\|), \ldots, \mathcal{D}\phi(\|\mathbf{x}_i - \mathbf{x}_{m_i}\|)](\hat{\phi}^i)^{-1}.$$

The local interpolants (4.4.7) and (4.4.8) are now substituted in (4.2.14), giving us

$$\frac{\partial \hat{u}_k^i}{\partial t} = \Psi_k^i \hat{u}_k^i(x,t) + \mathcal{I}\hat{u}_k(x,t) + \mathcal{E}\hat{u}_k(x,t) \tag{4.4.9}$$

where $\hat{u}^i = [\hat{u}_1(x_i,t), \hat{u}_2(x_i,t), \ldots, \hat{u}_{m_i}(x_i,t)]^T$.

The following global form is identical to the previous equation in local form.

$$\frac{\partial \hat{u}_k}{\partial t} = \Psi_k \hat{u}_k(x,t) + \mathcal{I}\hat{u}_k(x,t) + \mathcal{E}\hat{u}_k(x,t) \tag{4.4.10}$$

where $\frac{\partial \hat{u}_k}{\partial t} = [\frac{\partial \hat{u}_k(x_1)}{\partial t}, \frac{\partial \hat{u}_k(x_2)}{\partial t}, \ldots, \frac{\partial \hat{u}_k(x_{m-1})}{\partial t}]^T$, $\hat{u}_k = [\hat{u}_k(x_1), \hat{u}_k(x_2), \ldots, \hat{u}_k(x_{m-1})]^T$ and Ψ_k is the process of mapping Ψ_k^i from local to global by placing zeros in the proper locations. The system of equations (4.4.10) may be rewritten as

$$\frac{\partial \hat{u}}{\partial t} = \mathbf{A}_I \hat{\mathbf{u}} \tag{4.4.11}$$

where $\mathbf{A}_I = blkdiag(\Psi_1, \Psi_2, \ldots, \Psi_d) + \mathcal{I} \otimes I + \mathcal{E} \otimes I$, $\hat{\mathbf{u}} = [\hat{u}_1, \hat{u}_2, \ldots, \hat{u}_d]$.

Likewise, we may choose an influence domain Ω_{m_i} for every boundary point $x_i \in \Omega$, and use $\mathfrak{B}$ as a boundary operator, so we obtain

$$\mathfrak{B}\hat{u}_k(x_i) = \sum_{j=1}^{N} \ell_j \mathfrak{B}\phi(\|\mathbf{x}_i - \mathbf{x}_j\|) = \gamma_j^i \hat{u}_k^i \tag{4.4.12}$$

where

$$\gamma_k^i = [\mathfrak{B}\phi(\|\mathbf{x}_i - \mathbf{x}_1\|), \mathfrak{B}\phi(\|\mathbf{x}_i - \mathbf{x}_2\|), \ldots, \mathfrak{B}\phi(\|\mathbf{x}_i - \mathbf{x}_{\mathfrak{M}}\|)](\hat{\phi}^i)^{-1}. \tag{4.4.13}$$

The operator $\mathfrak{B}$ is the identity operator because we take into account the Dirichlet boundary condition in this study. We may extend the local system to the global form in a manner similar to that which we have done for interior points.

$$\gamma_k \hat{u}_k = G_k, \tag{4.4.14}$$

where G_k is associated with the Dirichlet boundary condition, and γ_k is the extension of γ_k^i, analogous to the mapping of Ψ_k^i to Ψ_k.
For every block of $\mathbf{A}_I$ that corresponds to each regime, we insert two rows pertaining to boundary grids produced in (4.4.14) in order to apply a system of boundary conditions (4.4.14) to (4.4.11). The following semi-discrete system of equations is finally concluded.

$$\frac{\partial \hat{u}}{\partial t} = \mathbf{A}\hat{u}, \tag{4.4.15}$$

where the discretization matrix for the interior and boundary points is $\mathbf{A}$.

4.5 Numerical Results

In this part, we carry out a series of computational experiments to prove that the numerical methods suggested for determining the Asian option's worth in the context of the Merton regime-switching jump-diffusion model are accurate and efficient. To approximate the spatial operator, we employed thin plate spline radial basis functions of the type $\tilde{r}^4 \ln \tilde{r}$, augmented with a second-degree polynomial space $\prod_2 := \{1, x, x^2\}$. An evenly spaced grid with $m_i = 3$ nearby nodes was employed for all computing situations. Given the Merton RSJD models, we discuss several numerical examples and analyze the convergence behavior of the proposed approaches for pricing Asian options. We conduct a numerical simulation in two and three economic states to study the pricing of the European style Asian put option under the regime-switching Merton principle. We prove the associated numerical method's option value and pointwise errors using M spatial and N temporal discretization points. For each j in the set Q, we may find the rate of convergence in space using the experimental formula below, as demonstrated in reference [93], as there is no analytical solution for the PIDE system (4.2.14).

$$\text{Convergence Order in Space} = \frac{\log \frac{M_1|u^k(M_1,N) - \tilde{u}^k(M_2,N)|}{M_2|u^k(M_2,N) - \tilde{u}^k(M_3,N)|}}{\log \frac{M_3}{M_2}}, \tag{4.5.1}$$

$$\text{Convergence Order in Time} = \frac{\log \frac{N_1|u^k(M,N_1)-u^k(M,N_2)|}{N_2|u^k(M,N_2)-u^k(M,N_3)|}}{\log \frac{N_3}{N_2}}, \tag{4.5.2}$$

where $u^k(M,N)$ is the numerical solution to the scheme at time $t=T$ using N temporal meshes, and M spatial meshes, and $\tilde{u}^k(M,N)$ is the numerical solution obtained by interpolating the cubic spline on the prior neighboring spatial mesh. Furthermore, the temporal direction computational formula is explained as in [93]. On a PC with an Intel(R) Core(TM) i5-10500 CPU at 3.10GHz, 3096 MHz, 6 Core(s), 12 Logical Processor(s), and 16.00GB RAM, we used MATLAB R2022b for computation.

Example 4.5.1. *Consider the function f given in (4.2.2), with $j=1,2$ and model parameters given as $[\varrho_1,\varrho_2]=[0.3,0.3]'$, $[\mu_1,\mu_2]'=[-0.1,-0.1]'$ and $Z=1.5$, $X=3$, $T=1$, $[r_1,r_2]'=[0.05,0.05]'$, $[\sigma_1,\sigma_2]'=[0.15,0.25]'$, $[d_1,d_2]'=[0,0]'$, $[\lambda_1,\lambda_2]'=[1,2]'$ and $A=\begin{bmatrix}-1 & 1\\ 1 & -1\end{bmatrix}$.*

First, we consider a two state RSJD model and demonstrate the convergence order of the RBF based BDF2 and CNLF schemes. For a fixed spatial point M the calculated convergence rate of the BDF2 scheme and the error that can occur at different temporal points are shown in Table 4.1. Similarly, Table 4.2 displays the temporal convergence rate and the errors for CNLF method. It is evident from Tables 4.1 and 4.2 that in the temporal direction, both the proposed methods have second order convergence rates. With the same parameters, the scheme in [25] has accuracy of order two, but the present methods have less errors at same temporal points. Thus, with the help of this example, we can observe that our scheme is better than the existing scheme in terms of accuracy.

Table 4.1: Errors and temporal convergence rate of the RBF-BDF2 method at different values of N, with a fixed $M=400$ using the parameters from the Example 4.5.1

	State 1		**State 2**	
N	Error	Order	Error	Order
400	7.724966e-07	...	2.374531e-07	...
450	5.282385e-07	2.0932	1.627789e-07	2.0719
500	3.770642e-07	2.0818	1.164239e-07	2.0631
550	2.785163e-07	2.0730	8.613334e-08	2.0562
600	2.115398e-07	2.0658	6.550645e-08	2.0507
650	1.644349e-07	2.0599	5.097577e-08	2.0462
700	1.303436e-07	2.0550	4.044493e-08	2.0425
750	1.050637e-07	2.0509	3.262674e-08	2.0393

Table 4.2: Errors and the temporal convergence rate of the RBF-CNLF method at different values of N, with a fixed $M = 400$ using the parameters from the Example 4.5.1

	State 1		State 2	
N	Error	Order	Error	Order
400	3.851254e-07	...	1.412960e-07	...
450	2.639214e-07	2.0748	9.686138e-08	2.0719
500	1.887215e-07	2.0652	6.927902e-08	2.0629
550	1.396002e-07	2.0577	5.125575e-08	2.0559
600	1.061589e-07	2.0518	3.898256e-08	2.0503
650	8.260554e-08	2.0470	3.033661e-08	2.0457
700	6.553805e-08	2.0430	2.407056e-08	2.0419
750	5.286828e-08	2.0396	1.941850e-08	2.0386

Furthermore, we showed the spatial convergence order and the error of the RBF-BDF2 and RBF-CNLF schemes that can occur at different points in spatial direction and for the fixed temporal points N. The computed convergence rate of the RBF-BDF2 scheme and the error that can occur at different spatial points are shown in Table 4.3. Similarly, Table 4.4 displays the spatial convergence rate and the errors for RBF-CNLF method.

Table 4.3: Errors and the spatial convergence rate of the RBF-BDF2 method at various values of M, with a fixed $N = 400$ using the parameters from the Example 4.5.1

	State 1		State 2	
N	Error	Order	Error	Order
200	2.942470e-03	...	2.159703e-03	...
250	1.404918e-03	2.0237	1.001362e-03	2.1552
300	7.767834e-04	2.0262	5.405856e-04	2.1572
350	4.734153e-04	2.0296	3.225397e-04	2.1673
400	3.092905e-04	2.0335	2.065821e-04	2.1820
450	2.128804e-04	2.0378	1.394996e-04	2.1998
500	1.525923e-04	2.0422	9.813945e-05	2.2199
550	1.129916e-04	2.0469	7.133282e-05	2.2418

Example 4.5.2. *Let's consider the function f given in (4.2.2) with $j = 1, 2$ and 3. Now, considering the model parameters as given in example* 3.2 *of [25],* $[\varrho_1, \varrho_2, \varrho_3] = [0.3, 0.25, 0.35]'$, $[\mu_1, \mu_2, \mu_3]' =$

Table 4.4: Errors and the spatial convergence rate of the RBF-CNLF method at different values of M, with a fixed $N = 400$ using the parameters from the Example 4.5.1

	State 1		State 2	
N	Error	Order	Error	Order
200	2.941493e-03	...	2.161904e-03	...
250	1.404485e-03	2.0236	1.001913e-03	2.1573
300	7.765669e-04	2.0260	5.407565e-04	2.1585
350	4.732961e-04	2.0294	3.226003e-04	2.1682
400	3.092200e-04	2.0333	2.066055e-04	2.1826
450	2.128364e-04	2.0376	1.395092e-04	2.2002
500	1.525636e-04	2.0421	9.814349e-05	2.2201
550	1.129722e-04	2.0467	7.133461e-05	2.2420

$[-0.1, -0.15, -0.05]'$, $[\sigma_1, \sigma_2, \sigma_3]' = [0.2, 0.3, 0.25]'$, $Z = 1.5$, $X = 3$, $T = 1$, $[r_1, r_2, r_3]' = [0.05, 0.05, 0.05]'$, $[d_1, d_2, d_3]' = [0, 0, 0]'$, $[\lambda_1, \lambda_2, \lambda_3]' = [1, 5, 2]'$, *and*

$$A = \begin{bmatrix} -2/3 & 1/3 & 1/3 \\ 1/3 & -2/3 & 1/3 \\ 1/3 & 1/3 & -2/3 \end{bmatrix}.$$

Next, we consider a three state RSJD model and display the convergence rate of the RBF based BDF2 and CNLF schemes. For a fixed spatial point M the calculated convergence rate of the BDF2 scheme and the error that can occur at different temporal points are shown in Table 4.5. Similarly, Table 4.6 displays the temporal convergence rate and the errors for CNLF method. It is evident from Tables 4.5 and 4.6 that in the temporal direction, both the proposed methods have second order convergence rates. With the same parameters, the scheme in [25] has accuracy of order two, but the present methods have less errors at same temporal points. Thus, with the help of this example, we can observe that our scheme is better than the existing scheme in terms of accuracy.

Moreover, under the three states RSJD model, we showed the spatial convergence rate and the error of the RBF-BDF2 and RBF-CNLF schemes that can occur at different spatial points and for the fixed temporal points N. The computed convergence rate of the RBF-BDF2 scheme and the error that can occur at different spatial points are shown in Table 4.7. Similarly, Table 4.8 displays the spatial convergence rate and the errors for RBF-CNLF method.

Example 4.5.3. *We consider the function f given in (4.2.2) with $j = 1, 2$ and 3 with model parameters* $[\varrho_1, \varrho_2, \varrho_3] = [0.3, 0.25, 0.35]'$, $[\mu_1, \mu_2, \mu_3]' = [-0.1, -0.15, -0.05]'$, $[\sigma_1, \sigma_2, \sigma_3]' = [0.2, 0.3, 0.25]'$, $Z = 1.5$,

Table 4.5: Errors and temporal convergence rate of the RBF-BDF2 method using the parameters from the Example 4.5.2 for different values of N, with a fixed $M = 400$

	State 1		State 2		State 3	
N	Error	Order	Error	Order	Error	Order
400	5.185740e-07	...	1.117038e-07	...	1.680320e-07	...
450	3.548664e-07	2.0869	7.653265e-08	2.0767	1.151737e-07	2.0731
500	2.534596e-07	2.0762	5.471196e-08	2.0676	8.236642e-08	2.0641
550	1.873079e-07	2.0678	4.046013e-08	2.0606	6.093134e-08	2.0571
600	1.423228e-07	2.0611	3.075913e-08	2.0551	4.633628e-08	2.0515
650	1.106690e-07	2.0556	2.392774e-08	2.0506	3.605566e-08	2.0470
700	8.775058e-08	2.0511	1.897845e-08	2.0468	2.860554e-08	2.0432
750	7.074956e-08	2.0472	1.530515e-08	2.0437	2.307486e-08	2.0400

Table 4.6: Errors and the temporal convergence rate of the RBF-CNLF method using the parameters from the Example 4.5.2 for different values of N, with a fixed $M = 400$

	State 1		State 2		State 3	
N	Error	Order	Error	Order	Error	Order
400	1.577304e-07	...	7.246324e-08	...	1.118337e-07	...
450	1.080807e-07	2.0756	4.967937e-08	2.0712	7.666537e-08	2.0718
500	7.728020e-08	2.0658	3.553476e-08	2.0623	5.483455e-08	2.0628
550	5.716283e-08	2.0582	2.629138e-08	2.0554	4.056935e-08	2.0558
600	4.346802e-08	2.0522	1.999657e-08	2.0499	3.085517e-08	2.0502
650	3.382296e-08	2.0473	1.556192e-08	2.0454	2.401189e-08	2.0457
700	2.683413e-08	2.0432	1.234784e-08	2.0416	1.905227e-08	2.0418
750	2.164624e-08	2.0398	9.961567e-09	2.0384	1.537012e-08	2.0386

$X = 3$, $T = 1$, $[r_1, r_2, r_3]' = [0.05, 0.05, 0.05]'$, $[d_1, d_2, d_3]' = [0.02, 0.03, 0.04]'$, $[\lambda_1, \lambda_2, \lambda_3]' = [3, 15, 6]'$ *and*

$$A = \begin{bmatrix} -2/3 & 1/3 & 1/3 \\ 1/3 & -2/3 & 1/3 \\ 1/3 & 1/3 & -2/3 \end{bmatrix}.$$

Subsequently, we examine an additional test case of the three-state RSJD model and demonstrate the convergence rate of the RBF based BDF2 and CNLF schemes. Table 4.9 displays the calculated convergence rate of the BDF2 scheme and the error that may occur at various temporal moments for a fixed spatial point M. In the same vein, Table 4.10 illustrates the temporal convergence rate and the errors associated with the CNLF method. It is clear from Tables 4.9 and 4.10 that both proposed methods have second-order convergence rates in the temporal direction. The present methods exhibit fewer errors at the

Table 4.7: Errors and the spatial convergence rate of the RBF-BDF2 method using the parameters from the Example 4.5.2 for different values of M, with a fixed $N = 400$

	State 1		State 2		State 3	
N	Error	Order	Error	Order	Error	Order
200	1.682243e-03	...	3.763072e-03	...	2.049840e-03	...
250	7.797641e-04	2.1565	1.732107e-03	2.1878	9.579519e-04	2.1198
300	4.208497e-04	2.1586	9.288160e-04	2.1941	5.214111e-04	2.1122
350	2.510418e-04	2.1688	5.505244e-04	2.2102	3.137430e-04	2.1124
400	1.607541e-04	2.1837	3.502498e-04	2.2322	2.027069e-04	2.1168
450	1.085308e-04	2.2015	2.348932e-04	2.2582	1.381171e-04	2.1236
500	7.633709e-05	2.2218	1.640763e-04	2.2875	9.807004e-05	2.1320
550	5.547458e-05	2.2439	1.183774e-04	2.3197	7.196592e-05	2.1417

Table 4.8: Errors and the spatial convergence rate of the RBF-CNLF method using the parameters from the Example 4.5.2 for different values of M, with a fixed $N = 400$

	State 1		State 2		State 3	
N	Error	Order	Error	Order	Error	Order
200	1.681444e-03	...	3.768254e-03	...	2.052900e-03	...
250	7.794416e-04	2.1562	1.733407e-03	2.1907	9.587566e-04	2.1228
300	4.207007e-04	2.1583	9.292230e-04	2.1958	5.216769e-04	2.1140
350	2.509661e-04	2.1685	5.506703e-04	2.2114	3.138445e-04	2.1137
400	1.607131e-04	2.1833	3.503067e-04	2.2330	2.027496e-04	2.1176
450	1.085074e-04	2.2012	2.349165e-04	2.2587	1.381363e-04	2.1242
500	7.632343e-05	2.2214	1.640859e-04	2.2879	9.807899e-05	2.1325
550	5.546647e-05	2.2436	1.183813e-04	2.3199	7.197020e-05	2.1420

same temporal locations despite the fact that the scheme in [25] has an accuracy of order two with the same parameters. Consequently, this example demonstrates that our scheme is more accurate than the existing scheme.

4.6 Conclusion

This chapter introduced an RBF-based implicit-explicit approach to solving partial integro-differential equations for pricing the moving boundary Asian option where the underlying asset undergoes a RSJD process. We used the IMEX-BDF2 and CNLF approaches for temporal discretization. Radial basis function-based finite difference methods were used for spatial discretization to solve the ensuing linear dif-

Table 4.9: Using the parameters from the Example 4.5.3, errors and temporal convergence rate of the RBF-BDF2 method at different values of N, with a fixed $M = 400$

	State 1		**State 2**		**State 3**	
N	Error	Order	Error	Order	Error	Order
400	1.070109e-07	...	3.467521e-08	...	7.323660e-08	...
450	7.330050e-08	2.0786	2.360530e-08	2.1312	5.016635e-08	2.0785
500	5.239293e-08	2.0692	1.676895e-08	2.1275	3.585655e-08	2.0694
550	3.874089e-08	2.0618	1.232442e-08	2.1255	2.651214e-08	2.0623
600	2.944992e-08	2.0559	9.312636e-09	2.1250	2.015259e-08	2.0567
650	2.290823e-08	2.0511	7.201088e-09	2.1254	1.567488e-08	2.0521
700	1.816937e-08	2.0472	5.677939e-09	2.1266	1.243125e-08	2.0484
750	1.465256e-08	2.0438	4.552332e-09	2.1283	1.002414e-08	2.0452

Table 4.10: Using the parameters from the Example 4.5.3, errors and the temporal convergence rate of the RBF-CNLF method at different values of N, with a fixed $M = 400$

	State 1		**State 2**		**State 3**	
N	Error	Order	Error	Order	Error	Order
400	8.837982e-08	...	2.387763e-08	...	5.427431e-08	...
450	6.058995e-08	2.0714	1.637047e-08	2.0710	3.721042e-08	2.0710
500	4.333814e-08	2.0625	1.170972e-08	2.0622	2.661646e-08	2.0622
550	3.206452e-08	2.0556	8.663882e-09	2.0553	1.969320e-08	2.0553
600	2.438724e-08	2.0500	6.589600e-09	2.0498	1.497831e-08	2.0498
650	1.897873e-08	2.0455	5.128262e-09	2.0453	1.165666e-08	2.0453
700	1.505887e-08	2.0417	4.069121e-09	2.0415	9.249216e-09	2.0415
750	1.214861e-08	2.0385	3.282761e-09	2.0383	7.461800e-09	2.0383

ferential equations produced by the time-dependent semi-discrete optimization of the governing equation. To approximate the integral term in PIDE, we used the composite trapezoidal rule. We showed the theoretical stability results for the proposed schemes. Our computational results show that both methods have a second-order convergence rate in the temporal and spatial directions. The computational experiments also reveal that the proposed methods exceed current literature methods in both accuracy and efficiency.

CHAPTER 5

RBF–BASED IMEX FINITE DIFFERENCE SCHEMES FOR PRICING OPTION UNDER LIQUIDITY SWITCHING [1]

This chapter aims to develop and analyze two accurate and efficient IMEX finite difference schemes for time semi discretization based on radial basis functions for pricing European and American options under liquidity shocks.

5.1 Introduction

Classical option pricing theory fails to accurately represent actual markets because it makes the fundamental assumption that markets are always liquid and that agents may trade anytime they want. Consequently, great effort has given in developing better models as a solution to these assumptions. Jump-diffusion models [79], such as Merton model [96], Lévy dynamics (see, for example, [30]), and stochastic volatility models are some examples of alternative models. Moreover, regime-switching is one of the rapidly emerging models that has received a lot of interest in option pricing. There are several studies on regime switching, but the fundamental concept was introduced by Hamilton [54] in econometric forecasting. Regime-switching methodologies offer a direct approach to capturing stochastic volatility and, consequently, fat tails, circumventing the limitation of the standard lognormality assumption in the Black-Scholes model. The concept of indifference pricing, which is connected to utility pricing, is something that [20] takes into consideration when the market is incomplete. The price at which an investor would retain the same amount of optimum utility, regardless of whether or not he has held options, is referred to as the indifference price. The non-

[1]The results discussed in this chapter have been published in it International Journal of Computer Mathematics, 101(7), 768-788 (2024). https://doi.org/10.1080/00207160.2024.2383757.

linear system (5.2.5) is satisfied by the buyer's indifference prices p (for state 0) and q (for state 1). The pricing and hedging problems associated with European options in a market vulnerable to liquidity shocks are examined in the study [92]. The authors use a distinct Markovian liquidity component to create a regime-switching description of market liquidity. The utility indifference method of valuing derivatives is then explained. The primary findings are the development and examination of a semi-linear coupled HJB equation that is satisfied by the indifference price. European options with liquidity shocks are modeled as a coupled system, where one is a degenerate parabolic equation, and the other has no diffusion factor. Koleva *et al.*[77] proposed a fourth-order compact scheme for a parabolic-ordinary system of liquidity shocks model for European options pricing. In this direction, other research can be found in [12, 78]. We present two RBF-based finite difference schemes that maintain the positivity of the differential problem solution. We focus on the numerical solution of the associated PDE systems for the European option and LCP system for the American style option, which is satisfied by the indifference prices of the writer and the buyer. More specifically, we construct and analyse the RBF-based finite difference schemes to approximate the parabolic-ordinary systems (5.3.3) and (5.3.4). Radial basis function mesh-free techniques are often used for solving partial differential equations because they provide spectral convergence for smooth solutions in complex geometry. RBF-FD does not achieve spectrum convergence. However, only RBF applied to the whole domain can achieve spectral convergence, although it may have stability problems. In this direction, Haghi *et al.*[52] presented an RBF-FD method for American options under the jump-diffusion models, Li *et al.*[87] extended the idea to solve the system of partial differential equations arising in options pricing under the regime-switching model. Bastani *et al.*[9] have developed a radial basis collocation approach, Rad *et al.*[109] introduced interpolation method using radial basis points to determine the price of European and American options. Using the local radial basis function as the basis, Kadalbajoo *et al.*[67, 69, 70] examined the efficacy of the meshfree approach in handling one and high-dimensional option pricing problems. Under jump-diffusion models, Shirzadi *et al.*[114, 115] developed the mesh-free moving least-squares approximation and obtained the best uniform error limits for the pricing option. We have provided the RBF-FD-based various IMEX techniques for pricing European and American options under the local volatility jump-diffusion framework [135]. Recently, to solve high-dimensional PDEs for multi-asset options using parabolic time-dependent models, [3] provide a hybrid RBF-FD solution that combines Gaussian and multiquadric functions. Other mesh-free work for option pricing can be found in [38, 100, 108, 116, 119, 136] and references therein.

A significant amount of research has been conducted in option pricing utilizing the RBF-FD approach; however, in the direction of coupled equations for option pricing, this method has been used comparatively less often. In the literature [24, 60, 111, 112], several approaches have been introduced to deal with the discretized linear complementarity problem that arises in American option pricing.

Gyulov *et al.*[51] used the interior penalty approach to price the American option to solve the complementarity system in a liquidity-switching market. For pricing the American option, we consider the operator splitting technique, described in [64]. The operator splitting approach has been effectively used by several authors [22, 65, 83] to solve the LCPs for option pricing.

This work aims to present the RBF-FD-based BDF1 and BDF2 time semi-discretization methods for pricing European and American options in a liquidity-switching framework and provide the stability estimates for these schemes. The remaining part of this chapter is organized as follows. We begin by defining the liquidity switching model, in addition to describing the basic abbreviations, symbols, and premises that will be used throughout this work, as well as the formation of coupled PDEs and LCPs and their associated features. In Section 5.3, we present the RBF-FD-based discretization techniques and give the stability analysis of the proposed schemes. Section 5.4 presents the BDF1 and BDF2 operator splitting time semi-discretization for the American option. In Section 5.5, numerical discussions are presented for pricing the European and American options to validate the theoretical results.

5.2 Liquidity Switching Model

The conventional theory of option pricing is based on a fundamental assumption, which is that markets are always liquid and that agents are free to trade anytime they want. On the other hand, this is not often the case in actual financial markets [91]. Regarding the availability of liquidity within financial markets or institutions, liquidity shocks are sudden changes or variations in the availability of liquidity. The mathematical ideas behind the liquidity shocks that are explored in option pricing will be addressed throughout this section. We discuss the market model in the context of possible liquidity shocks. Consider a complete probability space $(\Omega, \mathcal{F}, \mathbb{P})$ is a model of the financial market where $\mathbb{P}$ (the real-world probability) represents the physical measure. Also let $\mathcal{F}_\tau$ for $0 \leq \tau \leq T$ be the information set (filtration) available at time τ. We take into consideration a financial market that is vulnerable to liquidity shocks and consists of a stock and a risk-free asset (cash), as well as a limited investment time horizon $T < \infty$, which is selected to correspond with the expiry date of all securities in this model. To keep things simple, we use discounted pricing procedures, which guarantee that the cash value is always one and the interest rate is always zero. To represent total wealth, stock ownership as a percentage of total wealth, and the discounted stock price at time $\tau \in [0, T]$, we utilize $(X_\tau, \pi_\tau, S_\tau)$ defined on $\mathbb{R} \times \mathbb{R} \times \mathbb{R}^+$. This market is incomplete due to the existence of liquidity shocks, which is a source of liquidity risk. A more thorough examination of the liquidity switching model can be found in [92]. In addition, for a more precise explanation of a model of a financial market, one may refer to Etheridge's work (Financial Calculus) [47]. Ludkovski *et al.*[92] take into account an investor whose utility is defined in an exponential utility function $U(x) = -e^{-\gamma x}$, where $\gamma > 0$ represents the coefficient of risk aversion. The value functions $U^i(S, X, \tau)$ for the optimum investment problem in the presence of a contingent claim serve as a foundation for the utility-based pricing methodology,

$$U^i(S,X,\tau) = \sup_{\pi_\tau \in \mathbb{A}} \mathbb{E}^{\mathbb{P}}_{S,X,\tau,i}[-e^{-\gamma(X_T+hS_T)}], i=0,\ 1, \tag{5.2.1}$$

where the state variables in the liquidity state at time $\tau \in [0,T]$ are $(X_\tau, \pi_\tau, S_\tau)$. $\mathbb{A}$ is a collection of acceptable trading strategies π_τ, T is the expiry date of all assets, and $\mathbb{E}^{\mathbb{P}}$ stands for expectation taken under measure $\mathbb{P}$. Conventional techniques for stochastic control suggest the following: For a holder of a bounded contingent claim paying out $\Phi(S_T)$ at terminal time T, the optimum value functions $U^i(S,X,\tau)$ are provided by

$$U^i(S,X,\tau) = e^{-\gamma X - \gamma R^i(S,\tau)},$$

where the prices of the options in the two states are represented by $R^i(S,\tau)$, $i=0,1$, and γ is a risk aversion measure. Consequently, the coupled semi-linear parabolic-ordinary system's (5.2.2) unique viscosity solution [92] is represented by the pair (R^0, R^1).

$$\begin{cases} R^0_\tau + \frac{1}{2}\sigma^2 S^2 R^0_{SS} - \frac{\nu_{01}}{\gamma} e^{-\gamma(R^1-R^0)} + \frac{(d_0+\nu_{01})}{\gamma} = 0, \\ R^1_\tau - \frac{\nu_{10}}{\gamma} e^{-\gamma(R^0-R^1)} + \frac{\nu_{10}}{\gamma} = 0. \end{cases} \tag{5.2.2}$$

with the terminal conditions

$$R^i(S,T) = \Phi(S),\ \ i=0,\ 1, \tag{5.2.3}$$

where the underlying price $S \geq 0$, time $T \geq \tau \geq 0$, i.e., backward in time, $\sigma > 0$ represents the volatility of the stock, ν_{01} is the transition rate from state 0 to 1, ν_{10} is the transition rate from state 1 to 0 (assumed that the market has two states: liquid-0 and illiquid-1), $d_0 = \frac{\mu}{2\sigma^2}$, where μ is the drift. In the presence of illiquidity shocks, the value function for the optimal investment is given by

$$V^i(X,\tau) = \sup_{\pi_\tau \in \mathbb{A}} \mathbb{E}^{\mathbb{P}}_{X,\tau,i}[-e^{-\gamma X_T}] = -e^{-\gamma X} F_i(\tau), \qquad i=0,\ 1, \tag{5.2.4}$$

where $F_0(\tau)$ and $F_1(\tau)$ are the solutions of the ODE system $F'(\tau) = (\mathcal{D}-\mathcal{A})F(\tau)$ with

$$\mathcal{D} = \begin{bmatrix} d_0 & 0 \\ 0 & 0 \end{bmatrix}, \ \ \mathcal{A} = \begin{bmatrix} -\nu_{01} & \nu_{01} \\ \nu_{10} & -\nu_{10} \end{bmatrix}, \ \ F(\tau) \equiv [F_0(\tau), F_1(\tau)], \ \ F(T) \equiv [1,1].$$

Specifically, solutions can be written as

$$F_0(\tau) = c_1 e^{\lambda_1 \tau} + c_2 e^{\lambda_2 \tau}, \quad F_1(\tau) = \frac{1}{\nu_{01}}\{c_1(d_0+\nu_{01}-\lambda_1)e^{\lambda_1\tau} + c_1(d_0+\nu_{01}-\lambda_2)e^{\lambda_2\tau}\},$$

where

$$c_1 = \frac{\lambda_2 - d_0}{\lambda_2-\lambda_1} e^{-\lambda_1 T},\ c_2 = \frac{\lambda_1-d_0}{\lambda_1-\lambda_2} e^{-\lambda_2 T},\ \lambda_{1,2} = \frac{d_0+\nu_{01}+\nu_{10} \pm \sqrt{(d_0+\nu_{01}+\nu_{10})^2 - 4d_0\nu_{10}}}{2}.$$

The indifference prices $p = R^0 + \frac{\ln F_0(\tau)}{\gamma},\ q = R^1 + \frac{\ln F_1(\tau)}{\gamma}$, will satisfy the parabolic-ordinary system

$$\begin{cases} p_\tau + \frac{1}{2}\sigma^2 S^2 p_{SS} - \frac{\nu_{01}}{\gamma} e^{-\gamma(q-p)} + \frac{(d_0+\nu_{01})}{\gamma} - \frac{1}{\gamma}\frac{F_0^{'}}{F_0} = 0, \\ q_\tau - \frac{\nu_{10}}{\gamma} e^{-\gamma(p-q)} + \frac{\nu_{10}}{\gamma} - \frac{1}{\gamma}\frac{F_1^{'}}{F_1} = 0. \end{cases} \tag{5.2.5}$$

with the terminal conditions $p(S,T) = q(S,T) = \Phi(S)$. Although the problem (5.2.5) is degenerate and backward in time, we could transform it into a non-degenerate and forward in-time problem by using the transformations $t = T - \tau$, $u = \gamma R^0$ and $v = \gamma R^1$, i.e.

$$u_t = \frac{1}{2}\sigma^2 S^2 u_{SS} - ae^{-(v-u)} + b, \qquad v_t = c - ce^{-(u-v)}, \tag{5.2.6}$$

where $a = \nu_{01}$, $b = d_0 + \nu_{01}$, $c = \nu_{10}$, $\gamma = 1$, and the initial conditions are $u(S,0) = v(S,0) = \gamma\Phi(S)$.

Consider the solutions $u(S,t)$ and $v(S,t)$ of the following localised system of PDE (5.2.7) in the spatial domain $\Omega = (S_L, S_R)$,

$$\frac{\partial u}{\partial t} = \mathcal{L}u(S,t), \qquad \frac{\partial v}{\partial t} = \mathcal{L}^* v(S,t), \tag{5.2.7}$$

where, $\mathcal{L}u(S,t) = \frac{1}{2}\sigma^2 S^2 u_{SS} - ae^{-(v-u)} + b$, $\quad \mathcal{L}^* v(S,t) = c - ce^{-(u-v)}$, and the initial condition, $u(S,0) = v(S,0) = \max(S-K, 0)$. The boundary condition for a call option can be defined as:

$$u(S_L,t) = v(S_L,t) = 0,\ u(S_R,t) = v(S_R,t) = S_R - K. \tag{5.2.8}$$

The possibility of early exercise for the American option leads to the solution of a non-linear complementarity problem,

$$\begin{cases} \frac{\partial u}{\partial t} - \mathcal{L}u(S,t) \geq 0,\ \frac{\partial v}{\partial t} - \mathcal{L}^* v(S,t) \geq 0, \\ u(S,t) - \Phi(S) \geq 0,\ \left(\frac{\partial u}{\partial t} - \mathcal{L}u(S,t)\right)\left(u(S,t) - \Phi(S)\right) = 0, \\ v(S,t) - \Phi(S) \geq 0,\ \left(\frac{\partial v}{\partial t} - \mathcal{L}^* v(S,t)\right)\left(v(S,t) - \Phi(S)\right) = 0, \\ u(S,0) = \Phi(S),\ v(S,0) = \Phi(S),\ (S,t) \in \Omega \times J \end{cases} \tag{5.2.9}$$

where $J = (0, T]$ and the boundary conditions are defined in (5.2.8).

5.3 Discretization

In this section, we will discuss the temporal and spatial discretization techniques for the coupled PDEs (5.2.7) on the localised domain Ω.

5.3.1 Time Discretization

Let $k = T/N$ be the uniform temporal size, and denote $t_n = nk, n = 0, 1, 2, \ldots, N$. At time level n, u is abbreviated as $u_n(S)$.

We briefly discuss the semi-discretizations in time for the coupled PDEs in (5.2.7).

5.3.1.1 IMEX-BDF1 method

$$\begin{aligned} &\frac{u_{n+1}-u_n}{k} = \frac{1}{2}\sigma^2 S^2 (u_{SS})_{n+1} - ae^{(u_{n+1}-v_{n+1})} + b, \quad \frac{v_{n+1}-v_n}{k} = c - ce^{(v_{n+1}-u_{n+1})}, \\ &u_{n+1}(S_L) = v_{n+1}(S_L) = 0, \qquad u_{n+1}(S_R) = v_{n+1}(S_R) = S_R - K, \ n \geq 0, \end{aligned} \tag{5.3.1}$$

Using Taylor expansions up to second-order of the non-linear implicit term yields,

$$\begin{aligned} e^{u_{n+1}-v_{n+1}} &= e^{u_n - v_n}(1 + v_n - u_n) + e^{u_n - v_n}(u_{n+1} - v_{n+1}), \\ e^{v_{n+1}-u_{n+1}} &= e^{v_n - u_n}(1 + u_n - v_n) + e^{v_n - u_n}(v_{n+1} - u_{n+1}). \end{aligned} \tag{5.3.2}$$

The linearized IMEX BDF1 scheme is given by,

$$\begin{aligned} \tfrac{u_{n+1}-u_n}{k} &= \tfrac{1}{2}\sigma^2 S^2 (u_{SS})_{n+1} - a(e^{u_n - v_n}(1 + v_n - u_n) + e^{u_n - v_n}(u_{n+1} - v_{n+1})) + b, \\ \tfrac{v_{n+1}-v_n}{k} &= c - c(e^{v_n - u_n}(1 + u_n - v_n) + e^{v_n - u_n}(v_{n+1} - u_{n+1})), \ n \geq 0. \end{aligned} \tag{5.3.3}$$

5.3.1.2 IMEX-BDF2 method

Similarly, we can derive the IMEX-BDF2 scheme as:

$$\begin{aligned} \tfrac{3u_{n+1}-4u_n+u_{n-1}}{2k} &= \tfrac{1}{2}\sigma^2 S^2 (u_{SS})_{n+1} - a(e^{u_n - v_n}(1 + v_n - u_n) + e^{u_n - v_n}(u_{n+1} - v_{n+1})) + b, \\ \tfrac{3v_{n+1}-4v_n+v_{n-1}}{2k} &= c - c(e^{v_n - u_n}(1 + u_n - v_n) + e^{v_n - u_n}(v_{n+1} - u_{n+1})), \quad n \geq 1, \end{aligned} \tag{5.3.4}$$

with the boundary conditions

$$u_{n+1}(S_L) = v_{n+1}(S_L) = 0, \qquad u_{n+1}(S_R) = v_{n+1}(S_R) = S_R - K. \tag{5.3.5}$$

The backward difference technique of order one is used to determine the value (u_1, v_1). We now demonstrate the stability of time semi-discretization schemes. The Young's inequality will be applied often, for all $a, b \in \mathbb{R}$ with ϵ^* (valid for every $\epsilon^* > 0$), i.e,

$$(a, b) \leq \epsilon^* a^2 + \frac{1}{4\epsilon^*} b^2. \tag{5.3.6}$$

Consider the solutions u_n, v_n and $\tilde{u}_n, \tilde{v}_n$ to the equations (5.3.3) and the perturbed equations (5.3.7), respectively.

$$\begin{aligned} \tfrac{\tilde{u}_{n+1}-\tilde{u}_n}{k} &= \tfrac{1}{2}\sigma^2 S^2 (\tilde{u}_{SS})_{n+1} - a(e^{\tilde{u}_n - \tilde{v}_n}(1 + \tilde{v}_n - \tilde{u}_n) + e^{\tilde{u}_n - \tilde{v}_n}(\tilde{u}_{n+1} - \tilde{v}_{n+1})) + b + \mathcal{T}^u_{n+1}, \\ \tfrac{\tilde{v}_{n+1}-\tilde{v}_n}{k} &= c - c(e^{\tilde{v}_n - \tilde{u}_n}(1 + \tilde{u}_n - \tilde{v}_n) + e^{\tilde{v}_n - \tilde{u}_n}(\tilde{v}_{n+1} - \tilde{u}_{n+1})) + \mathcal{T}^v_{n+1}, \quad n \geq 0, \end{aligned} \tag{5.3.7}$$

combined with the conditions at the boundaries,

$$\tilde{u}_{n+1}(S_L) = \tilde{v}_{n+1}(S_L) = 0, \qquad \tilde{u}_{n+1}(S_R) = \tilde{v}_{n+1}(S_R) = S_R - K, \tag{5.3.8}$$

It is easy to check that for BDF1, truncation errors are as: $\mathcal{T}^u_{n+1}, \mathcal{T}^v_{n+1} \leq Ck$. We will examine the effects of the $\mathcal{T}^u_n, \mathcal{T}^v_n$ perturbations on the data at each subsequent time level t_n as we move in time.

Now that the error representation has a precise description, $\epsilon_n^u := \tilde{u}_n - u_n$, $\epsilon_n^v := \tilde{v}_n - v_n$. We define that, the numerical solution $\tilde{u}, \tilde{v}$ have the maximum limits as:

$$\tilde{C}_0 = \max_{\forall t \in J} |\tilde{u}_n|, \quad \tilde{C}_1 = \max_{\forall t \in J} |\tilde{v}_n|, \qquad \forall S \in \Omega, \quad n = 0, 1, 2, \cdots N. \tag{5.3.9}$$

The error equation for IMEX-BDF1 scheme is obtained by subtracting (5.3.7) from (5.3.3),

$$\begin{aligned} \frac{\epsilon_{n+1}^u - \epsilon_n^u}{k} &= \frac{1}{2}\sigma^2 S^2 (\epsilon_{SS}^u)_{n+1} + aC_u e^{\epsilon_n^u - \epsilon_n^v}(\epsilon_n^u - \epsilon_n^v + \epsilon_{n+1}^v - \epsilon_{n+1}^u) + \mathcal{T}_{n+1}^u, \\ \frac{\epsilon_{n+1}^v - \epsilon_n^v}{k} &= cC_v e^{\epsilon_n^v - \epsilon_n^u}(\epsilon_n^v - \epsilon_n^u + \epsilon_{n+1}^u - \epsilon_{n+1}^v) + \mathcal{T}_{n+1}^v, \quad n \geq 0, \end{aligned} \tag{5.3.10}$$

combined with the conditions at the boundaries $\epsilon_{n+1}^u(S_L) = \epsilon_{n+1}^v(S_L) = 0$, $\epsilon_{n+1}^u(S_R) = \epsilon_{n+1}^v(S_R) = 0$, where

$$C_u = \max_{0 \leq n \leq N} e^{\tilde{u}_n - \tilde{v}_n}, \quad C_v = \max_{0 \leq n \leq N} e^{\tilde{v}_n - \tilde{u}_n}, \quad \forall (S,t) \in \Omega \times \bar{J}.$$

Similarly, we can get the error equation for BDF2 scheme, where, $\mathcal{T}_{n+1}^u, \mathcal{T}_{n+1}^v \leq Ck^2$. To demonstrate the error estimate, we construct ν_1, ν_2, such that

$$\nu_1 = \max_{0 \leq t \leq T} \|u(\cdot,t)\|_{L^2} + 1 \qquad \nu_2 = \max_{0 \leq t \leq T} \|v(\cdot,t)\|_{L^2} + 1. \tag{5.3.11}$$

Throughout the analysis, C denotes a generic constant that is unaffected by the time step size, k, but that can vary depending on the data and the regularity of the analytical solution.

Lemma 5.3.1. *Let the exact solution be sufficiently smooth (at least first-order differentiable in time and second-order differentiable in spatial direction), and there is a constant $\mathcal{C}$, then the following outcomes hold for $k < \mathcal{C}$:*

$$\|u_n\|_{L^2} \leq \nu_1 \qquad \|v_n\|_{L^2} \leq \nu_2 \qquad n = 0, 1, 2, \cdots, N = \frac{T}{k}. \tag{5.3.12}$$

The proof of Lemma 5.3.1 is omitted, as it can be established by the same strategy that will be employed later to prove Lemma 5.3.3.

Theorem 5.3.2 (BDF1)**.** *Suppose there is sufficient regularity with L^2 norm for the exact solution (u,v) of equation (5.2.7). Let (u_{n+1}, v_{n+1}), be the numerical solution of the IMEX scheme (5.3.3), then for $k \to 0$, we have the following convergence results*

$$\|u - u_{n+1}\| + \|v - v_{n+1}\| \leq Ck.$$

Lemma 5.3.3. *Let the exact solution be sufficiently smooth (at least second-order differentiable in time and fourth-order differentiable in space), and there is a constant $\mathcal{C}$, then the following outcomes hold for $k < \mathcal{C}$.*

$$\|u_n\|_{L^2} \leq \nu_1 \qquad \|v_n\|_{L^2} \leq \nu_2 \qquad n = 0, 1, 2, \cdots, N = \frac{T}{k}. \tag{5.3.13}$$

Proof. Consider the error equation for system (5.3.4), we get,

$$\frac{3\epsilon^u_{n+1} - 4\epsilon^u_n + \epsilon^u_{n-1}}{2k} = \frac{1}{2}\sigma^2 S^2(\epsilon^u_{SS})_{n+1} + aC_u e^{\epsilon^u_n - \epsilon^v_n}(\epsilon^u_n - \epsilon^v_n + \epsilon^v_{n+1} - \epsilon^u_{n+1}) + \mathcal{T}^u_{n+1}, \tag{5.3.14}$$

$$\frac{3\epsilon^v_{n+1} - 4\epsilon^v_n + \epsilon^v_{n-1}}{2k} = cC_v e^{\epsilon^v_n - \epsilon^u_n}(\epsilon^v_n - \epsilon^u_n + \epsilon^u_{n+1} - \epsilon^v_{n+1}) + \mathcal{T}^v_{n+1}, \tag{5.3.15}$$

$$\epsilon^u_{n+1}(S_L) = \epsilon^v_{n+1}(S_L) = 0, \qquad \epsilon^u_{n+1}(S_R) = \epsilon^v_{n+1}(S_R) = 0. \tag{5.3.16}$$

The aforementioned conclusion will be supported by mathematical induction. It is evident that $\epsilon^u_0 \leq 1$ and $\epsilon^v_0 \leq 1$. We assume that at time t_n, the numerical error function has an L^2 bound, $\epsilon^u_n \leq 1$ and $\epsilon^v_n \leq 1$ such that $e^{|\epsilon^u_n - \epsilon^v_n|} \leq e^{C_{uv}}$. We will then demonstrate $\epsilon^u_{n+1} \leq 1$ and $\epsilon^v_{n+1} \leq 1$, remains valid.

Taking the inner product of both sides of the equation (5.3.14) with $4k(\epsilon^u_{n+1})$

$$\begin{aligned}\left(\frac{3\epsilon^u_{n+1} - 4\epsilon^u_n + \mathcal{E}^u_{n-1}}{2k}, 4k(\epsilon^u_{n+1})\right) \quad &= \quad \frac{1}{2}\sigma^2\left(S^2(\epsilon^u_{SS})_{n+1}, 4k\epsilon^u_{n+1}\right) \\ &\quad + aC_u e^{C_{uv}}\left(\epsilon^u_n - \epsilon^v_n + \epsilon^v_{n+1} - \epsilon^u_{n+1}, 4k\epsilon^u_{n+1}\right) \\ &\quad + \left(\mathcal{T}^u_{n+1}, 4k\epsilon^u_{n+1}\right)\end{aligned} \tag{5.3.17}$$

Using the identity $2(3A - 4B + C, A) = A^2 + (2A - B)^2 - B^2 - (2B - C)^2 + (A - 2B + C)^2$ in left side of equation (5.3.17), and after simplifying the equation we get

$$\begin{aligned}&\|\epsilon^u_{n+1}\|^2 - \|\epsilon^u_n\|^2 + \|2\epsilon^u_{n+1} - \epsilon^u_n\|^2 - \|2\epsilon^u_n - \mathcal{E}^u_{n-1}\|^2 \\ &= \frac{1}{2}\sigma^2\left(S^2(\epsilon^u_{SS})_{n+1}, 4k\epsilon^u_{n+1}\right) + 4kaC_u e^{C_{uv}}\|\epsilon^u_n - \epsilon^v_n + \epsilon^v_{n+1} - \epsilon^u_{n+1}\|\|\epsilon^u_{n+1}\| \\ &+ \left(\mathcal{T}^u_{n+1}, 4k\epsilon^u_{n+1}\right)\end{aligned} \tag{5.3.18}$$

Now simplifying the right side of (5.3.18), using $\left(S^2(\epsilon^u_{SS})_{n+1}, 4k\mathcal{E}^u_{n+1}\right) \leq 2k\|\epsilon^u_{n+1}\|^2$, and let $C_1 = 2aC_u e^{C_{uv}}$ then we have

$$\begin{aligned}&\|\epsilon^u_{n+1}\|^2 - \|\epsilon^u_n\|^2 + \|2\epsilon^u_{n+1} - \epsilon^u_n\|^2 - \|2\epsilon^u_n - \epsilon^u_{n-1}\|^2 \\ &\leq \sigma^2 k\|\epsilon^u_{n+1}\|^2 + 4kC_1\|\epsilon^v_{n+1}\|^2 + 5kC_1\|\epsilon^u_{n+1}\|^2 + 4kC_1\|\epsilon^u_n\|^2 + 4kC_1\|\epsilon^v_n\|^2 \\ &+ 2k\|\mathcal{T}^u_{n+1}\|^2 + 2k\|\epsilon^u_{n+1}\|^2.\end{aligned} \tag{5.3.19}$$

Now, taking the inner product of both sides of the equation (5.3.15) with $4k(\epsilon^v_{n+1})$, and let $C_2 = 2cC_v e^{C_{uv}}$, then we have

$$\begin{aligned}&\|\epsilon^v_{n+1}\|^2 - \|\epsilon^v_n\|^2 + \|2\epsilon^v_{n+1} - \epsilon^v_n\|^2 - \|2\epsilon^v_n - \epsilon^v_{n-1}\|^2 \\ &\leq k(5C_2 + 2)\|\epsilon^v_{n+1}\|^2 + 4kC_2\|\epsilon^u_{n+1}\|^2 + 4kC_2(\|\epsilon^u_n\|^2 + \|\epsilon^v_n\|^2) + 2k\|\mathcal{T}^v_{n+1}\|^2\end{aligned} \tag{5.3.20}$$

Adding up the inequalities (5.3.19) and (5.3.20), and let $C_3 = \max(C_1, C_2)$, then

$$\|\epsilon^u_{n+1}\|^2 - \|\epsilon^u_n\|^2 + \|\epsilon^v_{n+1}\|^2 - \|\epsilon^v_n\|^2 + \|2\epsilon^u_{n+1} - \epsilon^u_n\|^2 - \|2\epsilon^u_n - \epsilon^u_{n-1}\|^2 + \|2\epsilon^v_{n+1}$$

$$
\begin{aligned}
&-\epsilon_n^v\|^2 - \|2\epsilon_n^v - \epsilon_{n-1}^v\|^2 \\
&\leq \mathcal{C}k(\|\epsilon_{n+1}^u\|^2 + \|\epsilon_{n+1}^v\|^2) + 4kC_3(\|\epsilon_n^u\|^2 + \|\epsilon_n^v\|^2) + 2k(\|\mathcal{T}_{n+1}^u\|^2 + \|\mathcal{T}_{n+1}^v\|^2), \qquad (5.3.21)
\end{aligned}
$$

where $\mathcal{C} = \sigma^2 + 5C_3 + 2$. To keep the generality intact, let's assume that $0 \leq m \leq N$ is an integer. Then, after summing up the inequality (5.3.21), for $n = 0$ to $n = m$

$$
\begin{aligned}
&\|\epsilon_{m+1}^u\|^2 - \|\epsilon_0^u\|^2 + \|\epsilon_{m+1}^v\|^2 - \|\epsilon_0^v\|^2 + \|2\epsilon_{m+1}^u - \epsilon_m^u\|^2 + \|2\epsilon_{m+1}^v - \epsilon_m^v\|^2 \\
&-\|2\epsilon_1^u - \epsilon_0^u\|^2 - \|2\epsilon_1^v - \epsilon_0^v\|^2 \\
&\leq \mathcal{C}k(\|\epsilon_{m+1}^u\|^2 + \|\epsilon_{m+1}^v\|^2) + \mathcal{C}k\sum_{n=1}^{m}(\|\epsilon_n^u\|^2 + \|\epsilon_n^v\|^2) + 4kC_3\sum_{n=0}^{m}(\|\epsilon_n^u\|^2 + \|\epsilon_n^v\|^2) \\
&+k\sum_{n=0}^{m}(\|\mathcal{T}_{n+1}^u\|^2 + \|\mathcal{T}_{n+1}^v\|^2).
\end{aligned}
$$

Suppose that the k is small enough such that $(1 - k\mathcal{C}) > 0$ or $k < \frac{1}{\mathcal{C}}$, then the above inequality implies,

$$
\begin{aligned}
\|\epsilon_{m+1}^u\|^2 + \|\epsilon_{m+1}^v\|^2 \quad \leq \quad & C(\|\epsilon_0^u\|^2 + \|\epsilon_0^v\|^2 + \|2\epsilon_1^u - \epsilon_0^u\|^2 + \|2\epsilon_1^v - \epsilon_0^v\|^2 \\
&+k\sum_{n=1}^{m}(\|\epsilon_n^u\|^2 + \|\epsilon_n^v\|^2) + k\sum_{n=0}^{m}(\|\mathcal{T}_{n+1}^u\|^2 + \|\mathcal{T}_{n+1}^v\|^2)).
\end{aligned}
$$

We know that $mk \leq T$, then we have

$$
\begin{aligned}
\|\epsilon_{m+1}^u\|^2 + \|\epsilon_{m+1}^v\|^2 \quad \leq \quad & C(\|\epsilon_0^u\|^2 + \|\epsilon_0^v\|^2 + \|2\epsilon_1^u - \epsilon_0^u\|^2 + \|2\epsilon_1^v - \epsilon_0^v\|^2 \\
&+k\sum_{n=1}^{m-1}(\|\epsilon_{n+1}^u\|^2 + \|\epsilon_{n+1}^v\|^2) + mk\max_{0\leq n\leq m}(\|\mathcal{T}_{n+1}^u\|^2 + \|\mathcal{T}_{n+1}^v\|^2)),
\end{aligned}
$$

where C is a generic constant independent of the grid's size. Now, using the discrete Gronwall's inequality (for more information, see Lemma 3.1 in [68]), we get,

$$
\begin{aligned}
\|\epsilon_{m+1}^u\|^2 + \|\epsilon_{m+1}^v\|^2 \quad \leq \quad & C(\|\epsilon_0^u\|^2 + \|\epsilon_0^v\|^2 + \|2\epsilon_1^u - \epsilon_0^u\|^2 + \|2\epsilon_1^v - \epsilon_0^v\|^2 \\
&+\max_{0\leq n\leq m}(\|\mathcal{T}_{n+1}^u\|^2 + \|\mathcal{T}_{n+1}^v\|^2)). \qquad (5.3.22)
\end{aligned}
$$

From (5.3.22), we get, $\|\epsilon_{m+1}^u\|^2 + \|\epsilon_{m+1}^v\|^2 \leq Ck^4$. Now, if $k \leq \left(\frac{1}{C^{\frac{1}{4}}}\right)$, then we have

$$
\|\epsilon_{m+1}^u\| \leq 1 \qquad \text{and} \qquad \|\epsilon_{m+1}^v\| \leq 1. \qquad (5.3.23)
$$

This completes the proof of (5.3.13). □

Theorem 5.3.4 (BDF2)**.** *Suppose there is sufficient regularity with L^2 norm for the exact solution (u, v) of equation (5.2.7). Let (u_{n+1}, v_{n+1}), be the numerical solution of the IMEX scheme (5.3.4), then for $k \to 0$, we have the following convergence results:*

$$
\|u - u_{n+1}\| + \|v - v_{n+1}\| \leq Ck^2.
$$

5.3.2 Spatial Discretization

We will now discuss the implementation of the local radial basis function-based finite difference (RBF-FD) scheme for system (5.2.7). Let a collection of randomly selected discrete points within the domain Ω, denote $\Omega_{\mathfrak{M}} := \{\mathbf{x}_1, \mathbf{x}_2, \ldots, \mathbf{x}_i, \ldots, \mathbf{x}_{\mathfrak{M}}\}$. We can locally approximate the linear differential operator $\mathscr{L}$ at any node $\mathbf{x}_i \in \Omega_{\mathfrak{M}}$:

$$\mathscr{L}v(\mathbf{x}_i) = \sum_{j=1}^{m_i} \omega_j v(\mathbf{x}_j), \tag{5.3.24}$$

where $m_i (< \mathfrak{M})$ represents the stencil size in the sub-domain $\Omega_i \subset \Omega$ containing the approximation point $\mathbf{x}_i$, and ω_j denotes the unknown differential weights. It should be noted that the collection Ω_i contains exactly the nearest m_i nodes of $\Omega_{\mathfrak{M}}$ in the neighbourhood of $\mathbf{x}_i$.

The calculation of integral weight ω_j, which relies on the approximation point $\mathbf{x}_i$, is one of the key steps in the approximation of $\mathscr{L}v(\mathbf{x}_i)$ using expression (5.3.24). Typically, in the conventional finite difference approach, the discretization points are spaced evenly, and traditional polynomial interpolation is used to effectively determine the weights ω_j.

The interpolation technique in the radial basis function method, in contrast to the standard finite difference scheme, is not limited by the uniform distribution of discretization points and can be implemented efficiently on scattered node distributions. To estimate the integral weight ω_j, we have used the procedure, well defined in literature [87, 136].

5.3.3 RBF-FD Discretization

From (5.3.24), we consider the approximation of second order derivatives with respect to S as:

$$\frac{\partial^2 u}{\partial S^2} = \sum_{i=1}^{m_i} w_{SS}^i u^i(t). \tag{5.3.25}$$

Now substitute the equation (5.3.25) in (5.2.7), we get the system,

$$\frac{\partial u^j(t)}{\partial t} = \frac{1}{2}\sigma^2 (S^j)^2 \sum_{i=1}^{m_i} w_{SS}^i u^i(t) - ae^{-(v^j(t)-u^j(t))} + b, \; \frac{\partial v^j(t)}{\partial t} = c - ce^{-(u^j(t)-v^j(t))} \tag{5.3.26}$$

For $j = 1, 2, \cdots, M$, we can write the matrix vector form

$$\frac{\partial \mathbf{u}}{\partial t} = (\frac{1}{2}\sigma^2 (S^j)^2 W_{SS})\mathbf{u}(t) - ae^{-(\mathbf{v}(t)-\mathbf{u}(t))} + b, \quad \frac{\partial \mathbf{v}}{\partial t} = c - ce^{-(\mathbf{u}(t)-\mathbf{v}(t))}, \tag{5.3.27}$$

where,

$$\mathbf{u}(t) = [u^1(t)\ u^2(t) \quad u^{M-1}(t)\ u^M(t)]^T, \quad \mathbf{v}(t) = [v^1(t)\ v^2(t) \quad v^{M-1}(t)\ v^M(t)]^T.$$

The matrix structure of W_{SS} is based on the number of points in each stencil. For example, W_{SS} is a tridiagonal matrix if $m_i = 3$.

5.3.4 Full RBF-BDF2 Discretization

Now, we fully discretize the system (5.3.27) using IMEX-BDF2 combined with RBF-FD method, and let, $\mathbf{W} = \text{Diag}\left(\frac{1}{2}\sigma^2(S^j)^2\right) \cdot W_{SS}$,

$$\begin{aligned} \frac{3u^j_{n+1}-4u^j_n+u^j_{n-1}}{2dt} &= \mathbf{W}u^j_{n+1} - a(e^{u^j_n-v^j_n}(1+v^j_n-u^j_n)+e^{u^j_n-v^j_n}(u^j_{n+1}-v^j_{n+1}))+b \\ \frac{3v^j_{n+1}-4v^j_n+v^j_{n-1}}{2dt} &= c-c(e^{v^j_n-u^j_n}(1+u^j_n-v^j_n)+e^{v^j_n-u^j_n}(v^j_{n+1}-u^j_{n+1})),\ n\geq 1, \end{aligned} \tag{5.3.28}$$

By rearranging the terms of the system (5.3.28), we get

$$\mathcal{D}\mathbf{U}_{n+1} = \mathcal{A}\mathbf{U}_n + \mathcal{B}\mathbf{U}_{n-1} + \mathcal{C}, \tag{5.3.29}$$

where, $\mathbf{U} = [\mathbf{u},\ \mathbf{v}]$, is a $2M\times 1$ column vector and the $\mathcal{A}, \mathcal{B}, \mathcal{D}$ are block diagonal matrices of size $2M\times 2M$, $\mathcal{C}$ is a $2M\times 1$ order of column vector

$$\mathcal{D} = \begin{bmatrix} \mathcal{D}_1 & 0 \\ 0 & \mathcal{D}_2 \end{bmatrix},\ \mathcal{A} = \begin{bmatrix} \mathcal{A}_1 & 0 \\ 0 & \mathcal{A}_2 \end{bmatrix},\ \mathcal{B} = \begin{bmatrix} \mathcal{B}_1 & 0 \\ 0 & \mathcal{B}_2 \end{bmatrix},\ \mathcal{C} = \begin{bmatrix} \mathcal{C}_1 \\ \mathcal{C}_2 \end{bmatrix},$$

where $\mathcal{D}_1 = \text{Diag}\left(\frac{3}{2dt} + ae^{u^j_n-v^j_n} - ce^{v^j_n-u^j_n}\right) - \mathbf{W},\ \mathcal{D}_2 = \text{Diag}\left(\frac{3}{2dt} + ce^{v^j_n-u^j_n} - ae^{u^j_n-v^j_n}\right)$, $\mathcal{A}_1 = \text{Diag}\left(\frac{2}{dt} + ae^{u^j_n-v^j_n} - ce^{v^j_n-u^j_n}\right),\ \mathcal{A}_2 = \text{Diag}\left(\frac{2}{dt} + ce^{v^j_n-u^j_n} - ae^{u^j_n-v^j_n}\right), \mathcal{B}_1 = \text{Diag}\left(-\frac{1}{2dt}\right)$, $\mathcal{B}_2 = \text{Diag}\left(-\frac{1}{2dt}\right), \mathcal{C}_1 = b - ae^{u^j_n-v^j_n},\ \mathcal{C}_2 = c(1-e^{v^j_n-u^j_n})$, for $j = 1, 2, \cdots, M$.

5.4 American Option

In this section, we define the BDF1 and BDF2 operator splitting methods [64] to solve the LCP (5.2.9) for American option. The main goal of operator splitting approach is to obtain an equation such that $\psi = u_t - \mathcal{L}u$ by using the additional variable, ψ. Now in the region $\Omega\times J$, the LCP (5.2.9) can be reformulated as follows:

$$\begin{aligned} &\frac{\partial u}{\partial t} - \mathcal{L}u = \psi,\ \frac{\partial v}{\partial t} - \mathcal{L}^*v = \psi^*, (u(S,t)-\Phi(S))\cdot\psi = 0,\ (v(S,t)-\Phi(S))\cdot\psi^* = 0, \\ &u(S,t)-\Phi(S)\geq 0,\ v(S,t)-\Phi(S)\geq 0,\ \psi,\psi^*\geq 0. \end{aligned} \tag{5.4.1}$$

5.4.1 BDF1-OS Method

Let divide the governing equation $u_t - \mathcal{L}u = \psi$ into two discrete equations on the $(n+1)^{th}$ time level, as:

$$\left(\frac{\tilde{u}_{n+1}-u_n}{k}\right) - \mathcal{L}\tilde{u}_{n+1} = \psi_n,\ \left(\frac{\tilde{v}_{n+1}-v_n}{k}\right) - \mathcal{L}^*\tilde{v}_{n+1} = \psi^*_n, \tag{5.4.2}$$

$$\left(\frac{u_{n+1}-u_n}{k}\right) - \mathcal{L}\tilde{u}_{n+1} = \psi_{n+1},\ \left(\frac{v_{n+1}-v_n}{k}\right) - \mathcal{L}^*\tilde{v}_{n+1} = \psi^*_{n+1}. \tag{5.4.3}$$

Now, the discrete problem for LCP (5.4.1) is to search for the pairs (u_{n+1}, ψ_{n+1}), and $(u^*_{n+1}, \psi^*_{n+1})$ which satisfies both the discrete systems (5.4.2) and (5.4.3) as well as the constraints

$$u_{n+1}\geq\Phi,\ \psi_{n+1}\geq 0,\ \psi_{n+1}(u_{n+1}-\Phi) = 0,\ v_{n+1}\geq\Phi,\ \psi^*_{n+1}\geq 0,\ \psi^*_{n+1}(v_{n+1}-\Phi) = 0. \tag{5.4.4}$$

The first step is to find out the intermediate approximations $\tilde{u}_{n+1}$ and $\tilde{v}_{n+1}$ by solving the system (5.4.2) with known auxiliary terms ψ_n and ψ_n^* under boundary conditions :

$$\tilde{u}_{n+1}(S_L) = K, \qquad \tilde{u}_{n+1}(S_R) = 0, \qquad \tilde{v}_{n+1}(S_L) = K, \qquad \tilde{v}_{n+1}(S_R) = 0.$$

The second step of the operator splitting method is to establish a connection in (5.4.3) between u_{n+1}, v_{n+1} and ψ_{n+1}, ψ^*_{n+1} under the constraint (5.4.4). In order to secure this, we need to re-express the system (5.4.3) using results from equation (5.4.2) along with the constraints in (5.4.4) as a problem to search for the pair (u_{n+1}, ψ_{n+1}), such that

$$\begin{aligned} &\frac{u_{n+1} - \tilde{u}_{n+1}}{k} = \psi_{n+1} - \psi_n, \quad \frac{v_{n+1} - \tilde{v}_{n+1}}{k} = \psi^*_{n+1} - \psi^*_n, \\ &\psi_{n+1}(u_{n+1} - \Phi) = 0, \quad \psi^*_{n+1}(v_{n+1} - \Phi) = 0, \end{aligned} \tag{5.4.5}$$

with the constraints

$$u_{n+1} \geq \Phi \qquad v_{n+1} \geq \Phi \qquad \psi_{n+1} \geq 0 \qquad \psi^*_{n+1} \geq 0. \tag{5.4.6}$$

Again, by solving the problems (5.4.5)-(5.4.6), in (u_{n+1}, ψ_{n+1}) and (v_{n+1}, ψ^*_{n+1}) planes, we get

$$(u_{n+1}, \psi_{n+1}) = \begin{cases} (\Phi, \psi_n + \frac{\Phi - \tilde{u}_{n+1}}{k}) & \text{if } \tilde{u}_{n+1} - k\psi_n \leq \Phi, \\ (\tilde{u}_{n+1} - k\psi_n, 0) & \text{otherwise.} \end{cases} \tag{5.4.7}$$

$$(v_{n+1}, \psi_{n+1}) = \begin{cases} (\Phi, \psi^*_n + \frac{\Phi - \tilde{v}_{n+1}}{k}) & \text{if } \tilde{v}_{n+1} - k\psi^*_n \leq \Phi, \\ (\tilde{v}_{n+1} - k\psi^*_n, 0) & \text{otherwise.} \end{cases} \tag{5.4.8}$$

The pairs (u_0, ψ_0) and (v_0, ψ^*_0) at zeroth time level can be found with the aid of the given initial condition, followed by assigning the value $\psi_0 = 0$.

5.4.2 BDF2-OS Method

Using the same procedure of BDF1, we get the solution (u_{n+1}, v_{n+1}) for BDF2, with the correction terms as:

$$\begin{aligned} &\frac{3}{2}\frac{u_{n+1} - \tilde{u}_{n+1}}{k} = \psi_{n+1} - \psi_n, \ \frac{3}{2}\frac{v_{n+1} - \tilde{v}_{n+1}}{k} = \psi^*_{n+1} - \psi^*_n, \ u_{n+1} \geq \Phi, \ v_{n+1} \geq \Phi, \\ &\psi_{n+1} \geq 0, \ \psi^*_{n+1} \geq 0, \ \psi_{n+1}(u_{n+1} - \Phi) = 0, \ \psi^*_{n+1}(v_{n+1} - \Phi) = 0. \end{aligned} \tag{5.4.9}$$

By solving the problems (5.4.9), in (u_{n+1}, ψ_{n+1}) and (v_{n+1}, ψ^*_{n+1}) planes, we get

$$(u_{n+1}, \psi_{n+1}) = \begin{cases} (\Phi, \psi_n + \frac{3}{2}\frac{\Phi - \tilde{u}_{n+1}}{k}) & \text{if } \tilde{u}_{n+1} - \frac{2k}{3}\psi_n \leq \Phi, \\ (\tilde{u}_{n+1} - \frac{2k}{3}\psi_n, 0) & \text{otherwise.} \end{cases} \tag{5.4.10}$$

$$(v_{n+1}, \psi^*_{n+1}) = \begin{cases} (\Phi, \psi^*_n + \frac{3}{2}\frac{\Phi - \tilde{v}_{n+1}}{k}) & \text{if } \tilde{v}_{n+1} - \frac{2k}{3}\psi^*_n \leq \Phi, \\ (\tilde{v}_{n+1} - \frac{2k}{3}\psi^*_n, 0) & \text{otherwise.} \end{cases} \tag{5.4.11}$$

5.5 Numerical Results

In this part, we carried out different computational experiments to show the efficacy and accuracy of the suggested numerical techniques for estimating the value of European and American call options under the liquidity switching model. We utilized the second-degree space augmented polynomial ($\prod_2 := 1, x, x^2$) with the thin plate spline ($\tilde{r}^4 \ln \tilde{r}$) radial basis functions to approximate the spatial operator, and $m_i = 3$ is used in an uniformly spaced grid for all computational cases. In all three scenarios, when the option holder is in the money, at the money, or out of the money, we have shown the option value, errors, and convergence order of both suggested techniques. We used the piecewise cubic Hermite interpolation to get the option value at non-grid points.

We used MATLAB R2022b on a PC with Processor Intel(R) Core(TM) i5-10500 CPU @ 3.10GHz, 3096 Mhz, 6 Core(s), 12 Logical Processor(s) and 16.00GB RAM.

We used the following double mesh principle to calculate the errors: the difference between successive numerical solutions

$$\text{Error} = \left| u(k,h) - u\left(\frac{k}{2}, \frac{h}{2}\right) \right|,$$

and this formula is used to calculate the rate of convergence (Order):

$$\text{Order} = \log_2 \frac{|u(k,h) - u(\frac{k}{2}, \frac{h}{2})|}{|u(\frac{k}{2}, \frac{h}{2}) - u(\frac{k}{4}, \frac{h}{4})|},$$

where $u(k,h)$ represents the computed price of the option with temporal mesh length k and spatial mesh length h. We consider the N number of temporal points, and M number of spatial points. The following parameters are used to show the results at $S = 1.5,\ 2,\ 2.5$, in both the liquid and illiquid states:

$\mu = 0.06, \sigma = 0.3, \nu_{01} = 1, \nu_{10} = 12, K = 2, T = 1, S_{max} = 5,\ \gamma = 1,\ \Omega := [0, 5]$.

5.5.1 European Option

Table 5.1 reports the results from the first numerical simulation, which we used to price the European option. It display the option value, error, and temporal convergence rate of the BDF1 approaches at various asset prices under the liquidity switching model. We showed the results for liquid (R^0) and illiquid (R^1) states. Table 5.1 shows that when the temporal mesh was small enough in all states, the temporal convergence rate of BDF1 attained its asymptotic order one. Further, we conducted the same simulation using the BDF2 approach, and the results are shown in Table 5.2. When the temporal mesh was small enough in every state, we found that the temporal convergence rate of BDF2 attained its asymptotic order two. The option value for BDF2 is shown in Figure 5.1. Near the strike price, option prices exhibit little to no unpredictable fluctuation, according to the graphs. We also verified the convergence order for the BDF2 methods for pricing European option by plotting the error in Figure 5.2. From Figure 5.2, we can

Table 5.1: European option values for the liquid (upper) and illiquid state (below) for BDF1 at $M = 1024$.

	S=1.5			S=2			S=2.5		
N	Value	Error	Order	Value	Error	Order	Value	Error	Order
25	0.019770	-	-	0.168495	-	-	0.538758	-	-
50	0.019652	1.178973e-04	-	0.168892	3.970697e-04	-	0.538711	4.751057e-05	
100	0.019592	5.945299e-05	0.9877	0.169091	1.990627e-04	0.9961	0.538687	2.309818e-05	1.0404
200	0.019562	2.984385e-05	0.9943	0.169190	9.967456e-05	0.9979	0.538676	1.137017e-05	1.0225
400	0.019547	1.494993e-05	0.9972	0.169240	4.987524e-05	0.9989	0.538670	5.638101e-06	1.0119
800	0.019540	7.481771e-06	0.9986	0.169265	2.494750e-05	0.9994	0.538668	2.806953e-06	1.0062
25	0.015021	-	-	0.151819	-	-	0.530047	-	-
50	0.014842	1.788588e-04	-	0.152410	5.903113e-04	-	0.529897	1.498789e-04	-
100	0.014751	9.110646e-05	0.9731	0.152705	2.953554e-04	0.9990	0.529822	7.462257e-05	1.0061
200	0.014705	4.596749e-05	0.9869	0.152853	1.476719e-04	1.0000	0.529785	3.718255e-05	1.0049
400	0.014682	2.308621e-05	0.9935	0.152926	7.382813e-05	1.0001	0.529766	1.855202e-05	1.0030
800	0.014670	1.156853e-05	0.9968	0.152963	3.691148e-05	1.0001	0.529757	9.265217e-06	1.0016

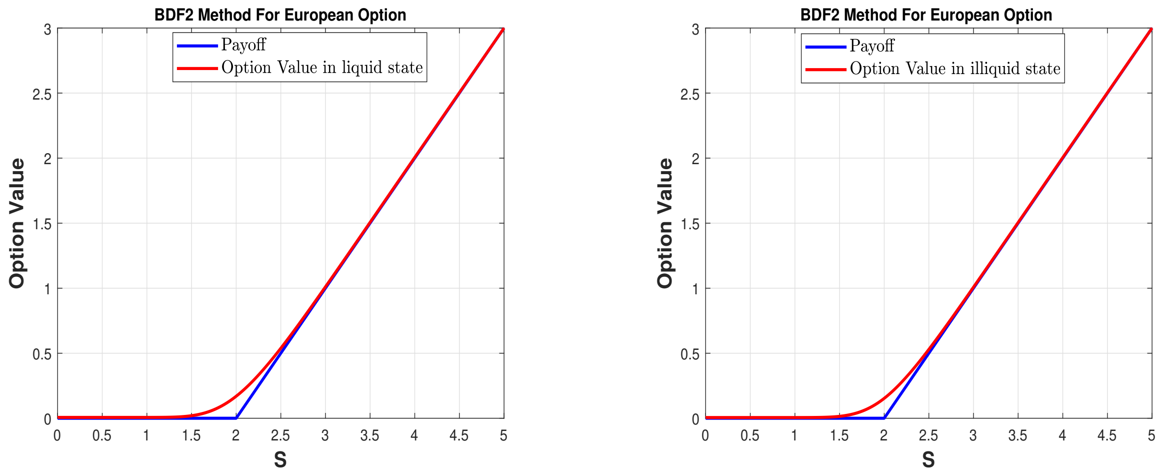

Figure 5.1: European option value using RBF-BDF2 method at $M = 1024, N = 800$.

see that the slope of the errors for BDF2 is approximately two. Using the same parameters in Table 5.3, we have also shown the option value, error, and spatial convergence order of the RBF-based BDF2 technique with the CPU time (in seconds) for different asset values in the liquid and illiquid stages of the economy. The suggested approach is shown to be second-order convergent in spatial dimension.

5.5.2 American Option

The penalty technique was used by the authors in [51] to address the linear complementarity problems in the pricing of American options. For pricing the American option under the liquidity switching model, we performed the same simulation using the operator splitting approach in conjunction with the RBF-

Table 5.2: European option values for the liquid (upper) and illiquid state (below) for BDF2 at $M = 1024$.

	S=1.5			S=2			S=2.5		
N	Value	Error	Order	Value	Error	Order	Value	Error	Order
25	0.019542	-	-	0.169244	-	-	0.538658	-	-
50	0.019535	6.788039e-06	-	0.169279	3.467573e-05	-	0.538663	5.314921e-06	-
100	0.019533	1.721656e-06	1.9791	0.169287	8.537609e-06	2.0220	0.538664	1.196427e-06	2.1513
200	0.019533	4.385892e-07	1.9728	0.169289	2.108965e-06	2.0172	0.538665	2.750843e-07	2.1207
400	0.019533	1.112810e-07	1.9786	0.169290	5.224311e-07	2.0132	0.538665	6.470497e-08	2.0879
800	0.019533	2.811407e-08	1.9848	0.169290	1.297212e-07	2.0098	0.538665	1.549929e-08	2.0616
25	0.014676	-	-	0.152946	-	-	0.529745	-	-
50	0.014663	1.311419e-05	-	0.152987	4.062634e-05	-	0.529747	2.094790e-06	-
100	0.014659	3.213764e-06	2.0287	0.152997	1.005790e-05	2.0140	0.529748	4.021876e-07	2.3808
200	0.014659	8.028527e-07	2.0010	0.152999	2.489735e-06	2.0142	0.529748	7.558820e-08	2.4116
400	0.014658	2.013179e-07	1.9956	0.153000	6.166180e-07	2.0135	0.529748	1.465443e-08	2.3668
800	0.014658	5.049012e-08	1.9954	0.153000	1.528752e-07	2.0120	0.529748	2.969693e-09	2.3029

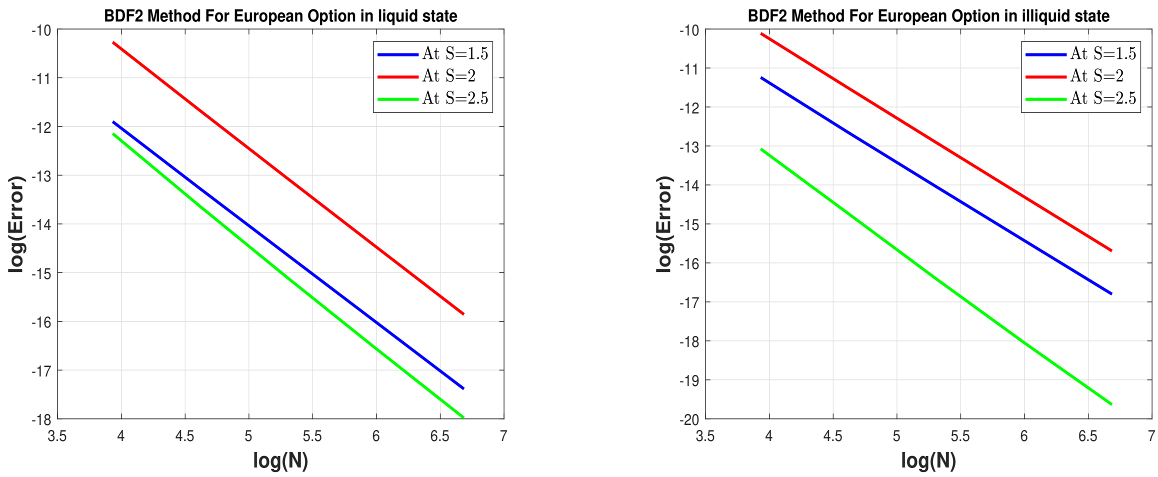

Figure 5.2: Convergence order of BDF2 in temporal direction for pricing European option at fixed $M = 1024$.

FD-based BDF1 and BDF2 methods. At each time step, the suggested methods with three time levels connected by the operator splitting approach provide a linear system that is easily solved using LU decomposition and no fixed-point iteration.

In this numerical simulation, we showed the option value, error, and the temporal convergence rate of the BDF1 techniques at different asset prices, and data are reported in Table 5.4.

Using the same simulation in Table 5.5, we have reported the data for BDF2 method. We found that when the temporal mesh was small enough in all states, the temporal convergence rate of BDF2 achieved its asymptotic order two. The option value for BDF2 is shown in Figure 5.3. Near the strike price, option

Table 5.3: Spatial convergence order of the RBF-based BDF2 method for pricing European option values in the liquid (upper) and illiquid states (below) at $N = 1600$.

	S=1.5			S=2			S=2.5			
M	Value	Error	Order	Value	Error	Order	Value	Error	Order	CPU Time
20	0.021808	-	-	0.161386	-	-	0.540612	-	-	0.089552
40	0.019958	1.850115e-03	-	0.167592	6.205910e-03	-	0.539207	1.404959e-03	-	0.114577
80	0.019620	3.381744e-04	2.4517	0.168933	1.341319e-03	2.2099	0.538802	4.046208e-04	1.7958	0.194867
160	0.019552	6.783236e-05	2.3177	0.169228	2.954829e-04	2.1825	0.538699	1.030361e-04	1.9734	0.443908
320	0.019537	1.512290e-05	2.1652	0.169285	5.673924e-05	2.3806	0.538673	2.579427e-05	1.9980	1.322748
640	0.019534	3.571569e-06	2.0821	0.169291	5.773206e-06	3.2969	0.538667	6.442386e-06	2.0013	13.983559
20	0.016989	-	-	0.143872	-	-	0.531713	-	-	0.087696
40	0.015125	1.863463e-03	-	0.151068	7.196518e-03	-	0.530324	1.389320e-03	-	0.112591
80	0.014757	3.679233e-04	2.3405	0.152600	1.531603e-03	2.2322	0.529895	4.283411e-04	1.6975	0.191622
160	0.014681	7.647072e-05	2.2664	0.152935	3.357396e-04	2.1896	0.529785	1.106001e-04	1.9534	0.453671
320	0.014664	1.733993e-05	2.1408	0.153000	6.410039e-05	2.3889	0.529757	2.779376e-05	1.9925	1.295155
640	0.014659	4.131082e-06	2.0695	0.153004	4.401208e-06	3.8643	0.529750	6.950444e-06	1.9995	13.812410

Table 5.4: American option values for the liquid (upper) and illiquid state (below) for BDF1 at $M = 1024$.

	S=1.5			S=2			S=2.5		
N	Value	Error	Order	Value	Error	Order	Value	Error	Order
25	0.019770	-	-	0.168495	-	-	0.538758	-	-
50	0.019652	1.178973e-04	-	0.168892	3.970697e-04	-	0.538711	4.751057e-05	-
100	0.019592	5.945299e-05	0.9877	0.169091	1.990627e-04	0.9961	0.538687	2.309818e-05	1.0404
200	0.019562	2.984385e-05	0.9943	0.169190	9.967456e-05	0.9979	0.538676	1.137017e-05	1.0225
400	0.019547	1.494993e-05	0.9972	0.169240	4.987524e-05	0.9989	0.538670	5.638101e-06	1.0119
800	0.019540	7.481771e-06	0.9986	0.169265	2.494750e-05	0.9994	0.538668	2.806953e-06	1.0062
25	0.015021	-	-	0.151819	-	-	0.530047	-	-
50	0.014842	1.788588e-04	-	0.152410	5.903113e-04	-	0.529897	1.498789e-04	-
100	0.014751	9.110646e-05	0.9731	0.152705	2.953554e-04	0.9990	0.529822	7.462257e-05	1.0061
200	0.014705	4.596749e-05	0.9869	0.152853	1.476719e-04	1.0000	0.529785	3.718255e-05	1.0049
400	0.014682	2.308621e-05	0.9935	0.152926	7.382813e-05	1.0001	0.529766	1.855202e-05	1.0030
800	0.014670	1.156853e-05	0.9968	0.152963	3.691148e-05	1.0001	0.529757	9.265217e-06	1.0016

prices exhibit little to no erratic fluctuation, according to the graphs. We also showed the convergence order for BDF2 method for the American option by plotting the error with respect to $\log(N)$ in Figure 5.4. From Figure 5.4, we can see that the slope of the errors for BDF2-OS is approximately two. Furthermore, we presented the numerical results using Tavella-Randal's [118] non-uniform spatial mesh at $S = K = 10$, with a fixed $M = 1600$ in $\Omega = [0, 20]$. The results of Table 5.6 and Table 5.7 show that the BDF2 approach has second-order temporal accuracy using non-uniform meshes. Additionally, we used the above-defined parameters with a fixed $N = 1600$ to illustrate the option value, error, and spatial convergence order of the RBF-based BDF2 technique with the CPU time (in seconds) for different asset values in the liquid

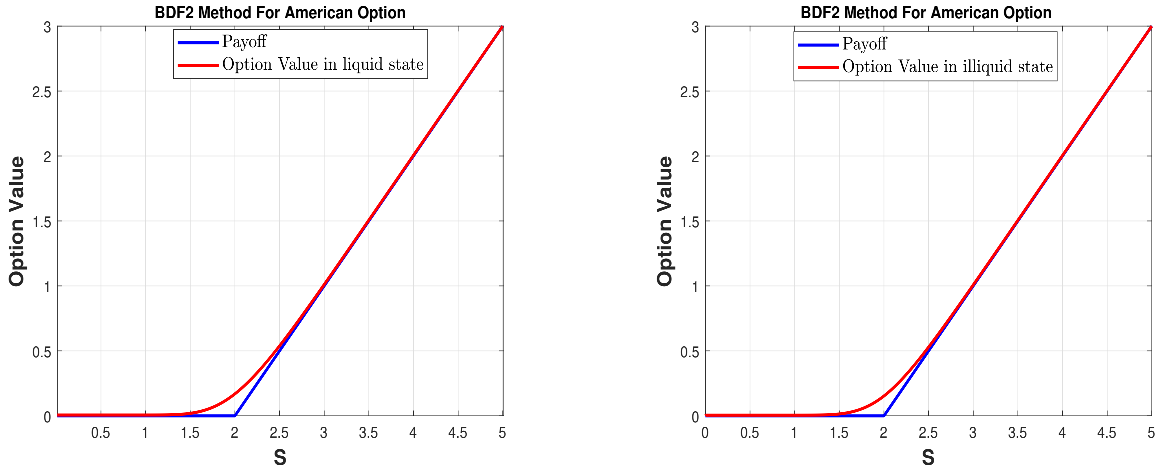

Figure 5.3: American option value using RBF-BDF2 method at $M = 1024, N = 800$.

and illiquid phases of the economy in Table 5.8. The suggested approach is shown to be second-order convergent in spatial dimension.

In Table 5.9, we showed the point-wise errors at $S = K$, with different discretization points and compared our results with the Table 5 of Gyulov [51], where the authors used the penalty method for the American constraints in order to indifference pricing of an American option. We can observe that the errors of the proposed method are reducing faster than those of Gyulov [51].

Table 5.5: American option values for the liquid (upper) and illiquid state (below) for BDF2 at $M = 1024$.

	S=1.5			S=2			S=2.5		
N	Value	Error	Order	Value	Error	Order	Value	Error	Order
25	0.019542	-	-	0.169244	-	-	0.538658	-	-
50	0.019535	6.788039e-06	-	0.169279	3.467573e-05	-	0.538663	5.314921e-06	-
100	0.019533	1.721656e-06	1.9791	0.169287	8.537609e-06	2.0220	0.538664	1.196427e-06	2.1513
200	0.019533	4.385892e-07	1.9728	0.169289	2.108965e-06	2.0172	0.538665	2.750843e-07	2.1207
400	0.019533	1.112810e-07	1.9786	0.169290	5.224311e-07	2.0132	0.538665	6.470497e-08	2.0879
800	0.019533	2.811407e-08	1.9848	0.169290	1.297212e-07	2.0098	0.538665	1.549929e-08	2.0616
25	0.014676	-	-	0.152946	-	-	0.529745	-	-
50	0.014663	1.311419e-05	-	0.152987	4.062634e-05	-	0.529747	2.094790e-06	-
100	0.014659	3.213764e-06	2.0287	0.152997	1.005790e-05	2.0140	0.529748	4.021876e-07	2.3808
200	0.014659	8.028527e-07	2.0010	0.152999	2.489735e-06	2.01426	0.529748	7.558820e-08	2.4116
400	0.014658	2.013179e-07	1.9956	0.153000	6.166180e-07	2.01354	0.529748	1.465443e-08	2.3668
800	0.014658	5.049012e-08	1.9954	0.153000	1.528752e-07	2.01202	0.529748	2.969693e-09	2.3029

Further, we look into numerical Greeks, Delta and Gamma for American option, which are computed by RBF–based IMEX-BDF2-OS method, to further demonstrate the numerical results generated by the

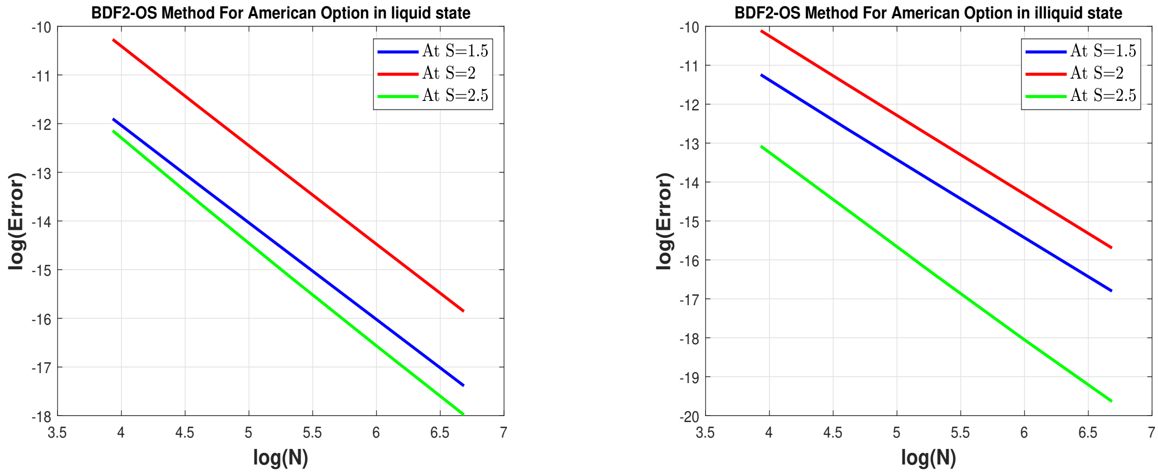

Figure 5.4: Convergence order of BDF2-OS in temporal direction for pricing American option at $M = 1024$.

Table 5.6: European option values for the liquid (upper) and illiquid state (below) for BDF2 at $M = 1600$.

	S=9			S=10			S=11		
N	Value	Error	Order	Value	Error	Order	Value	Error	Order
10	0.102555	-	-	0.432329	-	-	1.127627	-	-
20	0.102658	1.032201e-04	-	0.432859	5.302567e-04	-	1.127815	1.876837e-04	-
40	0.102679	2.122052e-05	2.2821	0.432984	1.250740e-04	2.0839	1.127855	4.032392e-05	2.2185
80	0.102684	4.259753e-06	2.3166	0.433014	2.971387e-05	2.0735	1.127864	8.757919e-06	2.2029
160	0.102684	8.611147e-07	2.3064	0.433021	7.112763e-06	2.0626	1.127866	1.937674e-06	2.1762
320	0.102685	1.788104e-07	2.2677	0.433023	1.718431e-06	2.0493	1.127866	4.396261e-07	2.1399
640	0.102685	3.836867e-08	2.2204	0.433023	4.187052e-07	2.0370	1.127866	1.021330e-07	2.1058
10	0.080180	-	-	0.388974	-	-	1.100708	-	-
20	0.080238	5.758298e-05	-	0.389636	6.617770e-04	-	1.100899	1.908212e-04	-
40	0.080253	1.557100e-05	1.8867	0.389784	1.479437e-04	2.1612	1.100943	4.397514e-05	2.1174
80	0.080256	2.825915e-06	2.4620	0.389819	3.510042e-05	2.0754	1.100953	9.353162e-06	2.2331
160	0.080256	4.914569e-07	2.5235	0.389827	8.369312e-06	2.0683	1.100955	2.043999e-06	2.1940
320	0.080257	8.514743e-08	2.5290	0.389829	2.006707e-06	2.0602	1.100955	4.612024e-07	2.1479
640	0.080257	1.488608e-08	2.5159	0.389830	4.839759e-07	2.0518	1.100955	1.069849e-07	2.1079

BDF2-OS. The Greeks of the numerical solution, calculated using the parameters $\mu = 0.06, \sigma = 0.3, \nu_{01} = 1, \nu_{10} = 12, K = 50, T = 1, S_{\max} = 100$ and $\gamma = 1$ in $\Omega = [0, 100]$ for the scheme IMEX-BDF2 for $M = 400$, $N = 1600$, are shown in Figure 5.5. We note that there are no oscillations in either Gamma or Delta. The absence of a diffusion component in the second equation of (5.2.7) results in a minor edge in the Greeks (Delta & Gamma) for the solution v (Figure 5.5). It is clear that the solution tends to a smooth function in time, since the jump of the Greeks (Delta & Gamma) at the strike price ($K = 50$) decreases as time passes. Moreover, when a market is liquid, it has a high trading volume and low bid-ask spreads. In this case, the gamma plot may exhibit smoother transitions and more predictable behavior when the underlying asset's price fluctuation. This is because there are enough market players eager to purchase and sell the option at multiple prices, resulting in effective price determination. In contrast, illiquid markets have less trading volume and large bid-ask spreads. In such situations, the gamma plot may show erratic movements and discontinuities. This is because it may be difficult to identify counterparties ready to trade at specific prices, resulting in more significant price gaps and sometimes exaggerated fluctuations in option prices. The little edge in the Greeks (Delta & Gamma) for the solution v (Figure 5.5) arises from the lack of the diffusion factor in the second equation in (5.2.7). We begin with a non-smooth initial function, the non-smoothness of the solution v remains for a long time, unlike the solution u, which is regulated by the parabolic equation in (5.2.7). Figure 5.5 depicts the profiles of the Greeks (Delta & Gamma) at various time levels. It is clear that the solution tends to a smooth function in time, since the jump of the Greeks (Delta & Gamma) at the strike point decreases over the time.

Table 5.7: American option values for the liquid (upper) and illiquid state (below) for BDF2 at M=1600.

	S=9			S=10			S=11		
N	Value	Error	Order	Value	Error	Order	Value	Error	Order
10	0.378072	-	-	0.817059	-	-	1.449758	-	-
20	0.378820	1.169094e-03	-	0.818054	1.273961e-03	-	1.450633	1.372050e-03	-
40	0.378981	2.366878e-04	2.3043	0.818275	2.614843e-04	2.2845	1.450824	2.785646e-04	2.3002
80	0.379016	5.098414e-05	2.2148	0.818324	5.645221e-05	2.2116	1.450866	6.058390e-05	2.2010
160	0.379023	1.132389e-05	2.1706	0.818335	1.216300e-05	2.2145	1.450875	1.359811e-05	2.1555
320	0.379025	2.580587e-06	2.1335	0.818338	2.618218e-06	2.2158	1.450877	3.051842e-06	2.1556
640	0.379025	5.967107e-07	2.1125	0.818338	5.220950e-07	2.3262	1.450877	4.194005e-07	2.8632
10	0.315517	-	-	0.736181	-	-	1.378073	-	-
20	0.316686	7.481711e-04	-	0.737455	9.945535e-04	-	1.379445	8.754007e-04	-
40	0.316922	1.608839e-04	2.2173	0.737717	2.214580e-04	2.1670	1.379723	1.910691e-04	2.1958
80	0.316973	3.457992e-05	2.2180	0.737773	4.905820e-05	2.1744	1.379784	4.189083e-05	2.1893
160	0.316985	7.507284e-06	2.2035	0.737786	1.095411e-05	2.1630	1.379798	9.309836e-06	2.1698
320	0.316987	1.660979e-06	2.1762	0.737788	2.459474e-06	2.1550	1.379801	1.932957e-06	2.2679
640	0.316988	3.629457e-07	2.1942	0.737789	4.545034e-07	2.4359	1.379801	1.941664e-07	3.3154

5.6 Conclusion

We proposed two numerical methods based on RBF-FD to solve semi-linear coupled PDEs and LCPs for indifference pricing of European and American options in a regime-switching model with exponential nonlinearity. The liquidity shocks model enhances pricing accuracy by incorporating liquidity risk, resulting in higher option prices in less liquid markets. This adjustment is crucial for traders and investors who need to manage risk effectively in real-world trading environments. To perform sensitivity analysis of

Table 5.8: Spatial convergence order of the RBF-based BDF2 method for pricing American option values in the liquid (upper) and illiquid states (below) at $N = 1600$.

	S=1.5			S=2			S=2.5			
M	Value	Error	Order	Value	Error	Order	Value	Error	Order	CPU Time
20	0.016989	-	-	0.143875	-	-	0.531713	-	-	0.148888
40	0.015125	1.863463e-03	-	0.151069	7.193672e-03	-	0.530324	1.389320e-03	-	0.163727
80	0.014757	3.679233e-04	2.3405	0.152600	1.531147e-03	2.2321	0.529895	4.283411e-04	1.6975	0.258627
160	0.014681	7.647072e-05	2.2664	0.152936	3.356058e-04	2.1897	0.529785	1.106001e-04	1.9534	0.591522
320	0.014664	1.733993e-05	2.1408	0.153000	6.404476e-05	2.3896	0.529757	2.779376e-05	1.9925	1.873720
640	0.014659	4.131082e-06	2.0695	0.153004	4.375042e-06	3.8717	0.529750	6.950444e-06	1.9995	14.768316
20	0.021808	-	-	0.161394	-	-	0.540612	-	-	0.111213
40	0.019958	1.850115e-03	-	0.167594	6.199666e-03	-	0.539207	1.404959e-03	-	0.137648
80	0.019620	3.381744e-04	2.4517	0.168934	1.340172e-03	2.2097	0.538802	4.046208e-04	1.7958	0.215557
160	0.019552	6.783236e-05	2.3177	0.169229	2.951198e-04	2.1830	0.538699	1.030361e-04	1.9734	0.469735
320	0.019537	1.512290e-05	2.1652	0.169285	5.658350e-05	2.3828	0.538673	2.579427e-05	1.9980	1.311562
640	0.019534	3.571569e-06	2.0821	0.169291	5.699174e-06	3.3115	0.538667	6.442386e-06	2.0013	14.328736

Table 5.9: Comparison of numerical errors with Table 5 of [51] for pricing American call option using the parameters in [51] under the liquidity switching model.

		Liquid State (u)		Illiquid State (v)	
M	N	Gyulov [51]	RBF-BDF2-OS	Gyulov [51]	RBF-BDF2-OS
64	128	-	-	-	-
128	256	2.77460e-04	3.374234e-05	2.28726e-04	3.337388e-05
256	512	7.00277e-05	9.267183e-06	5.78622e-05	9.341534e-06
512	1024	1.75479e-05	2.398951e-06	1.45077e-05	2.489551e-06

the proposed pricing model, the option value, Gamma, Delta, and computational errors have been shown with various parameters. The proposed schemes, BDF1 and BDF2, are first- and second-order convergent, respectively, and the stability analysis of the proposed techniques for coupled PDEs are presented. We used the operator splitting approach to deal with the inequality constraints in the system of semi-linear complementarity problems for American option pricing.

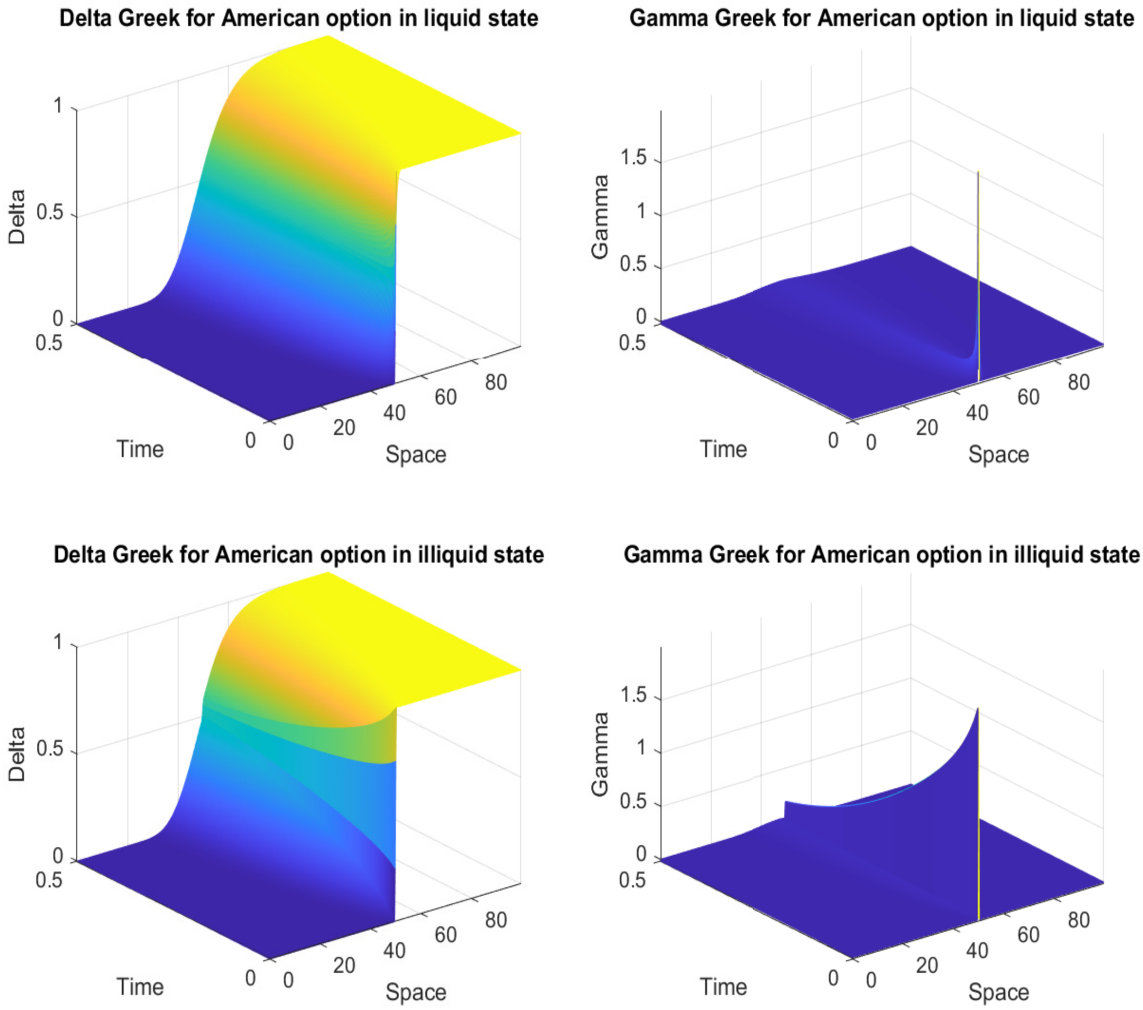

Figure 5.5: Greeks (Delta & Gamma) for pricing the American option using RBF–based IMEX-BDF2-OS under liquidity switching model at N=1600 and M=400.

CHAPTER 6

Conclusion and scope for future research

This chapter summarizes the thesis by highlighting the main contributions and novel aspects of the research work, and by outlining the scope for possible directions for future work that may be explored based on the findings of this study.

6.1 Summary

In this thesis, we developed radial basis function based grid-free schemes and investigated efficient and accurate numerical methods for partial differential and integro-differential equations (and inequalities) arising in finance. The main contributions include the construction of novel time semi-discretization finite-difference schemes for several option pricing problems, together with rigorous convergence and stability analyses under realistic regularity assumptions on the data. Due to their global support and smoothness properties, radial basis functions naturally enable higher-order accuracy. Thus, a radial basis function based approach was employed for spatial semi-descritization. This provides new radial basis function based implicit-explicit finite difference schemes for pricing of European, American, and Asian options under different market conditions, which accurately and efficiently approximate option values. By selecting appropriate radial basis functions and optimizing the associated shape parameters, higher convergence rates and reduced numerical errors were achieved. The proposed schemes effectively handle the singularities arising from non-smooth payoff functions through mesh condensation near the singular regions. Moreover, the resulting discretization leads to tridiagonal linear systems at each time step, allowing for efficient direct solution. The flexibility of the approach also permits implementation on non-uniform spatial grids. Extensive numerical experiments validate the efficiency, accuracy, and theoretical convergence rates of the proposed methods.

Following the introductory chapter (Chapter 1), in Chapter 2, we developed three radial basis function (RBF) based implicit-explicit finite-difference schemes, namely RBF-IMEX-BDF2, RBF-IMEX-CNLF and RBF-IMEX-CNAB, for solving the partial integro-differential equations arising from extended jump-diffusion asset price models. The proposed framework combines temporal IMEX discretization with an RBF-based spatial approximation and a composite trapezoidal rule for the integral term. For American option pricing, the RBF-IMEX-BDF2, RBF-IMEX-CNLF and RBF-IMEX-CNAB schemes were coupled with an operator-splitting approach to efficiently handle the linear complementarity constraints, resulting in linear systems that can be solved directly using LU decomposition without the use of fixed-point iteration. Numerical experiments for European and American put options under the Merton and Kou models with local volatility demonstrated the accuracy and efficiency of the proposed methods, as well as their ability to reliably compute option values and key 'Greeks'.

In Chapter 3, we extended the methodology proposed in Chapter 2 to regime-switching jump-diffusion asset price models. Three RBF based IMEX schemes, namely RBF-IMEX-BDF2, RBF-IMEX-CNLF, and RBF-IMEX-CNAB, were formulated to solve the resulting systems of partial integro-differential equations. The temporal IMEX discretization was combined with an RBF-based spatial approximation, while the integral terms were evaluated using a composite trapezoidal rule. For American option pricing, the schemes were coupled with an operator-splitting approach to efficiently handle the associated linear complementarity constraints, leading to linear systems at each time step that were solved by LU decomposition. Numerical experiments for European and American put options under the Merton and Kou models with local volatility demonstrated the accuracy, efficiency, and robustness of the proposed methods. In addition to option values, error measures and key Greeks, such as Delta and Gamma, were accurately computed. Numerical experiments for European and American put options were performed under the Merton and Kou models with local volatility to demonstrate the accuracy and efficiency of the proposed methods in computing option values.

In Chapter 4, an RBF based implicit-explicit approach was introduced for solving partial integro-differential equations arising in the pricing of moving boundary Asian options under a regime-switching jump-diffusion process. The IMEX-BDF2 and CNLF schemes were employed for temporal discretization, while RBF-based finite-difference techniques were used for spatial discretization of the resulting semi-discrete systems. The integral term in the PIDE was approximated using a composite trapezoidal rule. Rigorous stability results were established for the proposed schemes. Numerical experiments demonstrated that both methods achieved second-order convergence in time and space, and further showed that the proposed methods outperformed existing methods in the literature in terms of both accuracy and efficiency.

In Chapter 5, two numerical methods based on the RBF-finite difference framework were proposed for solving semi-linear coupled partial differential equations and linear complementarity problems arising in the indifference pricing of European and American options under a regime-switching model with exponential nonlinearity. The liquidity shocks model enhances pricing accuracy by incorporating liquidity risk, resulting in higher option prices in less liquid markets. This adjustment is important for effective risk management in real-world trading environments. Sensitivity analyses were conducted by examining option values, Delta, Gamma, and computational errors under various parameters. The proposed BDF1 and BDF2 schemes exhibited first and second order convergence, respectively, and stability analyses were established for the coupled PDE systems. For American option pricing, an operator-splitting approach was employed to efficiently handle the inequality constraints associated with the resulting semi-linear complementarity problems.

Each of the proposed IMEX time-stepping schemes has its own strengths in terms of accuracy, stability, and computational cost. The IMEX-CNLF and IMEX-CNAB schemes achieve second-order accuracy in time and are appealing because they are relatively straightforward to implement. However, their performance can become less reliable when dealing with highly stiff problems, such as those arising in jump-diffusion and regime-switching models. The IMEX-BDF2 scheme, on the other hand, demonstrates greater robustness and is more effective at controlling numerical oscillations, making it well suited for the stiff partial integro-differential equations commonly encountered in option pricing applications. For American options and liquidity-switching models, the operator-splitting approaches IMEX-BDF1-OS and IMEX-BDF2-OS provide additional flexibility by separating the differential and complementarity components of the problem, which simplifies the handling of early-exercise features. Overall, the numerical results suggest that IMEX-BDF2 and IMEX-BDF2-OS offer the best balance between accuracy, stability, and computational efficiency. Although all of the proposed schemes produce reliable approximations, the BDF-based methods consistently perform better for more challenging financial models that incorporate jumps, regime switching, and liquidity effects.

6.2 Future Research Directions

This section briefly describes some possible extensions of the present work.

- In the theoretical analysis, we restricted attention to uniform temporal discretization. Extending the convergence and stability analysis to non-uniform temporal and spatial discretizations simultaneously remains an important topic for future research.

- The proposed RBF based finite-difference method can be extended to investigate option pricing models involving mixed derivative terms and multi-asset dynamics.

- The RBF based finite-difference schemes can be further extended to solve higher-dimensional option pricing problems, including implementations on non-uniform spatial meshes.
- For option pricing problems, my future research interests include the development of new meshless approaches based on artificial intelligence and machine learning, particularly Physics-Informed Neural Networks (PINNs).

Bibliography

[1] Mostafa Abbaszadeh and Mehdi Dehghan. Reduced order modeling of time-dependent incompressible Navier–Stokes equation with variable density based on a local radial basis functions-finite difference (LRBF-FD) technique and the POD/DEIM method. *Computer Methods in Applied Mechanics and Engineering*, 364:112914, 2020.

[2] Yves Achdou and Olivier Pironneau. *Computational methods for option pricing*. SIAM, 2005.

[3] Nawzad M Ahmed, Fazlollah Soleymani, and Rostam K Saeed. Numerical investigation of high-dimensional option pricing PDEs by utilizing a hybrid radial basis function-finite difference procedure. *Engineering Analysis with Boundary Elements*, 163:211–222, 2024.

[4] Yacine Aıt-Sahalia, Yubo Wang, and Francis Yared. Do option markets correctly price the probabilities of movement of the underlying asset? *Journal of Econometrics*, 102(1):67–110, 2001.

[5] Ariel Almendral and Cornelis W Oosterlee. Numerical valuation of options with jumps in the underlying. *Applied Numerical Mathematics*, 53(1):1–18, 2005.

[6] Leif Andersen. Markov models for commodity futures: theory and practice. *Quantitative Finance*, 10(8):831–854, 2010.

[7] Leif Andersen and Jesper Andreasen. Jump-diffusion processes: Volatility smile fitting and numerical methods for option pricing. *Review of derivatives research*, 4(3):231–262, 2000.

[8] Ole E Barndorff-Nielsen, Thomas Mikosch, and Sidney I Resnick. *Lévy processes: theory and applications*. Springer Science & Business Media, 2001.

[9] Ali Foroush Bastani, Zaniar Ahmadi, and Davood Damircheli. A radial basis collocation method for pricing American options under regime-switching jump-diffusion models. *Applied Numerical Mathematics*, 65:79–90, 2013.

[10] David S Bates. Jumps and stochastic volatility: Exchange rate processes implicit in deutsche mark options. *The Review of Financial Studies*, 9(1):69–107, 1996.

[11] Erhan Bayraktar and Hao Xing. Pricing Asian options for jump diffusion. *Mathematical Finance: An International Journal of Mathematics, Statistics and Financial Economics*, 21(1):117–143, 2011.

[12] Dirk Becherer. Utility–indifference hedging and valuation via reaction–diffusion systems. *Proceedings of the Royal Society of London. Series A: Mathematical, Physical and Engineering Sciences*, 460(2041):27–51, 2004.

[13] Alain Bensoussan and J-L Lions. *Applications of variational inequalities in stochastic control*, volume 12. Elsevier, 2011.

[14] Fischer Black and Myron Scholes. The pricing of options and corporate liabilities. *Journal of political economy*, 81(3):637–654, 1973.

[15] Lynn Boen and Karel J In't Hout. Operator splitting schemes for American options under the two-asset merton jump-diffusion model. *Applied Numerical Mathematics*, 153:114–131, 2020.

[16] Phelim Boyle and Thangaraj Draviam. Pricing exotic options under regime switching. *Insurance: Mathematics and Economics*, 40(2):267–282, 2007.

[17] Phelim P Boyle. Options: A monte carlo approach. *Journal of financial economics*, 4(3):323–338, 1977.

[18] Michael J Brennan and Eduardo S Schwartz. The valuation of American put options. *The Journal of Finance*, 32(2):449–462, 1977.

[19] Mark Broadie, Paul Glasserman, and Shing-Gang Kou. Connecting discrete and continuous path-dependent options. *Finance and Stochastics*, 3:55–82, 1999.

[20] René Carmona. *Indifference Pricing: Theory and Applications.* Princeton University Press, 2008.

[21] P Carr, H Geman, DB Madan, and M Yor. The fine structure of asset returns; an empirical investigation journal of business 75. 2002.

[22] Chris Chen, Zeqi Wang, and Yue Yang. A new operator splitting method for American options under fractional black–scholes models. *Computers & Mathematics with Applications*, 77(8):2130–2144, 2019.

[23] Feng Chen and Jie Shen. Stability and error analysis of operator splitting methods for American options under the black–scholes model. *Journal of Scientific Computing*, 82(2):1–17, 2020.

[24] Feng Chen, Jie Shen, and Haijun Yu. A new spectral element method for pricing European options under the black–scholes and merton jump diffusion models. *Journal of Scientific Computing*, 52(3):499–518, 2012.

[25] Yong Chen. Second-order IMEX scheme for a system of partial integro-differential equations from Asian option pricing under regime-switching jump-diffusion models. *Numerical Algorithms*, pages 1–21, 2022.

[26] Zhuliang Chen and Peter A Forsyth. Implications of a regime-switching model on natural gas storage valuation and optimal operation. *Quantitative Finance*, 10(2):159–176, 2010.

[27] Rafael Company, Vera Egorova, Lucas Jódar, and Carlos Vázquez. Computing American option price under regime switching with rationality parameter. *Computers & Mathematics with Applications*, 72(3):741–754, 2016.

[28] Rafael Company, Vera N Egorova, and Lucas Jódar. A front-fixing etd numerical method for solving jump–diffusion American option pricing problems. *Mathematics and Computers in Simulation*, 189:69–84, 2021.

[29] Rama Cont. *Encyclopedia of quantitative finance*. Wiley, 2010.

[30] Rama Cont and Ekaterina Voltchkova. A finite difference scheme for option pricing in jump diffusion and exponential lévy models. *SIAM Journal on Numerical Analysis*, 43(4):1596–1626, 2005.

[31] Massimo Costabile, Arturo Leccadito, Ivar Massabó, and Emilio Russo. Option pricing under regime-switching jump–diffusion models. *Journal of Computational and Applied Mathematics*, 256:152–167, 2014.

[32] Georges Courtadon. A more accurate finite difference approximation for the valuation of options. *Journal of Financial and Quantitative Analysis*, 17(5):697–703, 1982.

[33] John C Cox, Stephen A Ross, and Mark Rubinstein. Option pricing: A simplified approach. *Journal of financial Economics*, 7(3):229–263, 1979.

[34] Min Dai, Qing Zhang, and Qiji Jim Zhu. Trend following trading under a regime switching model. *SIAM Journal on Financial Mathematics*, 1(1):780–810, 2010.

[35] Duy-Minh Dang, Duy Nguyen, and Granville Sewell. Numerical schemes for pricing Asian options under state-dependent regime-switching jump–diffusion models. *Computers & Mathematics with Applications*, 71(1):443–458, 2016.

[36] Mehdi Dehghan. Time-splitting procedures for the solution of the two-dimensional transport equation. *Kybernetes*, 36(5/6):791–805, 2007.

[37] Mehdi Dehghan, Ali Foroush Bastani, et al. Asymptotic expansion of solutions to the Black–Scholes equation arising from American option pricing near the expiry. *Journal of Computational and Applied Mathematics*, 311:11–37, 2017.

[38] Mehdi Dehghan, Ali Foroush Bastani, et al. On a new family of radial basis functions: Mathematical analysis and applications to option pricing. *Journal of Computational and Applied Mathematics*, 328:75–100, 2018.

[39] Mehdi Dehghan and Somayeh Pourghanbar. Solution of the Black-Scholes equation for pricing of barrier option. *Zeitschrift für Naturforschung A*, 66(5):289–296, 2011.

[40] Emanuel Derman and Iraj Kani. Riding on a smile. *Risk*, 7(2):32–39, 1994.

[41] Yann d'Halluin, Peter A Forsyth, and George Labahn. A semi-lagrangian approach for American Asian options under jump diffusion. *SIAM Journal on Scientific Computing*, 27(1):315–345, 2005.

[42] Darrell Duffie, Jun Pan, and Kenneth Singleton. Transform analysis and asset pricing for affine jump-diffusions. *Econometrica*, 68(6):1343–1376, 2000.

[43] Bernard Dumas, Jeff Fleming, and Robert E Whaley. Implied volatility functions: Empirical tests. *The Journal of Finance*, 53(6):2059–2106, 1998.

[44] Bruno Dupire et al. Pricing with a smile. *Risk*, 7(1):18–20, 1994.

[45] Yann d'Halluin, Peter A Forsyth, and George Labahn. A penalty method for American options with jump diffusion processes. *Numerische Mathematik*, 97:321–352, 2004.

[46] Vera N Egorova, Rafael Company, and Lucas Jódar. A new efficient numerical method for solving American option under regime switching model. *Computers & Mathematics with Applications*, 71(1):224–237, 2016.

[47] Alison Etheridge. *A course in financial calculus*. Cambridge University Press, 2002.

[48] Gregory E Fasshauer and Jack G Zhang. On choosing "optimal" shape parameters for rbf approximation. *Numerical Algorithms*, 45:345–368, 2007.

[49] Avner Friedman. Stochastic differential equations and applications. In *Stochastic differential equations*, pages 75–148. Springer, 1975.

[50] Ahmad Golbabai, Davood Ahmadian, and Mariyan Milev. Radial basis functions with application to finance: American put option under jump diffusion. *Mathematical and Computer Modelling*, 55(3-4):1354–1362, 2012.

[51] Tihomir B Gyulov and Miglena N Koleva. Penalty method for indifference pricing of American option in a liquidity switching market. *Applied Numerical Mathematics*, 172:525–545, 2022.

[52] Majid Haghi, Reza Mollapourasl, and Michèle Vanmaele. An rbf–fd method for pricing American options under jump–diffusion models. *Computers & Mathematics with Applications*, 76(10):2434–2459, 2018.

[53] Niels Haldrup and Morten Ørregaard Nielsen. A regime switching long memory model for electricity prices. *Journal of econometrics*, 135(1-2):349–376, 2006.

[54] James D Hamilton. A new approach to the economic analysis of nonstationary time series and the business cycle. *Econometrica: Journal of the econometric society*, pages 357–384, 1989.

[55] James D Hamilton. *Time series analysis*. Princeton university press, 2020.

[56] Mary R Hardy. A regime-switching model of long-term stock returns. *North American Actuarial Journal*, 5(2):41–53, 2001.

[57] Steven L Heston. A closed-form solution for options with stochastic volatility with applications to bond and currency options. *The review of financial studies*, 6(2):327–343, 1993.

[58] Desmond J Higham. Nine ways to implement the binomial method for option valuation in MATLAB. *SIAM review*, 44(4):661–677, 2002.

[59] Jian Huang, Zhongdi Cen, and Anbo Le. A finite difference scheme for pricing American put options under kou's jump-diffusion model. *Journal of Function Spaces and Applications*, 2013, 2013.

[60] Yunqing Huang, Peter A Forsyth, and George Labahn. Methods for pricing American options under regime switching. *SIAM Journal on Scientific Computing*, 33(5):2144–2168, 2011.

[61] John Hull and Alan White. The pricing of options on assets with stochastic volatilities. *The journal of finance*, 42(2):281–300, 1987.

[62] John Hull and Alan White. The use of the control variate technique in option pricing. *Journal of Financial and Quantitative analysis*, 23(3):237–251, 1988.

[63] John C Hull and Sankarshan Basu. *Options, futures, and other derivatives.* Pearson Education India, 2016.

[64] Samuli Ikonen and Jari Toivanen. Operator splitting methods for American option pricing. *Applied mathematics letters*, 17(7):809–814, 2004.

[65] Samuli Ikonen and Jari Toivanen. Operator splitting methods for pricing American options under stochastic volatility. *Numerische Mathematik*, 113(2):299–324, 2009.

[66] Michael Johannes. The statistical and economic role of jumps in continuous-time interest rate models. *The Journal of Finance*, 59(1):227–260, 2004.

[67] Mohan K Kadalbajoo, Alpesh Kumar, and Lok Pati Tripathi. Application of the local radial basis function-based finite difference method for pricing American options. *International Journal of Computer Mathematics*, 92(8):1608–1624, 2015.

[68] Mohan K Kadalbajoo, Alpesh Kumar, and Lok Pati Tripathi. An efficient numerical method for pricing option under jump diffusion model. *International Journal of Advances in Engineering Sciences and Applied Mathematics*, 7(3):114–123, 2015.

[69] Mohan K Kadalbajoo, Alpesh Kumar, and Lok Pati Tripathi. A radial basis function based implicit–explicit method for option pricing under jump-diffusion models. *Applied Numerical Mathematics*, 110:159–173, 2016.

[70] Mohan K Kadalbajoo, Lok Pati Tripathi, and Alpesh Kumar. Second order accurate IMEX methods for option pricing under Merton and Kou jump-diffusion models. *Journal of Scientific Computing*, 65:979–1024, 2015.

[71] Mohan K Kadalbajoo, Lok Pati Tripathi, and Alpesh Kumar. An error analysis of a finite element method with IMEX-time semidiscretizations for some partial integro-differential inequalities arising in the pricing of American options. *SIAM Journal on Numerical Analysis*, 55(2):869–891, 2017.

[72] Angelos Kanas. On real interest rate dynamics and regime switching. *Journal of Banking & Finance*, 32(10):2089–2098, 2008.

[73] Kamran Kazmi. An IMEX predictor–corrector method for pricing options under regime-switching jump-diffusion models. *International Journal of Computer Mathematics*, 96(6):1137–1157, 2019.

[74] Angelien Gertruda Zinnia Kemna and Antonius Cornelis Franciscus Vorst. A pricing method for options based on average asset values. *Journal of Banking & Finance*, 14(1):113–129, 1990.

[75] Namhyoung Kim and Younhee Lee. Estimation and prediction under local volatility jump–diffusion model. *Physica A: Statistical Mechanics and its Applications*, 491:729–740, 2018.

[76] Sangkwon Kim and Junseok Kim. Robust and accurate construction of the local volatility surface using the black–scholes equation. *Chaos, Solitons & Fractals*, 150:111116, 2021.

[77] Miglena N Koleva, Walter Mudzimbabwe, and Lubin G Vulkov. Fourth-order compact schemes for a parabolic-ordinary system of European option pricing liquidity shocks model. *Numerical Algorithms*, 74:59–75, 2017.

[78] Miglena N Koleva and Lubin G Vulkov. Numerical method for optimal portfolio in an exponential utility regime-switching model. *International Journal of Computer Mathematics*, 97(1-2):120–140, 2020.

[79] Steven G Kou. A jump-diffusion model for option pricing. *Management science*, 48(8):1086–1101, 2002.

[80] Alpesh Kumar, Gobinda Rakshit, Deepak Kumar Yadav, and Rajesh Yadav. RBF–based IMEX finite difference schemes for pricing option under liquidity switching. *International Journal of Computer Mathematics*, 101(7):768–788, 2024.

[81] Alpesh Kumar, Gobinda Rakshit, Deepak Kumar Yadav, and Rajesh Yadav. Radial basis function-based finite difference schemes for pricing Asian options under a regime-switching jump diffusion model. *Engineering Analysis with Boundary Elements*, 179:106400, 2025.

[82] Devendra Kumar and Komal Deswal. Haar-wavelet based approximation for pricing American options under linear complementarity formulations. *Numerical Methods for Partial Differential Equations*, 37(2):1091–1111, 2021.

[83] YongHoon Kwon and Younhee Lee. A second-order tridiagonal method for American options under jump-diffusion models. *SIAM Journal on Scientific Computing*, 33(4):1860–1872, 2011.

[84] Jaewook Lee and Younhee Lee. Stability of an implicit method to evaluate option prices under local volatility with jumps. *Applied Numerical Mathematics*, 87:20–30, 2015.

[85] Sunju Lee and Younhee Lee. Stability of numerical methods under the regime-switching jump-diffusion model with variable coefficients. *ESAIM: Mathematical Modelling and Numerical Analysis*, 53(5):1741–1762, 2019.

[86] Younhee Lee. Financial options pricing with regime-switching jump-diffusions. *Computers & Mathematics with Applications*, 68(3):392–404, 2014.

[87] Hengguang Li, Reza Mollapourasl, and Majid Haghi. A local radial basis function method for pricing options under the regime switching model. *Journal of Scientific Computing*, 79(1):517–541, 2019.

[88] Snorre Lindset and Arne-Christian Lund. A Monte Carlo approach for the American put under stochastic interest rates. *Journal of Economic Dynamics and Control*, 31(4):1081–1105, 2007.

[89] Jun Liu, Francis A Longstaff, and Jun Pan. Dynamic asset allocation with event risk. *The Journal of Finance*, 58(1):231–259, 2003.

[90] Ruihua Liu. Hybrid switching diffusions: Properties and applications (yin, gg and zhu, c.; 2010)[bookshelf]. *IEEE Control Systems Magazine*, 30(5):74–75, 2010.

[91] Francis A Longstaff. Financial claustrophobia: Asset pricing in illiquid markets, 2004.

[92] Michael Ludkovski and Qunying Shen. European option pricing with liquidity shocks. *International Journal of Theoretical and Applied Finance*, 16(07):1350043, 2013.

[93] Jingtang Ma and Han Wang. Convergence rates of moving mesh methods for moving boundary partial integro–differential equations from regime-switching jump–diffusion Asian option pricing. *Journal of Computational and Applied Mathematics*, 370:112598, 2020.

[94] Dilip B Madan and Frank Milne. Option pricing with vg martingale components 1. *Mathematical finance*, 1(4):39–55, 1991.

[95] Henry P McKean Jr. A free boundary problem for the heat equation arising from a problem in mathematical economics. *Indust. Manag. Rev.*, 6:32–39, 1965.

[96] Robert C Merton. Option pricing when underlying stock returns are discontinuous. *Journal of financial economics*, 3(1-2):125–144, 1976.

[97] Robert C Merton et al. Theory of rational option pricing. 1971.

[98] Vahid Mohammadi, Mehdi Dehghan, and Stefano De Marchi. Numerical simulation of a prostate tumor growth model by the RBF-FD scheme and a semi-implicit time discretization. *Journal of Computational and Applied Mathematics*, 388:113314, 2021.

[99] Reza Mollapourasl, Ali Fereshtian, Hengguang Li, and Xun Lu. Rbf-pu method for pricing options under the jump–diffusion model with local volatility. *Journal of Computational and Applied Mathematics*, 337:98–118, 2018.

[100] Reza Mollapourasl, Majid Haghi, and Ruihua Liu. Localized kernel-based approximation for pricing financial options under regime switching jump diffusion model. *Applied Numerical Mathematics*, 134:81–104, 2018.

[101] Michael Mongillo et al. Choosing basis functions and shape parameters for radial basis function methods. *SIAM undergraduate research online*, 4(190-209):2–6, 2011.

[102] Vasanttilak Naik. Option valuation and hedging strategies with jumps in the volatility of asset returns. *The Journal of Finance*, 48(5):1969–1984, 1993.

[103] Edgard Ngounda, Kailash C Patidar, and Edson Pindza. Contour integral method for European options with jumps. *Communications in Nonlinear Science and Numerical Simulation*, 18(3):478–492, 2013.

[104] Kuldip Singh Patel and Mani Mehra. Fourth-order compact finite difference scheme for American option pricing under regime-switching jump-diffusion models. *International Journal of Applied and Computational Mathematics*, 3(1):547–567, 2017.

[105] Kuldip Singh Patel and Mani Mehra. Fourth-order compact scheme for option pricing under the Merton's and Kou's jump-diffusion models. *International Journal of Theoretical and Applied Finance*, 21(04):1850027, 2018.

[106] David M Pooley, Kenneth R Vetzal, and Peter A Forsyth. Convergence remedies for non-smooth payoffs in option pricing. *Journal of Computational Finance*, 6(4):25–40, 2003.

[107] Michael JD Powell. The theory of radial basis function approximation in 1990. *Advances in numerical analysis*, pages 105–210, 1992.

[108] Jamal Amani Rad and Kourosh Parand. Numerical pricing of American options under two stochastic factor models with jumps using a meshless local petrov–galerkin method. *Applied Numerical Mathematics*, 115:252–274, 2017.

[109] Jamal Amani Rad, Kourosh Parand, and Luca Vincenzo Ballestra. Pricing european and American options by radial basis point interpolation. *Applied Mathematics and Computation*, 251:363–377, 2015.

[110] Alessandro Ramponi. Fourier transform methods for regime-switching jump-diffusions and the pricing of forward starting options. *International Journal of Theoretical and Applied Finance*, 15(05):1250037, 2012.

[111] Santtu Salmi and Jari Toivanen. An iterative method for pricing American options under jump-diffusion models. *Applied Numerical Mathematics*, 61(7):821–831, 2011.

[112] Santtu Salmi and Jari Toivanen. IMEX schemes for pricing options under jump–diffusion models. *Applied Numerical Mathematics*, 84:33–45, 2014.

[113] Eduardo S Schwartz. The valuation of warrants: Implementing a new approach. *Journal of Financial Economics*, 4(1):79–93, 1977.

[114] Mohammad Shirzadi, Mehdi Dehghan, and Ali Foroush Bastani. On the pricing of multi-asset options under jump-diffusion processes using meshfree moving least-squares approximation. *Communications in Nonlinear Science and Numerical Simulation*, 84:105160, 2020.

[115] Mohammad Shirzadi, Mehdi Dehghan, and Ali Foroush Bastani. Optimal uniform error estimates for moving least-squares collocation with application to option pricing under jump-diffusion processes. *Numerical Methods for Partial Differential Equations*, 37(1):98–117, 2021.

[116] Mohammad Shirzadi, Mohammadreza Rostami, Mehdi Dehghan, and Xiaolin Li. American options pricing under regime-switching jump-diffusion models with meshfree finite point method. *Chaos, Solitons & Fractals*, 166:112919, 2023.

[117] Tak Kuen Siu. Bond pricing under a markovian regime-switching jump-augmented vasicek model via stochastic flows. *Applied Mathematics and Computation*, 216(11):3184–3190, 2010.

[118] Domingo Tavella and Curt Randall. *Pricing financial instruments: The finite difference method*, volume 13. John Wiley & Sons, 2000.

[119] Nawdha Thakoor, Désiré Yannick Tangman, and Muddun Bhuruth. A new fourth-order numerical scheme for option pricing under the CEV model. *Applied Mathematics Letters*, 26(1):160–164, 2013.

[120] Nawdha Thakoor, Désiré Yannick Tangman, and Muddun Bhuruth. Rbf-fd schemes for option valuation under models with price-dependent and stochastic volatility. *Engineering Analysis with Boundary Elements*, 92:207–217, 2018.

[121] Jari Toivanen. Numerical valuation of European and American options under kou's jump-diffusion model. *SIAM Journal on Scientific Computing*, 30(4):1949–1970, 2008.

[122] Geraldine Tour, Nawdha Thakoor, Jingtang Ma, and Désiré Yannick Tangman. A spectral element method for option pricing under regime-switching with jumps. *Journal of Scientific Computing*, 83(3):1–31, 2020.

[123] Geraldine Tour, Nawdha Thakoor, Désiré Yannick Tangman, and Muddun Bhuruth. A high-order RBF-FD method for option pricing under regime-switching stochastic volatility models with jumps. *Journal of Computational Science*, 35:25–43, 2019.

[124] Pierre Van Moerbeke. On optimal stopping and free boundary problems. *Archive for Rational Mechanics and Analysis*, 60(2):101–148, 1976.

[125] Jan Vecer. A new PDE approach for pricing arithmetic average Asian options. *Journal of computational finance*, 4(4):105–113, 2001.

[126] Jan Vecer and Mingxin Xu. Pricing Asian options in a semimartingale model. *Quantitative finance*, 4(2):170, 2003.

[127] Lina von Sydow, Jari Toivanen, and Chi Zhang. Adaptive finite differences and IMEX time-stepping to price options under bates model. *International Journal of Computer Mathematics*, 92(12):2515–2529, 2015.

[128] Mohamed Ismail Mohamed Wahab, Z Yin, and NCP Edirisinghe. Pricing swing options in the electricity markets under regime-switching uncertainty. *Quantitative Finance*, 10(9):975–994, 2010.

[129] Wansheng Wang, Yingzi Chen, and Hua Fang. On the variable two-step IMEX BDF method for parabolic integro-differential equations with nonsmooth initial data arising in finance. *SIAM Journal on Numerical Analysis*, 57(3):1289–1317, 2019.

[130] Rafal Weron, Michael Bierbrauer, and Stefan Trück. Modeling electricity prices: jump diffusion and regime switching. *Physica A: Statistical Mechanics and its Applications*, 336(1-2):39–48, 2004.

[131] Zong-min Wu and Robert Schaback. Local error estimates for radial basis function interpolation of scattered data. *IMA journal of Numerical Analysis*, 13(1):13–27, 1993.

[132] Deepak Kumar Yadav, Akanksha Bhardwaj, and Alpesh Kumar. Errors in the IMEX-BDF-OS methods for pricing American style options under the jump-diffusion model. *Computational & Applied Mathematics*, 43(1):1, 2024.

[133] Deepak Kumar Yadav, Akanksha Bhardwaj, and Alpesh Kumar. Operator splitting method to solve the linear complementarity problem for pricing American option: An approximation of error. *Computational Economics*, 64(6):3353–3379, 2024.

[134] Deepak Kumar Yadav, Akanksha Bhardwaj, Gobinda Rakshit, and Alpesh Kumar. Implicit-Explicit BDF-OS Schemes for Pricing American Style Options in Markovian Regime-Switching Economy with Jumps: An Approximation of Error. *Computational Economics*, pages 1–40, 2026.

[135] Rajesh Yadav, Deepak Kumar Yadav, and Alpesh Kumar. RBF based some implicit–explicit finite difference schemes for pricing option under extended jump-diffusion model. *Engineering Analysis with Boundary Elements*, 156:392–406, 2023.

[136] Rajesh Yadav, Deepak Kumar Yadav, and Alpesh Kumar. RBF-FD based some implicit-explicit methods for pricing option under regime-switching jump-diffusion model with variable coefficients. *Numerical Algorithms*, pages 1–41, 2023.

[137] Rajesh Yadav, Deepak Kumar Yadav, and Alpesh Kumar. Adaptive Multiquadratic Radial Basis Function-based Explicit Runge–Kutta Methods. *arXiv preprint arXiv:2507.04261*, 2025.

[138] Hongtao Yang. A numerical analysis of American options with regime switching. *Journal of Scientific Computing*, 44(1):69–91, 2010.

[139] David D Yao, Qing Zhang, and Xun Yu Zhou. A regime-switching model for european options. *Stochastic Processes, Optimization, and Control Theory: Applications in Financial Engineering, Queueing Networks, and Manufacturing Systems: A Volume in Honor of Suresh Sethi*, pages 281–300, 2006.

[140] Muhammad Yousuf, AQM Khaliq, and Salah Alrabeei. Solving complex pide systems for pricing American option under multi-state regime switching jump–diffusion model. *Computers & Mathematics with Applications*, 75(8):2989–3001, 2018.

[141] Fei Lung Yuen and Hailiang Yang. Pricing Asian options and equity-indexed annuities with regime switching by the trinomial tree method. *North American Actuarial Journal*, 14(2):256–272, 2010.

[142] Jin E Zhang. Pricing continuously sampled Asian options with perturbation method. *Journal of Futures Markets: Futures, Options, and Other Derivative Products*, 23(6):535–560, 2003.

[143] Qing Zhang and Xin Guo. Closed-form solutions for perpetual American put options with regime switching. *SIAM Journal on Applied Mathematics*, 64(6):2034–2049, 2004.

[144] Qing Zhang and Xun Yu Zhou. Valuation of stock loans with regime switching. *SIAM Journal on Control and Optimization*, 48(3):1229–1250, 2009.

[145] Xin Zhang, Robert J Elliott, and Tak Kuen Siu. A stochastic maximum principle for a markov regime-switching jump-diffusion model and its application to finance. *SIAM Journal on Control and Optimization*, 50(2):964–990, 2012.

[146] You-lan Zhu, Xiaonan Wu, I-Liang Chern, and Zhi-zhong Sun. *Derivative securities and difference methods*. Springer, 2004.

List of Publications

Thesis Related Publication

1. **Rajesh Yadav**, Deepak Kumar Yadav, Alpesh Kumar: RBF based some implicit–explicit finite difference schemes for pricing option under extended jump-diffusion model. *Engineering Analysis with Boundary Elements* 156, 392-406 (2023). https://doi.org/10.1016/j.enganabound.2023.08.021

2. **Rajesh Yadav**, Deepak Kumar Yadav, Alpesh Kumar: RBF-FD based some implicit-explicit methods for pricing op- tion under regime-switching jump-diffusion model with variable coefficients. *Numerical Algorithms* 97(2), 645-685 (2024). https://doi.org/10.1007/s11075-023-01719-2

3. Alpesh Kumar, Gobinda Rakshit, Deepak Kumar Yadav, **Rajesh Yadav**: RBF Based Some IMEX Finite Difference Schemes For Pricing Option Under Liquidity Switching. *International Journal of Computer Mathematics* 101(7), 768-788 (2024). https://doi.org/10.1080/00207160.2024.2383757

4. Alpesh Kumar, Gobinda Rakshit, Deepak Kumar Yadav, **Rajesh Yadav**: Radial Basis Function-Based Finite Difference Schemes for Pricing Asian Options under a Regime-Switching Jump Diffusion Model. *Engineering Analysis with Boundary Elements* 179, 106400 (2025). https://doi.org/10.1016/j.enganabound.2025.106400

Other Publication

1. **Rajesh Yadav**, Deepak Kumar Yadav, Alpesh Kumar: Adaptive Multiquadratic Radial Basis Function-Based Explicit Runge-Kutta Methods. (*Communicated*).

2. Deepak Kumar Yadav, **Rajesh Yadav**, Gobinda Rakshit, Alpesh Kumar: An Extrapolated Implicit-Explicit Backward Difference Scheme for Utility Indifference Pricing of European and American Options in Liquidity-Switching Markets. (*Communicated*).

3. **Rajesh Yadav**, Deepak Kumar Yadav, Alpesh Kumar: Numerical approximation of blood flow in arteries using radial basis function based finite difference weighted essentially non-oscillatory scheme. (*Communicated*).

4. Deepak Kumar Yadav, **Rajesh Yadav**, Alpesh Kumar: A Conservative Sparse Augmented Compact IMEX-BDF2 Scheme for KdV and Zakharov-Kuznetsov Dispersive Equations. (*Communicated*).